SUHAYDA

NOAA Technical Report NWS 38

Hurricane Climatology for the Atlantic and Gulf Coasts of the United States

Francis P. Ho, James C. Su, Karen L. Hanevich,
Rebecca J. Smith and Frank P. Richards
Silver Spring, MD

April 1987

Study completed under agreement EMW-84-E-1589 for
FEDERAL EMERGENCY MANAGEMENT AGENCY

U.S. DEPARTMENT OF COMMERCE
Malcolm Baldrige, Secretary

National Oceanic and Atmospheric Administration
Anthony J. Calio, Under Secretary

National Weather Service
Richard E. Hallgren, Acting Assistant Administrator

TABLE OF CONTENTS

		Page
Abstract		1
1.	Introduction	1
1.1	Authorization	1
1.2	Purpose	2
1.3	Scope of report	2
1.4	Relation to flood insurance studies	4
1.5	Previous studies	5
2.	Data	5
2.1	Introduction	5
2.2	Sources of data	6
2.3	Hurricane central pressure (P_o) data	23
2.3.1	Central pressure criteria based on balanced wind model	24
2.3.2	Central pressure adjustments	24
2.3.3	Revised central pressure from previous studies	25
2.4	Hurricane radius of maximum winds (R) data	25
2.4.1	Source of radius of maximum winds	26
2.4.1.1	Radius of maximum winds from aerial reconnaissance	26
2.4.1.2	Radius of maximum winds from wind records	27
2.4.1.3	Radius of maximum winds from eye radius	28
2.4.1.4	Radius of maximum winds from pressure fit	28
2.4.1.5	Radius of maximum winds from **Monthly Weather Review**	28
2.5	Speed and (T) direction (θ) of forward motion	28
2.5.1	Source of T and θ data	28
2.5.2	T and θ data used in probability distributions	30
3.	Meteorological parameters and their interrelations	30
3.1	Introduction	30
3.1.1	Overview of the statistical study	30
3.1.2	Scope of the chapter	31
3.2	Considerations of data samples for statistical tests	31
3.2.1	Forward speed	32
3.2.2	Forward direction	34
3.3	Homogeneity of the hurricane data samples	34
3.3.1	Methods for testing the homogeneity of storm parameters	35
3.3.2	Comparison of results from different homogeneity tests	37
3.3.2.1	Meteorological method	37
3.3.2.2	Cluster analysis	38
3.3.2.3	Discriminant analysis	38
3.3.2.4	Principal component analysis	39
3.3.3	Selection of hurricane groups for independence testing	40
3.3.3.1	Gulf coast	42
3.3.3.2	Florida coast	42
3.3.3.3	Atlantic coast	43

Page

3.4 Interrelations between hurricane parameters..... 43
3.4.1 Brief review of previous studies..... 43
3.4.2 Methods for testing the interrelations between hurricane parameters..... 44
3.4.2.1 Contingency table with Chi-square test..... 44
3.4.2.2 Spearman test..... 44
3.4.3 Comparison of results from different independence tests..... 45
3.5 Discussion..... 45

4. The joint probability question: Central pressure versus radius of maximum winds..... 50
4.1 Introduction..... 50
4.2 Central pressure versus radius of maximum winds..... 50
4.3 Meteorological analysis..... 52
4.4 Discussion of analysis..... 55
4.5 Conclusions..... 59

5. Other joint probability questions..... 59
5.1 Introduction..... 59
5.2 Forward speed versus direction of storm motion..... 60
5.3 Central pressure versus direction of storm motion..... 61
5.3.1 Gulf coast..... 61
5.3.2 Atlantic coast..... 64
5.3.2.1 Atlantic coast, south of 33.5°N..... 64
5.3.2.2 North Atlantic coast..... 66
5.4 Cape Hatteras area..... 66
5.4.1 Parameters for landfalling hurricanes from northeast quadrant..... 66
5.4.2 Parameters for landfalling hurricanes from southeast quadrant..... 67
5.4.3 Landfalling track frequency..... 67

6. Frequency of hurricane and tropical storm occurrences..... 67
6.1 Classification of hurricanes and data..... 67
6.2 Frequency of landfalling tropical cyclones..... 72
6.2.1 Direct-count method..... 72
6.2.1.1 Objective smoothing procedure..... 75
6.2.1.2 Evaluation of procedure..... 75
6.2.2 Discussion of results..... 77
6.2.2.1 Areas of high entry frequencies..... 77
6.2.2.1 (a) Northwest Florida..... 77
6.2.2.1 (b) South Florida..... 77
6.2.2.1 (c) Upper Texas coast..... 78
6.2.2.1 (d) Cape Hatteras..... 78
6.2.2.2 Areas of low entry frequencies..... 78
6.2.2.2 (a) East coast..... 78
6.2.2.2 (b) Gulf coast..... 78
6.3 Frequency of exiting tropical cyclones..... 78
6.3.1 Analysis..... 78
6.3.2 Results and discussion..... 79
6.3.2.1 Gulf coast..... 79

Page

6.3.2.2 Atlantic coast..... 79
6.3.2.3 Application in tide-frequency analysis..... 79
6.4 Frequency of alongshore tropical cyclones..... 81
6.4.1 Analysis..... 81
6.4.2 Results and discussion..... 85

7. Central pressure..... 85
7.1 Introduction..... 85
7.2 Analysis..... 86
7.3 Results 89
7.3.1 Pressure minima..... 89
7.3.1.1 South Florida minimum..... 89
7.3.1.2 South Texas minimum..... 92
7.3.1.3 Carolinas and southern New England minima..... 92
7.3.1.4 Mississippi Delta minimum..... 92
7.3.2 Pressure maxima..... 92
7.3.2.1 Cross City, Florida, maximum..... 92
7.3.2.2 Delaware Bay maximum..... 93
7.3.2.3 Jacksonville maximum..... 93
7.3.2.4 Northern New England coastal maximum..... 93

8. Radius of maximum winds..... 94
8.1 Analysis..... 94
8.1.1 Gulf of Mexico..... 95
8.1.2 Atlantic coast..... 95
8.2 Evaluation of the analysis..... 95
8.2.1 Gulf coast..... 95
8.2.1.1 Florida and Mexico minima..... 95
8.2.1.2 Mississippi-Florida panhandle maximum..... 95
8.2.2 Atlantic coast..... 95
8.3 Radius of maximum winds for intense hurricanes..... 98

9. Speed and direction of storm motion..... 98
9.1 Speed of storm motion..... 98
9.1.1 Forward speed of landfalling tropical cyclones..... 98
9.1.1.1 Analysis..... 98
9.1.1.2 Results and discussion..... 98
9.1.2 Forward speed of bypassing tropical cyclones..... 102
9.2 Direction of storm motion..... 102
9.2.1 Direction of storm motion for landfalling tropical cyclones..... 102
9.2.1.1 Analysis..... 102
9.2.1.2 Results and discussion..... 103
9.2.1.2 (a) Gulf coast..... 106
9.2.1.2 (b) East coast, south of Cape Hatteras..... 107
9.2.1.2 (c) East coast, north of Cape Hatteras..... 107
9.2.1.3 Areas of discontinuous direction profile..... 107
9.2.2 Direction of storm motion for bypassing tropical cyclones... 107

10. Adjustment of hurricane intensity for filling overland..... 108
10.1 Introduction..... 108
10.2 Index for overland filling..... 108

Page

10.3 Previous observational studies..... 109
10.4 Analysis of data..... 109
10.5 Filling rates by region..... 110
10.6 Results 121
11. Application of hurricane parameters..... 123
11.1 Introduction..... 123
11.2 Landfall point..... 123
11.3 Peripheral pressure..... 124
11.4 Probability distributions of hurricane parameters and frequency of occurrence..... 124
11.5 Applications of profiles of probability distributions for hurricane parameters..... 127
11.6 Exiting tropical cyclones..... 136

12. Summary and discussion..... 136
12.1 Frequency of tropical cyclone occurrences..... 137
12.2 Probability distribution of storm parameters..... 138
12.3 Independence of parameters..... 138

Acknowledgments..... 139
References..... 140

Appendix A Detailed analysis of selected storms..... 147
A.1 Introduction..... 147
A.2 Hurricane Alicia, August 15-21, 1983..... 147
A.2.1 Introduction..... 147
A.2.2 Previous reports..... 147
A.2.3 Sources of data..... 148
A.2.4 General meteorological situation..... 149
A.2.5 Detailed meteorological analysis..... 149
A.2.5.1 Storm track..... 149
A.2.5.2 Forward speed..... 150
A.2.5.3 Central pressure..... 152
A.2.5.4 Wind analysis..... 154
A.2.5.5 Radius of maximum winds..... 156
A.2.6 Discussion..... 159
A.3 Hurricane David, September 2-5, 1979..... 160
A.3.1 Introduction..... 160
A.3.2 Previous studies..... 162
A.3.3 Aircraft data..... 163
A.3.4 Central pressure 164
A.3.4.1 P_o from aerial reconnaissance..... 164
A.3.4.2 P_o from land station observations..... 164
A.3.4.3 Pressure fit at the coast..... 164
A.3.4.4 Time variation of P_o..... 164
A.3.5 Radius of maximum winds 170
A.3.5.1 R from aerial reconnaissance..... 170
A.3.5.2 R from land station observations..... 170
A.3.5.3 Time variation of radius of R..... 174
A.4 Hurricane Allen, August 2-10, 1980..... 174
A.4.1 Introduction..... 174
A.4.2 Previous reports..... 176
A.4.3 Reconnaissance flight data..... 177

Page

A.4.4 Central pressure analysis..... 177
A.4.5 Wind analysis..... 177
A.4.6 Time variation of central pressure and radius of maximum winds..... 182
A.4.7 Relation of P_o and R in Hurricane Allen..... 182

Appendix B Statistical methods for tests of homogeneity and independence..... 185
B.1 Introduction..... 185
B.2 Methods for the test of homogeneity..... 185
B.2.1 Cluster analysis..... 185
B.2.1.1 Description of the method..... 185
B.2.1.2 Rationale for choice..... 186
B.2.1.3 Limitations of the method..... 187
B.2.1.4 Interpretation of the results..... 187
B.2.2 Discriminant analysis..... 187
B.2.2.1 Description of the method..... 187
B.2.2.2 Rationale for choice..... 187
B.2.2.3 Limitations of the method..... 187
B.2.2.4 Interpretation of the results..... 188
B.2.3 Principal component analysis..... 188
B.2.3.1 Description of the method..... 188
B.2.3.2 Rationale for choice..... 188
B.2.3.3 Limitations of the method..... 188
B.2.3.4 Interpretation of the results..... 188
B.2.4 Mann-Whitney test..... 189
B.2.4.1 Description of the method..... 189
B.2.4.2 Rationale for choice..... 190
B.2.4.3 Limitations of the method..... 190
B.2.4.4 Interpretation of the results..... 190
B.3 Methods for the test of independence..... 190
B.3.1 Spearman test..... 191
B.3.1.1 Description of the method..... 191
B.3.1.2 Rationale for choice..... 191
B.3.1.3 Limitations of the method..... 191
B.3.1.4 Interpretation of the results..... 191
B.3.2 Contingency table with Chi-square test..... 192
B.3.2.1 Description of the method..... 192
B.3.2.2 Rationale for choice..... 192
B.3.2.3 Limitations of the method..... 192
B.3.2.4 Interpretation of the results..... 192

Appendix C Plotting position formula..... 192
C.1 Introduction..... 192
C.2 Criteria for evaluation..... 192
C.3 Evaluation of plotting position formulae..... 194
C.4 Comparison of formulae..... 194

LIST OF FIGURES

Number		Page
1	Locator map with coastal distance intervals marked (nmi).....	3
2	Hourly observations of wind speed and direction, and distance of Allen's center from Brownsville, Texas.....	27
3	Radius of maximum winds versus inner radar eye radius.....	29
4	Difference between the radius of maximum winds and the inner radar eye radius versus maximum wind speed.....	29
5	Forward speed of landfalling hurricanes and tropical storms versus milepost (a) along the Gulf coast of Florida, and (b) along the Atlantic coast.....	33
6	Possible homogeneous regions for landfalling hurricane parameters.....	36
7	Plot of the second principal component versus the first principal component.....	40
8	Central pressure of landfalling hurricanes versus milepost.....	41
9	Interrelations between parameters of landfalling hurricanes for the Gulf and Atlantic coasts of the United States.....	46
10	Landfalling hurricane parameters versus milepost for the Atlantic coast.....	48
11	Location and minimum central pressure of extreme hurricanes.....	54
12	Tracks of extreme hurricanes.....	56
13	Same as Figure 12.....	57
14	Plot of P_o versus R for extreme hurricanes listed in Table 16.....	58
15	Scatter diagram of direction versus speed of forward motion for hurricanes landfalling on the Atlantic coast.....	60
16	Probability distribution of forward speed of (a) landfalling, and (b) alongshore hurricanes in the vicinity of Charleston, South Carolina, for the period 1886-1973.....	62
17	Plot of forward direction versus milepost for the landfalling hurricanes on the Gulf coast of the United States.....	63
18	Variation with latitude of direction of forward motion for hurricanes landfalling on the Atlantic coast.....	63

Number		Page
19	Histogram for direction of storm motion for the 2.5° latitude and longitude block centered about Key West, Florida	65
20	Track of tropical storms and hurricanes showing motion from northeast	68
21	Cumulative probability curve of central pressure for landfalling tropical cyclones near Wright Monument, North Carolina	69
22	Cumulative probability curve of speed of storm motion adapted for landfalling tropical cyclones near Wright Monument, North Carolina	69
23	Frequency of landfalling hurricanes and tropical storms	70
24	Smoothed coastline obtained by applying the objective smoothing function	71
25	Map showing extensions of west coast of Florida and the Atlantic coast through the Florida Keys	73
26	Count of landfalling tropical storms and hurricanes (1871-1984) by 50-nmi segments of a smoothed coastline	74
27	Frequency of landfalling tropical cyclones (1871-1984) for the Gulf and Atlantic coasts of the United States	76
28	Frequency of exiting hurricanes and tropical storms (1871-1974)	80
29	Tide frequencies at Wright Monument, North Carolina, for several classes of storms	81
30	Accumulative count of hurricane and tropical storm tracks passing the coast at sea (1871-1984)	82
31	Cumulative frequency of tropical cyclones bypassing the Gulf coast at selected distances offshore (1871-1984)	83
32	Cumulative frequency of tropical cyclones bypassing the Atlantic coast at selected distances offshore (1871-1984)	84
33	Cumulative probability curve of central pressure of hurricanes landfalling within (a) 250 nmi of milepost 250, near Corpus Christi, Texas, and (b) 200 nmi of milepost 1600 near Vero Beach Florida	88
34	Probability distribution of central pressure for hurricanes landfalling on the Gulf coast (1900-84)	90
35	Same as Figure 34, but for Atlantic coast hurricanes	91

Number		Page
36	Cumulative probability curve of radius of maximum winds for hurricanes landfalling within (a) 250 nmi of milepost 250, near Corpus Christi, Texas, and (b) 200 nmi of milepost 1600, near Vero Beach, Florida	94
37	Probability distribution of radius of maximum winds for hurricanes landfalling on the Gulf coast (1900-84)	96
38	Same as Figure 37, but for Atlantic coast hurricanes	97
39	Cumulative probability curve of forward speed of tropical cyclones landfalling within (a) 250 nmi of milepost 250, near Corpus Christi, Texas, and (b) 200 nmi of milepost 1600, near Vero Beach, Florida	99
40	Probability distribution of forward speed for tropical cyclones landfalling on the Gulf coast (1900-84)	100
41	Same as Figure 40, but for Atlantic coast tropical cyclones	101
42	Cumulative probability curve of direction of storm motion of tropical cyclones landfalling within (a) 100 nmi of milepost 250, near Corpus Christi, Texas, and (b) 100 nmi of milepost 1600, near Vero Beach, Florida	103
43	Probability distribution for direction of storm motion for tropical cyclones landfalling on the Gulf coast (1900-84)	104
44	Same as Figure 43, but for the Atlantic coast south of Cape Hatteras	105
45	Same as Figure 43, but for the Atlantic coast north of Cape Hatteras	106
46	Pressure profiles after landfall for (a) hurricane Frederick September 1979 and (b) Hurricane Alicia, August 1983	111
47	Map showing geographical regions used to study filling rates	112
48a	Variation with time after landfall of filling rate of hurricanes listed in region A of Table 19	114
48b	Same as Figure 48a	115
49	Filling rates for hurricanes of various intensities for region A (Gulf coast, west of Apalachicola, Florida)	116
50	Comparison of filling rates for various hurricanes crossing the Florida peninsula and the filling curve for region B from Schwerdt et al. (1979)	118

Number		Page
51	Filling rates for hurricanes of various intensities for region B (southern Florida)	119
52	Variation with time after landfall of filling rates for Hurricanes Hazel (1954), Gracie (1959), and David (1979)	120
53	Variation with time of filling rates for New England hurricanes	121
54	Filling rate for hurricanes in region C (Atlantic coast, north of Georgia)	122
55	Plot of cumulative counts of alongshore storms versus distance from coast for Vero Beach, Florida (milepost 1600)	126
56	Cumulative probability curves of P_o for designated locations	133
57	Cumulative probability curve for pressure deficit at Vero Beach, Florida	135
A.1	Hurricane track for Alicia, 0000 CST August 16 through 1200 CST August 18, 1983	150
A.2	Hurricane eye position obtained from radar, aircraft reconnaissance penetration fixes, and satellite observations	151
A.3	Minimum pressure recorded at land stations and by aircraft reconnaissance during Hurricane Alicia	152
A.4	Variation of minimum central pressure estimates for Hurricane Alicia	153
A.5	Hourly observations of sea-level pressure and surface wind speed recorded at Houston Intercontinental Airport, Texas	155
A.6	Same as Figure A.5, but for Baytown,Texas	156
A.7	Composite isotach analysis for Hurricane Alicia, centered at 2240 GMT, August 17, 1983	157
A.8	Streamline and 10-m isotach analysis for Hurricane Alicia, 0730 GMT, August 18, 1983	158
A.9	Flight-level winds recorded along radials through the center of Hurricane Alicia, 1352-1433 GMT, August 17, 1983	159
A.10	Radius of primary and secondary wind maxima in Hurricane Alicia, August 17-18, 1983	160
A.11	Track with central pressures for Hurricane David, September 2-5, 1979	161

Number		Page
A.12	Reconnaissance flight pattern, designated as star pattern used in Hurricanes David and Allen	163
A.13	Sea-level pressure observed during passage of Hurricane David, (September 1979) at (a) Shuttle Airport, Florida, and (b) Savannah (Municipal Airport), Georgia	165
A.14	Pressure-profile curve during Hurricane David (a) for Florida coast at 2100 GMT, September 3, 1979, (b) Georgia coast at 1800 GMT, September 4, 1979	166
A.15	Central pressure (sea-level) for Hurricane David, September 3-5, 1979	167
A.16	Flight-level winds recorded along radials through the center of Hurricane David, (a) 2308-2356 GMT, September 2, (b) 0644-0748 GMT, September 4, and (c) 1751-1841 GMT, September 4, 1979	169
A.17a	Wind speed and direction at Shuttle Airport, Florida, during the passage of Hurricane David, September 2-4, 1979	171
A.17b	Wind speed and direction at Savannah, Georgia, during the passage of Hurricane David, September 3-5, 1979	172
A.18	Radial distances (from eye center) of wind maxima in Hurricane David, September 2-5, 1979	173
A.19	Track of Hurricane Allen, August 2-11, 1980	175
A.20	Reconnaissance flight patterns used in Hurricane Allen	179
A.21	Central pressure for Hurricane Allen, (a) August 3-7, and (b) August 7-10, 1980	180
A.22	Flight-level winds recorded along radials through the center of Hurricane Allen, 1535-1627 GMT, August 5, 1980	181
A.23	Flight-level winds recorded along radials through the center of Hurricane Allen, 1844-1945 GMT, August 7, 1980	181
A.24	Composite map of flight-level winds recorded between 0200 and 0400 GMT, August 9, 1980	182
A.25	Central pressure and radial distances (from eye center) of wind maxima in Hurricane Allen, August 3-10, 1980	183
A.26	Concurrent observations of central pressure and radius of maximum winds for Hurricane Allen, August 3-9, 1980	184
B.1	Levels two through nine of the hierarchical clustering of landfalling hurricanes	186
C.1	Comparison of plotting position formulae for N = 10	195

LIST OF TABLES

Number		Page
1	Hurricanes with central pressure < 982 mb, ranked in chronological order from 1900-84. Gulf coast United States.....	7
2	Hurricanes with central pressure < 982 mb ranked in chronological order from 1900-84. East coast United States.....	14
3	Miscellaneous Florida hurricanes with central pressure < 982 mb ranked in chronological order from 1900-1984.....	20
4	Hurricanes with revised central pressure.....	26
5	Forward speed of hurricanes and tropical storms for selected portions of the coast.....	32
6	Initially selected coastal segments.....	35
7	Results of Mann-Whitney test for a **priori** selection of coastal segments in the Gulf of Mexico.....	37
8	Results of Mann-Whitney test for modified segments of the Gulf coast.....	38
9	Percentages of variance accounted for by principal components.....	39
10	Loading of hurricane parameters in the principal components which account for more than 12 percent of variance.....	39
11	Coastal segments that include homogeneous hurricane parameters for the test of independence.....	41
12	Breakpoint values for contingency tables.....	44
13	Sample sizes of paired parameters of landfalling hurricanes for coastal segments.....	45
14	An example of a general two-by-two contingency table.....	51
15	Frequency of occurrence of different storm radii in two different class intervals of hurricane intensity observed in the Gulf of Mexico, 1900-84.....	52
16	Severe hurricanes since 1900 with P_o < 930 mb.....	53
17	Comparison of speeds of landfalling and alongshore storms for the vicinity of Charleston, South Carolina.....	61
18	Partition of P_o and θ for landfalling hurricanes striking the Atlantic coast south of 33.5°N.....	64

Number		Page
19	Selected landfalling hurricanes (1928-1983) used to estimate overland filling rates	113
20	Changes in hurricane pressure deficits due to overland filling	117
21	Summary sheet of information needed from this report for surge-frequency computations	128
22a	Summary sheet for Vero Beach, Florida	130
22b	Summary sheet for 50 nmi north of Vero Beach, Florida	131
22c	Summary sheet for 50 miles south of Vero Beach, Florida	132
23	Tropical cyclone parameters Vero Beach, Florida	134
24	Data used in this report for probability analyses	137
A.1	Time, flight pattern, and flight level of NOAA/RFC missions into Hurricane David, September 1979	162
A.2	Time, flight pattern, and flight level of NOAA/RFC missions into Hurricane Allen, August 1980	178
C.1	List of plotting position formulae	193
C.2	List of plotting position formulae in the descending order of their p_m's	194

HURRICANE CLIMATOLOGY FOR THE ATLANTIC AND GULF COASTS OF THE UNITED STATES

Francis P. Ho, James C. Su, Karen L. Hanevich,
Rebecca J. Smith and Frank Richards

Water Management Information Division
Office of Hydrology
National Weather Service
National Oceanic and Atmospheric Administration

ABSTRACT A climatology of hurricane factors important to storm-surge modeling is presented for the Atlantic and Gulf coasts of the United States. A smoothed frequency of hurricanes and tropical storms entering, exiting, and passing within 150 nmi of the coast during the period 1871-1984 is given. The central pressure and radius of maximum winds for hurricanes occurring during the 85-year period, 1900-84, were obtained from analysis of available hurricane data. Direction and speed of storm motion for hurricanes and tropical storms at the time they crossed the coast were also analyzed for the same 85-year period. The cumulative probability curves of each factor were plotted and analyzed for each 50-nmi interval along the coast. Selected probability levels of each distribution were summarized, and smoothed variations along the coast were obtained. Statistical independence of hurricane parameters has also been examined and interrelations of central pressure and radius of maximum winds investigated.

1. INTRODUCTION

1.1 Authorization

The National Flood Insurance Act of 1968, Title XIII, Public Law 90-448, enacted August 1, 1968, authorized and provides for a National Flood Insurance Program to insure residences and small businesses against hazard of damage or destruction by flood. The Federal Insurance Administration (FIA), a part of the Federal Emergency Management Agency (FEMA), is the executive agency for the National Flood Insurance Program. In July 1982, a Joint Technical Assistance Work Plan was signed between FEMA and the National Oceanic and Atmospheric Administration (NOAA). The plan, among other things, allows for the National Weather Service (NWS), NOAA, to provide technical support to FEMA upon request. Authorization for this particular study is Project No. 53967 under agreement No. EMW-84-E-1589 between the FIA, FEMA and the NWS, NOAA, dated March 15, 1984 and duly signed April 25, 1984.

1.2 Purpose

The Federal Insurance Administration, FEMA, requested the NWS, NOAA, to develop a comprehensive and authoritative set of hurricane climatological statistics for the Atlantic and Gulf Coasts of the United States. These statistics are prerequisites in tidal flood-frequency analyses which are essential to establish flood insurance criteria for a given community. Coastal tidal inundations on the Gulf and Atlantic coasts of the United States are primarily caused by hurricanes. Therefore, the characteristics of these storms are the beginning point in making tidal flood-frequency analyses. The present study is a climatological assessment of the central pressure, radius of maximum winds, and other characteristics of hurricanes along the U.S. Atlantic and Gulf coasts in a manner suitable for determining the frequency of storm surge levels. It includes only the atmospheric characteristics of hurricanes and does not include surge levels that are the subject of other reports.

The present study is an update and revision of an earlier study published as NOAA Technical Report NWS-15 (Ho et al 1975), which will hereafter be referred to as TR 15. TR 15 presented a climatology of hurricane parameters important to storm-surge modeling along the U.S. Gulf and Atlantic Coasts. This climatology was an analysis of available hurricane data, with storm tracks from 1871 through 1973, and also included data for other meteorological variables since 1900. TR 15 included the cumulative probability distributions of each hurricane factor analyzed at 50-nmi intervals along the coast, and smoothed variations of each factor at selected probability levels along the coast were presented. A smoothed frequency of tropical storms and hurricanes entering and exiting the coast as well as those storms passing within 150 nmi of the coast was also given in TR 15. The question of joint probability among the various factors was discussed qualitatively, but formal statistical tests were not considered in TR 15.

The National Research Council of the National Academy of Sciences (NAS) reported on an evaluation of the FEMA Model for estimating potential coastal flooding from hurricanes (National Academy of Sciences 1983). This NAS report concluded that the basic approach used by FEMA is sound and appropriate for estimating 100-yr flood elevations in communities where severe flooding is caused by hurricane storm surges. However, the Advisory Committee of the NAS made several recommendations regarding the way in which coastal flood studies are conducted. The committee recommended, among other things, that the selection of storm samples and the adoption of appropriate interdependency assumptions should be carried out in a centralized way by an organization with the necessary expertise in hurricane climatology. The committee concluded that interdependencies among storm parameters, particularly among storm intensity, size, and direction, should be determined by that organization on a regional basis and an appropriate method for handling these interdependencies when applying the probability procedure to coastal flood elevations should be developed.

1.3 Scope of Report

The geographical region covered by the report is the U.S. Gulf and Atlantic coasts from Texas to Maine (fig. 1). The first objective was to define, climatologically, the frequency of hurricanes and tropical storms influencing each coastal segment. This was done for three classes of storms -- those entering the coast from the sea (entering or landfalling), those having entered the coast and then proceeding from land to sea (exiting), and those moving parallel to the

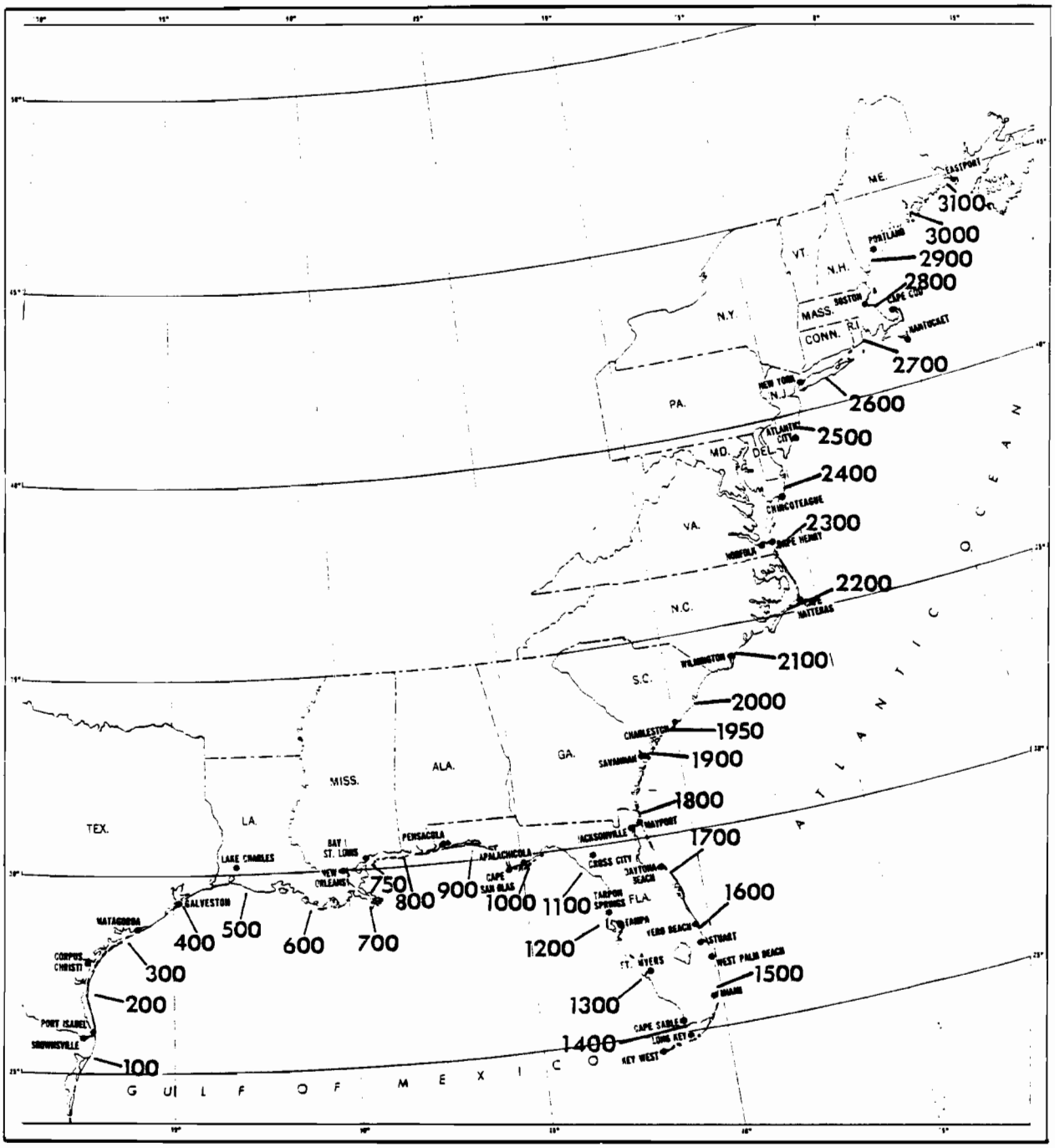

Figure 1.—Locator map with coastal distance intervals marked (nmi).

coast, with the center remaining at sea, but within 150 nmi of the point under consideration (alongshore or bypassing). These frequencies are presented in Chapter 6.

The second objective was to develop cumulative probability distributions for four hurricane parameters: (1) central pressure (P_o), an index of storm intensity, (2) the radius of maximum winds (R), an index of storm size, (3) forward speed of the storm (T), and (4) direction of storm motion (θ). Each of these factors influences the capability of the storm to produce storm tides. Chapter 2 discusses in detail the data sources and analyses from which the hurricane characteristics were obtained. Probability distributions and their along-coast variations for each parameter are presented in Chapters 7 through 9 of this report.

The statistical independence of hurricane parameters is considered in Chapter 3. The homogeneity of each parameter along the Gulf and Atlantic coasts was tested separately. Interrelations between pairs of parameters have been examined in Chapter 3. Non-linear relations between central pressure (P_o) and radius of maximum winds (R) are discussed both dynamically and statistically in Chapter 4. For this purpose, the data base for P_o and R was extended to include extreme hurricanes in the Caribbean and the Gulf of Mexico. Chapter 5 considers other conditional probability questions that are important to the currently used joint probability approach for tide-frequency analysis.

Chapter 10 examines changes in the wind and pressure fields due to the filling of hurricanes overland. Finally, Chapter 11 discusses application of the results of this study to flood insurance studies.

1.4 Relation to Flood Insurance Studies

Meteorological parameters P_o, R, θ and T can be used together with other conditions as input to storm-surge models. Other conditions include boundary conditions such as bathymetry, orientation of the coastline, etc. A storm-surge model can be used to compute the surge heights at the coast. The storm surge generated by a hurricane is the increase of the sea water surface elevation due to two physical processes. One process is the water surface elevation increase in the core region of a hurricane where the atmospheric pressure is extremely low. This is the so-called "inverse barometer effect." The other process is the convergence of the sea water, driven by the surface wind from the deeper ocean to the shallower coastal regions. This is related to surface wind stress and bathymetry. The atmospheric pressure gradient in a hurricane is the difference between the central pressure and a peripheral pressure. The surface wind stress in a hurricane is parameterized on the basis of the wind field near the water surface. Using appropriate meteorological assumptions, a wind field can be derived from knowledge of the pressure gradient, the radius of maximum wind speed, and the forward direction and speed of the hurricane.

The joint probability approach, as currently used in storm-surge frequency studies, assumes that each meteorological parameter used as input to the hydrodynamical model is independent. Development of storm-surge probabilities involves making computations for a range of meteorological parameters. The probability of occurrence of a given simulation is assumed to be the product of the probabilities represented by each input (meteorological) parameter. However, if the meteorological parameters are interrelated, a simple product of the individual probabilities is not appropriate. Hence, the need to evaluate the

possibility of interdependence among the factors that are the focus of this study. With this specific application in mind, there were a number of decisions made during the course of our analysis that ensured that the results would be tailored to the needs of the hydrodynamic modeling application. Some examples include the selection of the radius of maximum winds at the time of minimum pressure, and the assumption that the parameters represented steady-state storms. But these decisions also mean that the "climatology" described in this report **may not be appropriate for other more general meteorological applications.**

1.5 Previous Studies

One of the first systematic compilations of the characteristics of hurricanes affecting the United States coast was Tropical Cyclones (Cline 1926). Table 1 in Hydrometeorological Report No. 32 (Myers 1954) provided the first compilation of all hurricane central pressures and radii of maximum winds from 1900 to 1949. The National Hurricane Research Project Report No. 33 (Graham and Nunn 1959), hereafter referred to as NHRP 33, updated Myers' list and systematized the geographical distribution of the factors. Technical Paper No. 55 (Cry 1965) described all the hurricane tracks from 1871 to 1963, and cited the earlier works of this kind. HUR 7-97, Interim Report - Meteorological Characteristics of the Probable Maximum Hurricane, Atlantic and Gulf Coasts of the United States (Weather Bureau 1968) updated and revised the data in NHRP 33 and gave the geographical distribution of the characteristics of hypothetical hurricanes that had combinations of factors that made them the most severe hurricanes that can probably occur at a particular coastal location. NOAA Technical Report NWS 23 (Schwerdt, et al 1979) revised and updated the previous studies on meteorological criteria for engineering design hurricanes. Neumann et al. (1981) extended the period covered in Cry's hurricane tracks and prepared revised tracks where additional data indicated that they were necessary. This provided a firm climatological base describing tropical cyclones on the synoptic scale.

2. DATA

2.1 Introduction

Observations from hurricanes occurring near the United States Gulf and Atlantic coasts were used in this study to determine probability distributions of various parameters. Data presented in this chapter are used in later chapters of this report. If additional data were required for a specific purpose, it is discussed in the chapter where required.

The amount of observed data available from past hurricanes varies greatly and almost all of it required further analysis and interpretation before it could be of use for storm-surge computation. The amount of data available for any single storm also varies during different portions of the storm's life, from various geographic regions, and from different sections of the hurricane. These data are subject to numerous uncertainties in interpretation. We have attempted to bring this information together to make a comprehensive analysis, to develop accurate storm tracks from which speed and direction of storm motion are determined and to present an authoritative determination of central pressures and radius of maximum winds. Examples of detailed meteorological analyses are given in Appendix A.

Tables 1 through 3, for hurricanes during the years 1900-84, list most of the information used throughout this report. Parameter values in the tables are given for storms with P_o less than or equal to 982 mb (29.00 in.) occurring within 150 nmi of the Gulf and Atlantic coasts. The data are our update, revision and extension of Tables 1 and 2 in TR 15. There were a few changes made to the previously published data. In particular, to address the question of interdependence among parameters, available data were reviewed to ascertain their time of occurrence and to provide concurrent values of P_o and R where necessary.

Tables 1 through 3 give the date at which a hurricane entered, exited or came closest to the coast. The point along the coast where the hurricane parameters may be applied is indicated in the tables as the coastal reference point. The tables list parameters for the 85-yr period, 1900-84. The year 1900 was chosen to initiate estimation of the parameters by weighing the inaccuracies that would result from the sparse data of earlier years against the desirability of a longer period. Each of the P_o and R values listed in the tables is followed by a superscript letter or letters that refer to a legend at the end of the tables giving the source of the data value. The storm direction, measured from the north, denotes the track direction from which the hurricane crossed or bypassed the coast.

Tables 1 and 2 list a storm twice only if it crosses the coastline a second time (or if a bypassing storm makes another approach to the coast) after it has traveled a distance of 400 nmi (500 nmi along the Gulf Coast). An exception to this is Hurricane David: it was listed twice within 400 nmi, but only the second entry was included in the statistical computations discussed below. These duplicate storms are identified by a section mark (§) in the two tables. Hurricanes whose centers passed through the Florida Keys are listed in both the Gulf and Atlantic coast tables for the convenience of the user. The information on hurricanes which crossed the Florida Keys and eventually entered the west coast of Florida (within 500 nmi of its initial crossing), are listed separately in Table 3A.

If a hurricane crossed the coast on one side of the Florida peninsula, with a P_o less than or equal to 982 mb (29.00 in.) and weakened in intensity to P_o greater than 982 mb when it was more than 50 nmi from the opposite coast, it was listed for only the initial coastline it crossed (table 1 or 2). Those exiting storms, still of hurricane intensity at, or within 50 nmi of, the coast of exit, are included in Tables 1 and 2. Hurricanes which entered the Florida coasts and moved northward over land maintaining hurricane intensity within 50 nmi of the opposite coast are listed separately in Table 3B. They may be considered as bypassing hurricanes moving inland parallel to the coast.

2.2 Sources of Data

Original sources of hurricane data are barograph traces from land stations and ships, wind records from NWS and military stations, aircraft reconnaissance flight data, radar data, satellite data, miscellaneous pressure and wind reports and textual descriptions in the scientific literature. These descriptions have appeared in the Monthly Weather Review (published since June 1872), Climatological Data, National Summary (since 1950), National Hurricane Research Project Report No. 39 (Graham and Hudson 1960), NOAA Technical Memorandum NWS SR-56 (Sugg et al. 1971), the book Tropical Cyclones (Cline 1926), and a few other sources (e.g., data sources listed in append. A).

Table 1.--Hurricanes with central pressure < 982 mb (29.00 in.) ranked in chronological order from 1900-84. Gulf Coast United States

Date*	Approx.† coastal ref.	Storm dir.	P_o (mb)	P_o # (in.)	P_o value applied to	P_a (mb)	P_a was observed	R (nmi)	R was observed	T (kn)	Landfall point	Remarks
Sept. 9, 1900	378	130°	936.0	27.64[a']	coast	964.4	Galveston, TX	14[a]		10	29.1°N 95.1°W	
Aug. 15, 1901	773	195°	972.6	28.72[a']	coast	992.6	Mobile, AL	33[a]		14	30.4°N 88.8°W	
June 17, 1906	1398	185°	979.0	28.91[b']	24.7°N 81.0°W	997.6	Jupiter, FL	26[a]		10	25.1°N 81.0°W	
Sept. 27, 1906	779	160°	965.1	28.50[d']	coast	965.1	SS Winona	43[b]	Mobile, AL	16	30.4°N 88.7°W	SS Winona in eye of storm while anchored off Scranton, MS
Oct. 18, 1906	1405	270°	966.8	28.55[c']	coast	966.8	Navy tug near Dry Tortugas, FL	16[a]		16	24.9°N 81.0°W	
July 21, 1909	360	115°	958.7	28.31[b']	coast	982.1	Bay City, TX	19[a]		12	28.9°N 95.3°W	
Sept. 20, 1909	657	150°	965.1	28.50[b']	coast	989.8	New Orleans, LA	28[a]		11	29.1°N 90.2°W	
Oct. 11, 1909	1415 by	235°	957.0	28.26[c']	24.7°N 81.0°W	957.0	Knights Key, FL	22[b]	Key West, FL	10	-	
Oct. 17, 1910	-	200°	941.4	27.80[d']	24.4°N 82.7°W	941.4	SS Jean	28[a]		11	-	SS Jean in eye of storm at 24.4°N 82.7°W
Aug. 17, 1915	370	130°	948.5	28.01[a']	coast	952.9	Velasco, TX	29[b]	Houston, TX	11	29.0°N 95.2°W	
Sept. 29, 1915	671	170°	932.3	27.53[a']	27.0°N 89.3°W	935.0	HMS Hermione	26[ab]	New Orleans, LA and other stations	10	29.2°N 90.0°W	HMS Hermione experienced some eye effects at an unknown distance from the point of minimum pressure

See legend at end of Table 3

Table 1.--Hurricanes with central pressure < 982 mb (29.00 in.) ranked in chronological order from 1900-84. Gulf Coast United States (continued)

Date*	Approx.† coastal ref.	Storm dir.	P_o # (mb)	P_o # (in.)	P_o value applied to	P_a (mb)	P_a was observed	R (nmi)	R was observed	T (kn)	Landfall point	Remarks
July 5, 1916	805	160°	950.2	28.06[a']	coast	961.0	Fort Morgan, AL	26[a]		25	30.4°N 88.3°W	
Aug. 18, 1916	184	115°	948.2	28.00[c']	coast	948.2	Santa Gertrudis, TX	25[a]		11	26.8°N 97.4°W	
Oct. 18, 1916	842	220°	973.9	28.76[c']	coast	973.9	Pensacola, FL	19[b]	Pensacola, FL	21	30.3°N 87.5°W	
Sept. 29, 1917	886	230°	964.4	28.48[a']	coast	965.5	Pensacola, FL	33[b]	Pensacola, FL	13	30.4°N 86.7°W	
Sept. 10, 1919	-	110°	929.2	27.44[cd']	24.6°N 82.9°W	929.2	See remarks	15[a]		8	-	Lowest pressure obtained from mean of 2 ships (Lake Winona, Fred W. Weller) and Dry Tortugas, FL
$Sept. 14, 1919	207	105°	950.0	28.05[a']	coast	947.9	Port Aransas, TX	35[a]		20	27.2°N 97.3°W	
Sept. 21, 1920	630	155°	979.7	28.93[a']	coast	981.7	Houma, LA	28[a]		28	29.2°N 90.6°W	
June 22, 1921	309	175°	953.9	28.17[b']	coast	994.6	Houston, TX	17[a]		11	28.5°N 96.2°W	
Oct. 25, 1921	1201	235°	960.0	28.12[c']	coast	952.3	Tarpon Springs, FL	18[a]		10	27.9°N 82.8°W	
Oct. 20, 1924	-	220°	971.9	28.70[a']	24.6°N 82.9°W	-	See remarks	19[a]		8	-	Parameters obtained by interpolation between SS Toledo (off western end of Cuba) and Miami, FL and applied to the vicinity of Dry Tortugas, FL
Aug. 26, 1926	626	180°	958.7	28.31[ac']	coast	958.7	Houma, LA	27[a]		10	29.1°N 90.8°W	

See legend at end of Table 3

Table 1.—Hurricanes with central pressure < 982 mb (29.00 in.) ranked in chronological order from 1900-84. Gulf Coast United States (continued)

Date*	Approx.† coastal ref.	Storm dir.	P_o (mb)	P_o # (in.)	P_o value applied to	P_a (mb)	P_a was observed	R (nmi)	R was observed	T (kn)	Landfall point	Remarks
Sept. 18, 1926	1306 ex	125°	950.0	28.05[a']	26.4°N 81.9°W	950.0	Punta Rassa, FL	24[a]		17	-	
Sept. 20, 1926	842	140°	955.0	28.20[c']	coast	955.0	Perdido Beach, AL	17[b]	Pensacola, FL	7	30.3°N 87.5°W	
Oct. 21, 1926	1451 by	220°	931.9	27.52[a']	23.9°N 80.4°W	987.5	Key West, FL	21[a]		16	-	
June 28, 1929	296	130°	969.2	28.62[a']	coast	986.1	Port O'Connor, TX	13[a]		15	28.3°N 96.4°W	
Sept. 28, 1929	1445	100°	948.2	28.00[c']	coast	948.2	Key Largo, FL	28[a]		10	25.0°N 80.5°W	28.18 in. recorded at Long Key, FL
Aug. 14, 1932	378	135°	942.4	27.83[c']	coast	942.4	E. Columbia, TX	12[a]		15	29.1°N 95.1°W	SS Nicarao recorded lowest pressure of 27.82 in. near 29.0°N 94.8°W at 0130Z
Aug. 5, 1933	109	070°	975.3	28.80[a']	coast	981.4	Brownsville, TX	24[a]		10	25.5°N 97.2°W	
Sept. 5, 1933	135	090°	948.9	28.02[a']	coast	950.6	Brownsville, TX	20[b]	Brownsville, TX	8	26.0°N 97.2°W	
June 16, 1934	617	180°	965.8	28.52[a']	coast	967.8	Jeanette, LA	27[b]	Morgan City, LA	16	29.2°N 91.0°W	
Sept. 3, 1935	1425	130°	892.3	26.35[c']	coast	892.3	Long Key, FL	6[a]		9	24.8°N 80.8°W	
Nov. 5, 1935	1393 ex	065°	977.0	28.85[b']	25.2°N 81.1°W	972.9	Miami, FL	10[bcd]	Miami, FL	15	-	

See legend at end of Table 3

Table 1.—Hurricanes with central pressure < 982 mb (29.00 in.) ranked in chronological order from 1900-84. Gulf Coast United States (continued)

Date*	Approx.† coastal ref.	Storm dir.	P_o (mb)	P_o (in.)#	P_o value applied to	P_a (mb)	P_a was observed	R (nmi)	R was observed	T (kn)	Landfall point	Remarks
July 31, 1936	904	150°	963.8	28.46[ac']	coast	963.8	Ft. Walton, FL	19[ab]	Valparaiso, FL	9	30.4°N 86.4°W	
Aug. 8, 1940	462	140°	971.9	28.70[c']	coast	971.9	Sabine, TX	11[a]		8	29.7°N 93.7°W	
Sept. 23, 1941	348	180°	958.7	28.31[b']	coast	970.5	Houston, TX	21[a]		13	28.8°N 95.6°W	
Oct. 7, 1941	996	170°	981.4	28.98[a']	coast	982.1	Carrabelle, FL	18[ab]	Apalachicola, FL	11	29.8°N 84.7°W	
Aug. 30, 1942	309	135°	950.6	28.07[a']	coast	951.6	Seadrift, TX	18[a]		14	28.5°N 96.2°W	
July 27, 1943	419	110°	974.6	28.78[c']	coast	974.6	Ellington Field, TX	16[b]	Galveston, TX	8	29.5°N 94.6°W	
Oct. 18, 1944	-	195°	948.9	28.02[c']	24.6°N 82.8°W	948.9	Dry Tortugas, FL	29[a]		13	-	
Aug. 27, 1945	309	185°	967.5	28.57[c']	coast	967.5	Palacios, TX	18[a]		4	28.5°N 96.2°W	
Sept. 15, 1945	1465	130°	951.2	28.09[c']	coast	951.2	Homestead, FL	12[a]		10	25.3°N 80.3°W	Wind record at Miami, FL gives R = 24 at 2300Z-storm center was 22 nmi inland
Sept. 18, 1947	1312 ex	085°	960.0	28.35[a']	26.3°N 81.8°W	969.5	Captiva, FL	26[a]		7	-	Lowest pressure for the Gulf coast occurred some 50 nmi inland
§Sept. 19, 1947	716	115°	966.5	28.54[a']	coast	967.5	New Orleans WBO, LA	23[b]	New Orleans, LA	16	29.6°N 89.5°W	
Sept. 21, 1948	-	210°	935.3	27.62[a']	24.6°N 81.7°W	963.4	Boca Chica Airport, FL	7[a]		8	-	

See legend at end of Table 3

Table 1.—Hurricanes with central pressure < 982 mb (29.00 in.) ranked in chronological order from 1900-84. Gulf Coast United States (continued)

Date*	Approx.† coastal ref.	Storm dir.	P_o (mb)	P_o (in.)	P_o value applied to	P_a (mb)	P_a was observed	R (nmi)	R was observed	T (kn)	Landfall point	Remarks
Oct. 5, 1948	1410	230°	962.7	28.43[a']	24.8°N 81.0°W	975.3	Sombrero Key, FL	13[b]	Sombrero Key, FL	16	24.8°N 81.0°W	
Oct. 4, 1949	360	190°	963.4	28.45[a']	coast	978.0	5 mi SW of Freeport, TX	20[b]	Composite of many Texas stations	11	28.9°N 95.4°W	
Aug. 31, 1950 (Baker)	813	190°	979.3	28.92[c']	coast	979.3	Ft. Morgan, AL	21[a]		23	30.2°N 88.1°W	
Sept. 5, 1950 (Easy)	1162	230°	958.3	28.30[c']	coast	958.3	Cedar Key, FL	15[cd]		3	28.6°N 82.7°W	
Sept. 24, 1956 (Flossy)	904	250°	973.9	28.76[de']	coast	973.9	See remarks	18[b]	Pensacola, FL	10	30.4°N 86.4°W	Lowest pressure taken from the barometer of a dredge within the eye at Destin, FL and from a reconnaissance plane just off the coast at Pensacola, FL
June 27, 1957 (Audrey)	466	200°	946.5	27.95[a']	coast	958.4	Hackberry, LA	20[b]	Orange, LA	14	29.8°N 93.6°W	
Sept. 10, 1960 (Donna)	1422	140°	930.0	27.46[c']	24.8°N 80.9°W	930.0	Conch Key, FL	18[e]	Near Conch Key, FL	9	24.8°N 80.9°W	
Sept. 15, 1960 (Ethel)	747	175°	976.0	28.82[e']	26.6°N 89.3°W	979.0	Gulfport, MS	22[d]	Recon.	10	30.3°N 89.3°W	
Sept. 11, 1961 (Carla)	296	170°	930.9	27.49[e']	coast	930.9	Recon.	30[be]		6	28.3°N 96.4°W	

See legend at end of Table 3

Table 1.--Hurricanes with central pressure < 982 mb (29.00 in.) ranked in chronological order from 1900-84. Gulf Coast United States (continued)

Date*	Approx.† coastal ref.	Storm dir.	P_o (mb)	P_o (in.)#	P_o value applied to	P_a (mb)	P_a was observed	R (nmi)	R was observed	T (kn)	Landfall point	Remarks
Oct. 4, 1964 (Hilda)	579	175°	959.4	28.33[b']	coast	961.7	Franklin, LA	18[be]	Franklin, LA	7	29.5°N 91.5°W	
Oct. 14, 1964 (Isbell)	-	220°	964.1	28.47[e']	24.3°N 82.7°W	964.1	Recon.	10[e]	Near 24°N 83°W	15	25.8°N 81.3°W	
Sept. 8, 1965 (Betsy)	1445	090°	951.9	28.11[e']	coast	952.3	Tavernier, FL	22[be]	Plantation Key, FL	11	25.0°N 80.5°W	P_o = 947.9 mb observed by Recon. at 25.2°N 82.1°W
§Sept. 10, 1965 (Betsy)	664	135°	941.1	27.79[e']	28.2°N 89.2°W	941.1	Recon. at 27.9°N 88.8°W	32[be]	Port Sulphur, LA and Recon.	17	29.1°N 90.1°W	
June 8, 1966 (Alma)	-	200°	970.2	28.65[ce']	24.6°N 82.9°W	970.2	Dry Tortugas, FL	15[ce]	Dry Tortugas, FL Recon.	9	-	
Oct. 4, 1966 (Inez)	- by	065°	977.0	28.85[e']	24.1°N 84.1°W	977.0	Recon.	15[e]	Recon.	7	-	Lowest pressure 135 nmi WSW Key West, FL
Sept. 20, 1967 (Beulah)	123	155°	923.1	27.26[e']	24.8°N 96.3°W	923.1	Recon.	9[e]	Recon.	8	25.8°N 97.2°W	P_o = 939 mb at landfall
Oct. 19, 1968 (Gladys)	1162	235°	977.0	28.85[e']	coast	977.0	Recon.	17[e]	Recon.	10	28.6°N 82.7°W	
Aug. 18, 1969 (Camille)	747	160°	907.9	26.81[e']	28.2°N 88.8°W	907.9	Recon.	8[bc]	Near 28°N 89°W	16	30.3°N 89.3°W	
Aug. 3, 1970 (Celia)	243	115°	944.5	27.89[c']	coast	944.5	Ingleside, TX	9[b]	Corpus Christi, TX	14	27.7°N 97.1°W	
Sept. 12, 1970 (Ella)	11	100°	966.8	28.55[e']	coast	966.8	Recon.	21[e]	Recon.	7	23.9°N 97.7°W	

See legend at end of Table 3

Table 1.—Hurricanes with central pressure < 982 mb (29.00 in.) ranked in chronological order from 1900–84. Gulf Coast United States (continued)

Date*	Approx.† coastal ref.	Storm dir.	P_o (mb)	P_o # (in.)	P_o value applied to	P_a (mb)	P_a was observed	R (nmi)	R was observed	T (kn)	Landfall point	Remarks
Sept. 10, 1971 (Fern)	321	050°	979.0	28.91[e']	28.1°N 96.6°W	979.0	Recon.	12[e]	Recon.	5	28.6°N 96.0°W	Aircraft recon. observed lowest pressure just off TX coast south of Matagorda, TX
Sept. 16, 1971 (Edith)	500	230°	978.0	28.88[e']	coast	978.0	Recon.	15[e]	Recon.	15	29.7°N 93.0°W	
June 19, 1972 (Agnes)	966	195°	978.0	28.88[e']	29.3°N 85.8°W	978.0	Recon.	20[be]	Recon.	11	29.9°N 85.4°W	
Sept. 8, 1974 (Carmen)	575	155°	936.0	27.64[e']	28.0°N 90.7°W	936.0	Recon.	10[e]	Recon.	9	29.5°N 91.6°W	
Aug. 31, 1975 (Caroline)	30	110°	963.0	28.44[e']	coast	963.0	Recon.	15[e]	Recon.	5	24.3°N 97.7°W	
Sept. 23, 1975 (Eloise)	897	195°	955.0	28.20[c']	coast	955.0	Destin, FL	14[bc]	Hurlburt Field, FL and Valparaiso, FL	22	30.3°N 86.5°W	R > 30 nmi near 28°N 88°W
Sept. 2, 1977 (Anita)	15	060°	926.0	27.35[e']	24.2°N 97.1°W	926.0	Recon.	10[e]	Recon.	10	23.9°N 97.7°W	
Sept. 12, 1979 (Frederick)	806	160°	946.0	27.93[e']	coast	946.0	Recon.	33[e]	Recon.	11	30.4°N 88.3°W	
Aug. 10, 1980 (Allen)	151	155°	945.0	27.90[e']	coast	945.0	Recon.	40[e]	Recon.	8	26.2°N 97.2°W	
Aug. 18, 1983 (Alicia)	378	155°	962.0	28.40[e']	coast	962.0	Recon.	30[be]	Recon.	7	29.1°N 95.1°W	

See legend at end of Table 3

Table 2.--Hurricanes with central pressure < 982 mb (29.00 in.) ranked in chronological order from 1900-84. East Coast United States

Date*	Approx.† coastal ref.	Storm dir.	P_o (mb)	P_o # (in.)	P_o value applied to	P_a (mb)	P_a was observed	R (nmi)	R was observed	T (kn)	Landfall point	Remarks
Sept. 12, 1903	1510	120°	976.6	28.84[b']	coast	998.0	Tampa, FL	43[a]		8	26.1°N 80.1°W	
June 17, 1906	1584 ex	240°	979.0	28.91[b']	27.4°N 80.1°W	997.6	Jupiter, FL	26[a]		12	-	
Sept. 17, 1906	2018	105°	976.6	28.84[a']	coast	999.0	Columbia, SC	30[b]		16	33.3°N 79.2°W	
Oct. 18, 1906	1523 ex	220°	976.6	28.84[b']	26.4°N 80.1°W	990.9	Jupiter, FL	35[a]		6	-	
Oct. 11, 1909	1415 by	235°	957.0	28.26[c']	24.7°N 81.0°W	957.0	Knights Key, FL	22[b]	Key West, FL	10	-	
Aug. 28, 1911	1912	100°	979.3	28.92[b']	coast	982.7	Savannah, GA	27[b]	Savannah, GA	8	32.2°N 80.6°W	
Sept. 3, 1913	2177	115°	975.6	28.81[b']	coast	994.2	Raleigh, NC	38[ab]	Hatteras, NC	16	34.8°N 76.4°W	
Sept. 10, 1919	-	110°	929.2	27.44[cd']	24.6°N 82.9°W	929.2	See remarks	15[s]		8	-	Lowest pressure obtained from mean of 2 ships (Lake Winona, Fred W. Weller) and Dry Tortugas, FL
Oct. 26, 1921	1665 ex	260°	979.0	28.91[a']	28.6°N 81.8°W	960.0	Tarpon Spring FL, Gulf Coast	MSG		10	-	Lowest pressure for the East coast occurred as the storm was filling about 50 nmi inland from the coast
Aug. 26, 1924	2214 by	210°	971.9	28.70[a']	35.0°N 75.0°W	975.3	Hatteras, NC	34[b]	Hatteras, NC	22	-	

See legend at end of Table 3

Table 2.--Hurricanes with central pressure < 982 mb (29.00 in.) ranked in chronological order from 1900-84. East Coast United States (continued)

Date*	Approx.† coastal ref.	Storm dir.	P_o (mb)	P_o (in.)#	P_o value applied to	P_a (mb)	P_a was observed	R (nmi)	R was observed	T (kn)	Landfall point	Remarks
§Aug. 26, 1924	2732 by	220°	960.4	28.36[a']	41.1°N 69.8°W	972.2	Nantucket, MA	40[b]	Nantucket, MA Block Island, RI	24	-	Storm becoming extra-tropical
Dec. 2, 1925	2185	220°	980.4	28.95[a']	coast	987.8	Wilmington, NC	54[b]	Wilmington, NC	14	34.9°N 76.3°W	WB Technical Paper No. 55 implies that this storm was becoming extratropical and did not have hurricane-force winds when it struck the NC coast
July 28, 1926	1754	150°	959.7	28.34[a']	coast	975.3	Meritt Island FL	14[b]	Jacksonville, FL	8	29.9°N 81.3°W	
Sept. 18, 1926	1478	110°	931.0	27.49[a']	coast	935.0	Miami, FL	19[b]	Miami, FL	17	25.6°N 80.3°W	
Oct. 21, 1926	1451 by	220°	931.9	27.52[a']	23.9°N 80.5°W	987.5	Key West, FL	21[a]		16	-	
Sept. 17, 1928	1542	120°	935.3	27.62[c']	coast	935.3	W. Palm Beach, Everglades Drainage Dist. Office, FL	28[a]		13	26.7°N 80.0°W	
Sept. 28, 1929	1449	100°	948.2	28.00[c']	coast	948.2	Key Largo, FL	28[a]		10	25.0°N 80.5°W	
Aug. 23, 1933	2272	145°	966.5	28.54[bc']	coast	970.5	Cape Henry, VA	39[b]	Norfolk, Cape Henry, VA	18	36.4°N 75.8°W	
Sept. 4, 1933	1557	120°	947.5	27.98[c']	coast	947.5	Jupiter, FL	13[a]		11	26.9°N 80.1°W	
Sept. 16, 1933	2201	220°	956.7	28.25[c']	coast	956.7	Hatteras, NC	40[b]	Hatteras, NC	9	35.1°N 76.0°W	

See legend at end of Table 3

Table 2.--Hurricanes with central pressure < 982 mb (29.00 in.) ranked in chronological order from 1900-84. East Coast United States (continued)

Date*	Approx.† coastal ref.	Storm dir.	P_o (mb)	P_o (in.)#	P_o value applied to	P_a (mb)	P_a was observed	R (nmi)	R was observed	T (kn)	Landfall point	Remarks
Sept. 3, 1935	1425	130°	892.3	26.35[c']	coast	892.3	Long Key, FL	6[a]		9	24.8°N 80.8°W	
Nov. 4, 1935	1491	060°	972.9	28.73[c']	coast	972.9	Miami, FL	10[bc]	Miami, FL	12	25.9°N 80.1°W	
Sept. 18, 1936	2251 by	180°	965.8	28.52[d']	34.8°N 75.2°W	965.8	See remarks	34[a]		16	-	Lowest pressure is mean of 2 ships (El Occidente and Limon) off Cape Hatteras, NC
Sept. 21, 1938	2625	180°	943.0	27.85[a']	coast	946.2	Bellport, NY Coast Guard Sta.	45[b]	New Haven, CT	47	40.7°N 72.9°W	Storm becoming extra-tropical
Aug. 11, 1940	1902	100°	974.6	28.78[c']	coast	974.6	Savannah, GA	27[b]	Savannah, GA	9	32.1°N 80.8°W	
Sept. 14, 1944	2226 by	195°	944.1	27.88[a']	35.2°N 75.4°W	947.2	Hatteras, NC	17[b]	Hatteras, NC	23	-	
§Sept. 15, 1944	2649	220°	955.3	28.21[b']	coast	958.7	Pt. Judith, RI	29[b]	Fisher Island Pt. Judith, RI	30	40.9°N 72.3°W	Storm becoming extratropical
Sept. 15, 1945	1465	130°	951.2	28.09[c']	coast	951.2	Homestead, FL	12[a]		10	25.3°N 80.3°W	Wind record at Miami, FL gives R = 24 at 2300Z; storm center was 22 nmi inland
Sept. 17, 1947	1517	080°	946.8	27.96[a']	coast	947.2	Hillsboro, FL	26[ab]	Pineapple Plantation, FL	10	26.3°N 80.1°W	
Oct. 15, 1947	1890	080°	968.2	28.59[a']	coast	973.9	Savannah, GA	13[a]		17	31.9°N 81.1°W	
Sept. 22, 1948	1571 ex	230°	963.4	28.45[a']	27.2°N 80.2°W	964.8	St. Lucie Lock, FL	16[a]		11	-	

See legend at end of Table 3

Table 2.--Hurricanes with central pressure < 982 mb (29.00 in.) ranked in chronological order from 1900-84. East Coast United States (continued)

Date*	Approx.† coastal ref.	Storm dir.	P_o (mb)	P_o # (in.)	P_o value applied to	P_a (mb)	P_a was observed	R (nmi)	R was observed	T (kn)	Landfall point	Remarks
Oct. 6, 1948	1491 ex	230°	977.0	28.85[a']	25.9°N 80.1°W	979.3	Miami, FL	16[b]	Miami, FL	13	-	
Aug. 24, 1949	2214 by	220°	977.3	28.86[d']	35.1°N 75.2°W	977.3	Diamond Shoals Lightship, NC	24[a]		22	-	
Aug. 27, 1949	1557	130°	953.6	28.16[a']	coast	954.0	W. Palm Beach, FL	23[b]	W. Palm Beach, FL	14	26.9°N 80.0°W	
Oct. 18, 1950 (King)	1507	150°	955.0	28.20[c']	coast	955.0	Miami, FL	6[cd]	Miami, FL	6	26.1°N 80.1°W	
Aug. 30, 1954 (Carol)	2201 by	210°	960.0	28.35[e']	33.4°N 76.8°W	960.0	Recon.	23[b]	Ship data	10	-	
§Aug. 31, 1954 (Carol)	2646	200°	961.1	28.38[a']	coast	962.4	Suffolk Co. AFB, NY	22[b]	Suffolk Co. AFB, NY	33	40.9°N 72.4°W	
Sept. 10, 1954 (Edna)	2212 by	210	943.1	27.85[e']	34.0°N 75.6°W	943.1	Recon.	MSG		20	-	
§Sept. 11, 1954 (Edna)	2750	210°	947.2	27.97[e']	39.7°N 71.3°W	947.2	Recon.	20[e]	Recon.	40	41.7°N 70.1°W	
Oct. 15, 1954 (Hazel)	2057	190°	936.7	27.66[a']	coast	938.0	Tilgham Point, NC, by fishing boat Judy Ninda	25[b]	Myrtle Beach, SC	26	33.9°N 78.5°W	
Aug. 12, 1955 (Connie)	2187	180°	961.7	28.40[c']	coast	961.7	Fort Macon, NC	38[ab]	Cherry Point, NC (MCAS)	7	34.9°N 76.2°W	
Sept. 19, 1955 (Ione)	2162	175°	960.0	28.35[c']	coast	960.0	Morehead City, NC	22[b]	Cherry Point, NC (MCAS)	9	34.7°N 76.7°W	

See legend at end of Table 3

Table 2.--Hurricanes with central pressure < 982 mb (29.00 in.) ranked in chronological order from 1900-84. East Coast United States (continued)

Date*	Approx.† coastal ref.	Storm dir.	P_o (mb)	P_o (in.)#	P_o value applied to	P_a (mb)	P_a was observed	R (nmi)	R was observed	T (kn)	Landfall point	Remarks
Aug. 28, 1958 (Daisy)	2214 by	195°	949.0	28.03[e']	35.0°N 74.3°W	949.0	Recon.	18[e]	Near 35°N, 74°W	17	-	
§Aug. 29, 1958 (Daisy)	2750 by	240°	979.0	28.91[e']	40.9°N 68.5°W	979.0	Recon.	50[e]	40.9°N 68.5°W	21	-	
Sept. 27, 1958 (Helene)	2164 by	240°	932.0	27.52[e']	32.7°N 78.7°W	932.0	Recon.	25[e]	Recon.	14	-	
Sept. 29. 1959 (Gracie)	1935	150°	950.9	28.08[e']	coast	950.9	Recon.	26[b]	Beaufort, SC (MCAS)	12	32.5°N 80.4°W	
Sept. 10, 1960 (Donna)	1422	170°	930.0	27.46[c']	24.8°N 80.9°W	930.0	Conch Key, FL	18[e]	Near Conch Key, FL	9	24.8°N 80.9°W	
Sept. 11, 1960 (Donna)	1722 ex	210°	970.0	28.65[c']	coast	970.4	Orlando, FL	24[c]	Datona Beach, FL	16	29.5N 81.1°W	
§Sept 12, 1960 (Donna)	2122	215°	958.0	28.29[e']	coast	958.0	34.6°N 77.7°W	26[b]	Cherry Point, NC (MCAS)	26	34.4°N 77.6°W	
§Sept. 12, 1960 (Donna)	2612	205°	959.0	28.38[b']	coast	961.1	Brookhaven, NY	48[b]	Suffolk Co., NY AFB	32	40.6°N 73.2°W	Storm becoming extra-tropical
Sept. 20, 1961 (Esther)	2220 by	180°	948.0	27.99[e']	35.1°N 73.3°W	948.0	Recon.	MSG		14	-	
Aug. 27, 1964 (Cleo)	1482	160°	967.5	28.57[c']	coast	967.5	N. Miami, FL	7[be]	Miami, FL	9	25.7N 80.2°W	
Sept. 10, 1964 (Dora)	1756	100°	961.0	28.38[a']	29.8°N 80.4°W	965.8	St. Augustine, FL	34[e]	Recon.	7	29.9°N 81.3°W	
Oct. 15, 1964 (Isbell)	1557 ex	225°	977.7	28.87[c']	26.9°N 80.0°W	977.7	Juno Bch., FL	13[b]	W. Palm Bch., FL	17	-	

See legend at end of Table 3

Table 2.--Hurricanes with central pressure < 982 mb (29.00 in.) ranked in chronological order from 1900-84. East Coast United States (continued)

Date*	Approx.† coastal ref.	Storm dir.	P_o (mb)	P_o # (in.)	P_o value applied to	P_a (mb)	P_a was observed	R (nmi)	R was observed	T (kn)	Landfall point	Remarks
Sept. 8, 1965 (Betsy)	1445	090°	951.9	28.11[a']	coast	952.3	Tavernier, FL	22[be]	Plantation Key, FL	11	25.0°N 80.6°W	
Sept. 16, 1967 (Doria)	2278	020°	981.0	28.97[e']	38.0°N 71.9°W	981.0	Recon.	20[e]	Near 38°N 74°W	9	36.5°N 75.4°W	Lowest pressure 150 nmi east of Delmarva Peninsula
Sept. 10, 1969 (Gerda)	3080	195°	979.0	28.91[a']	42.1°N 68.7°W	979.0	Recon.	MSG		40	44.6°N 67.3°W	
Aug. 9, 1976 (Belle)	2214 by	190°	963.1	28.44[e']	32.5°N 75.2°W	963.1	Recon.	25[e]	Recon.	21	-	
§Aug. 10, 1976 (Belle)	2582	195°	975.0	28.79[e']	40.4°N 73.0°W	975.0	Recon.	31[e]	Recon.	21	40.6°N 73.5°W	P_o at landfall was 982 mb
Sept. 3, 1979 (David)	1567	135°	968.0	28.59[b']	coast	971.0	Melbourne, FL	27[bc]	West Palm Beach, FL	12	27.1°N 80.1°W	
§Sept 4, 1979 (David)	1857	160°	968.0	28.59[be']	coast	970.0	Savannah, GA	10[be]	Recon. and Savannah, GA	10	31.6°N 81.2°W	
Sept. 11, 1984 (Diana)	2081 by	210°	949.0	28.02[e']	33.8°N 77.7°W	949.0	Recon.	11[e]	Recon.	7	-	
§Sept. 13, 1984 (Diana)	2081	100°	972.0	28.70[e']	33.8°N 77.4°W	972.0	Recon.	16[e]	Recon.	5	33.9°N 78.0°W	

See legend at end of Table 3

Table 3.--Miscellaneous Florida Hurricanes with central pressure < 982 mb (29.00 in.) ranked in chronological order from 1900-1984
A. Hurricanes striking the West Coast of Florida after passing the Florida Keys

Date*	Approx.† coastal ref.	Storm dir.	P_o (mb)	P_o # (in.)	P_o value applied to	P_a (mb)	P_a was observed	R (nmi)	R was observed	T (kn)	Landfall point	Remarks
Oct. 18, 1910	1330	200°	953.3	28.15[a']	coast	980.0	Tampa, FL	32[a]		11	26.0°N 81.7°W	
Oct. 21, 1924	1338	240°	978.3	28.89[b']	coast	985.4	Miami, FL	21[a]		6	25.9°N 81.7°W	
Sept. 30, 1929	966	160°	975.3	28.80[c']	coast	975.3	Panama City, FL	MSG		6	29.9°N 85.4°W	Storm becoming extratropical
Sept. 4, 1935	1060	190°	960.0	28.35[b']	coast	980.0	Egmont Key, FL	21[a]		10	29.9°N 83.7°W	
Oct. 19, 1944	1262	190°	962.0	28.42[c']	coast	962.0	Sarasota, FL	34[a]		14	27.0°N 82.4°W	
Sept. 22, 1948	1337	225°	950.9	28.08[b']	coast	962.8	Belleglade, FL	16[ab]	Clewistown, FL	8	25.9°N 81.7°W	
Sept. 10, 1960 (Donna)	1301	170°	949.2	28.03[e']	coast	950.0	Naples, FL	11[be]	Fort Myers, FL	9	26.5°N 81.9°W	
Oct. 14, 1964 (Isbell)	1350	230°	970.0	28.64[e']	coast	973.6	Everglade City, FL	10[e]	Recon.	14	25.8°N 81.4°W	
June 9, 1966 (Alma)	1026	225°	977.0	28.85[e']	coast	977.0	Recon.	20[e]	Recon.	13	30.1°N 84.2°W	

See legend at end of Table 3

Table 3.—Miscellaneous Florida Hurricanes with central pressure < 982 mb (29.00 in.) ranked in chronological order from 1900-1984 (continued)
B. Hurricanes Over the Florida Peninsula with Central Pressure Measured 50 nmi Inland From Coast

Date*	Approx.† coastal ref.	Storm dir.	P_o (mb)	P_o (in.)#	P_o value applied to	P_a (mb)	P_a was observed	R (nmi)	R was observed	T (kn)	Landfall point	Remarks
Sept. 17, 1928	- by	120°	958.3	28.30[a']	50 nmi inland from coast	935.3 East coast	West Palm Beach, FL	MSG		12	-	Lowest pressure occurred 9 nmi W of Avon Park, FL, or about 50 nmi ESE of Tampa Bay, FL
Sept. 4, 1933	- by	120°	964.4	28.48[a']	50 nmi inland from coast	947.5 East coast	Jupiter, FL	29[b]	Tampa, FL	11	-	Lowest pressure for the Gulf coast occurred as the storm was filling just W of Avon Park, FL, or 50 nmi E-SE of Tampa Bay, FL
Aug. 27, 1949	- by	130°	960.7	28.37[a']	50 nmi inland from coast	954.0 East coast	West Palm Beach, FL	23[b]	West Palm Beach, FL	14	-	Lowest pressure occurred 10 nmi ESE of Lake Placid, FL, or 50 nmi NE of Charlotte Harbor (Gulf of Mexico)
Oct. 18, 1950 (King)	- by	150°	978.0	28.88[a']	50 nmi inland from coast	955.0 East coast	Miami, FL	MSG		17	-	Lowest pressure occurred 12 nmi ESE of Haines City, FL, or 50 nmi ENE of Tampa Bay, FL

See legend at end of Table 3

General Legend

P_a - lowest pressure detected by barometer or dropsonde

P_o - minimum central pressure (for either the Atlantic or Gulf Coast)

R - radius of maximum winds

T - forward speed of storm

by - bypassing storm

ex - exiting storm

MSG - missing

Recon. - aircraft reconnaissance

Legend

Source of Radius of Maximum Winds Data

a - computed from pressure profile

b - observed from wind speed record

c - extracted from Monthly Weather Review

d - approximation (about 5 or 6 nmi added to eye radius as observed by aircraft or radar)

e - aircraft reconnaissance wind data

Legend

Source of Minimum Central Pressure Data

a' - computed from pressure profile along or near coast

b' - computed from pressure profile and adjusted to the coast

c' - observed by land barometer

d' - observed by ship barometer

e' - observed by reconnaissance plane dropsonde

* Date applied to approximate coastal reference point in GMT

† Point at which storm entered, exited, or came closest to the coast (see fig. 1); not given to hurricanes passing the Florida Keys west of 81°W

\# Lower central pressures at distances greater than 150 nmi from the coast were not considered

§ Same hurricane as previous line

Tropical cyclone track information was used to determine the frequency of entering, exiting, and alongshore tropical storms and hurricanes, direction of forward motion and in some cases speed of motion. Smoothed best tracks have been given in several NOAA publications and periodicals previously cited. Cry (1965) combined data from available sources into a comprehensive report showing the most accurate and consistent locations of all tropical cyclones for the period 1871-1963. These tracks were designed to provide a smoothed track for all storms. Neumann et al. (1981) have extended the period covered and prepared revised tracks where additional data have indicated they were necessary. In addition, Jarvinen et al. (1984) have prepared a computer file of North Atlantic tropical cyclones (commonly referred to as the HURDAT tape). This file contains dates, tracks, windspeeds, and central pressure values (if available) for all tropical cyclones that occurred during the period 1886-1983. This file is maintained by the National Hurricane Center (NHC), NOAA, in Miami, Florida and is updated annually. This data file contains storm positions and wind speed information at 6-hourly intervals. They are subject to some degree of uncertainty, especially for the earlier years. It should be noted that linear interpolation of the data within 6-hourly intervals could lead to inaccurate instaneous storm track and wind speed information.

2.3 Hurricane Central Pressure (P_o) Data

The most important factor in storm surge modeling is the intensity of the hurricane, which is directly related to its central pressure. Harris (1959) demonstrated that storm surge height is approximately proportional to the central pressure depression, other factors being constant.

The specific pressure values in Tables 1 through 3 are the lowest pressures, generally determined from actual observations by either a barometer or dropsonde. For hurricanes of recent years, minimum pressure observed in penetrations of the hurricane eye by reconnaissance aircraft near the coast provided the central pressure in most cases. For earlier hurricanes, P_o values were estimated from observations taken at land stations. Observed pressures, P_a, were extrapolated inward to P_o (since P_a were rarely observed at the storm center) by using visually-fitted radial pressure profiles based on the formula (Schloemer 1954):

$$\frac{P - P_o}{P_n - P_o} = \exp(-R/r) \qquad (1)$$

where P is the pressure at radius r, P_o is the pressure at the storm center, P_n is the pressure at some large distance from the center at which the profile is asymptotic, and R is the radius at which the windspeed is greatest.

Schwerdt et al. (1979) computed pressure profiles for 19 past hurricanes using equation (1) and nine other pressure profile formulas and compared the results with observed data at radial distances of 40 and 80 nmi. They concluded that equation (1) gives a reasonably representative sea-level hurricane pressure profile. They also concluded that further refinements would not improve the reliability of the formula at this time because of the rather large scatter of pressure data around most hurricane profiles.

2.3.1 Central Pressure Criteria Based on Balanced Wind Model

Tables 1 through 3 also list the lowest pressure observed at a station (P_a), the observing station and a geographical reference to which P_o pertains (either at the coast or as far as 150 nmi offshore). The criterion used to select storm data for inclusion in Tables 1 through 3 ($P_o \leq 982$ mb) was based on consideration of the windspeed computed from a balanced wind model (after Myers 1954):

$$V_c^2 = \frac{1}{\rho}(P_n - P_o)\left(\frac{R}{r}\right)\exp(-R/r) \qquad (2)$$

where,

V_c = cyclostrophic windspeed, at which the centrifugal force exactly balances the horizontal pressure gradient force at radius, r,

ρ = density of air,

P_n = asymptotic pressure (same as defined in eq. 1),

P_o = central pressure, and

R = radius of maximum winds.

At the radius of maximum winds (R=r), with a central pressure of 982 mb (29.00 in.) and an asymptotic pressure of 1015.9 mb (30.00 in.), the cyclostrophic windspeed is 73 mph, or about the windspeed required for classification as a hurricane. The asymptotic pressure used by Myers is different from the peripheral pressure suggested in Chapter 11. Both pressures are intended to be representative of the environment removed from the dynamics of the tropical cyclone; Myers' pressure is that value to which an exponential pressure profile defined by equation 1 is asymptotic. It is a parameter for defining the intensity of the pressure gradient and does not actually have a physical counterpart in the pressure field. The peripheral pressure used in this report is the surface pressure at the outer limit of a hurricane where the cyclonic circulation ends and, therefore, has a physical meaning. The 982-mb criterion was used to put a specific bound on the data sample. We realize that there have been storms with hurricane-force winds and central pressures higher than 982 mb south of 35°N. It is not intended to be used as a forecasting criterion to distinguish hurricanes from tropical storms.

2.3.2 Central Pressure Adjustments

In some areas, barometric pressures could not be obtained near the coast. The central pressures were determined at the location nearest the coast where reliable observations could be obtained and adjusted downward to a coastal value. This was done for those central pressures for which the lowest observed pressure was from a station inland or at a coastal station when the storm was emerging from land to sea. These adjustments were made for 13 hurricanes and were carried over from TR 15 and earlier reports, including NHRP 33. Recomputations using filling rates given in Chapter 10 did not show significant differences; P_o values for 3 of 13 hurricanes were revised.

Questions have been raised about the minimum central pressure of Hurricane Camille which struck the northern Gulf coast in 1969. The best obtainable value is needed because Camille had the lowest central pressure on the mainland coast since record keeping began during the later part of the last century, and strongly influences the lower end of the probability distribution of central pressure. A minimum pressure of 905 mb was measured by an Air Force reconnaissance aircraft at 0016 GMT on August 17, 1969 near 25.2°N, 87.2°W, or 250 mi southeast of the mouth of the Mississippi River. Eighteen hours later, and only a few hours before the center made landfall, another reconnaissance aircraft penetrated the hurricane, and reported an even lower central pressure of 901 mb. A post-audit of the dropsonde computation at the National Climatic Center adjusted this to 908 mb. This value, which is quoted by Bradbury (1971), is the value in Table 1. The eye passed over Bay St. Louis, Mississippi, at landfall and an aneroid barometer a few blocks from the west end of the Bay St. Louis-Pass Christian bridge read 26.85 in. (909.4 mb). This barometer was later checked and found to be accurate by the New Orleans NWS Office (DeAngelis and Nelson 1969). One may assume then that Camille remained in a near steady state during its last 25 hours at sea.

2.3.3 Revised Central Pressure from Previous Studies

A virtual absence of pressure data made it necessary to omit the Louisiana hurricane of August 6, 1918, in which the closest recorded pressure was some 90 nmi from the path of the storm center. An estimate of P_o from such a distance would be highly questionable. Two hurricanes listed in NHRP 33 are not included in Tables 1 through 3. Upon reanalysis of the data, it was decided that both had weakened to tropical storm strength before they reached a point 50 nmi from where they exited the Florida coast. They are the storms of September 11, 1903 (Gulf coast) and October 20, 1924 (Atlantic coast).

On the basis of additional data discovered since the 1975 study, we revised the central pressure for several hurricanes. The most significant change involved the storm of September 20, 1909. The revision was based on a reconsideration of records available from the Weather Service Forecast Office in New Orleans. A few other changes of central pressures were made in hurricanes whose radius of maximum winds were revised. A recomputation using the pressure profile formula with the revised R values dictated these revisions. The dates of these hurricanes, and their previous and revised central pressure values are listed in Table 4.

2.4 Hurricane Radius of Maximum Winds (R) Data

Values of R for hurricanes were derived from various sources for the Gulf and Atlantic coasts of the United States. In TR 15 the values of R were for arbitrary locations and times. In this study, we reviewed all available data and determined concurrent values of P_o and R. The R values listed in Tables 1 through 3 are derived near the location and time where P_o applies. With aerial reconnaissance data, the R values are obtained from wind data recorded during the same traverse of the storm center in which the minimum P_o was observed. In a few cases, R could not be obtained by any reliable method. Storms with R's in this category are represented in Tables 1 through 3 by the abbreviation MSG (missing).

Table 4.--Hurricanes with revised central pressure

Date	Gulf Previous P_o (mb)	Gulf Revised P_o (mb)	Date	Atlantic Previous P_o (mb)	Atlantic Revised P_o (mb)
Oct. 18, 1906	976.6	966.8	Sept. 17, 1906	981.4	976.6
Sept. 20, 1909	980.0	965.1	Sept. 18, 1926	934.3	931.0
July 5, 1916	961.1	950.2	Aug. 23, 1933	969.5	966.5
Nov. 5, 1935	972.9	977.0	Sept. 21, 1938	939.7	943.0
Oct. 5, 1948	977.0	962.7	Sept. 15, 1944	958.7	955.3
Sept. 10, 1960 (Donna)	933.0	930.0	Sept. 17, 1947	940.1	946.8
Sept. 15, 1960 (Ethel)	972.0	976.0	Aug. 28, 1958 (Daisy)	957.0	949.0
			Sept. 12, 1960 (Donna)	961.1	959.0
			Sept. 10, 1964 (Dora)	965.8	961.0

2.4.1 Source of Radius of Maximum Winds

The values of R in the tables were developed from several sources: 1) windspeed records from aerial reconnaissance (for hurricanes since 1947), 2) windspeed records from land stations, whenever applicable, 3) approximations of eye radii deduced from airborne or land-based radar, 4) computations from an estimate of the pressure profile, or 5) on the basis of narrative or tabular data in the Monthly Weather Review.

2.4.1.1 Radius of Maximum Winds from Aerial Reconnaissance. Maximum flight-level winds and estimated maximum surface winds are usually included in flight reports from reconnaissance aircraft. Flight-level winds, recorded at one-second intervals by NOAA research aircraft flown into hurricanes have also been available since 1953. Recorded flight-level winds were processed and 10-second averages are stored on microfilm for data prior to 1973 and on magnetic tapes for recent years. Wind and pressure data on microfilm were tabulated, plotted, and analyzed for hurricanes affecting the U.S. coasts. From magnetic tape records since 1973, composite maps of flight-level winds relative to the storm center at given intervals and winds at various radial distances from the storm center recorded in a traverse through the eye were plotted by computer and made available to us by the Hurricane Research Division (HRD) of the Atlantic Oceanographic and Meteorological Laboratory (AOML) of NOAA. Analyses of these maps yielded another measure of the radius of maximum winds. Examples of these analyses are given in Appendix A.

It is generally accepted that, above the boundary layer, there is little vertical shear in a hurricane windfield in the lower troposphere (below about 600 mb). Miller (1958) developed a 3-dimensional description of the windfield in a tropical cyclone. Shea and Gray (1972) found that only the weaker storms exhibit a tendency for a slope of the radius of maximum winds with height; more intense storms do not. Willoughby et al. (1982) analyzed multi-level (1,500, 5,000 and 10,000 ft) flight data in Hurricane Allen (1980) and showed that

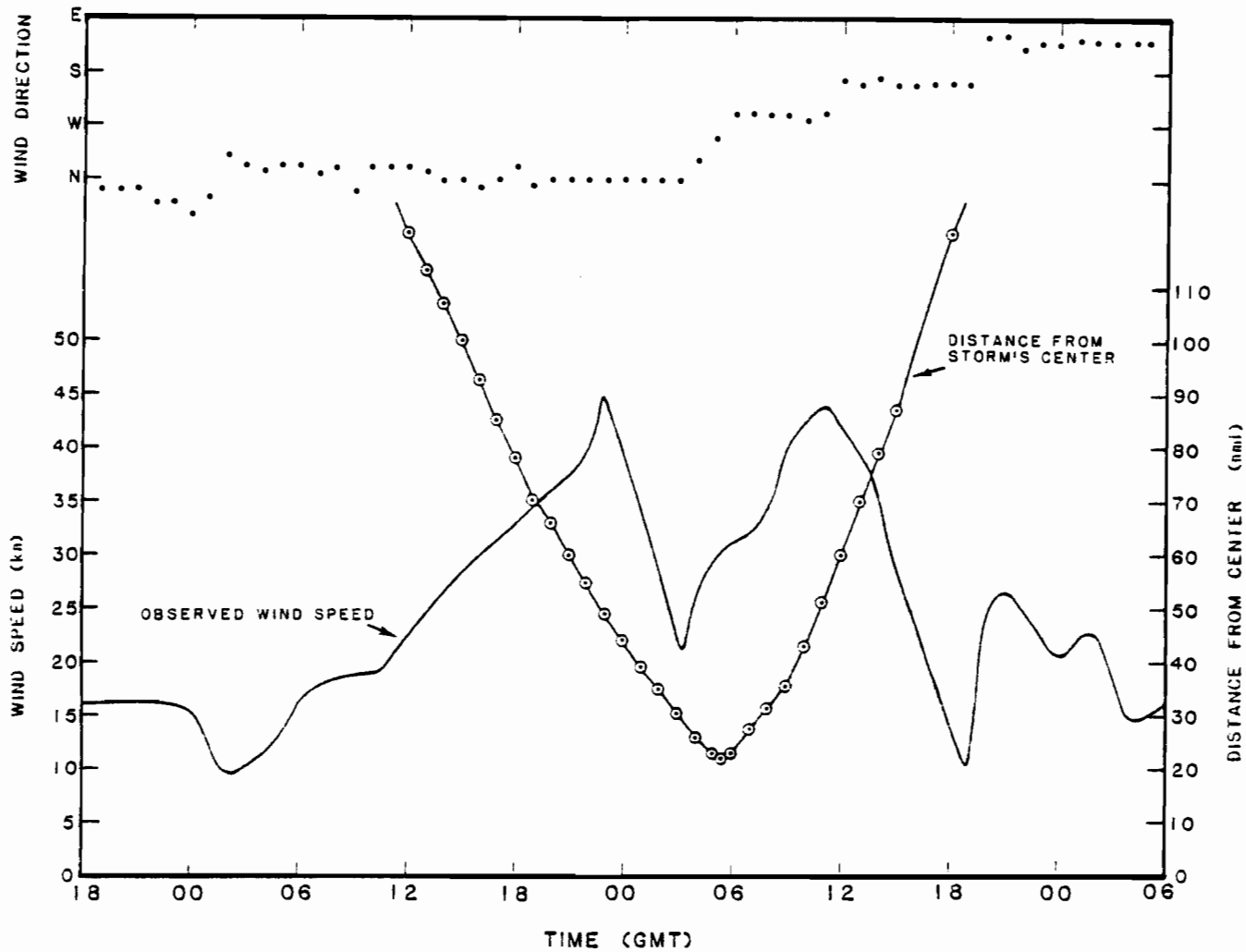

Figure 2.—Hourly observations of wind speed and direction, and distance of Allen's center from Brownsville, Texas for period 1800 GMT on August 8 through 0600 GMT on August 11, 1980.

the magnitudes of the maximum winds at different flight levels were generally quite similar. We concluded that flight-level wind data recorded at altitudes below the 600-mb level can be used to determine the surface value of R in hurricanes of moderate or greater than average intensity. Examples of this method of obtaining R are given in the data analysis in Appendix A.

2.4.1.2 Radius of Maximum Winds from Wind Records. Observed maximum winds are determined by noting the time when a wind-reporting station experienced the highest windspeed prior to the wind slackening in the hurricane's eye. From a knowledge of the location of the storm center at that time, one can deduce a value of R. Similar results can be obtained from various types of wind recorders. The windspeeds read off anemometer records were plotted on a time scale and a smooth curve drawn. A curve of distance from the storm center, as measured from the best track, was constructed on the same time scale. The two curves are shown for Hurricane Allen (1980) in Figure 2. The two peaks in the wind graph indicated that the storm's track took the center closer to the station than the radius of maximum winds. The 'observed' radius of maximum winds would

be the distance from the wind center at the time of these peaks. If the track had kept the storm center beyond R, there would have been only one peak in the wind profile. In this case, it was established that the radius of maximum winds was less than the distance of station from the storm track.

2.4.1.3 Radius of Maximum Winds from Eye Radius. In their work, The Structure and Dynamics of the Hurricane's Inner Core Region, Shea and Gray (1972) stated that, in the mean, the radius of maximum winds occurs at radii 5 to 6 nmi outside the inner radar eye radius (IRR) - assumed synonymous with the inner cloud wall. The IRR may be obtained from land-based radar, ships at sea, or aircraft. Figure 3, taken from Shea and Gray, shows the position of R relative to the IRR for 21 Atlantic Ocean and Gulf of Mexico hurricanes. Figure 4, also from Shea and Gray, shows the difference between R and IRR versus the maximum windspeed for radial flight legs. Note that the more intense the wind the better the agreement between R and IRR.

2.4.1.4 Radius of Maximum Winds from Pressure Fit. Computed R's can be estimated by fitting an exponential pressure profile to the data from a given hurricane. By their nature, computed values of R are more subject to error than observed R's. The procedure was used in previous studies to derive estimates that were carried over into the present study and was discussed by Myers (1954).

2.4.1.5 Radius of Maximum Winds from Monthly Weather Review. Reports of radii of maximum winds extracted from storm analyses in the Monthly Weather Review usually consist of estimates of the diameters from the measured time interval between the slackening and resumption of hurricane-force winds over some point near or along the coast. In other instances, researchers have reported their findings in the Monthly Weather Review, and these results (including estimates of the radius of maximum winds) have been accepted by the authors of this study.

2.5 Speed (T) and Direction (θ) of Forward Motion

The translation speed and direction of hurricane motion are, among others, important factors for determination of storm surges along the open coast. Forward speed and direction were determined primarily from analysis of hourly hurricane positions when they were available. Generally, the analyses of meteorological data are weighted toward synoptic-scale motions. The hurricane track, thus obtained, is a best estimate of the large-scale storm motion and not a precise location of the eye at discrete time intervals. In this report, direction of storm motion is measured clockwise from north and denotes the direction from which the storm crossed or bypassed the coast.

2.5.1 Source of T and θ Data

The T and θ information in Tables 1 through 3 were extracted from storm track charts. Hurricane tracks compiled by Cry (1965) and the charts for recent years published by the NHC, NOAA, in Miami, Florida (Neumann et al. 1981, and Jarvinen et al. 1984) were used. The speeds were derived mostly from detailed track charts, depicting hourly or bi-hourly positions in the vicinity of the coast, such as: Myers (1954), Graham and Hudson (1960), and Ho and Miller (1982, 1983). The listed T and θ pertain to the time of landfall, exit, or closest approach to the coast. In Tables 1 through 3, both the T and θ data prior to 1973 were carried forward from Tables 1 and 2 of TR 15.

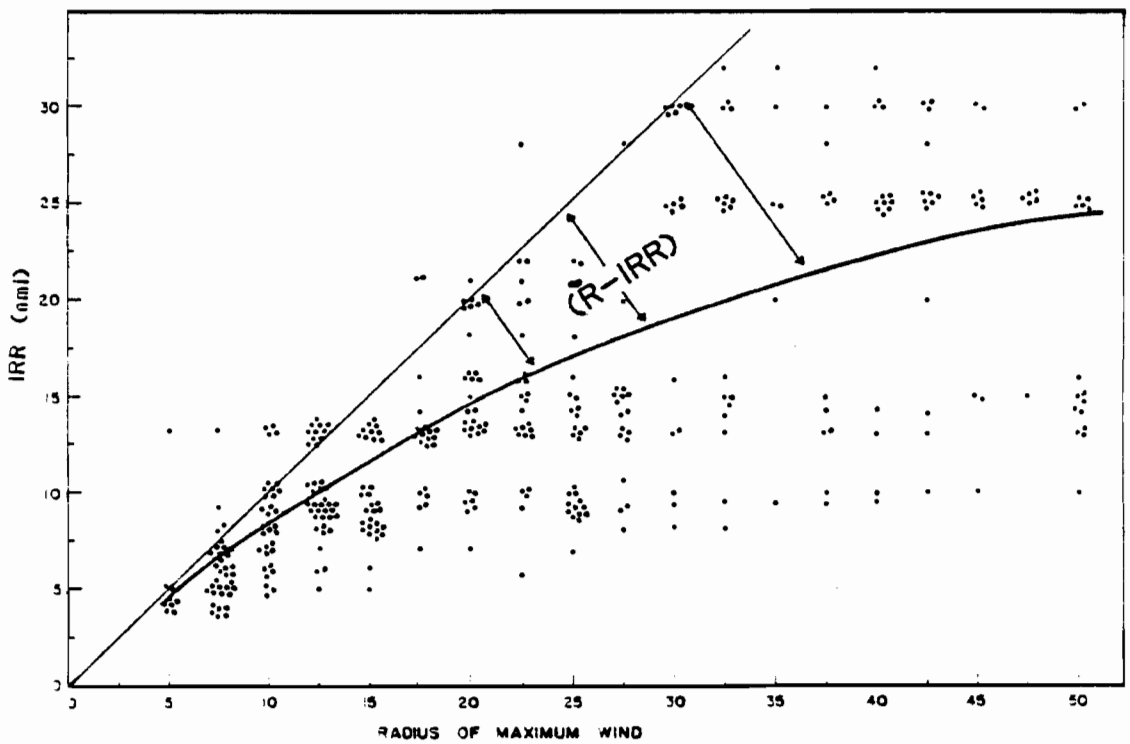

Figure 3.—Radius of maximum winds (R) versus inner radar eye radius (IRR). Points falling on the 45° line are those where the R and IRR coincide. The curved line indicates the best fit curve (from Shea and Gray 1972).

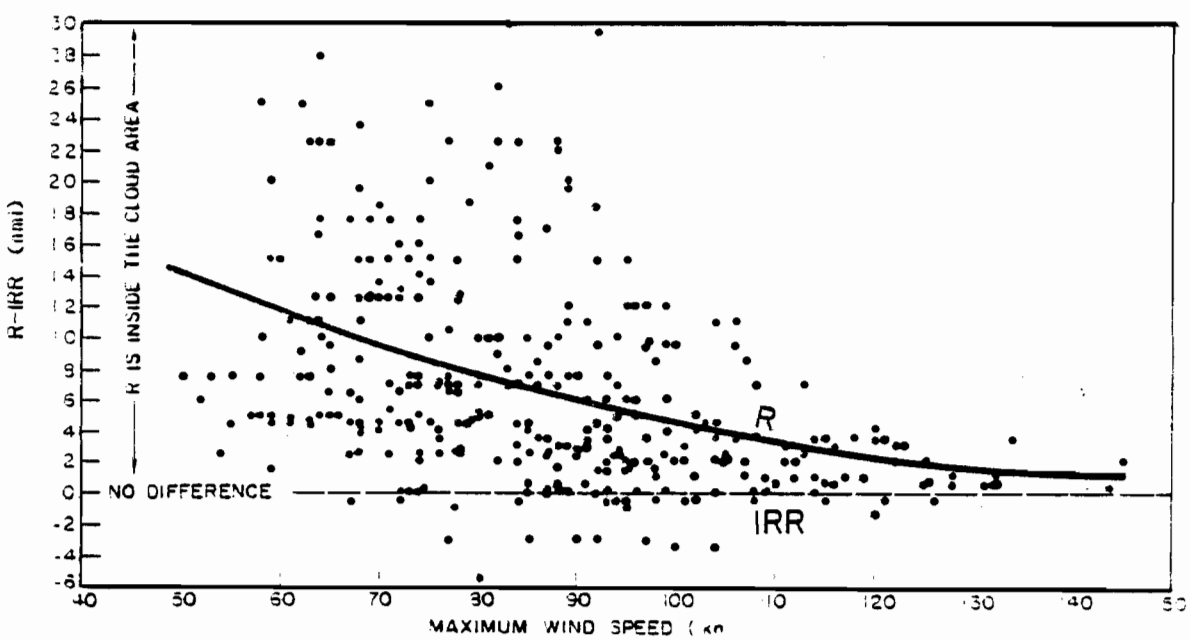

Figure 4.—Difference between the radius of maximum winds (R) and the inner radar eye radius (IRR) versus maximum wind speed. The best fit curve is indicated by the heavy line (from Shea and Gray 1972).

2.5.2 T and θ Data Used in Probability Distributions

In our present study, cumulative probability curves for T and θ were plotted for tropical cyclones since 1900. In TR 15, T data for hurricanes since 1886 were used in the plots. We made similar analyses using hurricane data from 1900-84 and found little difference in the results.

To expand our data sample for speed of forward motion, we utilized T data from all tropical cyclones landfalling on the Gulf and Atlantic coasts. In addition to the T data for landfalling hurricanes listed in Tables 1 through 3, average speeds for weaker storms were estimated from 6-hourly positions given on the HURDAT tape (Jarvinen et al. 1984). We chose the average speed, computed at synoptic hours, closest to the time of landfall as an approximation for landfalling tropical storms.

Directions of landfalling tropical cyclones were determined at the times they crossed the coast. In TR 15, the sample of θ included values from hurricanes and tropical storms since 1871. In the present study, θ data came from tropical cyclones that occurred during the 85-year period, 1900-84.

3. METEOROLOGICAL PARAMETERS AND THEIR INTERRELATIONS

3.1 Introduction

Meteorological parameters used in the hurricane climatology analysis are central pressure (P_o), radius of maximum winds (R), forward speed (T) and direction (θ) of storm motion. Since the computation of storm-surge frequencies using the joint probability approach assumes independence among the parameters, any interdependencies must be identified and taken into account.

In addition to the basic hurricane parameters, location parameters include a coastal reference milepost (m), the latitude (ϕ) and the longitude (λ). The mileposts are assigned such that m = 0 at the Mexican border and increases along the Gulf coast toward Florida, reaching a value of 1415 at the southern tip of Florida. The value of m further increases northward along the Atlantic coast to m = 3100 at the Canadian border (see fig. 1).

3.1.1 Overview of the Statistical Study

The ultimate purpose of the statistical tests was to find interrelations between the hurricane parameters, if any, so that those parameters could be properly accounted for in the storm-surge frequency computations. Because of large natural variability, our data sample did not provide a sufficient number of storms to estimate the underlying populations over coastal segments short enough to allow homogeneity to be assumed **a priori**. This made it desirable to pool data over as large an area as possible, to increase reliability of population estimation and hypothesis testing. However, the pooled data could only include coastal segments that were both statistically and meteorologically homogeneous. While determination of meteorologically homogeneous coastal segments was, of necessity, somewhat subjective, we complemented our judgments with consideration of statistical homogeneity. We felt that the variability in the data and limited sample sizes precluded a purely statistical determination of homogeneous regions.

The statistical methods used in this chapter are outlined in Appendix B, wherein the rationale for their choice, their limitations, and the interpretation of the results are discussed. We used two methods to delineate regions in which the hurricane parameters might be considered homogeneous: a meteorologically based method and a statistical method (based on cluster analysis).

For the meteorological method, hurricanes that struck a coastal segment that had relatively uniform orientation were grouped together. We then performed tests to determine whether the statistical characteristics of hurricane parameters among the various groupings were similar. The groups with no significant differences in statistical characteristics were considered for combination into a larger group. These pooled groups provided larger sample sizes for tests of interrelations between hurricane parameters.

We also performed a cluster analysis on the parameters of all hurricanes located along Gulf and Atlantic coasts; the hurricanes were separated into clusters (groups) based upon the characteristics of the sample data. The groups of hurricanes so obtained were then examined using principal component analysis and discriminant analysis to determine whether significant differences existed between the groups. The results were compared with those of the meteorological method.

3.1.2 Scope of the Chapter

In Section 3.2, a comparison of the statistical characteristics of forward speed of hurricanes and tropical storms is discussed. Practical problems with the treatment of the direction of motion of landfalling hurricanes and tropical storms is also discussed in this section. The homogeneity of hurricane parameters from different geographical regions is discussed in Section 3.3. The results of homogeneity test were used as guidelines for pooling the data samples used in the independence tests. In Section 3.4, interrelations between hurricane parameters are examined. In Section 3.5, the interdependence between hurricane parameters is discussed, and our conclusions are presented.

3.2 Considerations of Data Samples for Statistical Tests

Tropical storm data included forward direction and speed for the Gulf and Atlantic coasts of the United States. Central pressure and radius of maximum winds for individual tropical storms could not be adequately specified. However, central pressures of all tropical storms are, by our definition (see sec. 2.3.1), greater than 982 mb. Only landfalling tropical storm data were considered.

The landfalling tropical storm data were separated into two groups: one for the Gulf coast and the other for the Atlantic coast. For comparison, the landfalling hurricane data were also separated in the same manner. To examine whether the distributions of landfalling hurricanes and tropical storms should be considered separately, we set up the following data subsets:

GH: landfalling hurricanes on the Gulf coast,
GT: landfalling tropical storms on the Gulf coast,
AH: landfalling hurricanes on the Atlantic coast, and
AT: landfalling tropical storms on the Atlantic coast.

Table 5.--Forward speed of hurricanes and tropical storms for selected portions of the coast

Type of Storms	Sample Size	Average Speed (kn)	Standard Deviation (kn)
	West coast of Florida (1050 $\leq$ m <1415 nmi)		
Hurricanes	13	10.5	3.6
Tropical storms	28	15.8	7.6
	Northern Atlantic coast (m > 2400 nmi)		
Hurricanes	7	34.7	7.8
Tropical storms	12	22.8	6.7

We performed the (1) Mann-Whitney test, (2) Wilcoxon two-sample test with normal approximation, and (3) Kruskal-Wallis test with Chi-square approximation on the data set pairs GH and GT, and AH and AT. Part of the Mann-Whitney test, and all of the Wilcoxon and Kruskal-Wallis tests were conducted using SAS procedures.*

3.2.1 Forward Speed

The results of the three tests show no significant difference between the distributions of landfalling hurricanes and landfalling tropical storms for either the Gulf or Atlantic coasts. We also inspected scatter diagrams of forward speed vs. milepost for landfalling hurricanes and landfalling tropical storms. Figures 5a and 5b show that the distribution of forward speed of landfalling hurricanes and tropical storms for the west coast of Florida (m = 1050-1415) differs from that for mileposts greater than 2400. The latter is located north of Chesapeake Bay. Table 5 shows that tropical storms that struck land, on average, moved faster than did hurricanes along the west coast of Florida, but moved more slowly than hurricanes for the northern portion of the Atlantic coast. The variation along the Florida coast appears to be reasonable, and is explained by the fact that storms that recurve tend to move faster as they become embedded in stronger westerly flow. Strong westerlies also tend to disrupt the delicate thermal circulation necessary to support intense storms. Therefore, storms that recurve tend to be weaker (tropical storms) and move more rapidly. We concluded that hurricanes and tropical storms in this area represented complementary portions of the same distribution, not separate distributions.

Clearly, the observations north of milepost 2400 cannot be explained this way. While we have no fully satisfactory explanation for what the data indicate, we note that the sample size is rather small, and for the hurricanes, the variability is considerably higher than the Florida sample (see table 5). Furthermore, most storms, whether hurricanes or tropical storms, that reach

* SAS is the Statistical Analysis System. Mention of a commercial product does not constitute endorsement by the Federal Government.

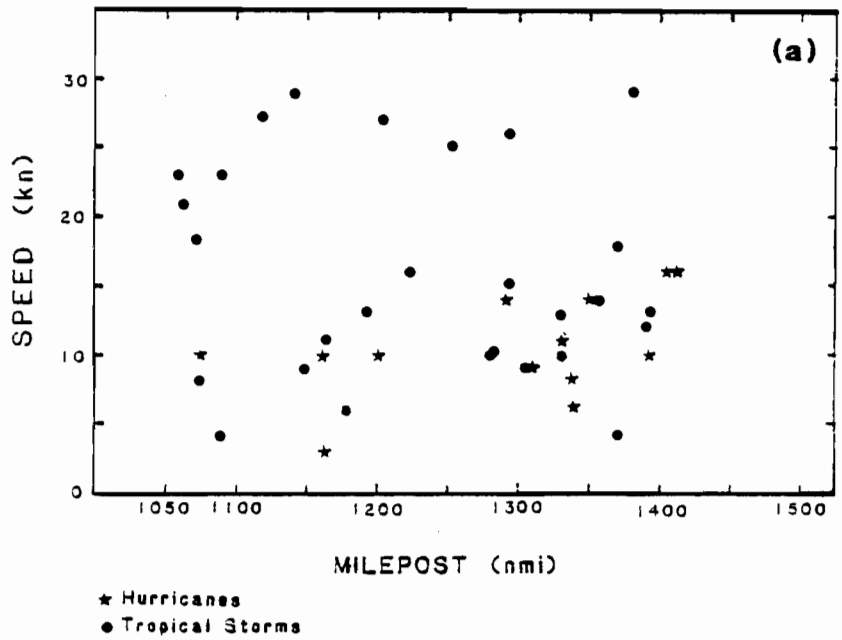

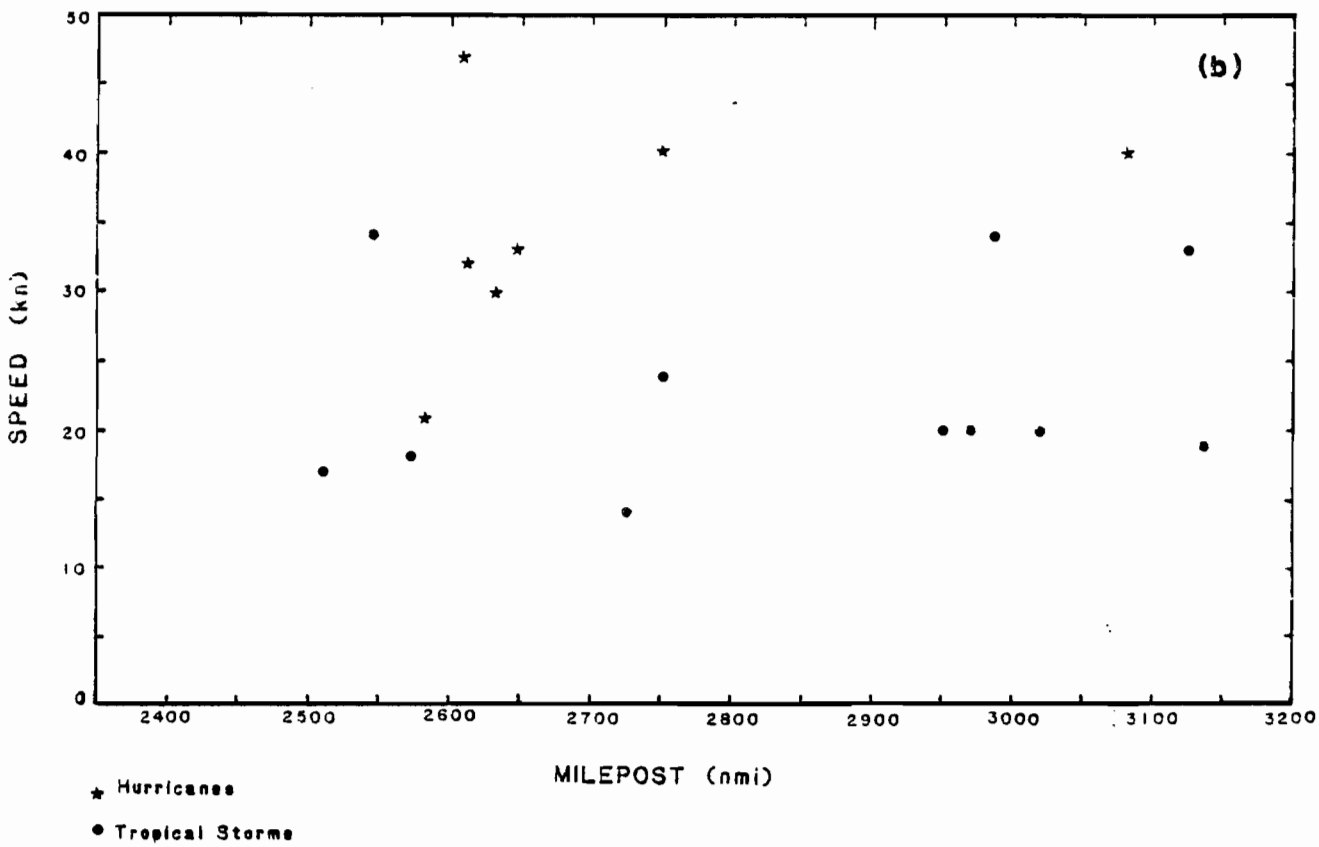

Figure 5.--Forward speed of landfalling hurricanes and tropical storms versus milepost (a) along the Gulf coast of Florida, and (b) along the Atlantic coast.

these northern latitudes are moving quite rapidly. They appear to have been transformed into systems whose circulations have extratropical characteristics. The fastest moving storms are probably propagating as waves along a baroclinic zone. Because of the small sample size, the generally large variability and the indication that the dynamics of the storms north of milepost 2400 appear to be quite unlike classical tropical cyclones, we exercised judgment in our analysis of these data. We felt that the best estimate of the underlying population could be achieved by consideration of the forward speed of both hurricanes and tropical storms. Based upon the test results and on our judgment, we treated the speed of motion for tropical storms the same as for hurricanes for both the Gulf and Atlantic coasts.

3.2.2 Forward Direction.

The data only include landfalling storms. In our data sample, landfalling hurricanes outnumber hurricanes in the other categories (bypassing and exiting) by a large amount. The sample sizes in the bypassing and exiting categories are so small that it would not be possible to make meaningful inferences based on statistical analysis.

Landfalling tropical cyclones are defined as those that strike the coast, hence their range of forward directions is limited by the coastal orientation. The range of directions can vary greatly as the coastal orientation changes over short distances. This variation can limit the range of directions in the category of landfalling storms in a way totally unrelated to real meteorological variability. For this reason, we decided that it was not appropriate to treat direction of motion as a random variable for the purposes of hypothesis testing, and in particular, for examination of interrelations with other parameters. Possible interrelations between θ and the other hurricane parameters will be considered further in Chapter 5.

3.3 Homogeneity of the Hurricane Data Samples

For the purposes of this study, homogeneity for a given coastal segment means that parameter estimates from a sample of storms for one location appear to be drawn from the same population as the parameter estimates for any other location in the segment.

We separated the storms into groups so that each group consisted of the storms that made landfall on a coastal segment that had relatively uniform orientation. Presumably, if the segment was properly selected, the data would be meteorologically homogeneous. We then performed statistical tests to determine whether the frequency distribution of the parameters from one group appeared to be the same as other groups. The groups which appeared to show no significant difference in their distributions were considered for combination into a larger group.

Cluster analysis of the parameters provided another method to separate the hurricanes into groups based on the characteristics of the data sample. The groups of storms so obtained were tested using principal component analysis and discriminant analysis to determine whether they appeared to be reasonable partitions. The results were then compared with those of the meteorological method (based on coastal orientation).

Table 6.--Initially selected coastal segments

Segment Number	Number of Hurricanes	Milepost Range (smoothed coastline)	Description
1	23	0-400	Gulf coast from Mexican border to Galveston, Texas
2	12	400-700	Gulf coast from Galveston, Texas to Mississippi delta
3	19	700-1100	Gulf coast from Mississippi delta to Suwannee Sound, Florida
4	12	1100-1415	Gulf coast from Suwannee Sound, Florida to the southern tip of Florida peninsula
5	17	1415-1800	Whole Atlantic coast of Florida
6	12	1800-2200	Atlantic coast from Georgia to Cape Hatteras
7	9	2200-2700	Atlantic coast from Cape Hatteras to Rhode Island
8	2	2700-3100	Atlantic coast from Rhode Island to Canadian border

3.3.1 Methods for Testing the Homogeneity of Storm Parameters

In the meteorological method, we first selected eight segments along the Gulf and Atlantic coasts of the United States. These eight segments were located in the milepost ranges shown in Table 6 and are shown schematically in Figure 6 (see also fig. 1). The number of landfalling hurricanes in each segment is also listed in Table 6.

There were four segments on the Gulf coast and another four segments on the Atlantic coast. Milepost 1415 is located at the southern tip of Florida. Along each segment, the orientation of the coastline is relatively uniform, except for the two most northern segments along the Atlantic coast. For the first six segments we used the Mann-Whitney test to examine the relation of P_o, R, and T among pairs of segments. Segments 7 and 8 were not included in the testing because of the small numbers of observations. The test was used to determine whether the distribution functions of a given parameter appeared to be significantly different between two segments of the coastline. If no difference in distribution functions for two segments was detected for all parameters, those two segments could be combined if the meteorological conditions in each segment were deemed to be similar enough.

The seven parameters used in the cluster analysis were P_o, R, θ, T, the milepost value (m), the latitude (ϕ), and longitude (λ) of the landfalling point. For each grouping, principal component analysis and discriminant analysis

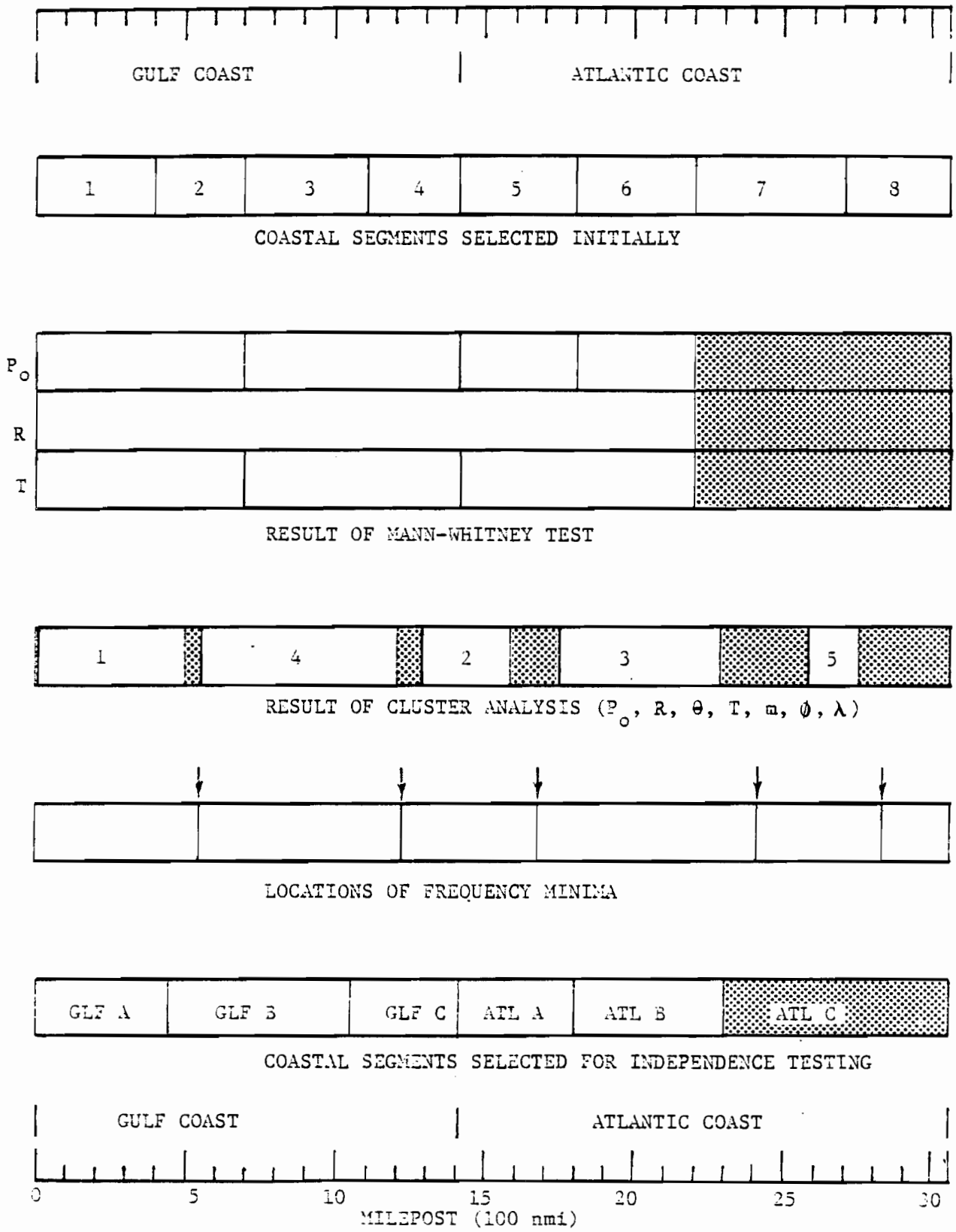

Figure 6.--Possible homogeneous regions for landfalling hurricane parameters. Shaded areas have insufficient or no data.

Table 7.--Results of Mann-Whitney test for a priori selection of coastal segments in the Gulf of Mexico

Segment Number	P_o Segment Number 1	2	3	R Segment Number 1	2	3	T Segment Number 1	2	3
1									
2	*			*			*		
3	0	*		*	*		0	*	
4	0	*	*	*	*	*	*	*	*

Segments as given in Table 6
* indicates segments with similar distributions
0 indicates segments with different distributions

were used to examine the similarity between the groups. The most distinctively separated groups were selected and the parameters within each group were examined for possible interrelations.

3.3.2 Comparison of Results from Different Homogeneity Tests

3.3.2.1 Meteorological Method. After the coastal segments were selected (table 6), the Mann-Whitney test (Conover 1971) was performed to compare pairs of segments. Adjacent segments with no significant difference in distribution functions were considered for combination.

The results for the Gulf coast are shown in Table 7. In all cases, adjacent segments appeared to have similar distributions. However, for P_o and T, some segments that were separated by one or two segments appeared to come from different distributions. For instance, for both parameters, segments 1 and 3 had different distributions, even though they both had distributions similar to that of segment 2. To explore the variation along the Gulf coast further, we divided the data sample into different segments. An example is shown in Table 8, where only 3 segments were used. Again, all segments appeared to have similar distributions of R, but different distributions of P_o and T. Our analysis of shifting the segment boundaries led us to conclude that the data appear to be

Table 8.--Results of Mann-Whitney test for modified segments of the Gulf coast

Segment Number	P_o Segment Number 1	2	R Segment Number 1	2	T Segment Number 1	2	Milepost Range
1							0-500
2	0		*		0		500-1000
3	0	*	*	*	*	*	1000-1415

* indicates segments with similar distributions
0 indicates segments with different distributions

"locally homogeneous." It appears that there may be variations along the smoothed coastline in the Gulf that could result in samples that would not be homogeneous if the segments were too large. However, it is not clear what "too large" is. By that, we mean that the variation appears continuous and that there are no obvious breakpoints between homogeneous regions. Therefore, the data can be considered homogeneous locally. In Section 3.3.3, we combine this with an evaluation of the statistically based cluster analysis to specify homogeneous segments for the independence testing.

The concept of local homogeneity was also assumed to apply for the Atlantic coast. As indicated in Table 6, the number of storms beyond milepost 2200 was too small to consider formal statistical testing. The results of the Mann-Whitney test for the region south of milepost 2200 were variable, depending on the segments chosen. However, the results were not inconsistent with the concept of local homogeneity. This is reasonable, considering the known variation of the hurricane parameters with latitude.

3.3.2.2 Cluster Analysis. The results of the cluster analysis were generally consistent with the results of the meteorological method. In application of the cluster analysis procedure, the number of clusters was assigned **a priori**, and the cluster boundaries were then determined. Analyses for two through nine clusters were conducted. When five clusters were selected, the partitioning was most similar to that determined by the meteorological method. The cluster analysis technique assigns each storm to a particular cluster and assigns it an identification (ID) number. These ID numbers are shown in the schematic in Figure 6. Somewhat surprisingly, each of the clusters included storms that struck land over a continuous extent of the coast. That is, milepost alone could be used to totally delineate which storms were included within each cluster. This is consistent with our judgment used in specifying regions by the meteorological approach (sec. 3.3.2.1). The cluster boundaries for the five-cluster partition were generally located in regions of storm-frequency minima (see fig. 27). Because of this, the last storm in one cluster (largest milepost value) could be at a considerable distance (40 nmi or more) from the first storm in the adjacent cluster. With this in mind, a cluster boundary in Figure 6 should be considered a point somewhere in the transition region - cluster boundaries are not precise delineations.

3.3.2.3 Discriminant Analysis. To determine how well the clusters of hurricanes were separated, discriminant analysis was performed on them. In addition to providing the seven parameters mentioned in Section 3.1 (P_o, R, T, θ, m, ϕ, λ), a cluster identification number (as shown in fig. 6, for a 5-cluster partition) was also used as input to the procedure. The results showed that hurricanes were not distinctively separated by the cluster analysis for 3 through 9 clusters. For example, in the case of five clusters, Hurricane Hazel of 1954, which made landfall at milepost 2077, was put in cluster 3 by the cluster analysis but classified into cluster 1 by the discriminant analysis. In this case, cluster 1 includes hurricanes which made landfall in the milepost range 1-500 and cluster 3 includes those in the milepost range 1752-2294. The discriminant analysis and the cluster analysis agree only on classifying all landfalling hurricanes into two clusters: one includes those in the milepost range 1-1201 and the other in the milepost range 1292-2750, with missing data outside of these ranges. However,

Table 9.--Percentages of variance accounted for by principal components

Principal Component	Percentage of Variance	Cumulative Percentage of Variance
1	44.6	44.6
2	15.2	59.8
3	14.3	74.1
4	12.2	86.3
5	9.0	95.3
6	4.5	99.8
7	0.2	100.0

examining these milepost ranges, we felt that these two clusters cannot be meteorologically homogeneous, especially the second cluster, because it includes hurricanes which are generally larger in size and faster in forward motion as compared to hurricanes in the lower latitudes.

3.3.2.4 Principal Component Analysis. Principal component analyses were conducted to examine the relative importance of the parameters. The percentage of variance that each principal component accounted for is shown in Table 9. The first principal component accounts for almost 45 percent of the total variance, and each of the next three principal components account for more than 12 percent of the total variance. "Loadings" provide a measure of the contribution of the parameters to each component. The loading of the hurricane parameters in the four most significant principal components is shown in Table 10. Each column in the table is an eigenvector normalized to have a unit length. This means that the square root of the sum of squares of numbers in each column is unity. Table 10 shows high positive loadings on the milepost (m) and landfalling latitude (ϕ) and high negative loading on the landfalling longitude (λ) in the first principal component, and high positive loading on central pressure (P_o) in the second principal component. The loading and importance of the first component confirms our meteorological judgment that location is an important factor in delineating homogeneous regions.

Table 10.--Loading of hurricane parameters in the principal components which account for more than 12 percent of variance

Parameter	Principal Component 1	2	3	4
P_o	0.13	0.87	-0.14	-0.16
R^o	0.31	0.33	0.11	0.60
θ	0.20	0.13	0.73	-0.57
T	0.39	-0.28	0.39	0.26
m	0.50	-0.14	-0.38	-0.21
ϕ	0.47	0.01	0.11	0.25
λ	-0.48	0.14	0.36	0.34

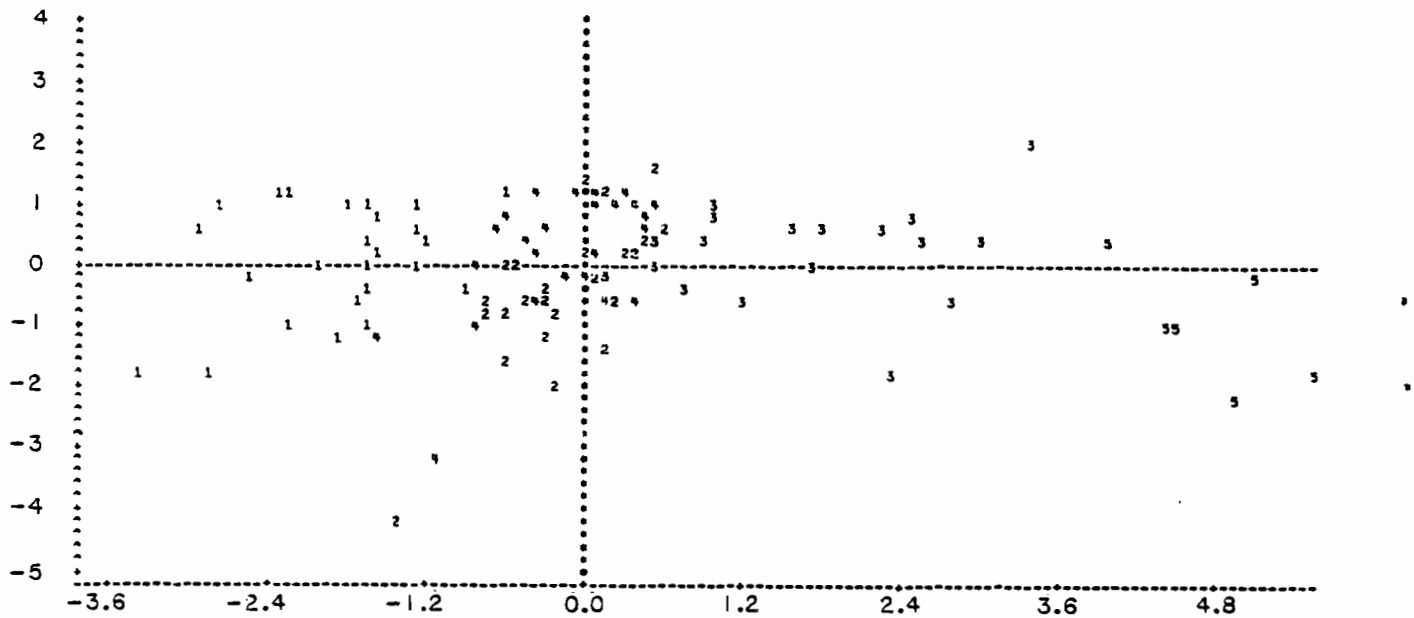

Figure 7.—Plot of the second principal component versus the first principal component. Each symbol represents a landfalling hurricane and indicates the cluster to which it belongs.

Using the classification provided by the cluster analysis, the second principal component was plotted versus the first principal component as shown in Figure 7. In this graph, each symbol represents a landfalling hurricane and the symbol indicates the cluster to which it belongs. The figure shows that clusters 1, 3, and 5 are distinctively separated with few "misclassifications," and clusters 2 and 4 are mixed. Cluster 2 includes landfalling hurricanes in the milepost range 1292-1584 which covers the southwest and southeast Florida coast. Cluster 4 includes landfalling hurricanes in the milepost range 560-1201 which covers the Gulf coast from eastern Louisiana to the Florida panhandle. Thus the landfalling hurricanes in the milepost range 560-1584 are difficult to classify into distinctive subgroups on the basis of principal component analysis. Note that location parameters played an important role in the first component, and P_o in the second component (see table 10). Figure 8 is a scatter diagram showing the distribution of P_o as a function of milepost for clusters 2 and 4. While there are fewer landfalling storms for mileposts 1000-1250, the range of pressures does not indicate any obvious clustering. In both the western and eastern portions, most P_o's range upwards from 930 mb, with an intense storm in each section. It seems reasonable to group these data together on the basis of the characteristics of their pressures.

3.3.3 Selection of Hurricane Groups for Independence Testing

The fact that the location parameters play an important role both in the principal component analysis and in the cluster analysis supports our use of coastal segments for the delineation of homogeneous regions of hurricane parameters. Consideration of meteorological factors and the results of the statistical analysis suggest boundaries between milepost 400-700, 1000-1200, 1600-1800, 2200-2300 and near 1415. Milepost 1415 is chosen as a boundary because it is a dividing point between the Gulf and Atlantic coasts. The regions we ultimately judged to be homogeneous are summarized in Table 11 (see also fig. 6).

Table 11.—Coastal segments that include homogeneous hurricane parameters for the test of independence

Segment ID	Milepost Range	Description
GLF A	0-450	Texas coast
GLF B	450-1050	Gulf coast from Louisiana to Florida Panhandle
GLF C	1050-1415	West coast of Florida south of 30°N
ATL A	1415-1800	East coast of Florida
ATL B	1800-2300	Atlantic coast from Georgia to North Carolina, including Cape Hatteras
ATL C	2300-3100	Atlantic coast from Virginia to Canadian border

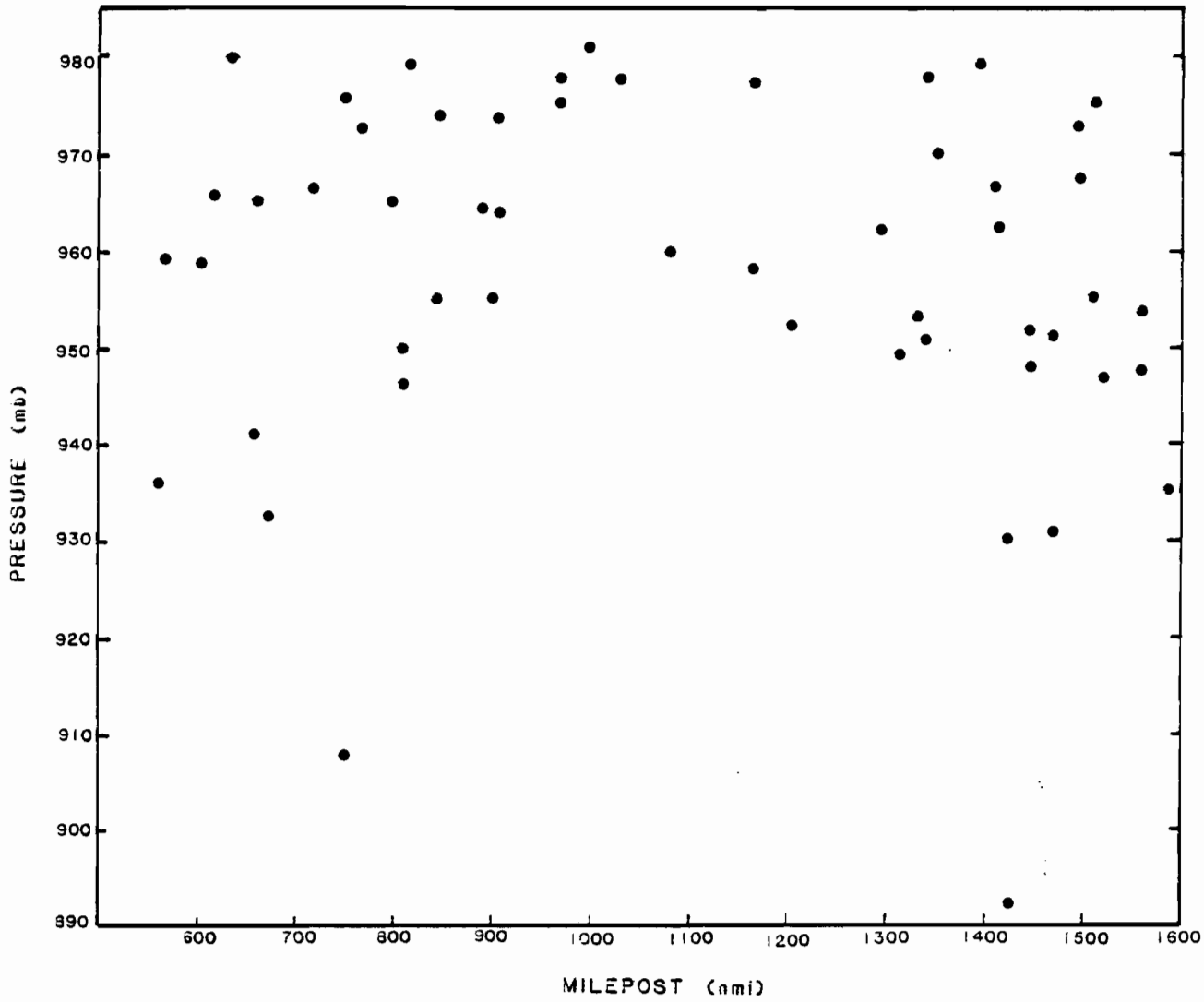

Figure 8.—Central pressure of landfalling hurricanes versus milepost.

3.3.3.1 Gulf Coast. Both our meteorological judgment and statistical analyses suggested that the region along the coast of Texas could be considered meteorologically homogeneous. Our initial boundary was at milepost 400 and the analyses in Sections 3.3.2.2 through 3.3.2.4 suggested a break near milepost 500. Since the Gulf coast turned most sharply around milepost 450, we decided to select this point to delineate our first homogeneous region. We had initially divided the south-facing portion of the Gulf coast (mileposts 400-1100) into two portions, with the break near the Mississippi delta (milepost 700). We did this to consider the possibility that storms affecting the eastern and western portions might be different. The results of the statistical analysis did not support this division. The statistical analysis suggested extending this region to the middle portion of the west coast of Florida. However, the storms affecting the west coast of Florida tend to be weaker (see fig. 8). Since the frequency of landfalling storms on the west coast of Florida is low, we felt that the statistical techniques were not able to discriminate this difference. We selected milepost 1050 as the dividing point between the two regions. Again, the coastal orientation changes most rapidly near this point.

3.3.3.2 Florida Coast. The Gulf and Atlantic coasts of the United States were considered separately because of their differences in geographical and meteorological conditions. Division of the Florida peninsula involves consideration of a number of factors, some of which suggest contradictory groupings. The statistical analyses as well as meteorological considerations (e.g., Kuo 1959) demonstrate that hurricane characteristics vary noticeably with latitude. This is due to both latitudinal variations in atmospheric circulation patterns and generally decreasing sea-surface temperature with increasing latitude. Warm water has been identified as an important factor in supporting the energy transformations necessary to maintain a hurricane circulation. These facts suggest that the data for all of Florida be considered homogeneous. In fact, the results of the cluster analysis support such a grouping for the southern portion of the peninsula. However, coastal orientation suggests dividing the data sample near the southern tip of Florida. Tropical circulation typically is associated with easterly flow. Therefore, storms moving from the east would strike the east coast of Florida. The synoptic scale meteorological patterns under such flows are most conducive to development and maintenance of hurricanes. On this basis, we suggest that there is the potential for strong hurricanes to affect the east coast of Florida.

For a hurricane to strike the west coast of Florida, it must have a westerly component in the direction from which it approaches the coast. Usually such motion is associated with storms that have undergone recurvature. Recurvature, as opposed to more random variations in storm direction, is almost always associated with the tropical cyclone becoming embedded in the westerlies. This is usually a critical transition in the hurricane's lifecycle. When this happens, the upper-level outflow necessary to maintain the warm-core circulation is impeded. Such storms tend to weaken and some take on extratropical characteristics. Occasionally, hurricanes that formed in the Gulf of Mexico moved across the Florida peninsula in a west to east direction before recurving northeastward. Though intense hurricanes were reported to have struck near Cedar Key and Tampa Bay in the mid-1800's (Ludlum 1963), it is reasonable to expect that, on the average, hurricanes striking the west coast of Florida will probably be weaker. The data (since 1900) in Figure 8 lends support to this observation.

3.3.3.3 Atlantic coast. When five clusters were used, the cluster analysis suggested that the Atlantic coast include 3 regions: (1) the southern half of Florida peninsula, including the west coast, (2) a segment from about Vero Beach (milepost 1600) to the vicinity of Cape Hatteras (milepost 2250), and (3) a region including all the coast north of Cape Hatteras. Our **a priori** judgment suggested four segments, with only the boundary in the vicinity of Cape Hatteras being common with the cluster analysis. The reasons for selecting milepost 1415 at the tip of Florida have been discussed in the previous section. As mentioned in Section 3.3.2.2, the boundaries of a cluster represents a region, rather than a clearly defined point. Examination of Figure 27 shows that from mileposts 1600-1800 there is a broad minimum in frequency of landfalling storms. In fact, it is probably reasonable to place the boundary between clusters any place within this region. For this reason, we chose to maintain milepost 1800 as the divider between the homogeneous cluster of storms striking the east coast of Florida and those affecting the coast to the north. This point is near the Florida-Georgia state line where the coastal orientation changes from NNW-SSE to NE-SW.

Both our judgment and the statistical analysis support considering the region from Florida-Georgia state line to the vicinity of Cape Hatteras as homogeneous. Conditions to the north of Cape Hatteras may not be homogeneous, either meteorologically or statistically. However, the region north of milepost 2300 is specified as "homogeneous" because of the very limited number of observations of landfalling storms in this area. In general, we did not base our analysis for this portion of the coast on the results of formal statistical techniques. We believed that the only way to treat this area was by exercising meteorological judgment. Our analysis ensured consistency and a smooth transition from the more data-rich areas to the south of this area.

3.4 Interrelations Between Hurricane Parameters

3.4.1 Brief Review of Previous Studies

Previous studies have suggested that some interrelations between hurricane parameters may exist. TR 15 suggested specifically that:

1. hurricanes with P_o below 920 mb have small R;
2. for P_o from 920 to 970 mb, there is "no detectable interrelation" between P_o and R when the entire Atlantic coast was considered;
3. "if the latitudinal trend [along the Atlantic coast] is removed from P_o and R, little local interrelation between P_o and R remains"; and
4. hurricanes that have recurved and move toward the north-northeast tend to be faster (larger T) than those that are at the same latitude and have a more westward component in the forward velocity.

National Academy of Sciences (1983) evaluated the FEMA storm-surge model and indicated that:

1. The Tetra Tech report claimed no strong linear relations among any hurricane parameters were found for the Gulf region as a whole;

Table 12.--Breakpoint values for contingency tables

Region:	GLF A ($0 \leq m < 450$)	GLF B ($450 \leq m < 1050$)
Parameter	Breakpoint	Breakpoint
P_o	951 mb	965.5 mb
R	18 nmi	20.5 nmi
T	11 kn	13 kn

2. Earle indicated that there was no significant relation between forward speed and central pressure depression over or near southwest Florida (see p. 111, National Academy of Sciences 1983). This implies no significant relation between T and P_o because central pressuredepression is defined as the difference between P_o and a peripheral pressure that is usually near 1013 mb.

3. For the middle section of western Florida coast, R and θ seem to be dependent upon central pressure depression (implying dependence on P_o).

Among suggestions listed above, Tetra Tech's claim was based on factor analysis applied to all storm parameters. Others were based mostly upon qualitative reasoning and no rigorous statistical tests were used to support the hypotheses.

3.4.2 Methods for Testing the Interrelations Between Hurricane Parameters

Two methods were used to examine the question of statistical independence: contingency tables with a Chi-square test and the Spearman test. The contingency table test is a categorical test while the Spearman test is a rank test. Both methods are described in more detail in Appendix B.

3.4.2.1 Contingency Table with Chi-Square Test. Since the contingency table analysis was designed for categorical data, the hurricane parameters had to be separated into categories. Because the hurricane data are continuous, the choice of boundaries between categories was somewhat arbitrary. The separation of the data also had to meet the requirement that the expected count in each cell could not be less than five in more than 20 percent of the cells in the contingency table. Because of the limited sample sizes, we only used two-by-two contingency tables. Only two segments had enough data to allow the Chi-square test to be performed: the two western-most segments along the Gulf coast (GLF A and GLF B). The breakpoints selected to create the categories are given in Table 12. These breakpoint values divide the parameters into two groups - values of the parameter less than the given value and those equal to or above the breakpoint value.

3.4.2.2 Spearman Test. The Spearman test is based on interrelations between the ranking (from one extreme to the other) of the observed values instead of on the observed values themselves. This test does not require assumptions about the distribution of the data; it is a non-parametric test. The Spearman test statistic can be computed for a sample size as small as four (Conover 1971). It can be used to test independence, positive correlation or negative correlation between ranks of two random variables. The minimum sample size that is required for reliable inference based on this test has not been established. Thus, the test results obtained for small samples must be interpreted with caution. In the

Table 13.--Sample sizes of paired parameters of landfalling hurricanes for coastal segments

	GLF A	GLF B	GLF C	ATL A	ATL B	ALT C
Milepost Range	0-450	450-1050	1050-1415	1415-1800	1800-2300	2300-3100
(P_o, R)	23	28	13	17	16	6
(P_o, T)	24	29	13	17	16	7
(R, T)	23	28	13	17	16	6

discussion of test results, we also present the sample sizes to provide a qualitative indication of the reliability of test results, i.e., the larger the sample size the more reliable the result is likely to be.

3.4.3 Comparison of Results from Different Independence Tests

The comparison between results of the Spearman test and those of the contingency table with a Chi-square test are shown in Figure 9. In each block, the upper triangle shows the results of the Spearman test and the lower triangle shows those of the contingency table with a Chi-square test. A symbol is given for each intersection of a column of one parameter and a row of a different parameter. The symbol I means that the pair of parameters are mutually independent and the symbol * indicates that the sample size for the pair of parameters was too small for the contingency table with a Chi-square test.

The sample sizes of paired parameters of landfalling hurricanes are listed in Table 13. For coastal segment ATL C, there were only seven landfalling hurricanes recorded, and for one hurricane the R value was not available. The sample size for ATL C was considered so small that no formal statistical testing was done for this coastal segment. Only segments with sample sizes greater than 20 were sufficient to apply the Chi-square test.

Figure 9, indicates that each pair of parameters for the combinations of P_o, R and T are mutually independent. For the pairs that have large enough sample sizes, the results from the Spearman test and the Chi-square test agree with each other.

3.5 Discussion

In general, the parameters P_o, R and T for landfalling hurricanes are mutually independent for the coastal segments throughout the milepost range 0-2300. For mileposts greater than 2300 (north of Chesapeake Bay), the small sample size prevents the determination of meaningful statistical results. The direction of storm motion is limited by the coastal orientation and cannot be treated as a random variable. For the purposes of storm-surge frequency computations, it is our recommendation, based on the results of the statistical tests and on our meteorological judgment, that all parameters be considered locally independent for the entire Gulf and Atlantic coast, except for the special cases discussed in Chapters 4 and 5.

The data available for tropical storms, and bypassing and exiting hurricanes were inadequate to allow a statistical treatment. For landfalling tropical storms, only forward direction and speed were available. For bypassing and

GLF A ($0 \leq m < 450$)

	P_o	R	T
P_o		I	I
R	I		I
T	I	I	

SPEARMAN

CHI-SQUARE

GLF B ($450 \leq m < 1050$)

	P_o	R	T
P_o		I	I
R	I		I
T	I	I	

SPEARMAN

CHI-SQUARE

ATL B ($1800 \leq m < 2300$)

	P_o	R	T
P_o		I	I
R	*		I
T	*	*	

SPEARMAN

CHI-SQUARE

GLF C ($1050 \leq m < 1415$)

	P_o	R	T
P_o		I	I
R	*		I
T	*	*	

SPEARMAN

CHI-SQUARE

ATL A ($1415 \leq m < 1800$)

	P_o	R	T
P_o		I	I
R	*		I
T	*	*	

SPEARMAN

CHI-SQUARE

Figure 9.—Interrelations between parameters of landfalling hurricanes for the Gulf and Atlantic coasts of the United States. Symbol m denotes milepost, I means independent, and * means insufficient data.

exiting hurricanes, except for limited coastal segments, the sample sizes were too small for meaningful statistical tests. In practical applications, these classes of storms are treated as individual entities with separate frequency counts and different probability distributions for corresponding parameters, if warranted. The question of their interdependency was not resolved in this study, but, based on the results for landfalling storms, we feel it is reasonable to assume that these parameters can also be considered independent.

While consideration of the statistical analysis was integral to our conclusions, our recommendations rely heavily on our meteorological judgment. This situation arose because the data sample was characterized by large natural variability. While the sampling period is on the order of a century, there are generally fewer than 10-15 storms per year that reach an intensity sufficient to be classified as tropical cyclones. In general, this amount of data is not sufficient to counteract the natural variability of the sample, and to allow standard statistical procedures to provide reliable guidance in answering the question of whether the parameters are mutually independent.

We want to emphasize that our conclusion that the data can, in general, be considered independent should be interpreted narrowly. We feel that, given the data sample, there is no evidence to support quantifiable interrelations. Because of the variation along the coast, both in the Gulf as discussed in Section 3.3.2.1, and along the Atlantic coast due to the "latitude effect," independence should be considered to be applicable locally. This concept is analogous to the idea of local homogeneity, discussed in Section 3.3.2.1. For example, Figure 10 shows scatter diagrams of P_o, R, θ, and T as a function of milepost for the Atlantic coast. There is a fairly clear tendency for all four parameters to increase with the milepost value - this is the "latitude effect." This correlation of all parameters with latitude could lead to the conclusion, based on any number of statistical tests, that the parameters are interrelated. However, this interrelation would not necessarily be between the parameters themselves, but could be due to the latitude effect. For any limited area, even if sufficient data were available, we feel that it is likely that the parameters would be mutually independent. Because we present our results (chapts. 6-9) with respect to milepost, the latitude effect, while being incorporated into the analysis, has effectively been removed for the purposes of local storm-surge computations.

Our recommendation that the parameters be treated as locally independent **is not meant to imply that we feel there are no interrelations between the four parameters.** Meteorologically, there are good reasons to suspect such relations. What we are proposing is that the natural variability in the data sample completely overwhelms any interrelations that may exist. The recommendation is a practical one - there is no way, within the limits of this study, to quantify interrelations between the parameters. Except for the special cases discussed in Chapters 4 and 5, there is no justification for attempting to specify, rather arbitrarily, possible interrelations. Further analysis of data from areas beyond those considered in this study may be sufficient to determine whether interrelations do exist, and to support quantification of such relations. However, if such work were to be pursued, care should be taken to assure that conclusions drawn from such a study were applicable to storm-surge computations along the Gulf and Atlantic coasts.

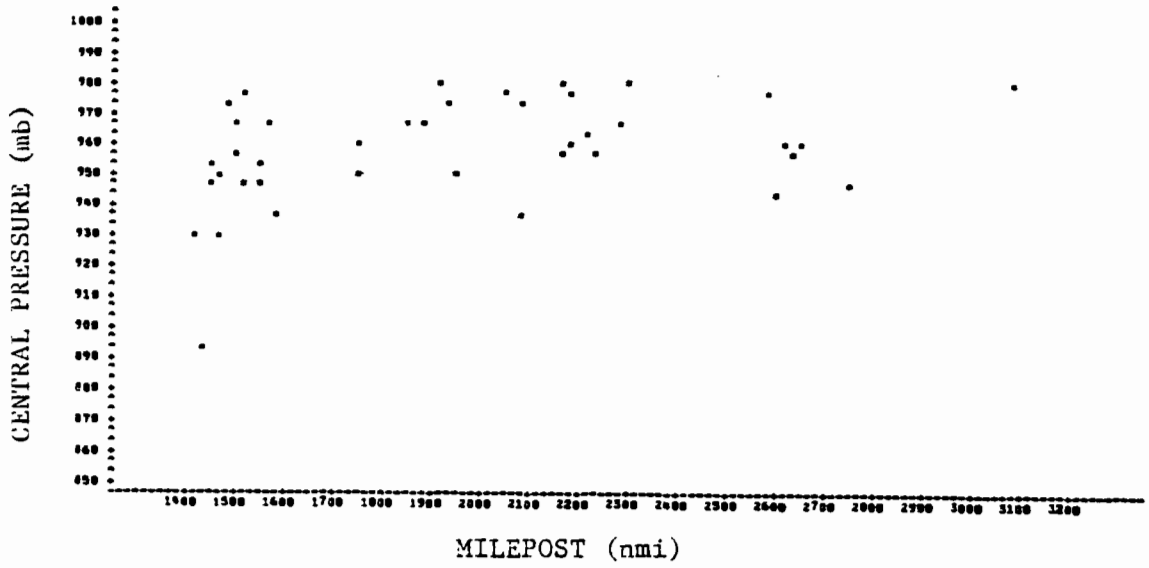

(a) Central Pressure

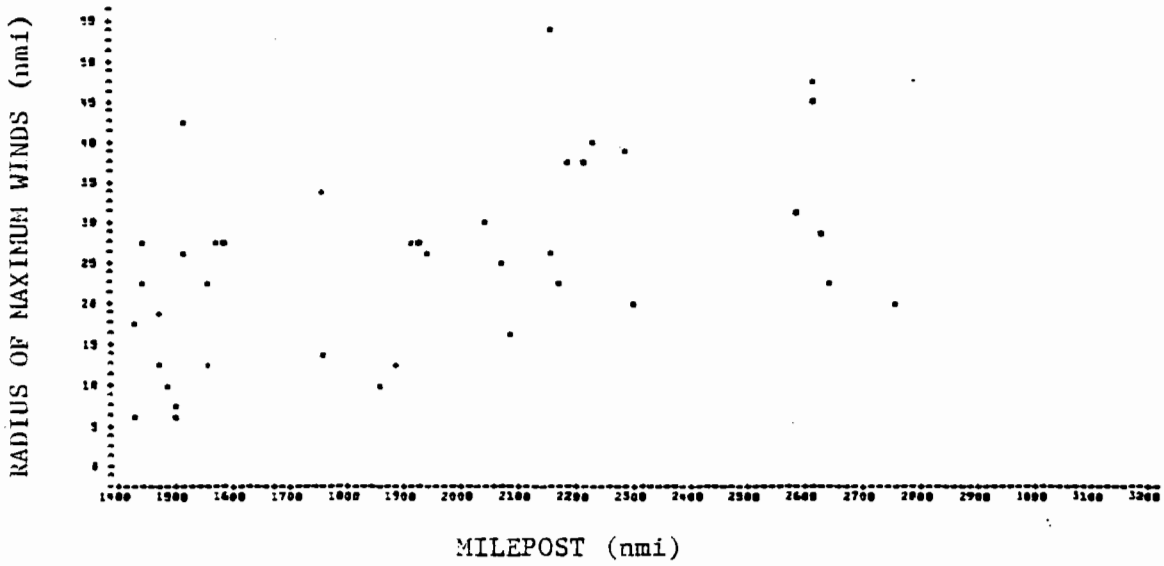

(b) Radius of maximum winds

Figure 10.—Landfalling hurricane parameters versus milepost for the Atlantic coast.

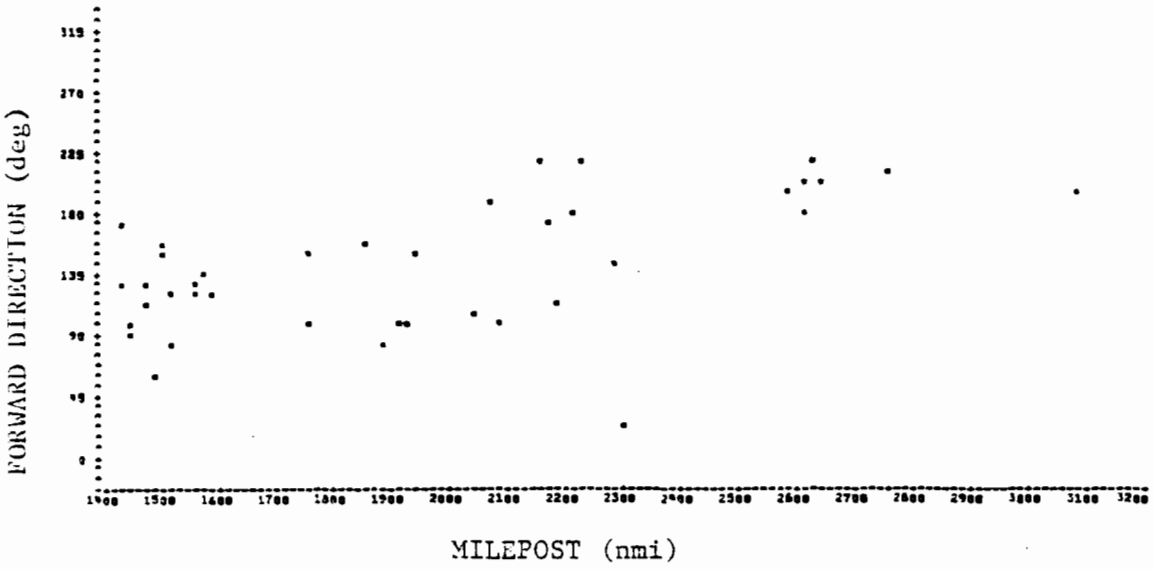

(c) Forward direction

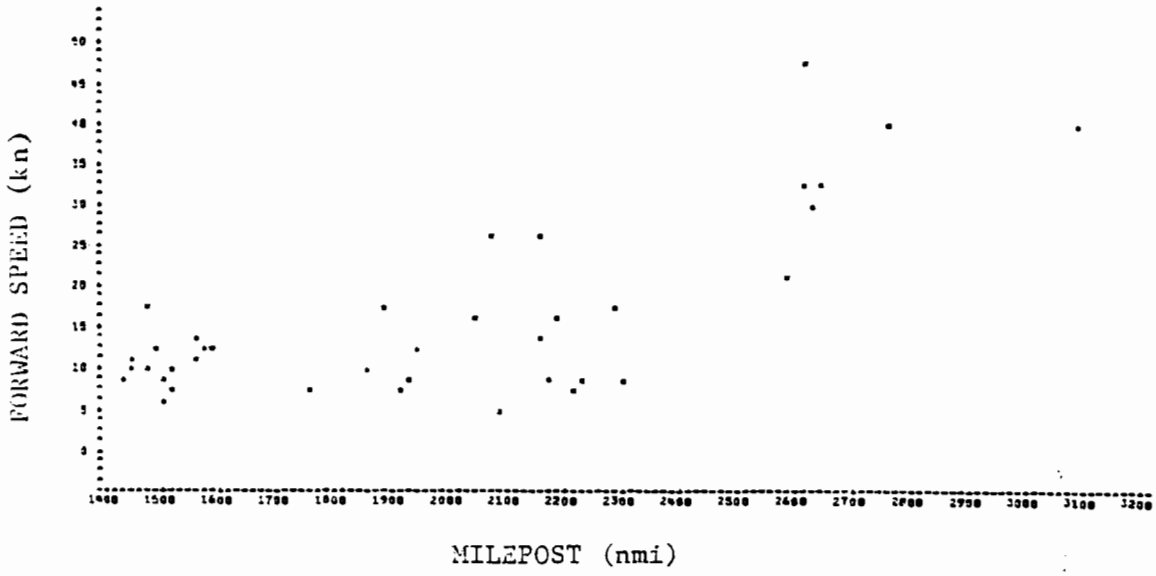

(d) Forward speed

Figure 10.—(continued).

4. THE JOINT PROBABILITY QUESTION: CENTRAL PRESSURE VERSUS RADIUS OF MAXIMUM WINDS

4.1 Introduction

An objective of this report was to define climatological probability distributions of hurricane central pressure (P_o), radius of maximum winds (R), forward speed (T), and direction of motion (θ) along the Atlantic and Gulf coasts. In calculating frequency distributions of hurricane-induced surges on the coast it is necessary to combine the probabilities from the individual distributions. In such applications, the question of statistical independence among the individual probability distributions has to be addressed. For example, of all the hurricanes affecting a given coastal stretch over a long period of time, what fraction of the storms are in **both** the upper 10 percent in intensity (P_o) and size (R)? If P_o and R are independent, the probabilities can be multiplied. In this case, there would be a 1-percent chance of their joint occurrence. If P_o and R are positively correlated, there would be more than a 1-percent chance of the simultaneous occurrence of a storm both this intense and this large. Similarly, if P_o and R are negatively correlated, the joint probability is less than 1 percent.

Statistical tests may be inappropriately biased toward acceptance of independence if the significance level chosen for the test is too low, especially considering the high variability and relatively small sample sizes available for this study. Dependencies which are meteorologically based may be present, but may not lead to rejection of the null hypothesis of independence. Another point that must be considered is whether or not certain interdependencies are expected to extend across the entire spectrum of a given parameter or whether such relations might be important only within some limited range of values.

4.2 Central Pressure Versus Radius of Maximum Winds

A significant joint probability question is whether hurricane size (R) and intensity (P_o) are independent. A storm that is both large and intense would have enormous destructive power. Hurricanes with very large R's (in excess of 45 nmi) are generally found to be of moderate or weak intensity. In hurricanes that have undergone recurvature and are moving northward in the Atlantic, often becoming extratropical, the radius of maximum winds tends to become larger and more ill-defined, and the central pressure rises. Extremely intense hurricanes (low P_o) and those with small radii of maximum winds tend to occur together because, if angular momentum is conserved, a vortex contracts in size as it increases its rotational speed.

If we examine the data for P_o and R for the Gulf coast (table 1), it is not surprising that the calculated correlation coefficient was only 0.16. A correlation coefficient this low indicates that the linear relation between P_o and R is not likely to be significant. However, a low correlation could occur if a nonlinear relation existed between these two variables. It is also possible that a relation between P_o and R could be masked by the high degree of natural variability inherent in hurricane observations. If such a relation exists, it is likely to be most prominent for intense storms where the dynamics that couple the variation of both P_o and R are stongest and less susceptible to the masking influences of environmental factors external to the storm. To test the interdependence of P_o and R, we choose to employ non-parametric statistics. A nonparametric test does not require specification of the form of the distribution,

Table 14.--An example of a general two-by-two contingency table

	Condition 1	Condition 2	Total
Group 1	a	b	a + b
Group 2	c	d	c + d
Total	a + c	b + d	n

thus, the statistical test avoids the assumption of linearity. It can also provide insight into behavior of the extreme portion of the distribution by judicious selection of the P_o and R groupings. (See below.)

The test of interdependence of P_o and R involves comparing the two samples of observations to see if the populations appear to be related. In other words, to determine if a given P_o value is more likely to be associated with a limited range of R values (interdependence), or whether any R from the complete spectrum of values has the same probability as the distribution specified for R for every P_o value (independence). We set up a contingency table, the form of the tabulation is displayed conventionally in Table 14. The letters a, b, c, and d are the count of occurrences in each group for a given condition.

We used Fisher's exact probability test (Conover 1971) to compare our groupings. Fisher's test assumes that the marginal totals of Table 14 are fixed (that is, the number of observations in each group and for each condition are fixed), and tests whether the partitioning of frequencies (a, b, c, d) could have arisen by chance. The probability of such an occurrence is calculated as,

$$p = \frac{\binom{a+c}{a}\binom{b+d}{b}}{\binom{n}{a+b}},$$

where $\binom{a+c}{a}$ is a binominal coefficient $\frac{(a+c)!}{a!c!}$, hence

$$p = \frac{(a+b)!\ (c+d)!\ (a+c)!\ (b+d)!}{n!\ a!\ b!\ c!\ d!}$$

Table 15.--Frequency of occurrence of different storm radii in two different class intervals of hurricane intensity observed in the Gulf of Mexico, 1900-84

	$R \leq 15$ nmi	$R > 15$ nmi	Total
$P_o > 930$ mb	16	47	63
$P_o \leq 930$ mb	3	0	3
Total	19	47	66

Table 15 shows the number of occurrences of hurricanes making landfall on the Gulf coast, within different categories of central pressure and storm size. We formed a null hypothesis, H_o, that there was no significant difference between R associated with group 1 ($P_o > 930$ mb) and group 2 ($P_o < 930$ mb). Fisher's test gives a probability of occurrence by chance a value of 0.02. At the 5-percent level we rejected H_o and concluded that there was a significant difference between the two groups of hurricanes, in terms of occurrence of the specified hurricane radius.

A similar test was applied to the parameters, P_o and R, for hurricanes landfalling on the Atlantic coast. With a small sample size and a much larger degree of scatter, the formal statistical test could not detect any significant interdependence of these two parameters for Atlantic coast hurricanes. While it is clear that a relation appears to be reasonable for the extremely intense hurricanes, natural variability seems to overwhelm this effect for most of the other (weaker) storms. Furthermore, it requires a much larger sample of data to establish the functional form of the joint probability of two parameters with a degree of reliability, as compared to specifying a single probability distribution.

The hurricanes listed in Tables 1 and 2 are insufficient to quantify any joint probability relation that might exist over the full range of P_o and R. The data must be supplemented by a measure of deduction and meteorological judgment. Before reaching a conclusion, we supplemented our data base by including extremely intense hurricanes that occurred outside our main area of interest (within 150 nmi of the Gulf and Atlantic coasts).

4.3 Meteorological Analysis

The basic observations used in our analysis of extremely intense hurricanes ($P_o \leq 930$ mb) were based primarily on wind and pressure data recorded by reconnaissance aircraft. In some cases, central pressures were also obtained from a search of other sources, including studies of individual hurricanes in the literature. Table 16 gives a list of hurricanes with P_o less than or equal to 930 mb recorded during the period 1900-85, together with the radius of maximum winds taken at the time of minimum central pressure. The R values for Hurricane Janet of 1955 could not be determined because of a lack of wind data. Janet was a very compact storm with winds reaching hurricane force only about 2 hr before the arrival of the eye (Dunn et al. 1955). Estimated maximum winds of 200 mph were reported just about 30 min prior to the passage of the eye over Swan Island. The table also lists locations where the P_o and R data were observed. In all cases,

Table 16.--Severe hurricanes since 1900 with P_o < 930 mb

Storm	Date	P_o(mb)	Source	R (nmi)	Source	Location
	Sept. 9, 1919*	926.5	Steamship Fred W. Weller	15	Pressure profile	Dry Tortugas, FL
	Sept. 3, 1935*	892.3	Long Key, FL	6	Pressure profile	24.8N 80.8W
Carol	Sept. 3, 1953*	929.0	Navy	25	Navy	19.8N 60.4W
Janet	Sept. 28, 1955	914.0	Chetumal, MX	No data	-	18.4N 87.9W
Donna	Sept. 10, 1960*	930.0	Conch Key, FL	18	NOAA	24.8N 80.9W
Esther	Sept. 17, 1961*	927.0	Navy	10	NOAA	25.0N 66.4W
Hattie	Oct. 30, 1961	923.0	Navy	12	Wind composite	18.3N 85.0W
Inez	Sept. 28, 1966	927.0	NOAA	7.5	NOAA	16.9N 67.4W
Beulah	Sept. 19, 1967	923.0	NOAA	9	NOAA	24.2N 96.3W
Camille	Aug. 17, 1969	905.0	Air Force	10	Wind composite	25.2N 87.2W
Carmen	Sept. 2, 1974	929.0	Air Force	8	Navy	17.9N 86.8W
Anita	Sept. 2, 1977	926.0	NOAA	10	NOAA	24.2N 97.1W
David	Aug. 30, 1979	924.0	NOAA	8	NOAA	16.3N 65.2W
Allen	Aug. 7, 1980	899.0	NOAA	8	NOAA	21.8N 86.4W
Gloria	Sept. 24, 1985*	919.0	Air Force	15	Air Force	24.3N 70.1W

* Atlantic hurricanes

the central pressure (P_o) given in Table 16 is the lowest pressure observed in the entire life span of each hurricane. The notation P_o used to designate the central pressures in Tables 1 through 3 carries a different connotation. Tables 1 through 3 list the pressure that would generate a realistic surge on the open coast in steady-state models currently used in flood insurance studies (relative to the coast). In this chapter, P_o is used to signify the central pressure values without reference to the time or place of observation (absolute minimum P_o).

Figure 11 shows the locations of the 15 extreme hurricanes at the time of their lowest central pressure. Out of the 15 extreme hurricanes, 6 occurred in the Atlantic Ocean. The hurricane of 1935 which struck the Florida Keys had the lowest central pressure ever recorded in Atlantic hurricanes (892.5 mb). The most intense hurricanes affecting the Gulf coast were Hurricanes Camille (1969) and Allen (1980). A record low central pressure for the Gulf of Mexico (899 mb) was reported in Hurricane Allen as it entered the Gulf of Mexico through the Yucatan Channel.

Figures 12 and 13 show the tracks of these severe hurricanes together with locations of reported lowest pressures at various times during the life span of each hurricane. Central pressures of 905, 908, and 909 mb were observed in Hurricane Camille (1969) near 25°N, 28°N, and at the time of landfall. There was insufficient data to show detailed time variation of Camille's intensity between the time she crossed 25°N and the coast. We assumed that Camille's central pressure remained almost steady during this time period of about 36 hours. Hurricane David (1979) reached its minimum pressure of 924 mb when the hurricane was located some 100 nmi south-southeast of Puerto Rico. Its central pressure rose above 930 mb and then dropped to 926 mb just before crossing the coast of Hispaniola. Low pressures in Hurricane Allen (1980) were plotted at three different locations because Allen went through three weakening/deepening cycles in its life span. The occurrence of these three cycles in Allen strongly suggests that geographical location is not a limiting factor in the occurrence of extreme hurricanes.

4.4 Discussion of Analysis

Figure 14 shows a plot of P_o versus R for the hurricanes listed in Table 16. Data from Hurricane Carla (1961) and a few data points from Allen (1980) (when P_o was slightly higher than the minimum of 899 mb) were plotted in the same figure to aid in determining the envelope of possible R values for extreme hurricane conditions. An envelope was drawn through the highest R values for selected intervals of central pressures. This curve indicates that observations of extremely intense hurricanes with P_o less than 920 mb consistently have small R values. The question of possible interdependence of P_o and R appears to be clearest for the most intense hurricanes.

The second question which follows is whether the group of hurricanes included in Figure 14 are representative of landfalling hurricanes. Of the six Atlantic hurricanes, the 'Labor Day' hurricane (1935) which had the lowest central pressure ever recorded in the Atlantic, struck the Florida Keys. Hurricane Camille reached its maximum intensity in the Gulf of Mexico; its central pressure appears to have remained almost steady for the 36 hours before it crossed the coast. Hurricanes David, Inez, Hattie, Carmen, Janet and Anita (see fig. 11)

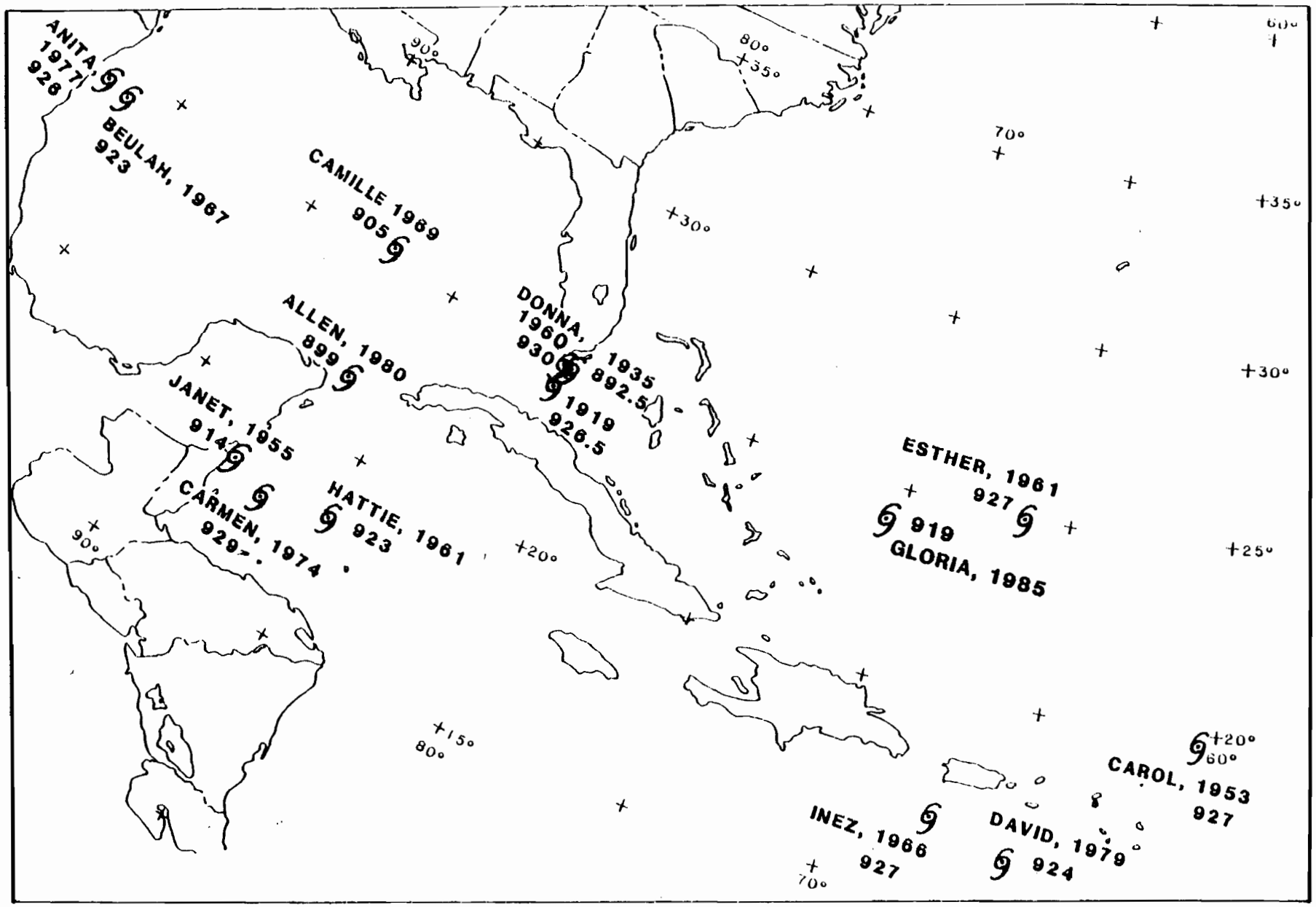

Figure 11.--Location and minimum central pressure of extreme hurricanes.

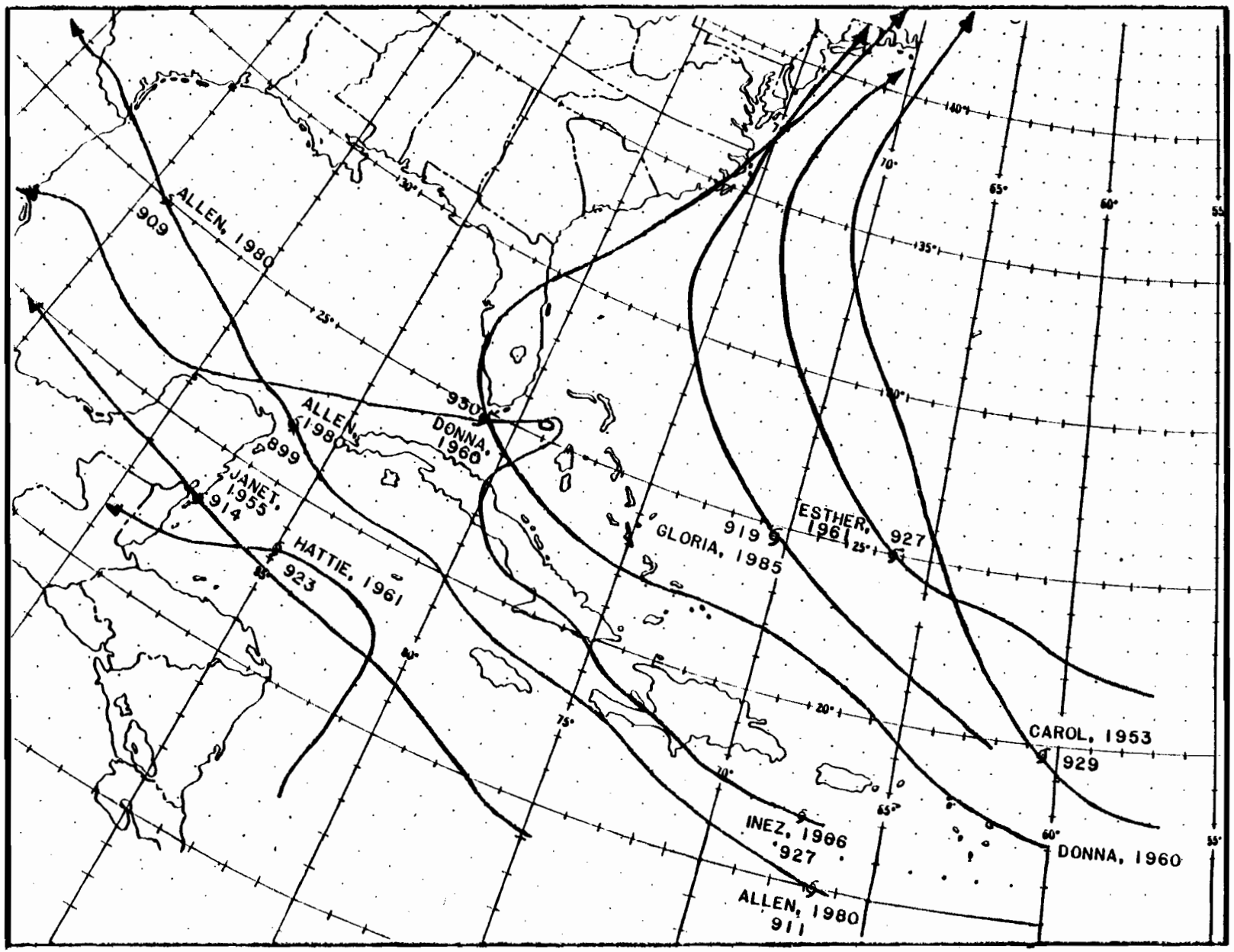

Figure 12.--Tracks of extreme hurricanes.

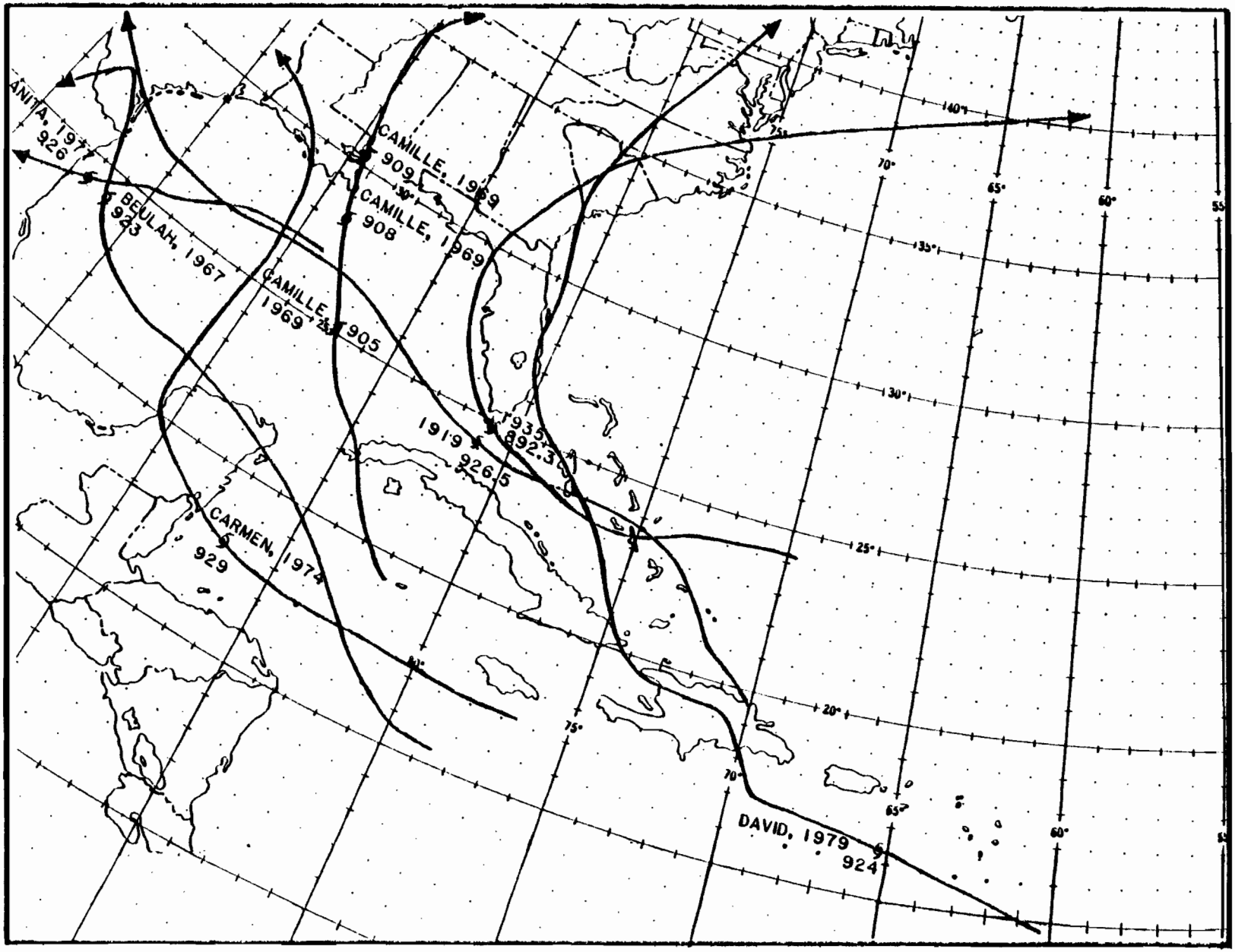

Figure 13.--Same as Figure 12.

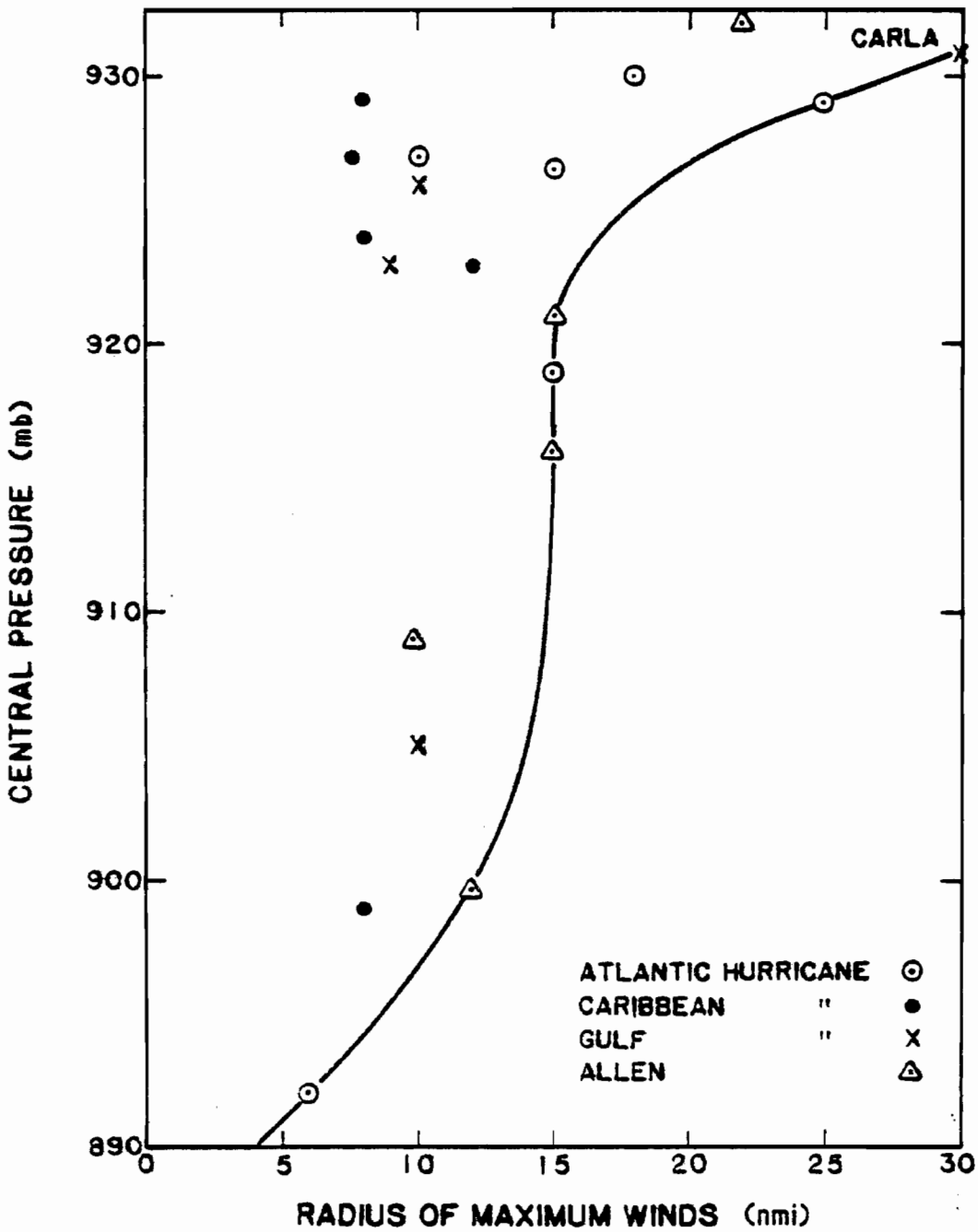

Figure 14.--Plot of P_o versus R for extreme hurricanes listed in Table 16. Additional data points from hurricanes Carla (1961) and Allen (1980) have been included.

reached their maximum intensity prior to the time of landfalling. The weakening of Hurricane Allen (1980) prior to the time of landfall can be explained by the presence of a warm high pressure ridge over the southern states. Similarly, other cases of decreasing intensity prior to landfall could not be simply explained due to the close proximity of the land mass. There is no reason to believe that, under reasonable meteorological conditions, any of these hurricanes could not have reached the coast while maintaining their maximum intensity.

4.5 Conclusions

There are insufficient data to specify a joint probability distribution of P_o and R for extreme hurricanes on a regional basis. Intense hurricanes were experienced on the Gulf coast, extending from the Florida Keys (1935 hurricane) through the Mississippi coast (Camille 1969) to locations off the Texas coast (Hurricanes Allen, Anita and Beulah). Small R's tended to be associated with these hurricanes when their pressures were lowest. These facts suggest that small R's are associated with intense hurricanes. There are seven observed R values for hurricanes with central pressure less than 920 mb. These R values, ranging from 6 nmi to 15 nmi, have both mean and median values of 10 nmi. It appears that 10 nmi is a representative R value* for intense hurricanes. A refinement can be accomplished by separating the intensity of the storms into two different class intervals. **We believe that an R value of 13 nmi assigned to the class interval of 920-908 mb and an R value of 9 nmi assigned to storms with P_o less than 908 mb would provide reasonable estimates consistent with observations and accepted meteorological principles.** We recommend the adoption of these R values for the most intense hurricane categories.

5. OTHER JOINT PROBABILITY QUESTIONS

5.1 Introduction

Unlike P_o, R and T, θ is restricted to ranges that depend on coastal orientation, and, as discussed in Section 3.2.1.2, creates problems in treating the direction data as a random sample. This chapter will attempt to examine possible interrelations between P_o and θ, and between T and θ. While we will use some formal statistical procedures, we want to emphasize that it is only for the purpose of guiding our judgment about possible interrelations. Ho and Tracey (1975) discussed in some detail possible relations between P_o and θ. It appears that this interrelation is a localized problem for North Carolina, north of Cape Hatteras. With the limited number of observations, it is not feasible to specify the joint probability of the two parameters. To establish such a joint probability relation requires a much larger sample size than that required for a single probability distribution. An alternative approach in dealing with this problem is to segregate the sample into subgroups.

---

*It should be emphasized that the representative R value is a climatological mean which excludes probable extreme values and may not be applicable in engineering design and forecasting.

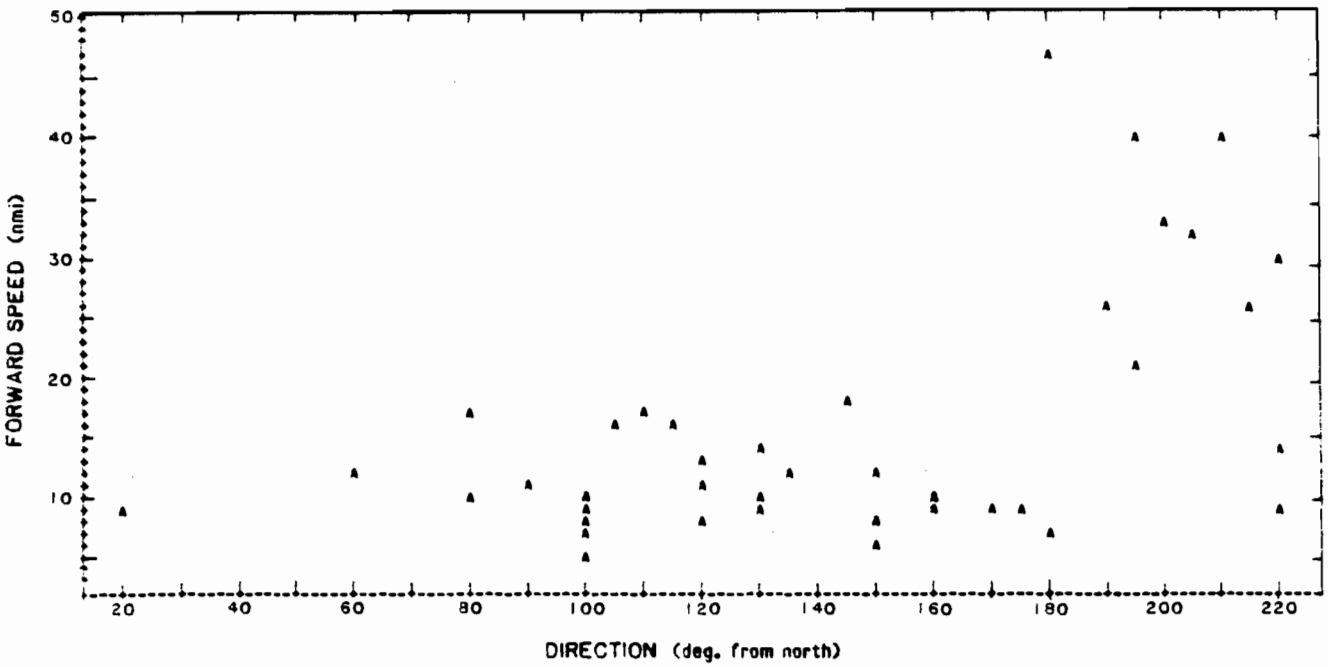

Figure 15.--Scatter diagram of direction versus speed of forward motion for hurricanes landfalling on the Atlantic coast.

5.2 Forward Speed versus Direction of Storm Motion

In the Atlantic, hurricanes tend to move north-northeastward to northeastward after they recurve. These hurricanes generally move faster than westward moving hurricanes at the same latitudes. Atlantic hurricanes that recurve near the coast often strike either the North Carolina coast or the south shore of Long Island or New England. Figure 15 shows a scatter diagram of direction versus speed of forward motion for hurricanes landfalling on the Atlantic coast. This figure reveals that a direction of about 180° appears to separate the speeds into two groups. The group with high speeds (right hand side of fig. 15) is associated with directions from 180-220°, while the slower speeds are associated with the full range of directions. This suggests that landfalling hurricanes moving north-northeastward tend to have higher speeds of translation than those coming from a direction with an easterly component. It is of interest to note that these fast-moving storms entered the coast north of 33.5°N. These hurricanes crossed the coast either near Cape Hatteras, North Carolina or in the Long Island-New England area. These are the only areas along the Atlantic coast whose coastal orientation allows storms moving from this general direction to be classified as landfalling hurricanes. Storms entering the coast south of Cape Hatteras, North Carolina, are generally hurricanes of Atlantic origin that move in a northerly direction after recurvature or those that exited the Florida and Georgia coast. Storms landfalling on the south shore of Long Island or New England are usually hurricanes that moved parallel to the coast of Maryland, Delaware and New Jersey. They could be classified as alongshore storms for coastal locations to the south of the point where they made landfall. There are no landfalling hurricanes coming from the directions 180-220° south of 33.5°N because of the way storms are classified: by definition, storms coming from those directions (180-220°) are either exiting or alongshore storms.

Table 17.--Comparison of speeds of landfalling and alongshore storms for the vicinity of Charleston, South Carolina

Percent of storms	5	20	40	60	80	95
Landfalling storms (kn)	5.6	7.2	9.5	12.2	15.1	19.2
Alongshore storms (kn)	6.6	8.6	10.8	13.5	17.6	23.5
Difference	1.0	1.4	1.3	1.3	2.5	4.3

As indicated in Chapter 3, θ and T for landfalling storms generally vary with increasing latitudes. The correlation coefficient of T and landfalling latitude on the Atlantic coast is 0.71, and 0.45 for θ and latitude. An examination of the scatter diagram for T versus latitude (see fig. 10d) reveals that hurricanes with speeds greater than 20 kn struck the coast north of 33°N, and that all the hurricanes which crossed the Long Island-New England coast were fast-moving storms. Thus, hurricanes landfalling at the northern latitudes tend to move at higher speeds than those making landfall to the south. Though there are limitations in the data samples for θ and T as previously indicated, it appears that hurricanes landfalling on the northern Atlantic coast may be different from those making landfall to the south. However, when we examined the data within homogeneous regions (concept of local homogeneity, as discussed in sec. 3.3.2.1), θ and T for landfalling hurricanes appeared to be independent. The apparent relation is attributed to the latitude effect, as discussed in Section 3.5.

Figure 16 (from Myers 1975) shows cumulative probability curves of forward speed for alongshore and landfalling storms for the Charleston, South Carolina area. The plots suggest that alongshore storms move only slightly faster than landfalling storms. Twenty percent of alongshore storms move at speeds faster than 17.5 kn, while 20 percent of landfalling storms move at speeds faster than 15 kn. Differences for the other 80 percent of storms are typically just over 1 kn, as shown in Table 17. This difference is within the range of expected error in measuring storm speeds and suggests no relation between T and θ.

5.3 Central Pressure versus Direction of Storm Motion

5.3.1 Gulf Coast

Hurricanes landfalling on the Gulf coast generally arrive at the Texas coast from an easterly direction, or strike the Florida Panhandle, Alabama, Mississippi and Louisiana coasts from a southerly direction or cross the west coast of Florida from the south-southwest to the southwesterly directions, as shown in Figure 17. It would be easy to assume that these track directions come from different populations. The Mann-Whitney test, which can be used to evaluate the homogeneity of two samples, indicates that there are significant differences among track directions in the three different zones on the Gulf coast. However, the solid line in Figure 17 is the variation of the perpendicular drawn to the smoothed coastline of Figure 1. The close correspondence between the data and this line is simply a result of the restriction in directions imposed by classifying these storms as landfalling hurricanes. Tests of interdependence of P_o and θ using contingency tables and the Spearman rank tests for the three zones

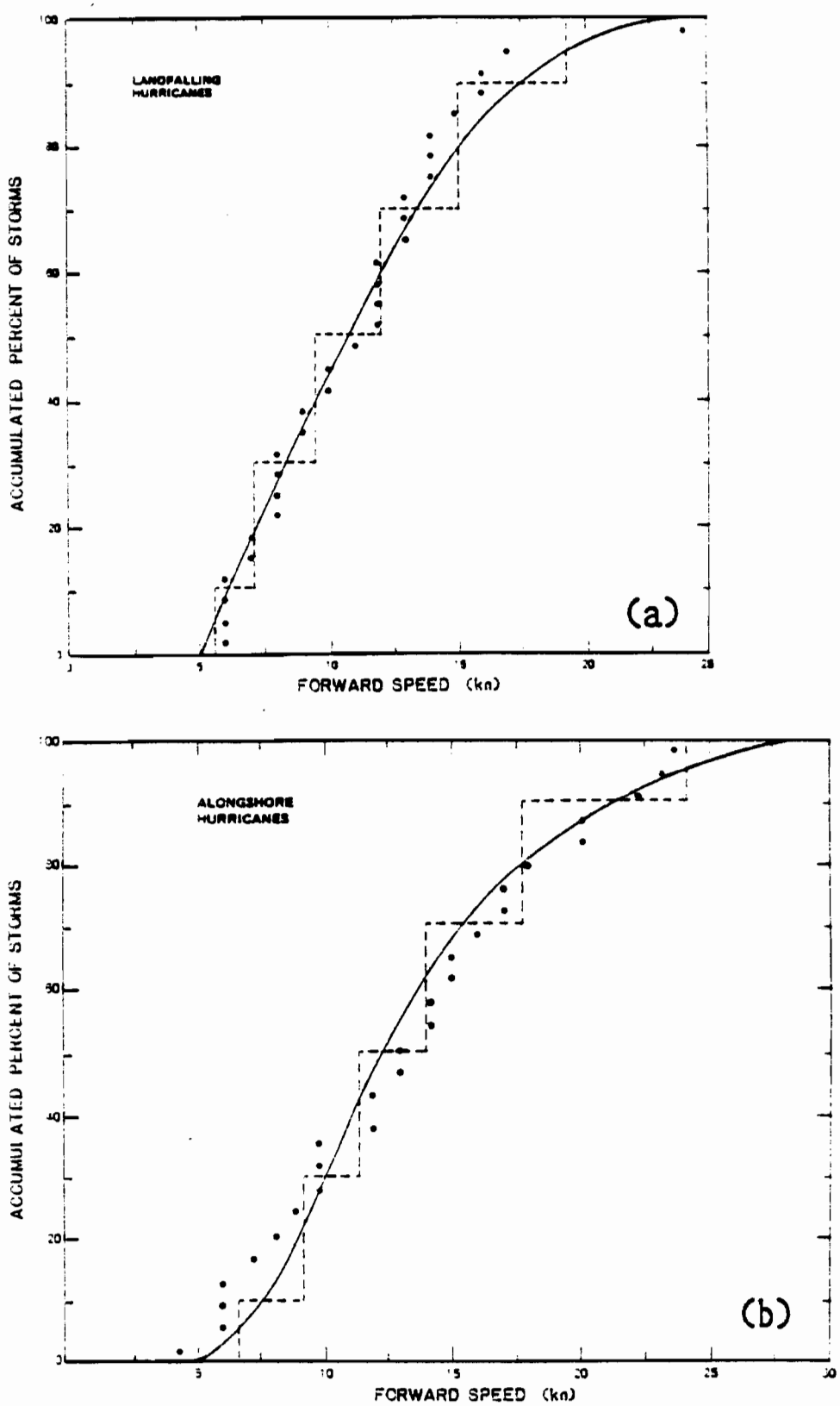

Figure 16.--Probability distribution of forward speed of (a) landfalling, and (b) alongshore hurricanes in the vicinity of Charleston, South Carolina, for the period 1886-1973 (from Myers 1975).

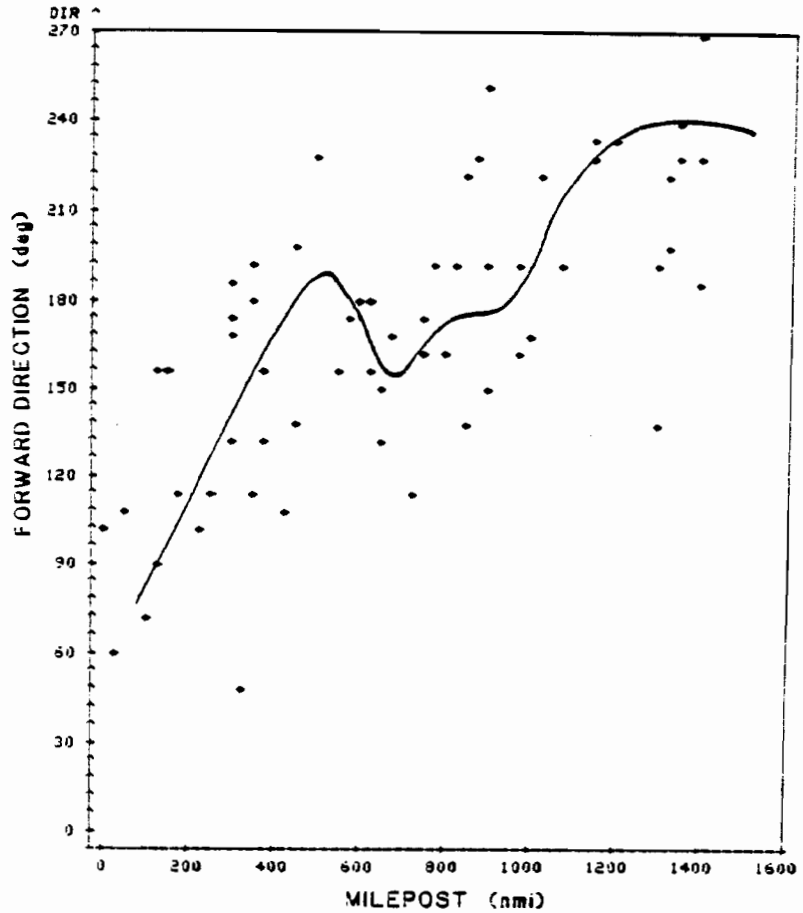

Figure 17.--Plot of forward direction versus milepost for the landfalling hurricanes on the Gulf coast of the United States. The solid line is the perpendicular to the coastal orientation as a function of milepost value.

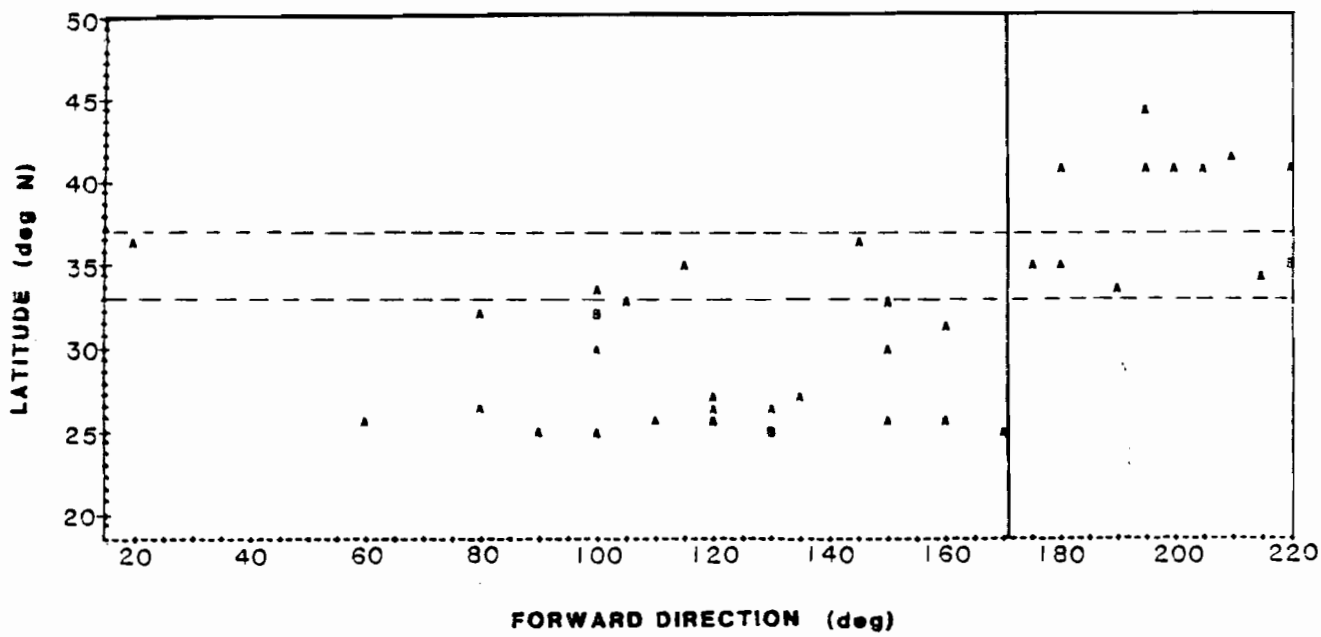

Figure 18.--Variation with latitude of direction of forward motion for hurricanes landfalling on the Atlantic coast.

Table 18.—Partition of P_o and θ for landfalling hurricanes striking the Atlantic coast south of 33.5°N

	$P_o \leq 945$ mb	$P_o > 945$ mb	Total
$\theta \geq 95°$	3	15	18
$\theta < 95°$	0	4	4
Total	3	19	22

separately show no evidence of interrelations between the parameters. However, this conclusion must be interpreted narrowly: independence is with respect to landfalling storms. Because of the variation of the coastline, this should also be considered locally independent, in the same sense as described in Section 3.5. It should not be extended to the underlying populations that contain the full range of possible values without more detailed and extensive analysis.

5.3.2 Atlantic Coast

On the Atlantic coast, the interrelations of P_o and θ are masked by their correlations with latitude. Figure 18 shows the variation with latitude of the direction of motion for hurricanes landfalling on the Atlantic coast. The plot suggests two groups of storm track directions. These two groups appear to be separated by a forward direction of about 170° (vertical line on fig. 18). From a meteorological standpoint, the data sample suggests the existence of two distinct groups: (1) landfalling hurricanes crossing the Atlantic coast from easterly directions (20-170°), which are westward moving hurricanes embedded in the basic easterly current, and (2) landfalling hurricanes coming from 170-220°, which are hurricanes moving northeastward after recurvature. There is also a stretch of the coast, from 33.5-37°N, which apparently includes hurricanes from both groups (dashed horizontal lines in fig. 18).

Statistical tests of homogeneity, using contingency tables and the Mann-Whitney test, indicate that storm track data north of 37°N are significantly different from similar data to the south. These results also suggest that there are two distinct groups of storm-track directions for landfalling hurricanes along the Atlantic coast. Since the data along the entire Atlantic coast cannot be considered homogeneous, it is inappropriate to consider the interdependence of P_o and θ for these data without separating the sample into separate groups.

5.3.2.1 Atlantic Coast, South of 33.5°N. We considered the data sample of landfalling hurricanes for the Atlantic coast, south of 33.5°N, in the form of a 2 X 2 contingency table. We estimated the probability that specific partitionings of the frequencies arose by chance. One partition of the data can be made as shown in Table 18. This contingency table shows the number of occurrences (frequencies) of hurricanes within different categories of P_o and θ. We then formed a null hypothesis that the noted distribution of observations (frequencies) arose by chance, that is, there was no significant difference between $\theta \geq 95°$ and $\theta < 95°$. The Fisher exact probability test gives a 0.53 probability of occurrence by chance. This indicates that we cannot reject the null hypothesis at the 5-percent level. We further tested for different groupings by changing the dividing line for both track directions and central pressures. These tests also yielded results which did not allow us to reject the

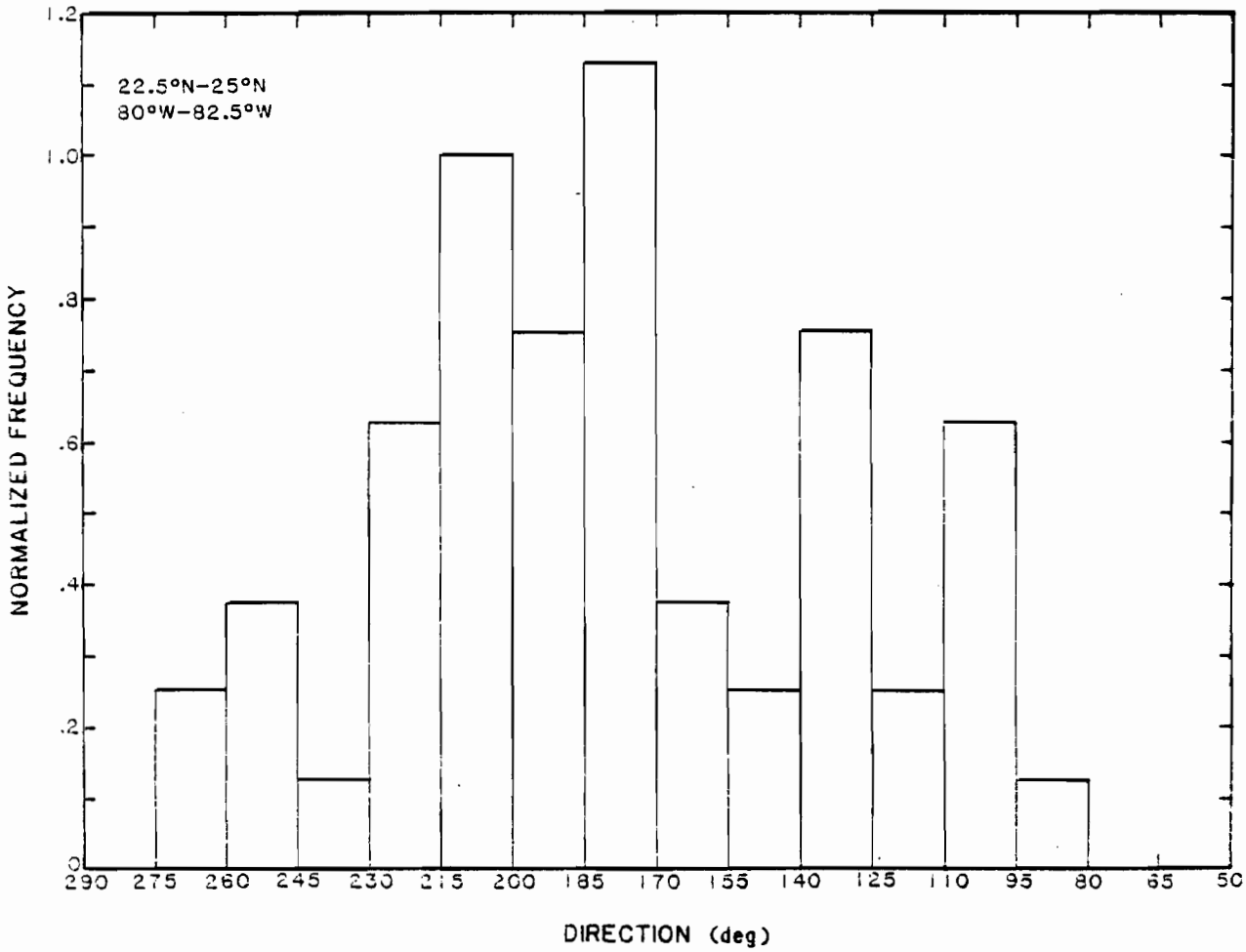

Figure 19.--Histogram for direction of storm motion for the 2.5° latitude and longitude block centered about Key West, Florida.

null hypothesis. We concluded that, at the 5-percent level, there is no significant difference between the two groups of hurricanes, in terms of occurrence of the specified direction of storm motion. In other words, there is no detectable relation between P_o and θ.

This conclusion is based on the total data sample. However, there may be localized areas that could exhibit characteristics different from this general conclusion. The data sample is inadequate to detect such situations. For instance, an interrelation between P_o and θ might occur locally near the southern tip of the Florida peninsula and the Florida Keys. Figure 19 shows a histogram for direction of storm motion for a 2.5 degrees latitude and longitude block centered about Key West. This histogram indicates a bimodal distribution for direction of storm motion with storms traversing the 2.5 degree block both from the southeast and the southwest. It is generally observed that storms coming from an easterly direction are more intense than those coming from a westerly direction. These localized interrelations between P_o, θ, and possibly between other parameters need further scrutiny. It is left to the user of this report to look at conditions at specific locations more closely. The treatment of storms affecting the Cape Hatteras area that follows in Section 5.4 may be used as a guide.

5.3.2.2 North Atlantic Coast. Examination of Figure 10a showing the latitudinal variation of pressure suggests no noticeable variation with milepost for the northern Atlantic coast. Meteorological conditions associated with the increase in central pressure with increasing latitude are discussed in Chapter 7. This feature is not obvious from Figure 10a. Consideration of Figure 10c for storm direction shows a variation due in part to variations in coastal orientation, but primarily due to synoptic-scale meteorological conditions. A large scale high pressure system (the Azores-Bermuda high) usually is centered off the coast creating a clockwise flow around it during the hurricane season. In association with this high pressure system, storm direction tends to turn clockwise as the storms move northward. This is the main explanation for the variation shown in Figure 10c. In the absence of adequate data to test for interrelations independent of latitude, it is our judgment that the concept of local independence is appropriate for the northern part of the Atlantic coast.

5.4 Cape Hatteras Area

There are a number of coastal locations that, because of geographical features, are probably not well represented by the generalized results presented in this report. Such areas include protrusions, such as the Mississippi delta, the southern part of Florida, Cape Hatteras and Cape Cod. It also includes major bays and partially enclosed bodies of water, such as Chesapeake Bay, Delaware Bay and the New York Bight. The paucity of storms affecting any one of these areas makes generalized analysis such as done in this report impossible. They must be examined on an individual basis. To illustrate some factors that might be considered in such an analysis, we studied the area around Cape Hatteras. What follows includes consideration of the more important factors for this particular location. Some aspects of the approach might not be equally appropriate for other locations.

One reason for selecting Cape Hatteras was based on consideration of Figure 18. It appears that between 33.5 to 37.0°N, the storms may include different types of hurricanes. For the coastal region from Cape Hatteras, North Carolina to Virginia Beach, Virginia on the Atlantic coast, hurricanes landfalling from the southeast quadrant cover the full range of intensities from severe to weak. Occasionally, a hurricane meanders and strikes this stretch of the coast from the northeast quadrant; observations indicate that these storms have been weaker than those coming from the southeast. They have been weakened either by unfavorable conditions in the troposphere or by the reduction of energy supply while drifting over cold water. These storms, which typically move at less than 15 kn, generally have slower speeds of translation than storms entering the coast from the southeast quadrant. Therefore, a separation of P_o and T, as well as P_o and θ, between landfalling storms from the southeast and northeast quadrant was considered. The data for all landfalling hurricanes do not suggest that R differs much depending on θ. Therefore, the R probability distribution as given in Chapter 8 is recommended for both storm categories. Portions of the statistical treatments used below were formulated by Ho and Tracey (1975).

5.4.1 Parameters for Landfalling Hurricanes from Northeast Quadrant

A special analysis was made of tropical cyclones landfalling from the northeast quadrant. Hurricane Doria (1967), which was a tropical storm at landfall, was used from Table 2, and, to expand the sample, data from other tropical cyclones

(1886 to 1984) moving from a northeasterly direction within an area west of 70°W and north of 32°N were also used. Tracks for Doria and these seven additional storms are shown in Figure 20. These eight central pressure values were used in the estimation of the cumulative probability curve shown in Figure 21 (curve A). The speeds of forward motion for the same storms were measured from storm track maps (Neumann et al. 1981), and were used to help establish the probability distribution shown in Figure 22 (curve A).

5.4.2 Parameters for Landfalling Hurricanes from Southeast Quadrant

To obtain the probability distribution of central pressure for storms landfalling from the southeast quadrant, the probabilities for northeast quadrant tropical cyclones were subtracted from the overall probability for all landfalling storms. The probability distribution thus obtained was also checked against a direct sample of storm data. The resultant distribution for the southeast storms (fig. 21, curve B) differs only slightly from that of all landfalling storms. Speed of forward motion probabilities were evaluated in a similar manner (fig. 22, curve B).

5.4.3 Landfalling Track Frequency

A discontinuity of track directions at Cape Hatteras can be seen between the curves in Figures 44 and 45. The frequency of storms landfalling from the sector 91-160° is approximately the same immediately north and south of the Cape. Landfalling storms from the other possible directions - 160-240° south of the Cape and from the northeast quadrant north of the Cape - are not of equal frequency. The overall frequency of landfalling storms (fig. 27), which was averaged along the coast by using a smoothing function, was adjusted to define this discontinuity. A track count of storms from the northeast quadrant and the 91-160° sector crossing overlapping two-degree latitude and longitude squares was examined separately. The sum of these frequencies was checked against the frequencies of all landfalling tropical cyclones. Figure 23 shows the resulting frequencies with which hurricanes and tropical storms entered the coast from different sections both north and south of the Cape. The plotted points show the frequencies of all tropical cyclones at 50-nmi intervals (determined from fig. 27).

6. FREQUENCY OF HURRICANE AND TROPICAL STORM OCCURRENCES

6.1 Classification of Hurricanes and Data

The frequency with which a coastal area has experienced tropical storms and hurricanes during the period 1871-1984 is analyzed in this chapter. The data have been divided into three categories of storms that affect the coast in different ways: 1) landfalling storms, 2) exiting storms, and 3) alongshore storms. The frequency of storm occurrences is defined as the number of tracks of each category of storms per year per nautical mile along a smoothed coast. The term "smoothed coastline" is discussed further in Section 6.2.1.2 and a smoothed coastline, defined objectively, is shown in Figure 24.

The statistics on the frequency of hurricane and tropical storm occurrences are based on the yearly storm track charts by Neumann et al. (1981) from 1871-1980, and from their annual updates between 1981-1984 (published in Monthly Weather Review). Following the criteria used in the track charts, tropical storms are

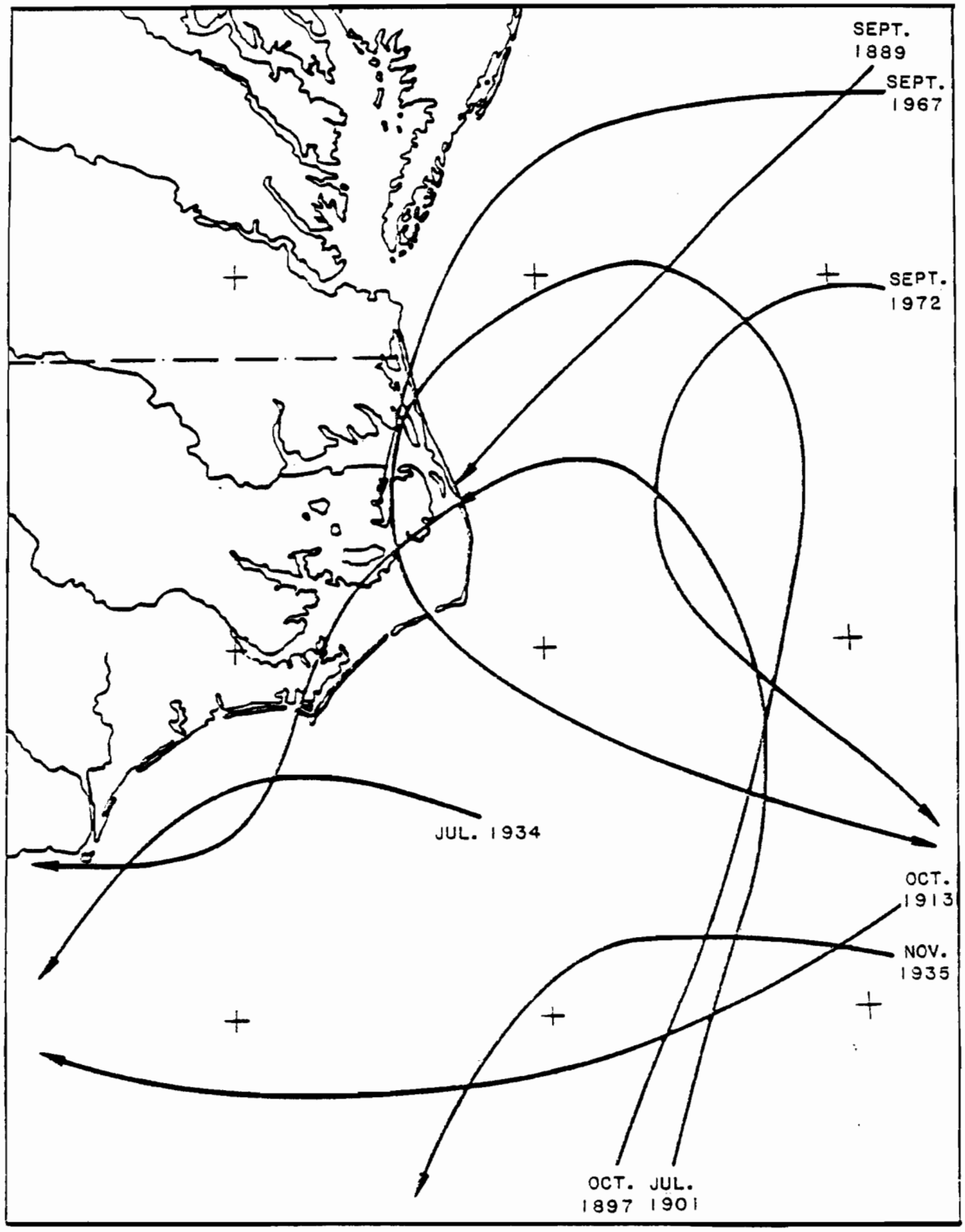

Figure 20.--Track of tropical storms and hurricanes showing motion from northeast (from Ho and Tracey 1975).

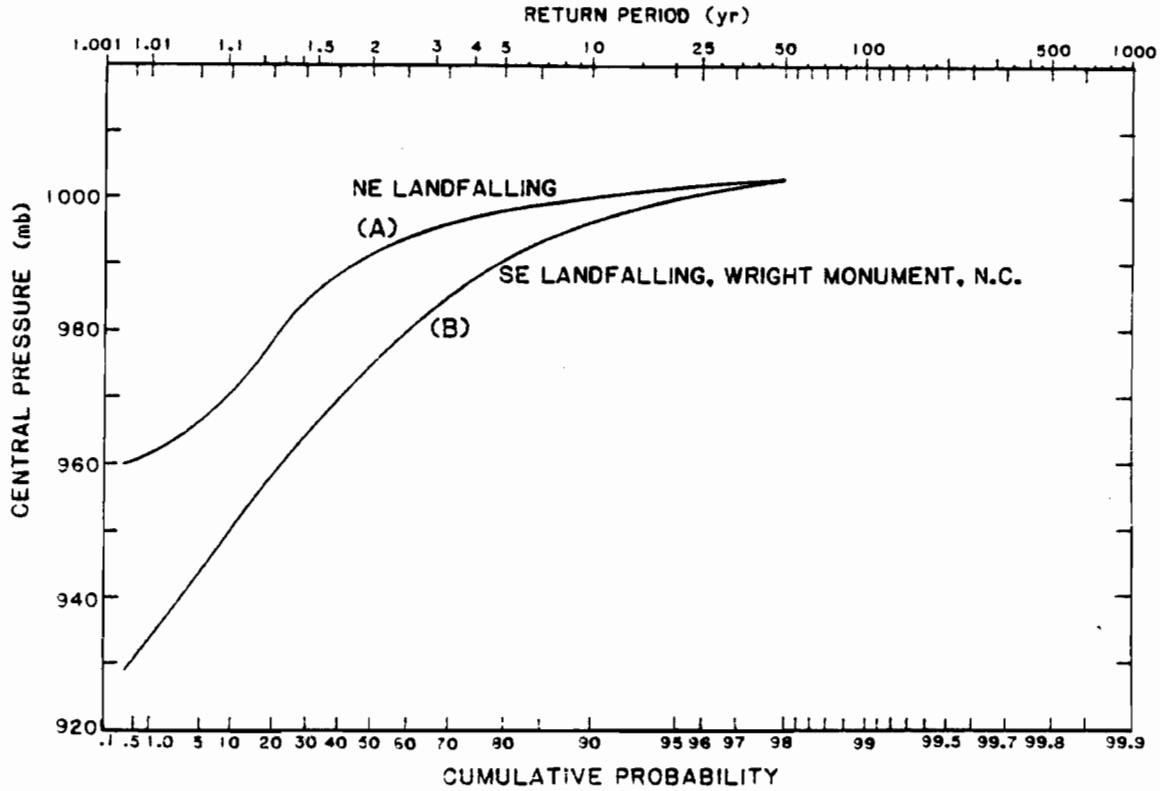

Figure 21.—Cumulative probability curve of central pressure for landfalling tropical cyclones adapted for Wright Monument, North Carolina.

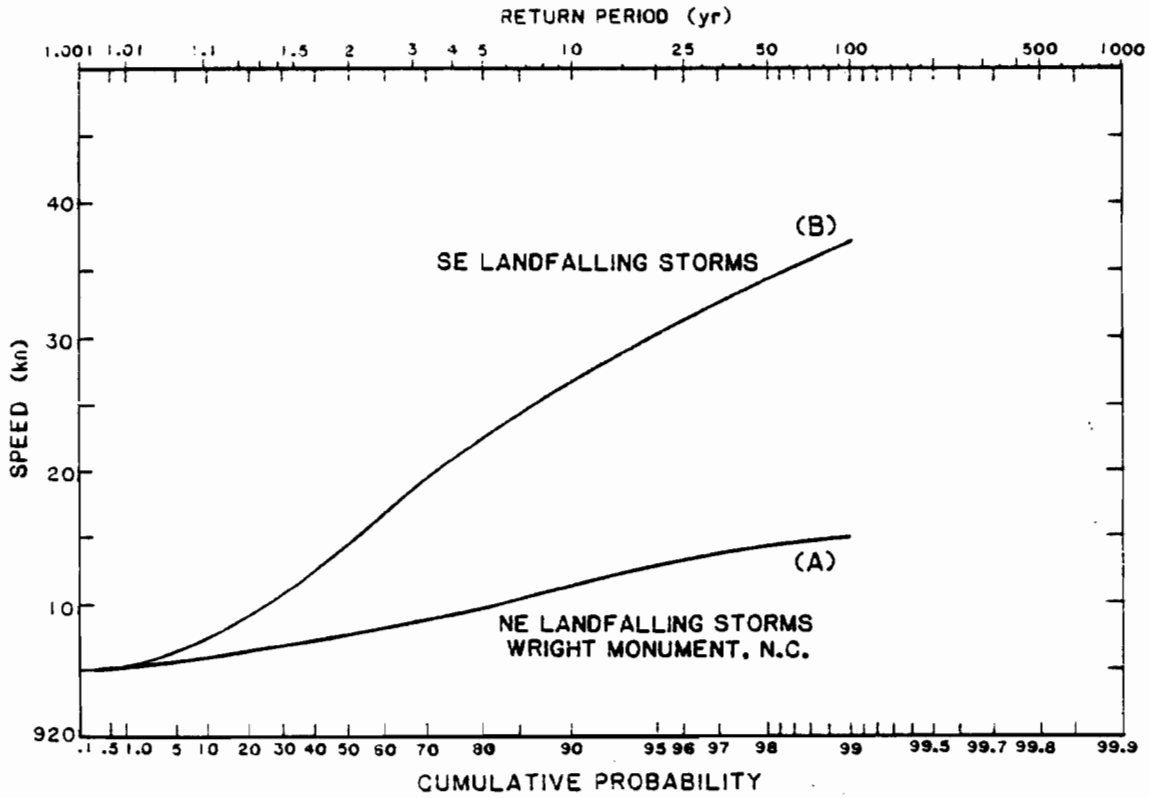

Figure 22.—Cumulative probability curve of speed of storm motion adapted for Wright Monument, North Carolina.

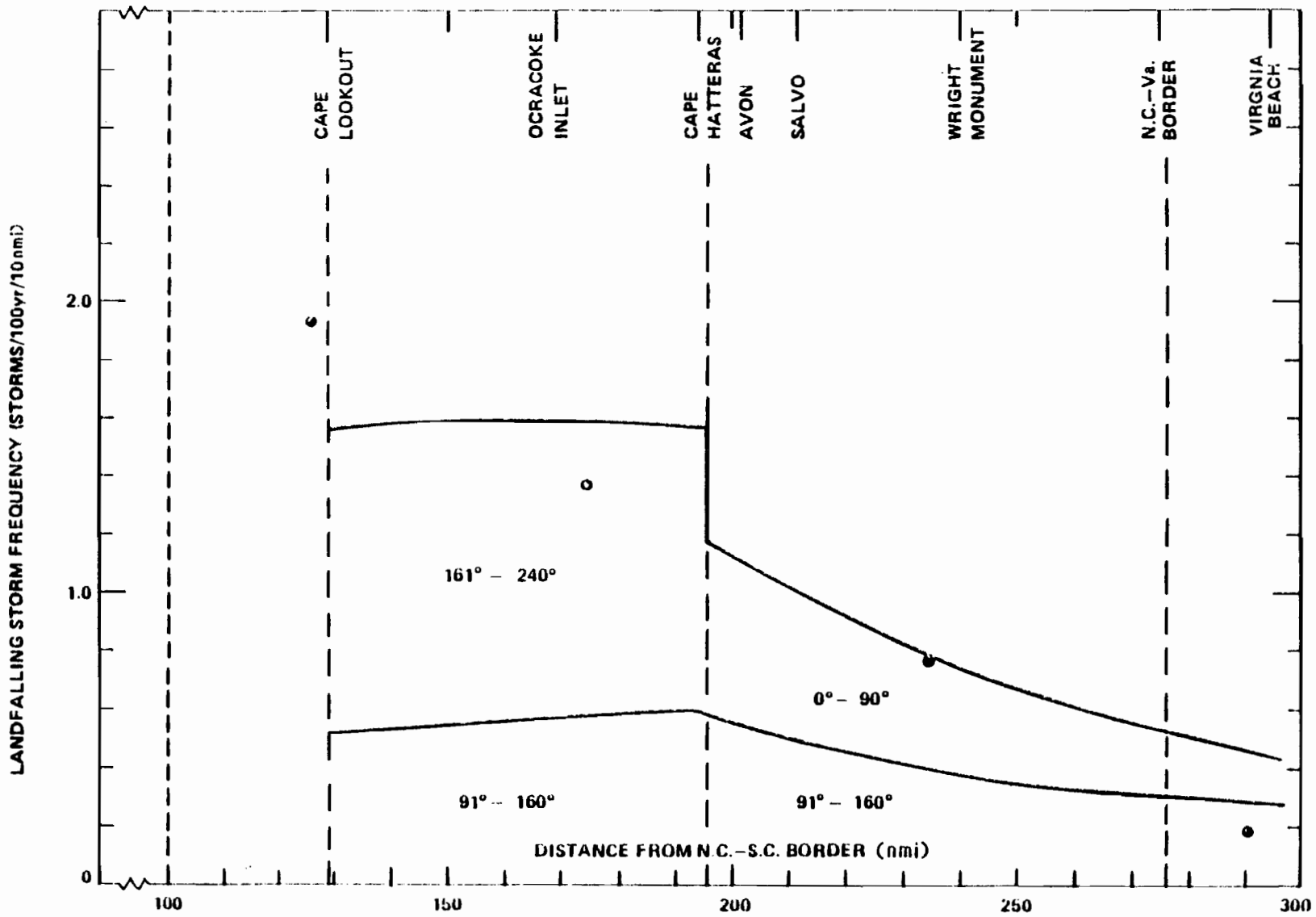

Figure 23.--Frequency of landfalling hurricanes and tropical storms. Frequencies count for 50-nmi segments from Section 6.2 are denoted by dots.

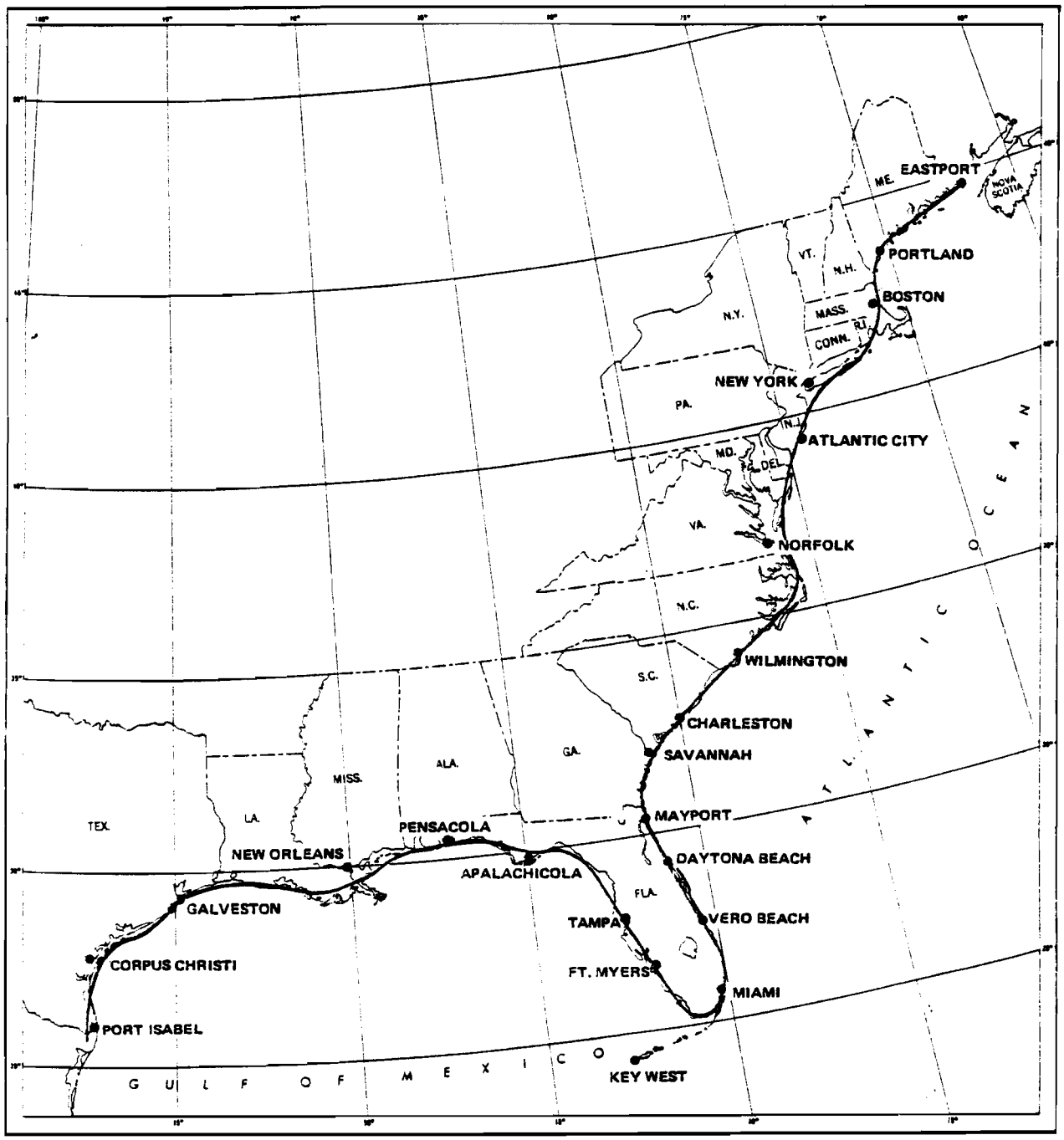

Figure 24.--Smoothed coastline obtained by applying the objective smoothing function.

defined as storms with maximum winds 34 to 63 kn, and hurricanes as storms with winds 64 kn or greater. The track charts also show extratropical stages of the cyclone tracks when the tropical circulation was modified as the cyclone moved into a nontropical environment. Beginning in 1972, the term subtropical was adopted as official terminology to describe such storms. Satellite imagery and other observational evidence enabled Hebert and Poteat (1975) to reexamine the official Atlantic hurricane tracks and to identify subtropical portions of the cyclone tracks since 1968. We included, in our frequency counts, subtropical storms and extratropical storms which have intensity equal to or greater than that of a tropical storm. For conciseness we use the term "tropical cyclone" in this report to include all four classifications. Storms classified as "tropical depressions" and "subtropical depressions" (maximum winds less than 34 kn) are not included in the statistics.

6.2 Frequency of Landfalling Tropical Cyclones

Determination of the frequency of landfalling storms in a given area would be relatively simple if a sufficiently large sample were available. However, data are available for only 114 years, from 1871-1984. Inspection of this sample reveals variations within short coastal strips which are likely to be chance occurrences due to the relatively small sample size. A goal of this report was to smooth out such variations, and to portray the characteristics of the population, not the variability of the samples. Special effort was made to take into account the effect of coastal orientation on the frequency of storms.

6.2.1 Direct-Count Method

The most direct method of assessing the frequency of landfalling tropical cyclones is to count the number of storms striking the coast. The number of entries was totaled for each 50-nmi segment along the smoothed coastline from a point some 250 nmi south of the Texas-Mexico border to the Maine-Canada border (see fig. 24). We created extensions of the Gulf and Atlantic coastlines at the tip of Florida. We "extended" the Gulf coast from Cape Sable to the Keys, stopping at its intersection with 81°W longitude, as shown in Figure 25. We "began" the Atlantic coastline at approximately 82.5°W, and continued it eastward along the Florida Keys to the mainland (see fig. 25). A storm could only be counted once on each "coast." The extensions were used for estimation of the probability distributions of storm frequency, P_o and R. We did not use the coastal extensions for T and θ, since these data sets included both hurricanes and tropical storms; we felt that the data were adequate to resolve the variation of T and θ along this part of the coast. The Gulf coast analysis stopped, and the Atlantic coast analysis began at coastal reference point 1415.

For the period 1871-1984, 307 tropical cyclones entered the Gulf coast, and 193 entered the Atlantic coast, not including storms passing the Florida Keys west of 81°W. The 50-nmi segment counts were smoothed by using the smoothing function described in Section 6.2.1.1. Figure 26 shows the frequency plot of these discrete storm entry values at 50-nmi intervals (points joined by a dashed line) and the smoothing obtained as described in the next section. These frequencies depict tracks of storm centers, but do not take into consideration the lateral extent of coast affected by an individual hurricane. The damage swath from a major hurricane can cover more than 100 nmi of coastline. The frequencies of occurrences given in terms of storms per 100 yr per 10 nmi of the coast (vertical scale in fig. 26) represent long-term averages of tropical cyclones which include

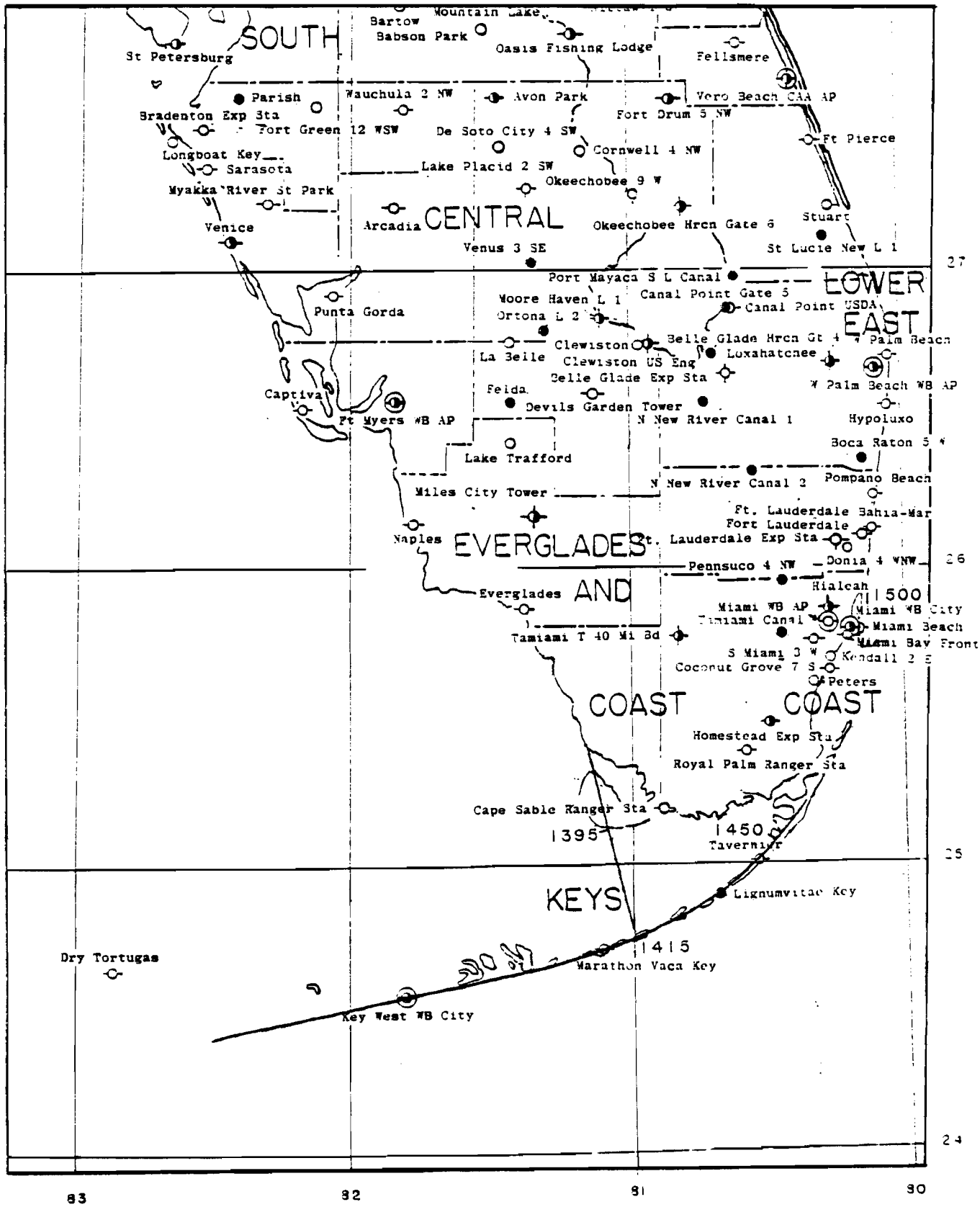

Figure 25.—Map showing extensions of west coast of Florida and the Atlantic coast through the Florida Keys. Numerals are milepost between 1395 and 1500 (see fig. 1).

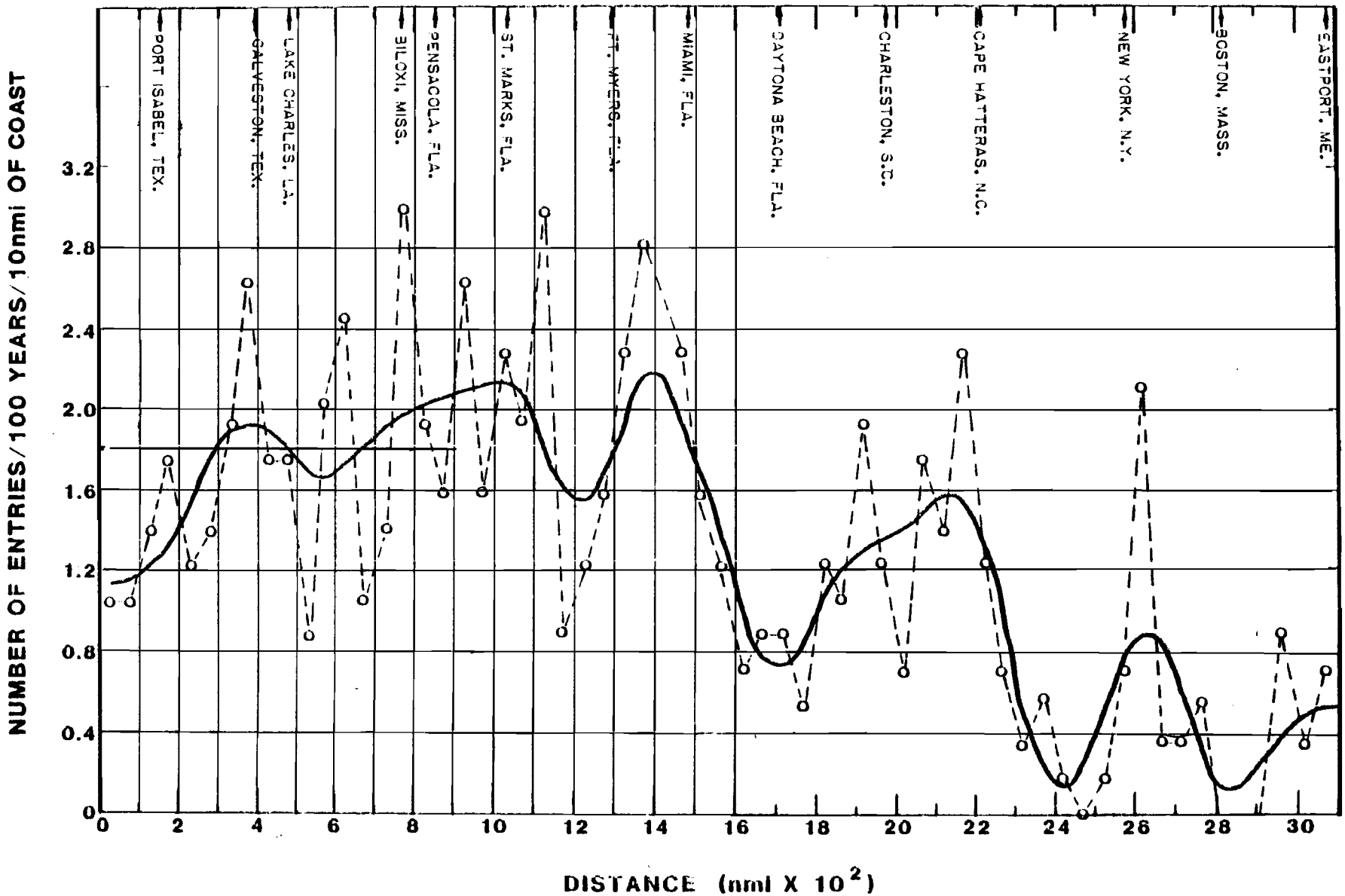

Figure 26.--Count of landfalling tropical storms and hurricanes (1871-1984) by 50-nmi segments of a smoothed coastline (points plotted and connected by dashed lines). Solid line denotes the entry frequency curve obtained by applying the objective smoothing function.

storms ranging in intensity from weak tropical storms to intense hurricanes. In a probabilistic sense, one storm per 100 years should be interpreted as that event which has a 1-percent chance of occurrence per year over a 10-nmi coastal segment.

6.2.1.1. Objective Smoothing Procedure. The 50-nmi segment counts were smoothed by weighted averaging over 11 data points. We used a weight function in the same manner as in low-pass filtering in time series analysis. The adopted function has the following assigned weights (after Craddock 1969):

$$W_n = 0.300,\ 0.252,\ 0.140,\ 0.028,\ -0.040,\ -0.030;\ \text{for}$$

$$n = 0,\ \pm1,\ \pm2,\ \pm3,\ \pm4,\ \pm5,\ \text{respectively.}$$

An alternative smoothing procedure sometimes applied in climatological analyses uses a running-mean $[W_n = 1/(2N+1)]$. The results thus obtained may have distortions in phase angle variation (shifting of maximum or minimum positions). The weighting function adopted here is designed to maintain the average frequencies and phase angles of the original input series. These weights were applied to all successive discrete values from south of Texas to the southern portion of Florida, and from Key West to Maine. The end of the input series was extended as a mirror image of the original series. Thus, smoothed frequency estimates of landfalling tropical cyclones for each 50-nmi interval were obtained along the smoothed coastline, from Texas all the way to the Canadian border. The two series were then connected to give a continuous smoothed curve of frequency of landfalling tropical cyclones (solid curve of fig. 26). Figure 27 shows the final frequency curve including an extension at the southern tip of Florida depicting the frequencies for the Florida Keys (upper portion of the curve).

6.2.1.2 Evaluation of Procedure. The direct count method derives its data from a count of tropical cyclones at the coast and not out over the water. It gives the best estimate of the variation along a smooth coastline of the frequency of landfalling storms. However, it tends to obscure variations due to coastal shape. A stretch of the coast that turns sharply in a direction almost parallel to that of the predominant storm motion is less exposed than adjacent coastal segments more nearly normal to the track direction. We have implicitly smoothed sampling variability associated with small scale variations of the coast.

To identify areas where the implied smooth coastal direction differs significantly from the actual coastline, a smoothed coastline was constructed. Coastal locations at 50-nmi intervals along the Gulf coast and Atlantic coast were smoothed using the smoothing function described in Section 6.2.1.1. These points were plotted and a continuous line joining these points was drawn for both the Gulf and Atlantic coastlines (fig. 24). This diagram reveals that this smooth line cuts across the actual coastline at several places -- most significantly, across the Mississippi Delta, along the west coast of Florida and across Cape Cod. For the most part, the smoothed coastline approximates quite well the orientation of the actual coast.

Areas where a smoothed coastal direction differs substantially from the actual direction may be detected in Figure 24. These areas may either be sheltered from or exposed to the prevailing direction of storm motion more than the smoothed coastal direction would suggest. Differences between these coastal directions on

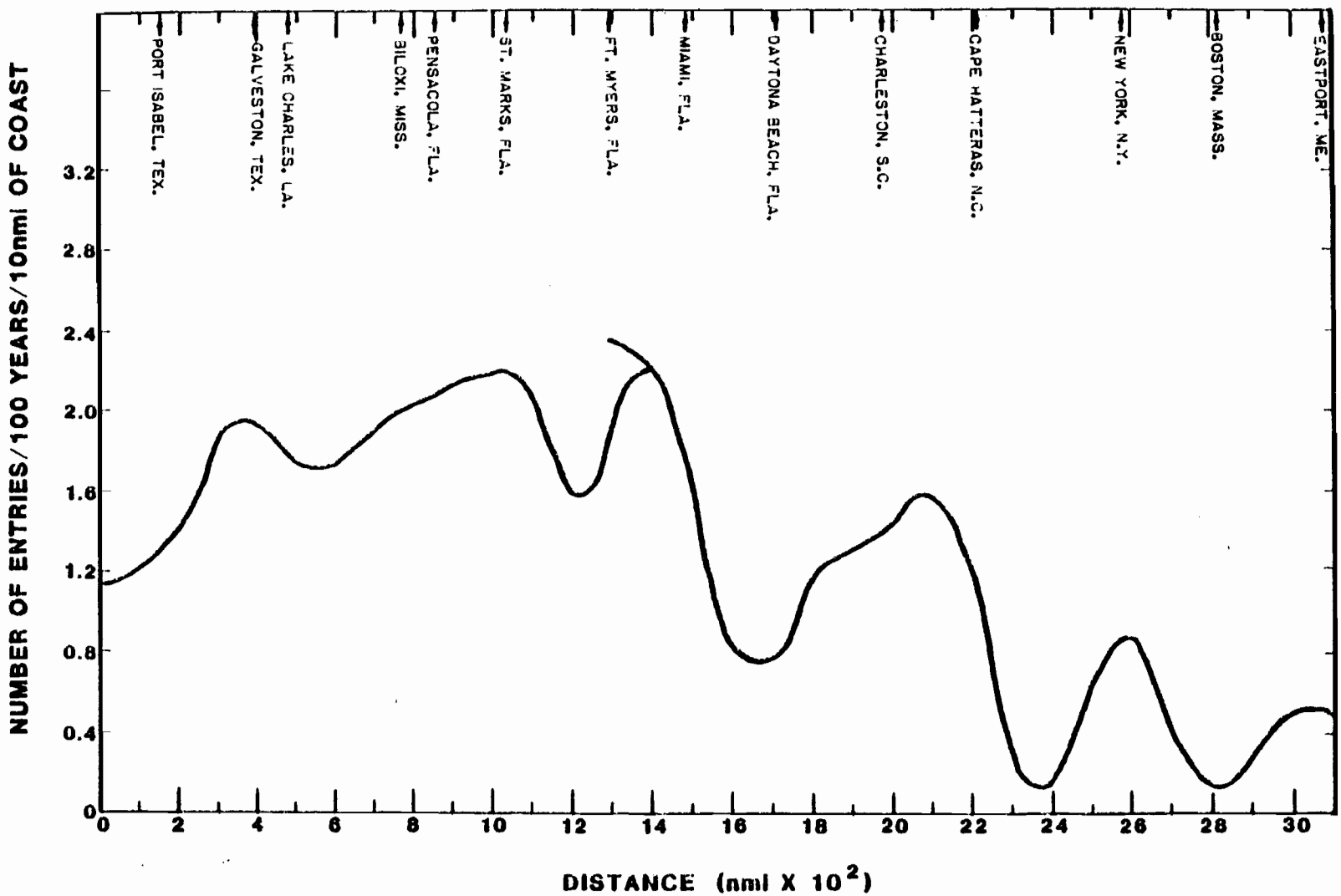

Figure 27.--Frequency of landfalling tropical cyclones (1871-1984) for the Gulf and Atlantic coasts of the United States.

the Gulf coast may be large enough to cause significant differences in frequencies of landfalling tropical cyclones obtained from the direct-count method. The effect of the coastal orientation on the frequency count can be illustrated by differences in frequencies between the north-south segment of the southern portion of the west coast of Florida and the east-west segment of the Florida Keys. Because of the coastal orientation, the west coast of Florida is subject to landfalling storms from the southwesterly direction, while the Florida Keys are at risk from both the southwesterly and southeasterly directions. The coastal extensions discussed in Section 6.2.1 helped in analyzing the data near the southern tip of Florida.

Other areas that required special attention are the Cape Hatteras area and the Apalachee Bay area. The treatment of a discontinuity in the track count at Cape Hatteras was discussed in Chapter 5 (sec. 5.3). Assessing the frequency with which tropical cyclones struck the coast along the Gulf of Mexico was more complicated than for the Atlantic coast because of the small angle between prevailing track directions and the coast, on the one hand, and varying coastal directions on the other hand. In order to treat these problems in the Gulf, we also made use of the track-density method in which storm paths are considered independent of coastal orientation. For a detailed discussion of this approach, see the Appendix in TR 15.

6.2.2 Discussion of Results

Figure 27 reveals that the range of occurrence of landfalling tropical cyclones over a 100-yr period varies from a minimum of 0.1 storms per 10 nmi of smoothed coastline near Boston, Massachusetts, to a maximum of 2.2 in the middle of the Gulf coast of northwest Florida and the Florida Keys. A frequency of close to 2.0 storms per 10 nmi per 100 years appears to the south of Galveston, Texas. Highest frequency of landfalling tropical cyclones on the east coast is in southern Florida, and a comparatively high frequency appears to the south of Cape Hatteras, North Carolina. The frequency of entries drops off rapidly from Miami to Daytona Beach, Florida and from Cape Hatteras northward to Maine, except around Long Island.

6.2.2.1 Areas of High Entry Frequencies.

6.2.2.1 (a) Northwest Florida. The high frequency of storm entries along the northwest Florida coast near St. Marks suggests that this stretch of the coast is a favorable crossroad for tropical cyclones that pass east of the Yucatan Peninsula and those that recurve in the Gulf of Mexico. This coastal region is also vulnerable to Atlantic storms that cross the Florida Peninsula.

6.2.2.1 (b) South Florida. A maximum in landfalling storm frequency appears near the tip of the Florida peninsula and along the Florida Keys. The southernmost portion of this area is exposed to both Atlantic and Caribbean hurricanes. Generally, tropical cyclones strike the east coast of south Florida from an east-southeasterly direction - a predominant direction for Atlantic hurricanes before recurvature. The west coast of south Florida is vulnerable to tropical cyclones moving in a northeastward direction after recurvature. The most frequent areas of recurvature in the month of October have been near the Bahamas and in the northwestern Caribbean (Cry 1965).

6.2.2.1 (c) Upper Texas Coast. The comparatively high frequency along the upper Texas coast is partially caused by the predominantly westward-moving storms in the Gulf of Mexico during the early hurricane season. Only six storms have recurved and moved northeastward (away from the southern Texas coast) during the months of June, July, and August since 1901. These early season storms accounted for more than half the total number of storms that struck the Texas coast.

6.2.2.1 (d) Cape Hatteras. The high frequency of storm entries just south of Cape Hatteras, North Carolina (1.6 storms per 10 nmi per 100 years), is the combined result of the number of northeastward moving storms that reentered the North Carolina coast after exiting the east coast of Florida and Georgia in addition to hurricanes of Atlantic origin that moved in a northerly direction after recurvature. Almost 90 percent of the storms entered the North Carolina coast, south of Cape Hatteras, in a northwesterly to a northeasterly direction.

6.2.2.2 Areas of Low Entry Frequencies. The frequency of storm entries is less than 1 per 10 nmi of coastline per 100 years over the northern section of the east coast from a point some 50 nmi north of Cape Hatteras northward to the Canadian border and also in the vicinity of Daytona Beach, Florida. The significantly lower frequency of entries north of Cape Hatteras, North Carolina, is easily understandable. With a few exceptions, hurricanes recurving south of Cape Hatteras either enter the North Carolina coast or move northeastward away from the United States mainland.

6.2.2.2 (a) East Coast. Colon (1953) has shown the locus of points of highest frequency of recurvature for different months of the hurricane season. Hurricanes off the east coast of the United States frequently recurve between latitudes 27° and 29°N during the months of July and September. For the other months of the hurricane season, recurvatures occur at latitudes farther south, following the shift of the subtropical ridge (Alaka 1968). The northern limit of hurricane recurvature at about 29°N appears to coincide with an area of minimum frequency of landfalling hurricanes along the east coast. Hurricane Dora of September 1964 was the only hurricane that struck the northeastern Florida coast in recent years.

6.2.2.2 (b) Gulf Coast. The relative minimum in storm entry frequency along the west coast of Florida (compared to the mid-Gulf coast and the southern tip of the Florida peninsula) can be explained by the prevailing westward motion of hurricanes of Atlantic origin. The relatively low frequency of storm entries (before 1985) along the Louisiana coast west of the Mississippi Delta is most likely due to sampling variability. The inclusion of storm data for the 1985 and 1986 hurricane seasons which were not included in this study would have increased the entry frequency for this area.

6.3 Frequency of Exiting Tropical Cyclones

6.3.1 Analysis

The frequency of exiting tropical cyclones was defined by a subjective smoothing of 50-nmi segment coastal crossings. These counts were obtained from the storm track information previously cited. A total of 152 tropical cyclones exited the Atlantic coast and 20 from the Gulf coast during the period 1871-1984. The shape of the coast, relative to storm tracks, and meteorological considerations were taken into account in the smoothing. For storms exiting the coasts of

Florida, consistency in frequency and direction of movement was maintained with the frequency of landfalling storms on the opposite coast. The objective smoothing technique was not used in this analysis because the observed data are closely related to the geographical features of the coasts and because of physical considerations (such as direction of storm motion). For these reasons, the smoothing of sampling variations of exiting storms that concentrated in these areas of the Atlantic coast was done subjectively, taking into account meteorological factors.

6.3.2 Results and Discussion

Figure 28 shows the smoothed frequency distribution of exiting tropical cyclones. This curve indicates high frequencies along the coasts of northern Florida and Georgia and along the North Carolina coast north of Cape Hatteras.

6.3.2.1 Gulf Coast. The comparatively few exiting storms along the northern portion of the west coast of Florida agrees with the decrease of landfalling storms northward along the Atlantic coast of Florida. A local maximum of exiting storm frequency occurred near Fort Myers, Florida.

6.3.2.2 Atlantic Coast. The maximum frequency of exiting storm occurrence appears near Jacksonville, Florida, near milepost 1800, with 3 storms per 100 yr per 10 nmi of the smoothed coastline (see fig. 28). The frequencies decrease southward with 2.2 storms/100 yr/10 nmi near Daytona Beach, 1 storm/100 yr/10 nmi near West Palm Beach, and 0.3 storms/100 yr/10 nmi near Miami, Florida. The frequency diminishes rapidly north of Jacksonville. Higher values appear between Cape Hatteras, North Carolina, and Cape Henry, Virginia.

Many exiting storms along the Atlantic coast originally were eastward-moving storms in the Gulf of Mexico. They can also be traced to storms that recurved over the Gulf or over the Florida peninsula south of the 29th parallel and moved northeastward north of the subtropical ridge. This last group accounts for the high frequency of exiting storms over the northeastern portion of the Florida peninsula. The concentration of exiting storms just north of Cape Hatteras and Cape Cod reflects the orientation of the coastline and the comparatively high counts of entering storms south of these capes.

6.3.2.3 Application in Tide-Frequency Analysis. The treatment of exiting storms in tide-frequency analysis for the area north of Cape Hatteras was considered by Ho and Tracey (1975). They noted that grouping the parameters into fewer class intervals was sufficient for storm-tide computations because exiting storms produced lower tides. They concluded that exiting storms made little contribution to the overall storm-tide frequencies. Figure 29 (from Ho and Tracey) is a graph of tide frequencies at Wright Monument, North Carolina, for several classes of storms. Curve 'd' shows the computed frequencies of exiting storms contributing little to the total tide frequencies. Such minimal contributions from exiting storms can be attributed to lower intensities associated with them and from dynamic ocean conditions associated with exiting storms. All things being equal, exiting storms give smaller surges than landfalling storms. Speed of storm motion works inversely for surge generation between exiting/landfall storm.

Sensitivity tests should be conducted to determine whether omission of the contribution of exiting storms could affect the desired level of accuracy of the overall storm-surge frequencies. Exiting storms on the Florida coasts should be considered because of their generally higher frequency of occurrence and stronger

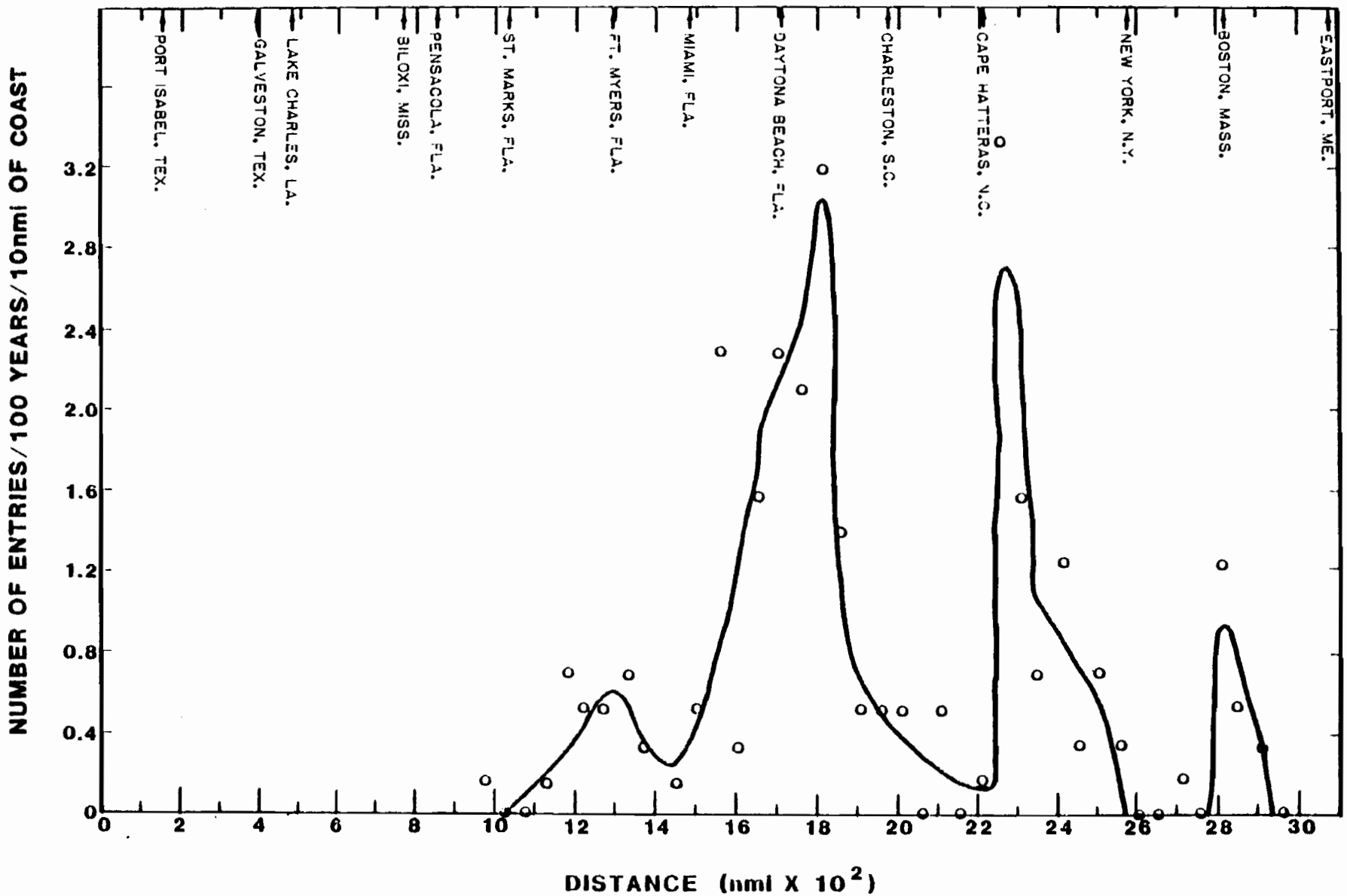

Figure 28.--Frequency of exiting hurricanes and tropical storms (1871-1984). Curve fitted subjectively.

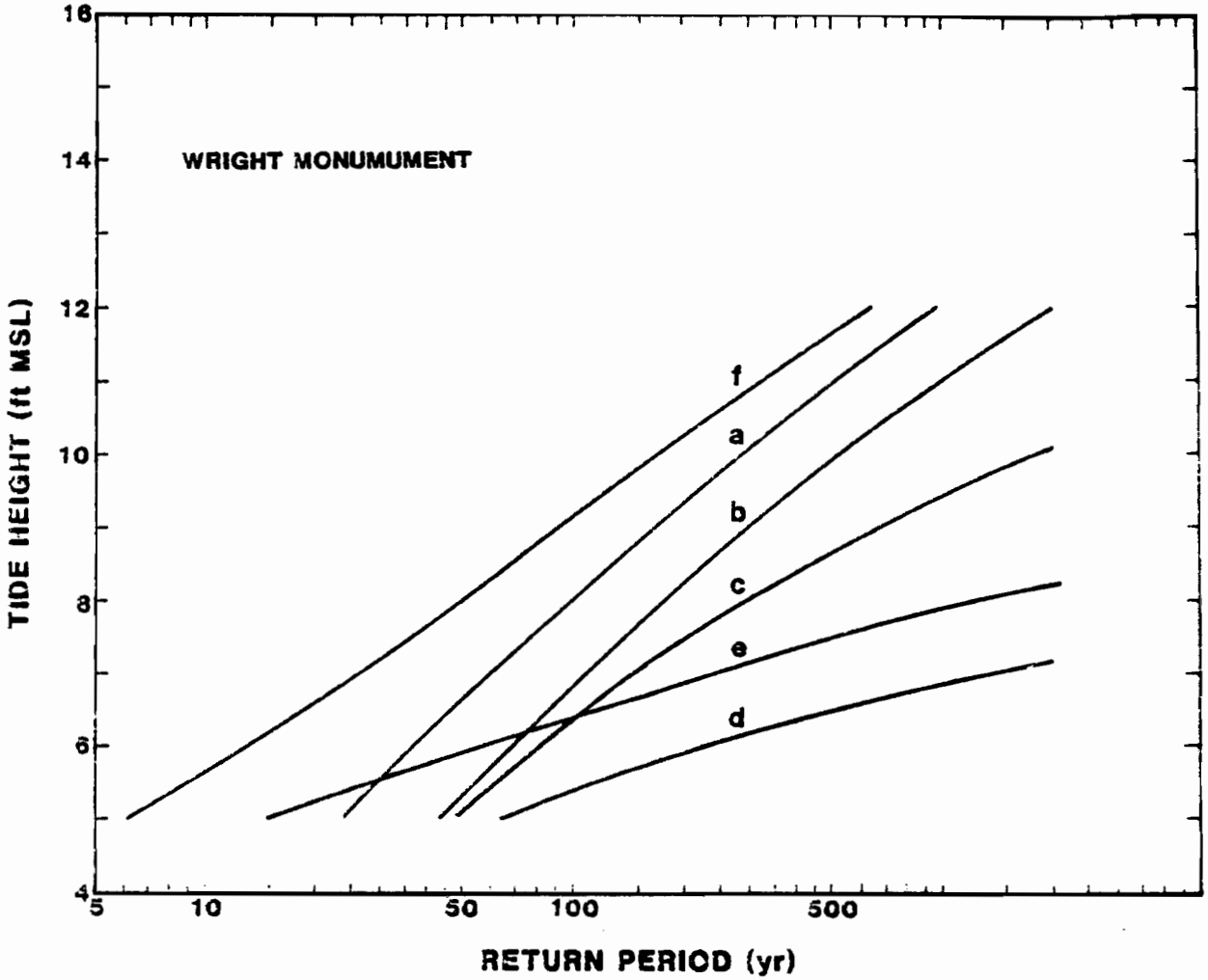

Figure 29.—Tide frequencies at Wright Monument, North Carolina, for several classes of storms: (a) landfalling, (b) alongshore, (c) inland, and (d) exiting hurricanes and tropical storms; (e) winter storms; (f) all storms (from Ho and Tracey 1975).

intensities due to limited overland reduction as they move across the relatively narrow Florida peninsula. For estimating exiting storm intensities, the reader is referred to Chapter 10 for consideration of overland filling rates and Chapter 11 for application procedures.

6.4 Frequency of Alongshore Tropical Cyclones

6.4.1 Analysis

The frequency estimates for tropical cyclones that bypassed the coast were based on the same maps and data period used above. A count was made of storms intersecting 5-nmi intervals along lines drawn perpendicular to a smoothed coastline centered at each of the coastal locations (A to Z) in Figure 30. The same storm may have been counted several times as it moved parallel to the coast. The cumulative track counts along each of the 26 lines normal to the coast were plotted against the distance from the coast. A smooth curve was then fit to the data on each of these frequency plots.

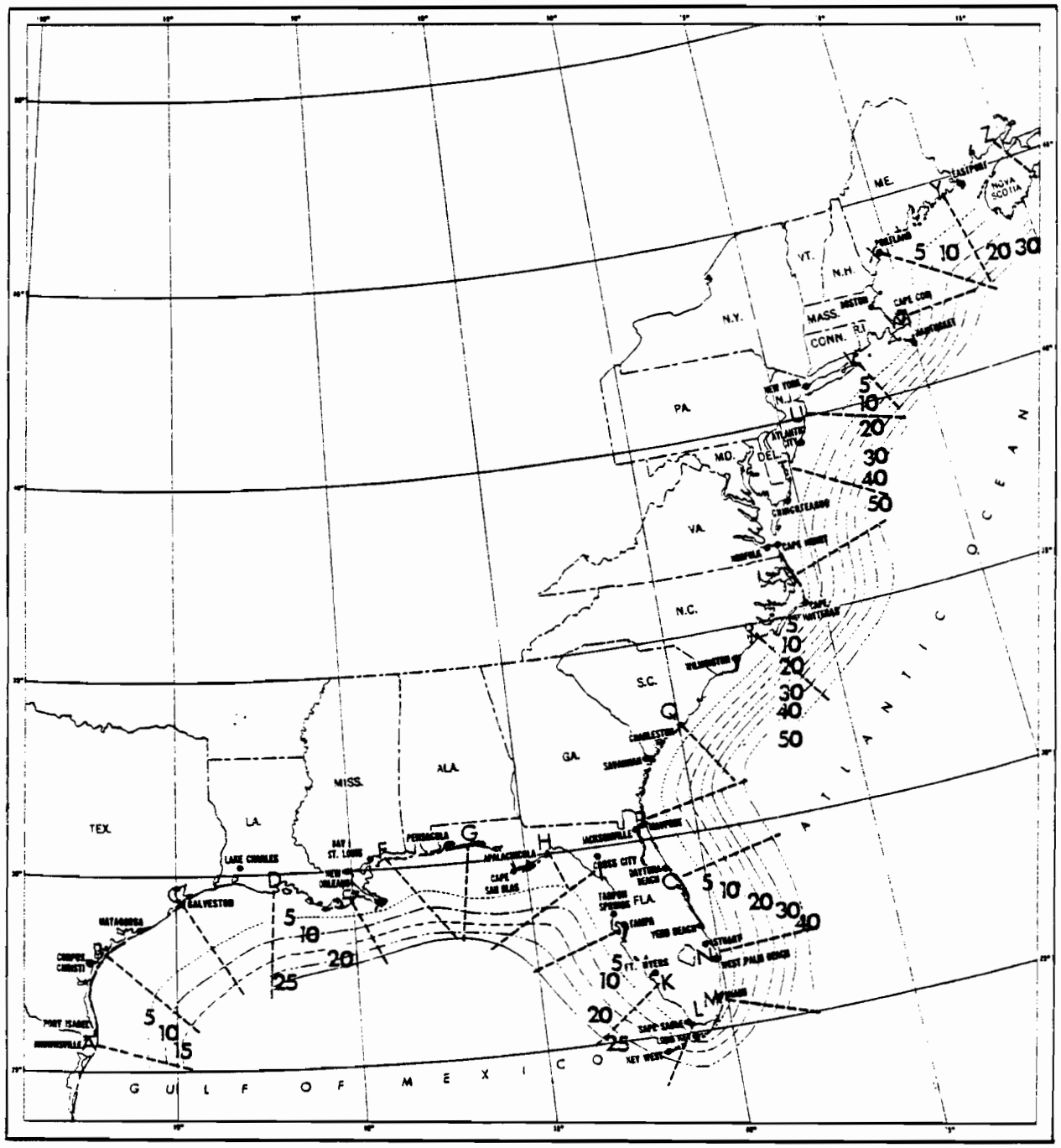

Figure 30.--Accumulative count of hurricane and tropical storm tracks passing the coast at sea (1871-1984). Based on counts along heavy dashed lines shown projected normal to coast.

The frequency distributions were smoothed subjectively both along the coast and perpendicularly outward. These results are shown on Figure 30 by isolines of accumulated number of storm tracks bypassing the coast at sea for the period 1871-1984. We then read from the map accumulated track counts at discrete distances of 10, 20, 30, 50, 75 and 100 nmi from the coast and plotted them as alongshore profiles. Additional track counts and frequency plots were made at close intervals near areas where the alongshore profiles fluctuated greatly because of either a geographic protrusion or a concave coastline. Analysis was then undertaken to obtain a set of smooth frequency curves for the Atlantic and Gulf coasts. The resultant curves are shown in Figures 31 and 32 depicting the accumulated storm track counts in storms per 100 years at selected distances off the Gulf and Atlantic coasts, respectively.

6.4.2 Results and Discussion

Figure 30 reveals that the maximum concentration of alongshore storms occurred off Cape Hatteras, North Carolina. Fewer than five tropical cyclones bypassed within 50 to 80 nmi off the coasts of northwest Florida, Alabama, and Mississippi and within some 100 nmi of the Texas coast. The higher values off the Mississippi Delta may be caused by geographic protrusion. There is a high frequency of bypassing storms off the coast of Cape Hatteras for the same reason that there is a high frequency of landfalling storms south of Cape Hatteras. The gradient at a distance of 100-150 nmi off the Atlantic coast indicates that storms frequently traverse at some greater distances off the coast rather than bypassing near the coast. This may be explained by the existence of the semi-permanent high pressure system (the Bermuda High) in the Atlantic and the location of the Gulf Stream off the coast. Atlantic hurricanes approaching these latitudes tend to recurve along the western edge of the high pressure cell. The higher track counts between 100 to 150 nmi off the coast seem to be associated with the mean position of the Gulf Stream. Because of the steep gradient of bypassing storm frequencies at some distance off the coast, caution should be used in determining a representative frequency over finite distance intervals from the coast.

Figure 31 shows a higher number of storms bypassing the Mississippi Delta and the southern tip of the Florida peninsula in the Gulf of Mexico. An analysis of storm track counts passing through two and a half degree latitude and longitude blocks in the Gulf yielded maximum concentration of storm tracks in an area extending from south of the Mississippi Delta to western Cuba (diagram not shown). This explains the high values shown in Figure 31. The minimum values occurred off the Texas coast and the Apalachee Bay area because of the concave coastline in those areas which minimized the count of bypassing storms near the coast. Figure 32 shows similar peaks and troughs in the alongshore profile of bypassing storm frequencies off the Atlantic coast. These extreme values also appear to be associated with geographic features of the coastline.

7. CENTRAL PRESSURE

7.1 Introduction

Central pressure (P_o) is a commonly used index of hurricane intensity. Harris (1959) demonstrated that storm surge height is approximately proportional to the central pressure deficit ($\Delta P = P_n - P_o$), other factors being constant. This chapter develops probability distributions of central pressure for tropical cyclones along the coast.

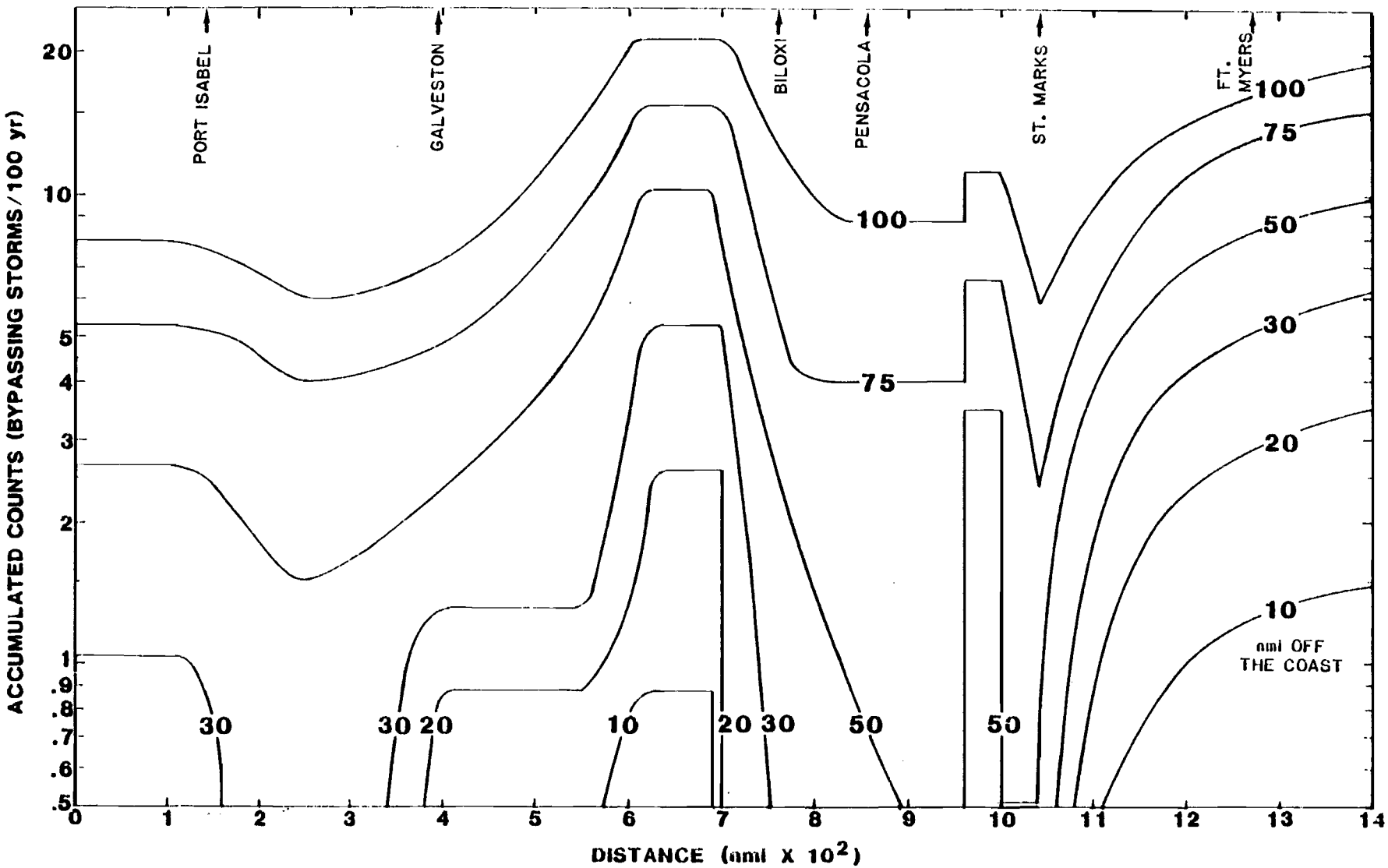

Figure 31.--Cumulative frequency of tropical cyclones bypassing the Gulf coast at selected distances offshore (1871-1894).

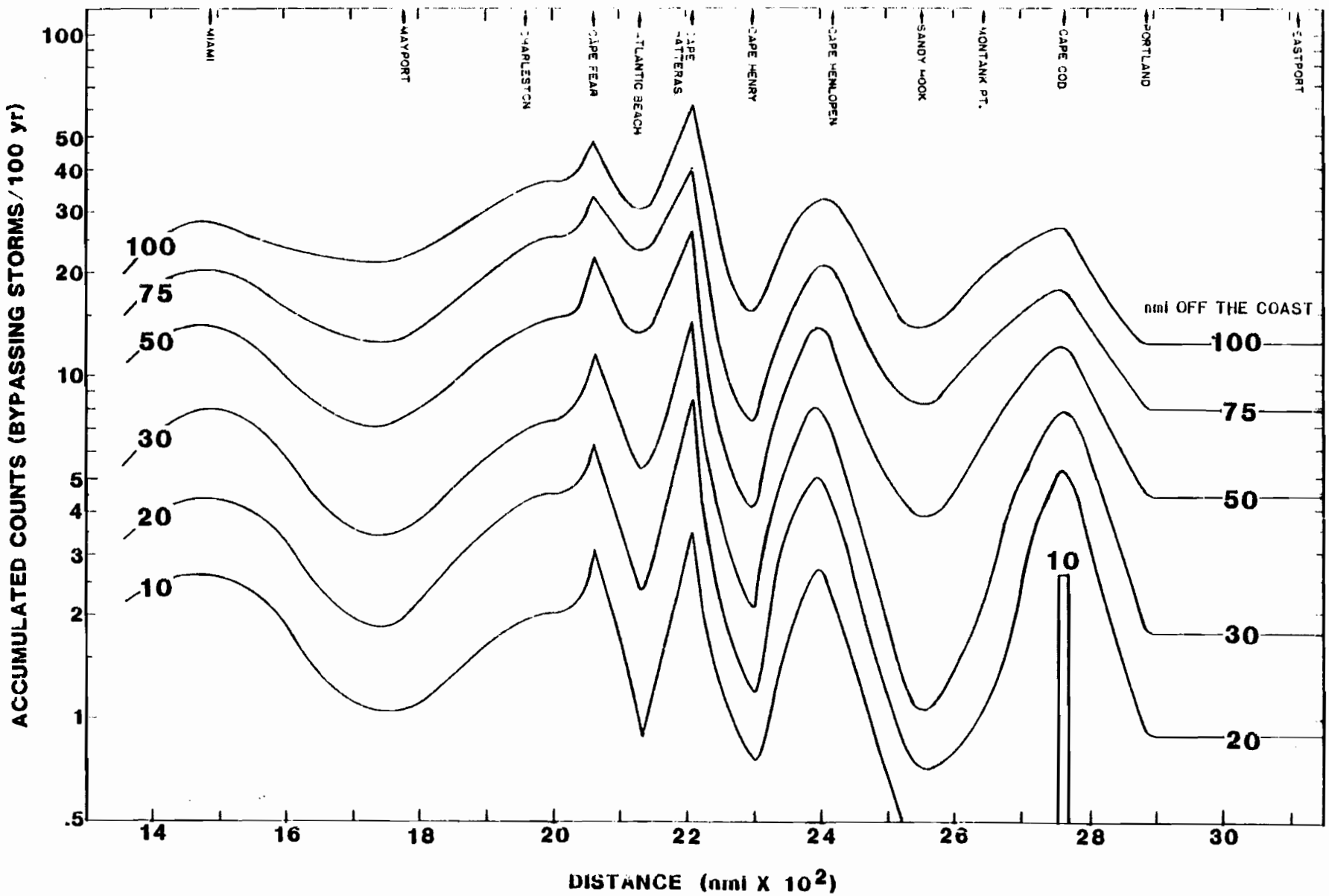

Figure 32.--Cumulative frequency of tropical cyclones bypassing the Atlantic coast at selected distances offshore (1871-1984).

The data on which we developed the P_o probability distributions for the Atlantic and Gulf coasts of the United States have been collected in Tables 1 through 3. Original sources of data are described in Section 2.2. Revisions were made in P_o data from TR 15 where we verified suspect data not accepted in previous reports and, in a very few cases, as an analysis judgment after reviewing all the data. A description of the data analyses was included in Section 2.3, and revised hurricane central pressures were listed in Table 4.

Tables 1 through 3 list parameters of all storms with a central pressure less than 982 mb (29.00 in.) that crossed the Atlantic and Gulf coasts or passed within 150 nmi on the seaward side of the coast. The criterion that central pressure be less than 982 mb was based on the consideration that the computed magnitude of cyclostrophic wind using this pressure value (as described in sec. 2.3.1) is approximately the wind speed required for classification as a hurricane*. With central pressure available for an average of less than one hurricane per year for the period of record for each coast (Gulf and Atlantic), the data in Tables 1 through 3 form a limited sample.

7.2 Analysis

Cumulative probabilities of hurricane P_o were determined from tabulated values listed in Tables 1 through 3 for overlapping zones, generally centered 50 nmi apart along the coast (see fig. 1). The lateral extent of the zone over which the data were pooled was 400 nmi along the Atlantic coast, and 500 nmi on the Gulf coast. We used a shorter distance along the Atlantic coast because latitudinal variations were more important than along the Gulf coast. The 50-nmi criterion was modified in areas where the data were sparse.

On the Atlantic coast, between the mouth of Chesapeake Bay and eastern Long Island, the overlapping 400-nmi zones were separated by 100 nmi, and a single zone was used from Long Island to the Canadian border. Near the southern tip of Florida, hurricanes that passed near Dry Tortugas, and those that crossed the Florida Keys, together with Atlantic coast hurricanes were used to determine the probability distributions of P_o at locations on the Florida Keys. The cumulative probability curves, thus obtained, were used in the extension of the Atlantic coast along the Florida Keys (see fig. 25).

In southern Florida, along the Gulf coast, the overlapping 500-nmi zones were centered 100 nmi apart (instead of 50 nmi). Hurricanes that pass the Florida Keys and make landfall in western Florida usually become weaker as they approach the coast. Parameters for hurricanes passing the Florida Keys are listed in

*Following the criteria used by NHC, hurricanes are defined as tropical storms with winds 64 kn or greater. We realize that there have been storms with hurricane-force winds and central pressures as high as 990 mb south of 35°N. The 982-mb criterion was used to put definite bounds on the data sample. In our statistical analysis, cumulative probability curves for central pressure are extended to cover the full range of hurricanes and tropical storms.

Table 1 and their characteristics near the time of landfall are given in Table 3a. As discussed in Section 7.3.2.1, P_o values tend to be higher north of Cape Sable. Treatment of the data near the southern tip of Florida was handled differently because of the break at milepost 1415 (see sec. 6.2.1 and fig. 25). In determining the cumulative probabilities for P_o at coastal reference points 1350 and 1400 (near Cape Sable), we used P_o values for 6 hurricanes observed near Dry Tortugas instead of the weaker intensities measured near landfall points at some distance north of the points of interest. This was done to minimize the biasing influence of the large number of generally weaker storms to the north.

Tables 1 through 3 include only hurricanes with P_o below 982 mb. However, the track count on which the storm frequency (chapt. 6) is based includes tropical cyclones of both hurricane and tropical storm intensities. In the application of hurricane climatology, frequency of a representative, climatologically specified hurricane of given characteristics is the product of the frequency of all storms and the probability of a storm having those particular characteristics. In order to ensure a higher level of consistency in our analysis, we expanded the central pressure probability distribution to include weaker hurricanes and tropical storms, in the manner described below.

The first step in the analysis of central pressure data was to construct cumulative probability curves for each 400- or 500-mile zone. The magnitude of central pressure versus probability of occurrence was plotted. Determining the probability to be assigned to a data point is commonly referred to as determining the plotting position. A plotting position may be expressed as a percent from 0-100. Probability plotting of hydrologic or meteorologic data requires that individual observations or data points be independent of each other and that the sample data be representative of the population.

Gumbel (1958) proposed five criteria for plotting position relationships. Several plotting relationships have been presented by Chow (1964). Benson (1962) in a comparative study of several plotting position relationships found, on the basis of theoretical sampling from extreme value and normal distributions, that the Weibull relationship provided estimates that were consistent with experience. The Weibull plotting position formula meets all five of the criteria proposed by Gumbel. An evaluation of plotting position formulae is included in Appendix C. All of the relationships give similar values near the center of the distribution, but they vary in the tails. In TR 15, the Hazen plotting position formula was used to assess the probabilities. One objection to the Hazen plotting position is that the return period for the largest event is twice the record length. In the present study, the Weibull relationship was used in assessing the probabilities of all parameters. This plotting position relationship can be expressed as:

$$p = \frac{m}{n + 1} \times 100$$

where p is the probability expressed as a percent of the total number of storms, n, and m is the rank from lowest to highest. To get n for all tropical cyclones, the count of central pressures (up to 982 mb) was adjusted similar to TR 15, using the ratio of hurricanes to the total number of tropical cyclones based on a direct count of storm tracks. The upper part of the curve for each graph is extended smoothly to 1003 mb at the 100-percent level to arbitrarily represent

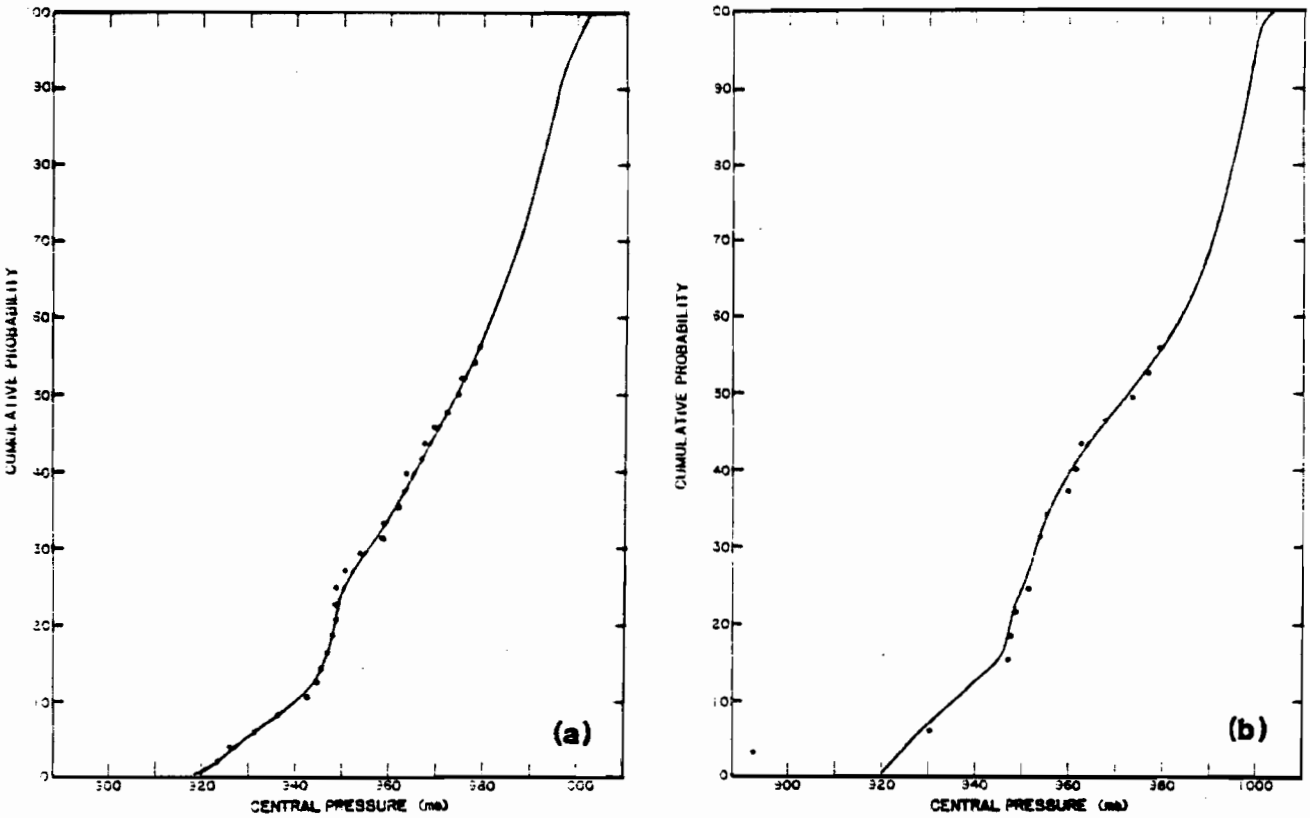

Figure 33.—Cumulative probability curve of central pressure of hurricanes landfalling within (a) 250 nmi of milepost 250, near Corpus Christi, Texas, and (b) 200 nmi of milepost 1600, near Vero Beach, Florida.

tropical cyclones with central pressure greater than or equal to 982 mb. Examples of cumulative frequency curves for two coastal zones are shown in Figures 33a and 33b. The first is centered near Corpus Christi, Texas and the second near Vero Beach, Florida.

It should be noted that the best fit cumulative probability curves were not always the most consistent solution for successive 50-nmi increments. The question of how to deal with an outlier in an extreme value distribution analysis is always debatable. The central pressure determined for engineering design hurricanes (called standard project hurricanes) along the Atlantic and Gulf coasts by Schwerdt et al. (1979) was used extensively as a guide in analyzing the lower end of the cumulative probability curves for central pressure (see fig. 2.1 of Schwerdt's report). In the example given in Figure 33b, central pressure data which was used in plotting the cumulative probability curve for milepost 1600 near Vero Beach, Florida, included a P_o value of 892 mb from the 1935 hurricane. Earlier studies (e.g., Schwerdt et al. 1979) indicated that a hurricane with such a low P_o would have approached the intensity of a "probable maximum hurricane" with a probability of occurrence as much as an order of magnitude less than 0.1 percent. Undoubtedly, this P_o value would be considered an outlier for the purposes of our analyses. In treating this outlier, more weight was given to this storm in the analysis for the Florida Keys, where the hurricane made landfall, than at Vero Beach, Florida. The decrease in intensity of a "standard project hurricane" from the Florida Keys to Vero Beach was also used as a guide in the analysis.

Using the smoothed set of cumulative probability curves of minimum central pressure, we read off the 1-, 5-, 15-, 30-, 50-, 70, and 90-percentile points for each increment and plotted then as alongshore profiles. Analysis was then undertaken to obtain a set of curves representing a consistent view of the probability distribution of P_o for the Atlantic and Gulf coasts. The resultant central pressure values at selected percentiles for each increment were smoothed using the same weighting function employed in Chapter 6 (see sec. 6.2.1.1).

The relative infrequency of hurricanes near the Canadian border and of P_o data near the Mexican border forced us to subjectively adjust the results of the objective smoothing in these end areas. A discontinuity in the analysis with respect to all but the uppermost class interval was found to exist between the chain of Florida Keys and Cape Sable. This was a result of the geographical features associated with the tip of the Florida peninsula. Gulf storms striking the southern tip of Florida are generally weaker than those moving from the east and striking the Atlantic coast of southern Florida and the Keys. Treatment of this area was discussed in Section 6.2.1.

7.3 Results

An inspection of Figures 34 and 35 reveals that there is an overall increase in central pressure from south to north, a well-known fact, caused, in part, by decreasing water temperature toward the north. Distinct minima ranked in order from lowest pressure at the 5-percent level are found on 1) the tip of the Florida peninsula, 2) at the Texas-Mexico border, 3) near Louisiana's Mississippi Delta, 4) at the South Carolina-North Carolina state line, and 5) over the southern New England coast.

The primary maximum occurs near the (until recently) sparsely populated coastal area west of Cross City, Florida (mile 1,100 in fig. 34). Secondary maxima lie near the mouth of Delaware Bay (mile 2,400 in fig. 35), and near Jacksonville, Florida (mile 1,800 in fig. 35). The Jacksonville maximum exceeds the Delaware Bay maximum for the higher percentile levels. Pressures also rise northward along the upper New England coast.

Reasons for the increase in central pressure from south to north include the entrance of colder and drier air at low levels, which destroys the upward slope of the isotherms from outside to inside the circulation and decreases the amount of energy available to the storm. According to Riehl (1954), jet streams at high levels which are detrimental to tropical cyclones are stronger and more common in temperate latitudes. Riehl states that "the arrival of the equatorward margin of a westerly jet stream at high levels will destroy a [tropical cyclone] circulation rapidly since it favors upper convergence, entrance of cold air aloft, subsidence, and drying."

7.3.1 Pressure Minima

7.3.1.1 South Florida Minimum. The lowest accepted sea-level barometer reading (892.3 mb), not including tornadoes, in the Western Hemisphere occurred at Long Key, Florida, in the hurricane of September 2, 1935. This contributed to the south Florida minimum.

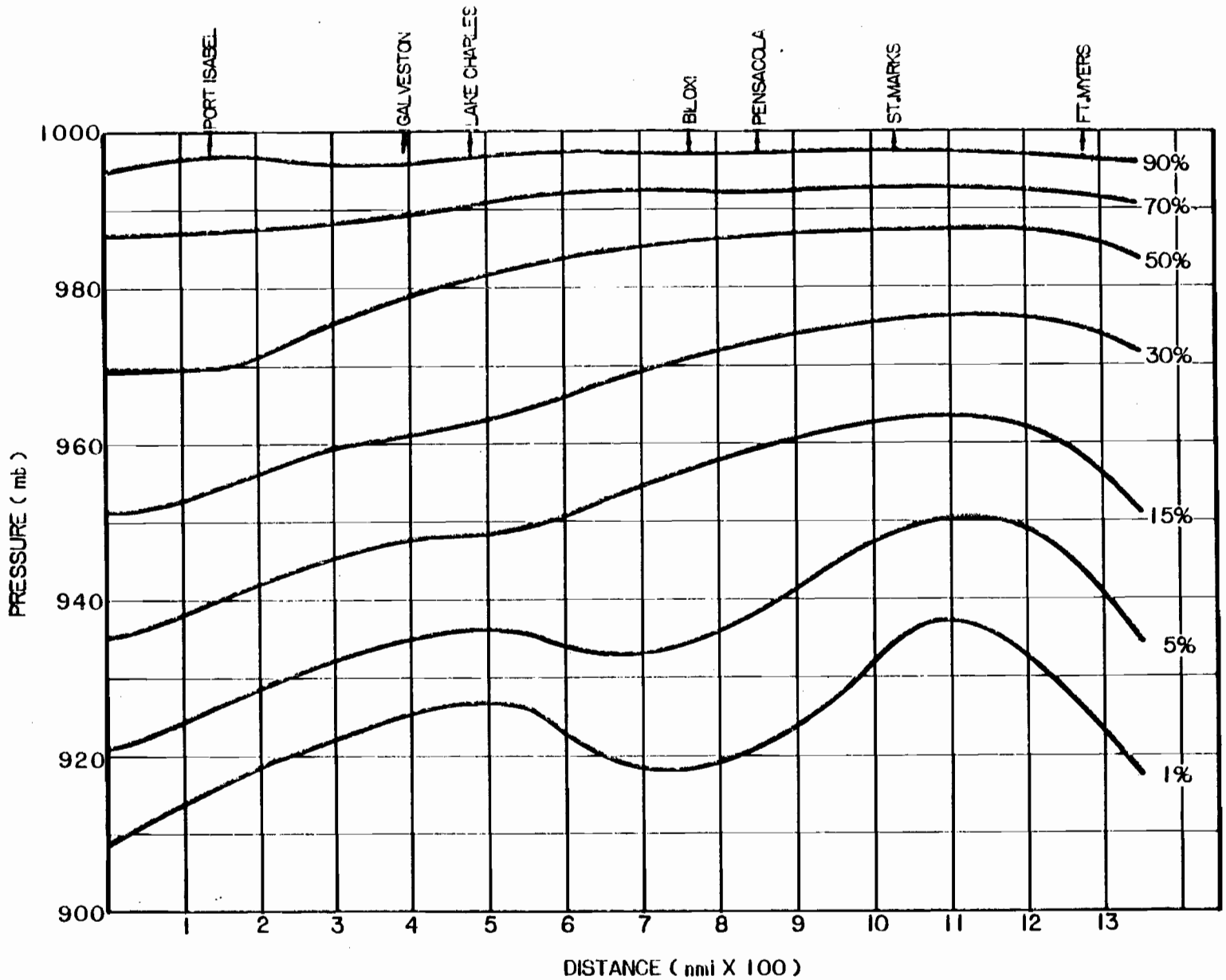

Figure 34.--Probability distribution of central pressure for hurricanes landfalling on the Gulf coast (1900-84). Numbered lines denote the percentage of storms with P_o equal to or less than the value indicated along the ordinate.

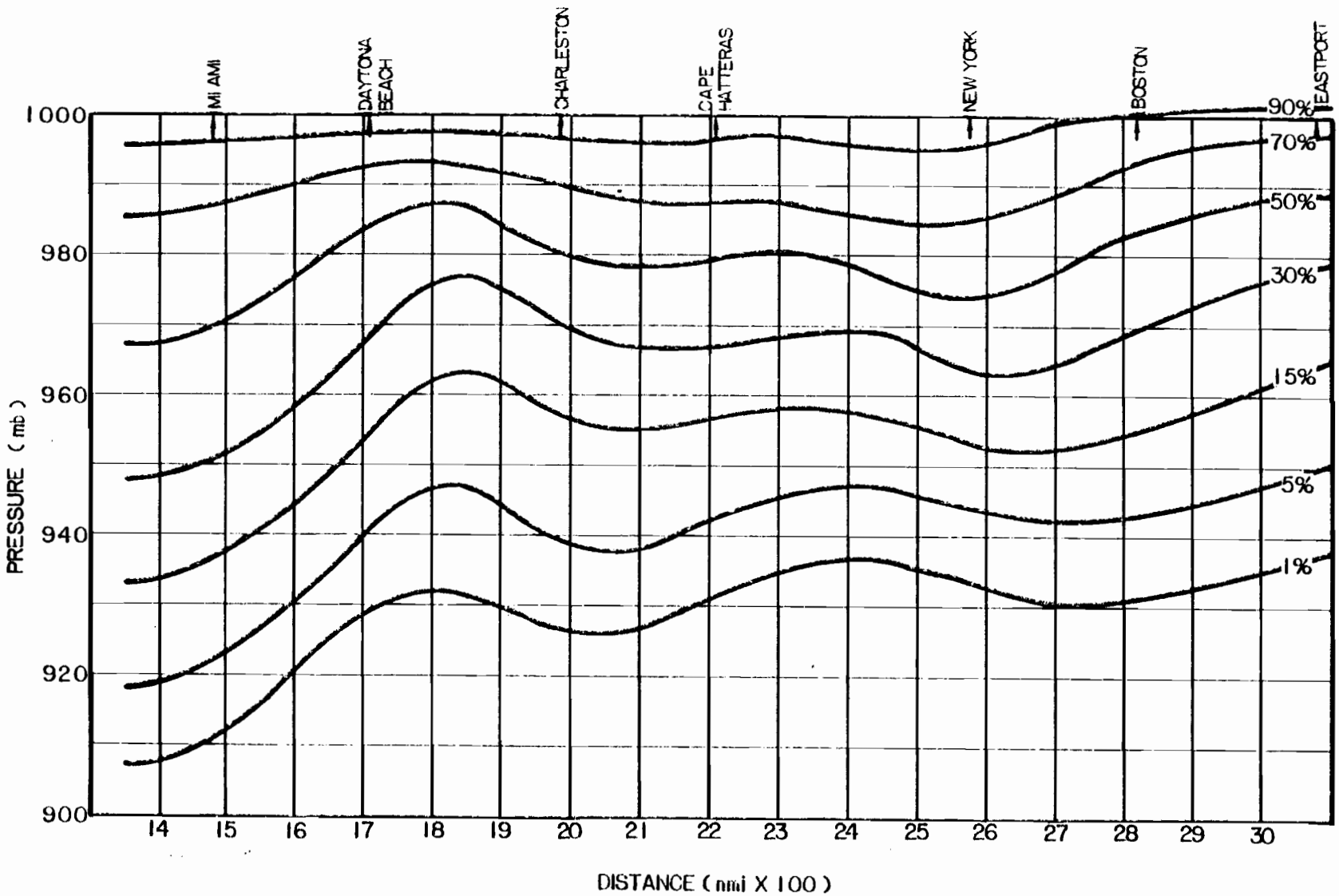

Figure 35.--Same as Figure 34, but for Atlantic coast hurricanes.

7.3.1.2 South Texas Minimum. Hurricane Beulah (923 mb), the third most intense storm (in terms of P_o) included in this study, struck the Port Isabel area of Texas in September 1967. Hurricane Carla (931 mb) and the Galveston hurricane of September 1900 (936 mb), two other notably severe hurricanes, struck the Texas coast between Matagorda and Galveston Islands. There is no reason why Carla or the Galveston storm would not have been at least as strong if they had struck the south Texas coast. If we look at storms outside the bounds of the main area of interest in this study, Hurricanes Janet and Allen also lend strong support for the south Texas minimum. Janet brought a P_o of 914 mb to Chetumal, Mexico (18°N) in September 1955 (Dunn et al. 1955). Allen had the lowest central pressure (899 mb) ever observed in the western Caribbean while passing through the Yucatan Channel on September 7, 1980 (see append. A).

7.3.1.3 Carolinas and Southern New England Minima. The two lowest tropical cyclone central pressures observed along the coasts of Georgia, South Carolina, North Carolina and Virginia, occurred during the passage of Hurricane Hazel (1954) and Helene (1958). Hazel struck the coast near the North Carolina-South Carolina state line. Helene aimed her winds at the same area but turned away to the northeast a few hours before the center would have made landfall. In the Carolinas and in southern New England where the coast projects eastward, there is increased exposure to north-northeastward moving cyclones, some of which, like Hazel and Helene, can be of great intensity.

7.3.1.4 Mississippi Delta Minimum. This minimum was caused principally by Hurricane Camille (1969), and its effect is most prominent in the lower percentiles. Even though Camille passed east of Louisiana on her way to the Mississippi coast, the minimum appears near the mouth of the Mississippi River because this portion of the coast is further south (lower latitude). The data at the 1-percent level indicate a well-defined minimum; the analysis of the 5-percent curve in Figure 34 was lowered to provide continuity with the 1-percent curve.

7.3.2 Pressure Maxima

7.3.2.1 Cross City, Florida, Maximum. The lowest central pressure recorded in a hurricane entering the northern Gulf coast of the Florida peninsula was 958 mb in the storm of September 1950, which entered the coast near Cedar Key. This is not nearly as low as hurricane central pressures observed on the mid-Gulf coast (Mississippi, Alabama, and the Pensacola area) and on the southwest coast of Florida to the south. Is an extremely low P_o here less likely climatologically or is this simply a sampling variation during the period of record? Present indications suggest that there is a real variation and the 1- through 15-percent curves in Figure 34 reflect this judgment.

Our judgment was based on the following. A good many storms have paralleled the west coast of Florida close to shore from the Keys northward. Although the eyes of these hurricanes remained over water, substantial amounts of air entering the storm at the surface had trajectories over the Florida peninsula. Miller (1963) has shown that sensible heat is lost from a parcel of air as it travels overland. His calculations for Hurricane Donna (1960) show that the surface inflow over land is essentially a moist adiabatic process, which leads to the hypothesis that, since the major portion of the eastern semicircle of an alongshore west Florida hurricane is over land, a portion of the storm's surface latent and sensible heat source is removed, the equivalent potential temperature

of the surface air is lowered, and the radial gradient of equivalent potential temperature at the surface is weakened. Movement of a storm out of tropical waters can further weaken the gradient. The Labor Day hurricane of 1935 is a good example of what can happen when an intense hurricane leaves the Florida Keys and heads up the west coast of Florida. After crossing Long Key with a central pressure of 892.3 mb (26.35 in.), the hurricane brushed Cape Sable and paralleled the west coast of Florida for about 30 hours before entering the coast near Dead Mans Bay. By then, the storm had weakened to minimal hurricane intensity. The air mass north of the hurricane and surface water temperatures had remained essentially constant as the storm skirted no more than 50 nmi off the coast for those 30 hours.

Although the area has not experienced a severe storm in over 100 years, it should be noted that the Cross City area is exposed to hurricanes moving in from the southwest. For a storm moving from this direction, the land effect would not be significant. For example, a hurricane could develop over the Bay of Campeche, attain great strength over the central Gulf, and then aim its destructive winds directly at the area as in the storm of October 1842 (Ludlam 1963). Figure 34 is intended to combine these possibilities.

7.3.2.2 Delaware Bay Maximum. The strongest tropical cyclone to move inland on the New Jersey coast during this century was a minimal hurricane (Sept. 1903) with central pressure above 982 mb. Storms heading north-northeastward over the Delmarva peninsula after having entered the coast at a point farther south are more common, but these storms have usually filled to a considerable degree by the time they reach Delaware Bay. The raw data have been deliberately undercut in the Delaware Bay area because our method of data analysis is more sensitive to landfalling storms than to bypassing storms. Most of the hurricanes affecting this part of the coast pass offshore before striking or bypassing the southern New England coast, but it is possible that they could turn into the Delmarva-New Jersey coast. These storms have central pressures comparable with landfalling storms of southern New England. Therefore, in an attempt to provide the best estimate of the underlying population and to ensure consistency along this section of the coast, the curves for the Delaware Bay area reflect both the raw data and the possibility of more intense storms striking the coast.

7.3.2.3 Jacksonville Maximum. The P_o probabilities achieve another high point along the northeast coast of Florida. Again, the shape of the coastline has an effect. The direction of the coastline is from 160° to 340° (measured from north) in this region. When a storm recurves sufficiently to miss the southeast coast, it usually misses the northeast coast. Until 1964, the city of Jacksonville was unique in that it was the only major city on the Atlantic coast south of Connecticut that had never sustained winds of hurricane force in modern times. Hurricane Dora spoiled this fortuitous record in September 1964, lashing the Jacksonville area with 82-mph winds and demonstrating that Jacksonville was <u>not</u> immune from hurricanes.

7.3.2.4 Northern New England Coastal Maximum. P_o rises steadily going from southeastern Massachusetts northward to Canada. The "cold wall" of the Labrador Current contributes to this effect. During August, the month of warmest sea-surface temperatures, water temperatures average between 65° and 70°F from Long Island to Cape Cod. Along the coast of Maine during the same month, the temperature is in the upper 50's - cold enough to give any tropical cyclone an extratropical character.

8. RADIUS OF MAXIMUM WINDS

8.1 Analysis

Cumulative frequencies of R's included in Tables 1 through 3 for the same overlapping zones, centered 50 nmi apart, as used for the P_o analysis were analyzed. R's for southern Florida were treated in the same way as pressure. The same hurricanes were used for both P_o and R. For each 400- or 500-nmi coastal segment, the R values were plotted on cumulative frequency graphs. The percentages were determined by the plotting position formula (see sec. 7.2 and append. C). Examples of the frequency analysis for specific coastal segments are shown in Figure 36. Greater freedom was taken in analyzing the cumulative frequency curves of R, and the final coastal variation of the probability distributions, than with P_o, because the R data were considered less reliable. Because data were sparse along the northern portion of the Atlantic coast, the cumulative frequencies were developed using both landfalling and bypassing storms.

We did not expand the R distribution, as was done with P_o, in an attempt to account for tropical storms that were not included in the analysis. Tropical storms, especially weaker ones, often have no well-defined R, and when they do, it can frequently be as much as a hundred miles from the apparent storm center. Assigning values of R to such storms would be haphazard, at best. Only hurricanes (those in tables 1-3) were considered in the frequency analysis of R along the coast. The R values were determined near the location where P_o applies.

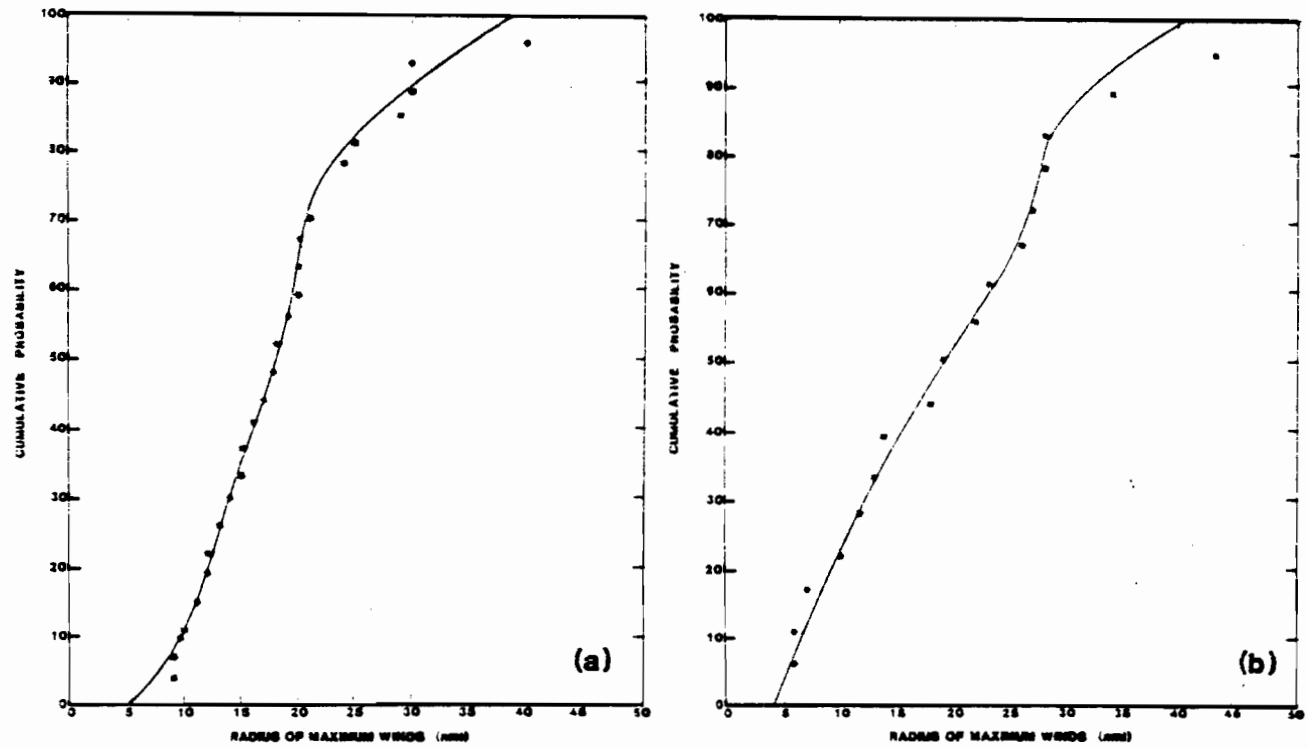

Figure 36.—Cumulative probability curve of radius of maximum winds for hurricanes landfalling within (a) 250 nmi of milepost 250, near Corpus Christi, Texas, and (b) 200 nmi of milepost 1600, near Vero Beach, Florida.

Five discrete probability levels were chosen to portray the results of the analysis. The coastal variation of R for the Gulf coast and the Atlantic coast is shown in Figures 37 and 38, respectively. The data along the west coast of Florida and along the Atlantic coast were limited and were only used to guide analysis of the final probability distributions. In these areas, the final results reflect a higher level of meteorological judgment.

8.1.1 Gulf of Mexico

When the five percentiles for each 50-nmi increment along the Gulf coast were plotted and analyzed, the resulting curves (fig. 37) depicted a trend of increasing R's with latitude, which is consistent with previous studies (e.g., Weather Bureau (1957), NHRP 33). Data proved to be too sparse to obtain cumulative frequencies of R for the central Texas coast southward. The five curves were extended smoothly down the coast to Mexico (about 24°N), keeping in mind that as we proceeded southward along the coast the value of R should not increase with decreasing latitude.

8.1.2 Atlantic Coast

Cumulative frequency variation of R along the Atlantic coast as shown in Figure 38 displays increasing R with latitude. There were only eight observations of R north of Virginia. The smoothing procedure discussed in Section 6.2.1.1 was not applied for these latitudes; rather, subjective smoothing was used to extend the curves to the Canadian border.

8.2 Evaluation of the Analysis

Because of a few additional storms and due to revisions made to several R values previously used in TR 15, our analysis resulted in somewhat different probability estimates for R than in TR 15. The majority of the revisions were decreases in R values.

8.2.1 Gulf Coast

8.2.1.1 Florida and Mexico Minima. As mentioned above, there is a variation of R with latitude, and, as expected, minima occur on both the eastern and western edges of the Gulf of Mexico portion of Figure 37. For example, with the exception of Hurricane Camille (1969), an R less than 14 nmi has not been observed over the central Gulf coast, while four hurricanes with R's less than 14 nmi have affected the western and eastern rims of the Gulf. The analysis shows moderately lower values on the western rim of the Gulf compared to the same latitude on the eastern rim and agrees with NHRP 33, which shows the same trend.

8.2.1.2 Mississippi-Florida Panhandle Maximum. The northernmost extension of the Gulf coast is at Mobile Bay. From what has been discussed so far with regard to variation of R with latitude, it is reasonable to expect the maximum in this general area.

8.2.2 Atlantic Coast

The curves in Figure 38 reflect the fact that the radius of maximum winds tends to increase with latitude between the Florida Keys and Canada. The five probability curves attain their greatest slope between coastal Georgia and the Cape

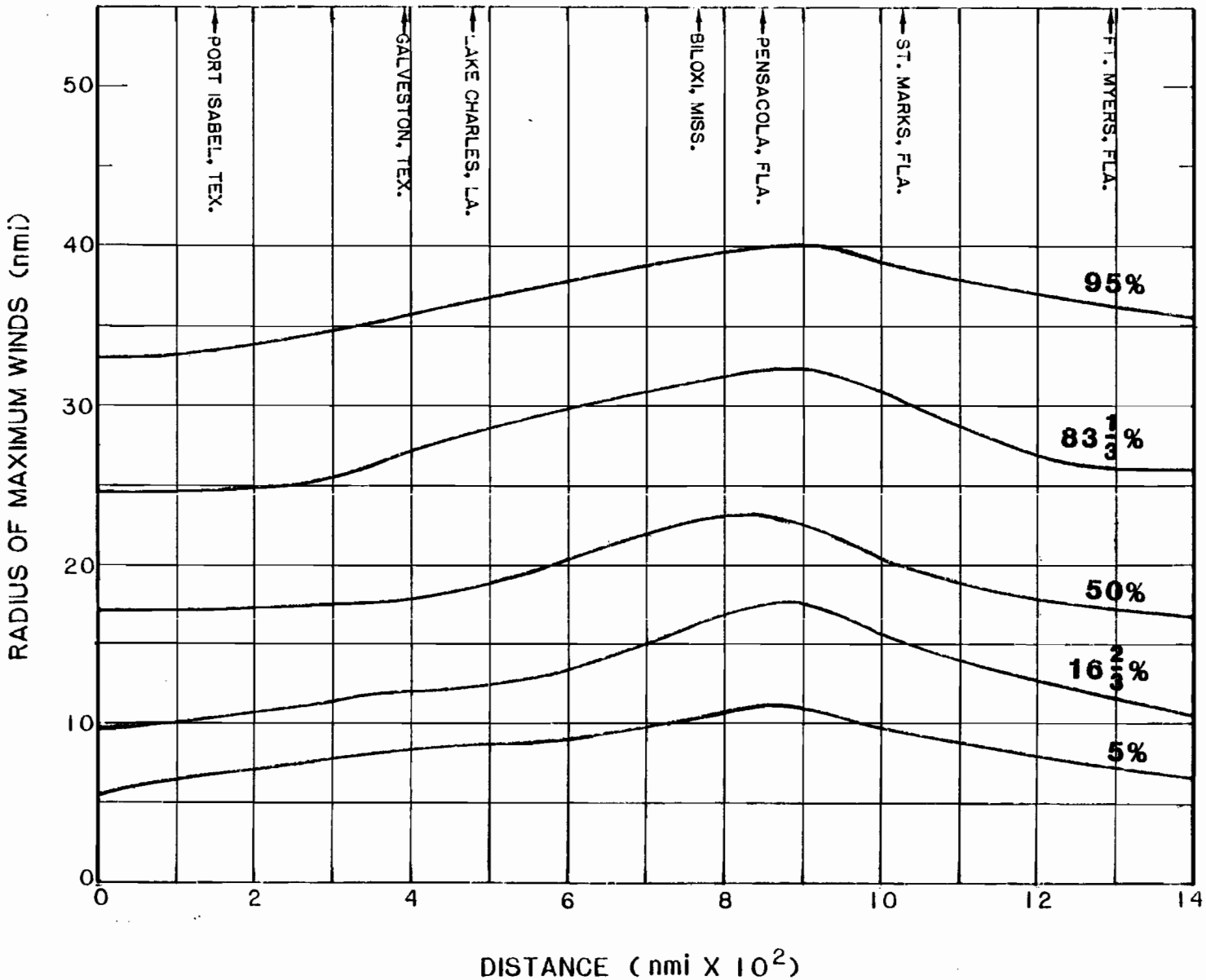

Figure 37.--Probability distribution of radius of maximum winds for hurricanes landfalling on the Gulf coast (1900-84). Numbered lines denote the percentage of storms with R equal to or less than the value indicated along the ordinate.

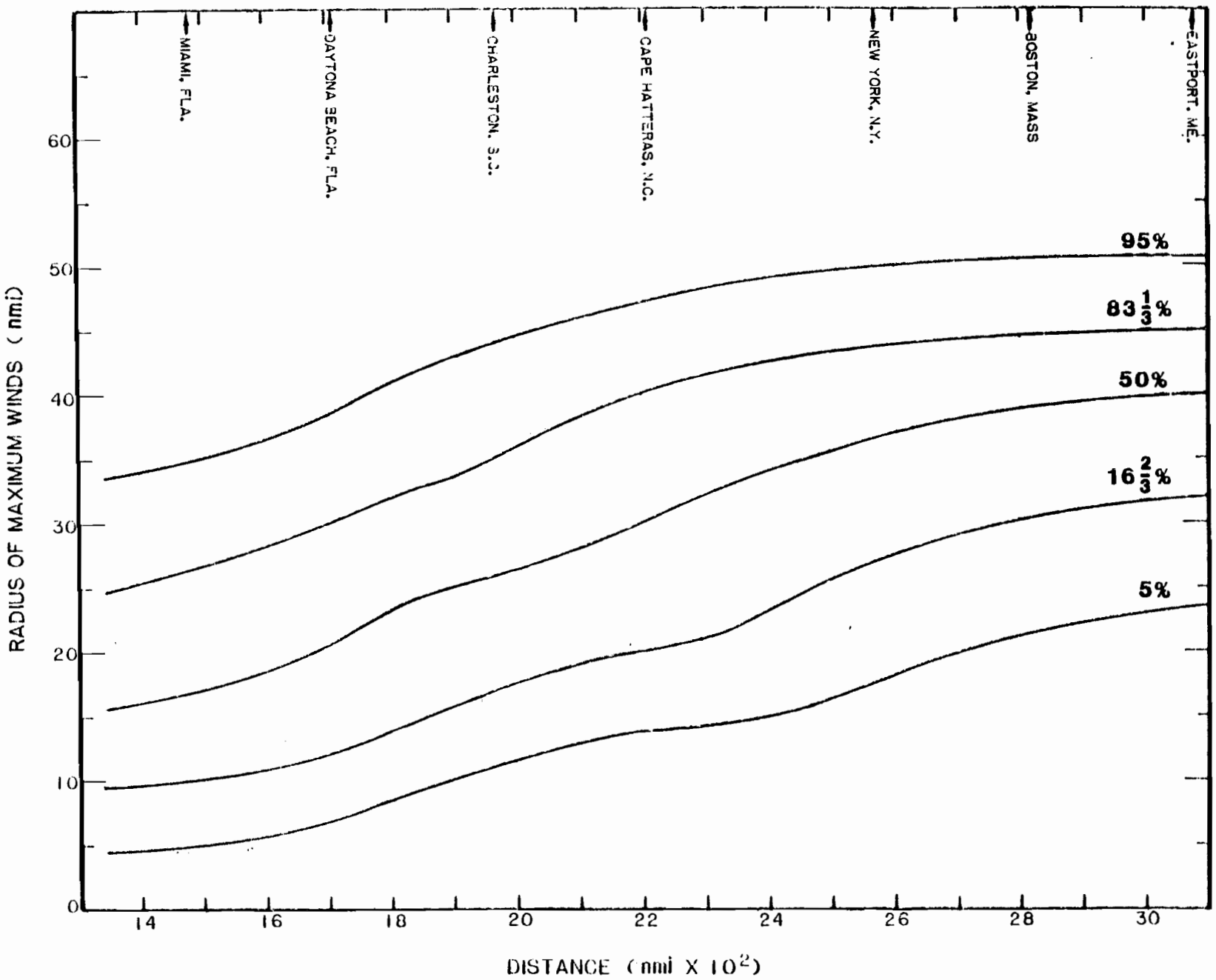

Figure 38.--Same as Figure 37, but for Atlantic coast hurricanes.

Hatteras area. It is in these latitudes that hurricanes most often pass from a tropical to a temperate environment, and it is in this region where one would expect R to show its greatest increase for the reasons discussed in Section 8.3. The slope of the lower probabilities curves change less between Georgia and Cape Hatteras because there are a few storms with small R in the data sample.

8.3 Radius of Maximum Winds for Intense Hurricanes

Observations indicate that hurricanes with very large R's are of moderate or weak intensity. In hurricanes moving northward in the Atlantic and becoming extratropical, R tends to become larger and more diffuse and P_o generally rises. Data from intense hurricanes of record (see table 16 and fig. 14) indicate that the most extreme hurricanes (P_o less than 920 mb) tend to have small R's. The question of interdependence of P_o and R was discussed in Chapter 4. We recommend that an R value of 13 nmi be used for hurricanes with P_o in the range of 908-920 mb, and R = 9 nmi be used with P_o less than 908 mb.

9. SPEED AND DIRECTION OF STORM MOTION

9.1 Speed of Storm Motion

Data for the speed of storm motion is discussed in Section 2.5. Included in these data are a few subtropical storms. We chose to include them since they also have the ability to produce storm surges.

9.1.1 Forward Speed of Landfalling Tropical Cyclones

9.1.1.1 Analysis. Cumulative frequencies of forward speed for landfalling tropical cyclones were determined for the same overlapping zones used for both P_o (sec. 7.2) and R (sec. 8.1). As indicated in Section 2.5, both T and θ could be reliably determined for tropical storms as well as hurricanes, thus increasing the sample size. Cumulative probability curves of forward speeds were determined using Weibul's plotting position formula (see sec. 7.2). Figure 39 shows examples of the cumulative frequency analysis of raw data at two points along the coast (near Corpus Christi, Texas and Vero Beach, Florida). Percentage values at each 50-nmi location were determined from analyses such as Figure 39 for 5-, 20-, 40-, 60-, 80- and 95-percent levels. The values were then analyzed to ensure consistency along the coast. The resulting curves are shown in Figures 40 and 41.

9.1.1.2 Results and Discussion. Figures 40 and 41 show that tropical cyclone speed generally increases with northward progression of each storm, especially after recurvature to a northerly or northeasterly direction. The upper 50 percent of forward speeds increases from 11-17 kn near Daytona Beach, Florida, to 35-53 kn at the northern extent of the United States' Atlantic coastline.

Overall, there was a marked increase in values of T along the west coast of Florida as compared with the variation shown in values of TR 15. In this study, we omitted hurricanes prior to 1900 that had been used in TR 15. This was done to ensure a consistent sampling period for all parameters (P_o, R, T and θ). Before finalizing this decision, however, we examined the effect of omitting storms prior to the turn of the century. We found that there were no significant

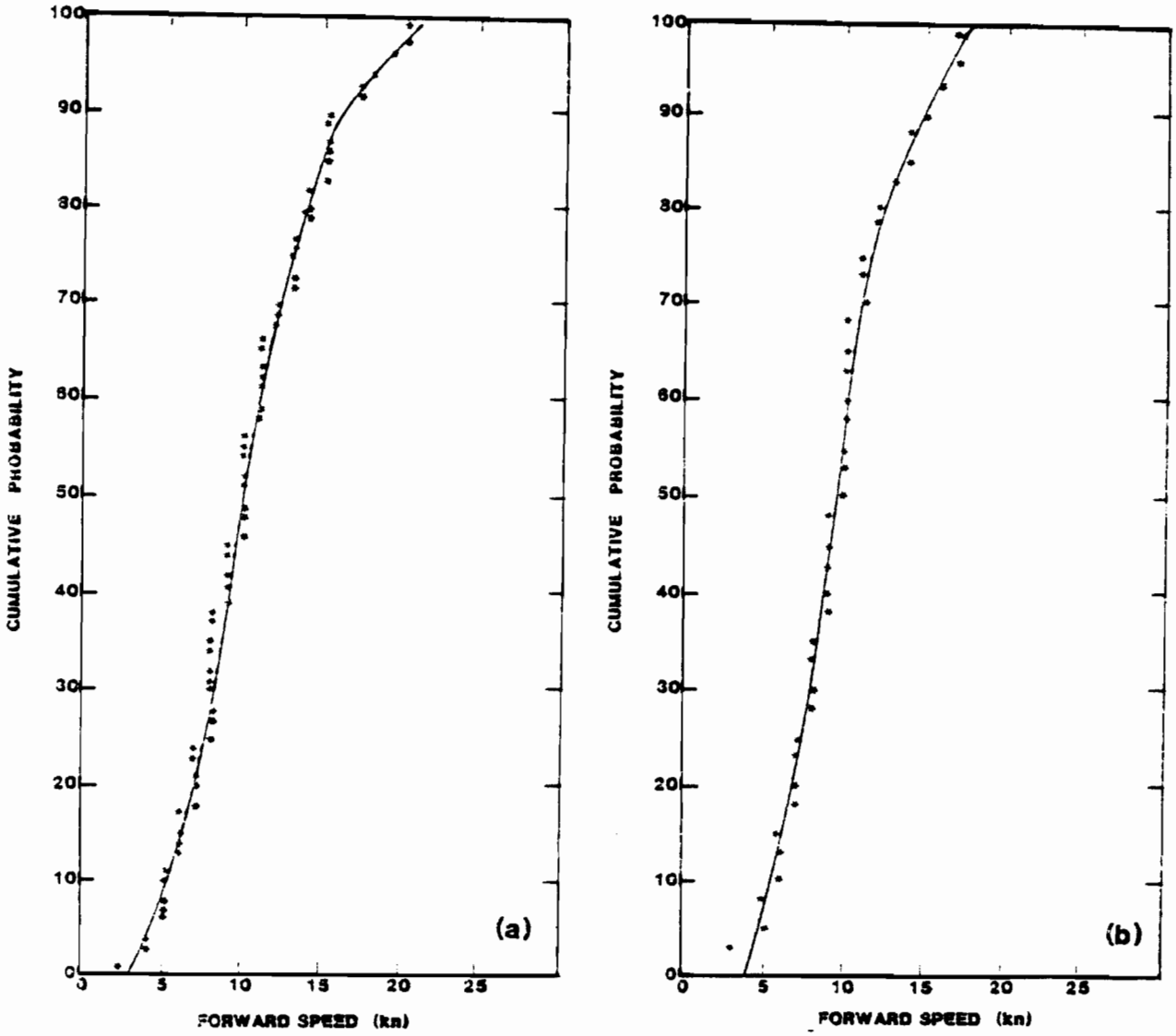

Figure 39.--Cumulative probability curve of forward speed of tropical cyclones landfalling within (a) 250 nmi of milepost 250, near Corpus Christi, Texas, and (b) 200 nmi of milepost 1600, near Vero Beach, Florida.

differences in the probability distribution of speed for hurricanes by this truncation of the period of record. TR 15 had based its speed distribution on hurricanes only. To provide a sample that was consistent with the storms used for the direction distributions, and to increase the sample size, the speeds of tropical storms were used in determining the speed distribution.

The substantial increase in the speeds in the higher percentile levels along the west coast of Florida (see fig. 40) was due, not to the change in period of record, but to the addition of tropical storms. Between coastal reference points 900 to 1300, 12 storms with speeds greater than 20 kn were added to the data sample. All were less than hurricane intensity. Storms that exceed 20 kn at these latitudes generally have become embedded in a broader-scale circulation that usually leads to these higher translation speeds. These same meteorological conditions involve recurvature, usually into an environment associated with horizontal temperature gradients that create conditions that are not favorable to the thermal circulation associated with strong hurricanes (see discussion in sec. 7.3.2.1). Therefore, the faster translation speeds appear to be associated with weaker storms. However, the small number of storms and high degree of

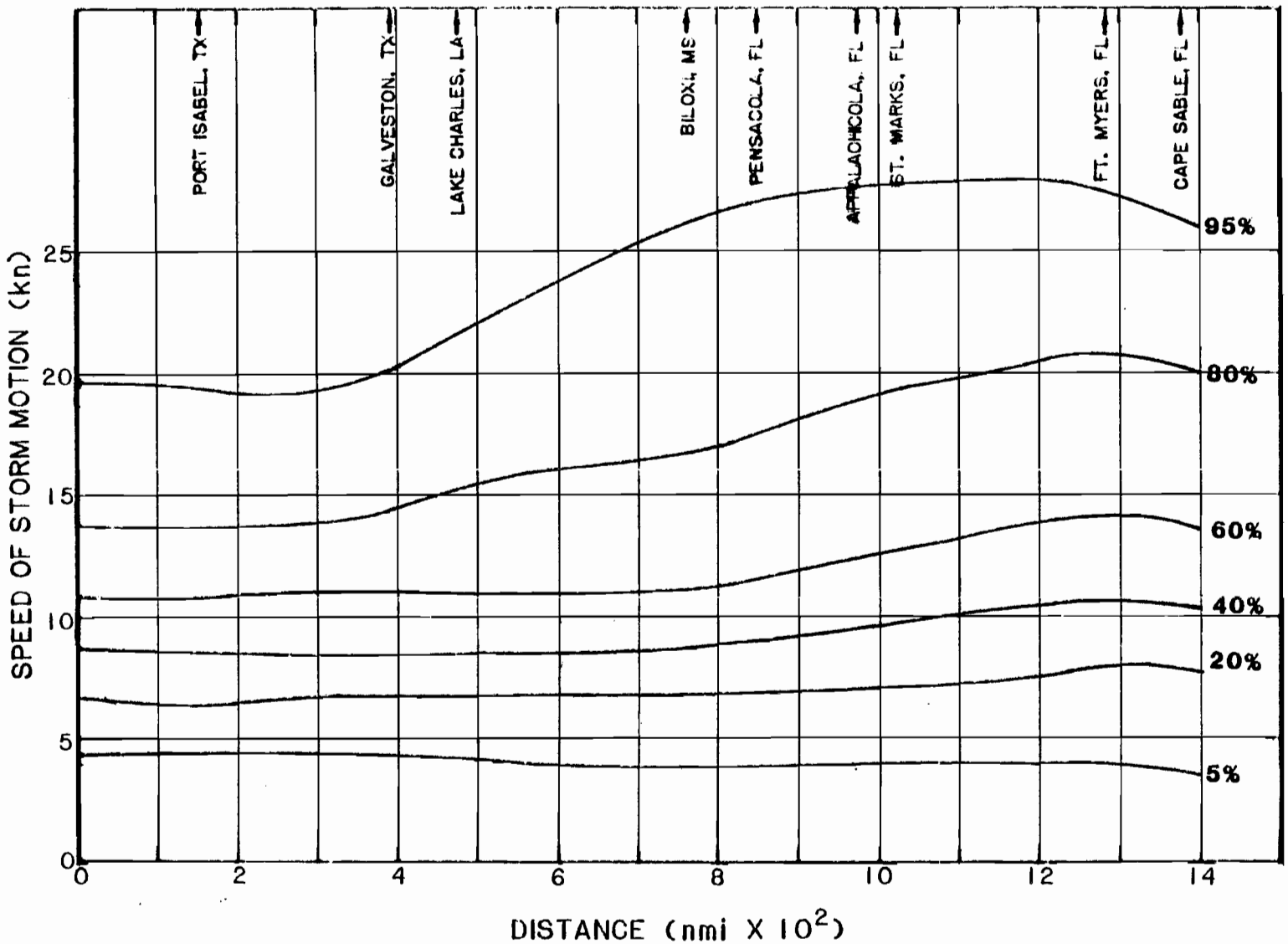

Figure 40.--Probability distribution of forward speed for tropical cyclones landfalling on the Gulf coast (1900-84). Numbered lines denote the percentage of storms with T equal to or less than the value indicated along the ordinate.

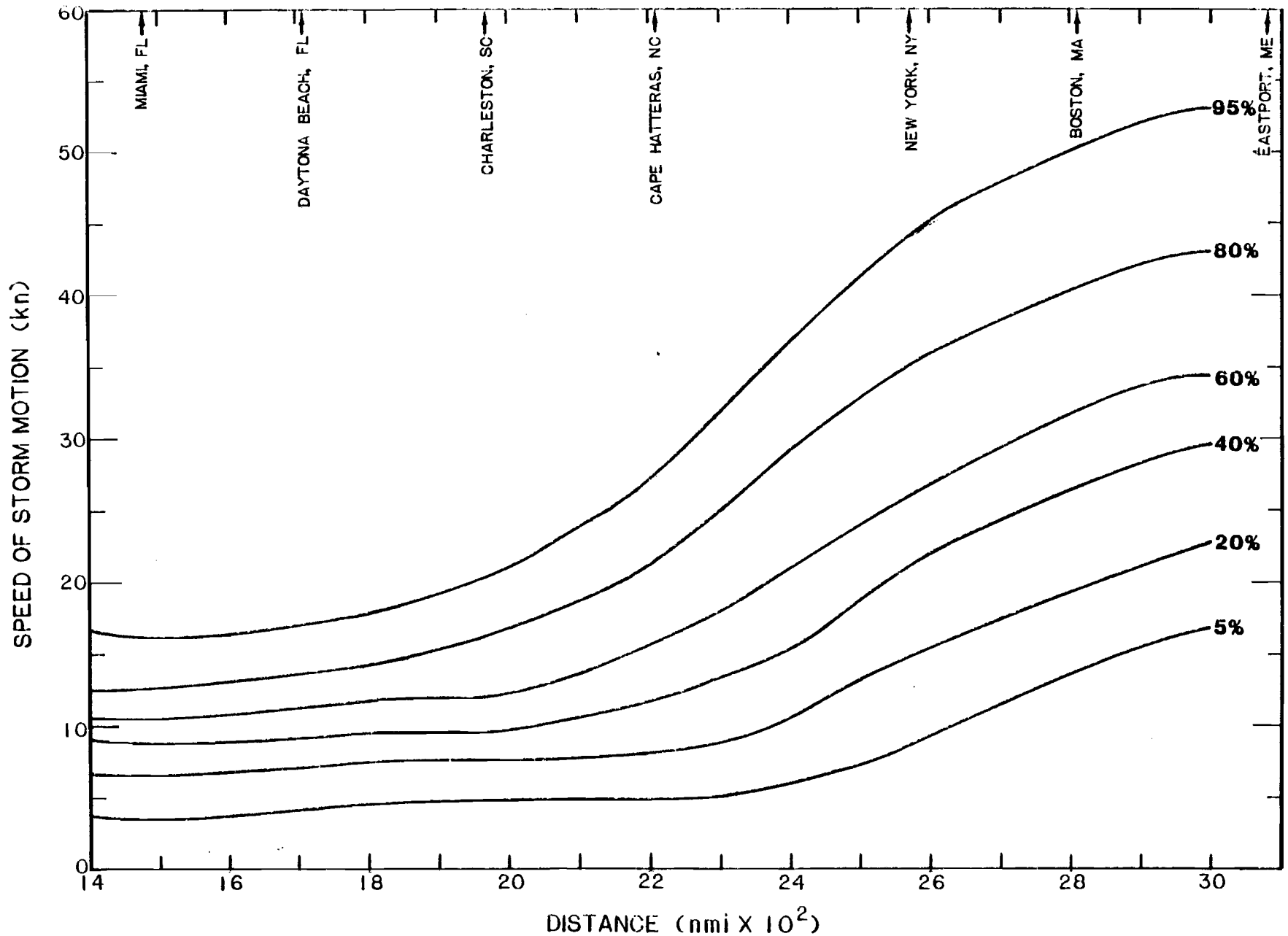

Figure 41.--Same as Figure 40, but for Atlantic coast tropical cyclones.

variability from storm to storm precluded us from establishing whether a joint probability relation actually exists, let alone what form the relation might take. Inclusion of these tropical storms also leads to discontinuities in the speed distributions between the west and east coasts of southern Florida for all but the lowest percentiles.

9.1.2 Forward Speed of Bypassing Tropical Cyclones

Observations of bypassing storms are more limited than for those storms striking the coast, especially for storms from earlier years. Additionally, the frequency of occurrence of bypassing storms, subject to the criteria in this study, is lower than for landfalling storms. Given the high degree of natural variability of tropical cyclones and the limitations just mentioned, we felt it would be unlikely that we could develop an adequate probability distribution for the speed of bypassing storms. Consideration of meteorological factors affecting the speed of storm motion suggests that there is likely to be little difference in the speed distribution between landfalling and bypassing tropical cyclones. The speed is primarily dependent on conditions of the larger-scale meteorological environment. In general, the controlling circulation patterns that affect the speed are not sensitive to coastal orientation, the factor that leads to the segregation of landfalling and bypassing storms. **We recommend using the speed distribution for landfalling storms as a reasonable approximation for bypassing storms.**

9.2 Direction of Storm Motion

9.2.1 Direction of Storm Motion for Landfalling Tropical Cyclones

9.2.1.1 Analysis. Tropical cyclone tracks compiled by Cry (1965) and updated track charts (Neumann et al. 1981) were used in summarizing the directions of storm motion. Directions of landfalling tropical cyclones were measured at the time they crossed the coast. Cumulative frequencies of the entry direction for overlapping 200-nmi zones (100 nmi either side of the central point) were used in plotting cumulative probability curves at 50-nmi intervals along the Atlantic and Gulf coasts. In TR 15, cumulative frequencies were counted for overlapping zones of 75 nmi on each side. In both cases the zones along the coast were smaller than those used for the other three parameters (P_o, R and T) because the landfall directions are totally dependent on coastal orientation which can change significantly over relatively short intervals. The smaller zones minimized pooling inconsistent directions. We used storm data since 1900 in the present study instead of the longer period used in TR 15. We believe the decrease in sample size due to a shorter observational period is partially compensated by the increased number of storms taken from a somewhat larger sampling area.

In areas where the coastal orientation changes significantly within 100 nmi of the point of interest, the direction of entry with reference to the coast was taken into consideration. For example, a storm that crossed the coast from 250° near Key West would not be counted as a landfalling storm for another point on the Florida Keys, some distance to the east. In areas where the coastline turns abruptly, frequency counts were taken over shorter distances. Because of insufficient data north of Cape Hatteras, analyses there were made over larger distance increments.

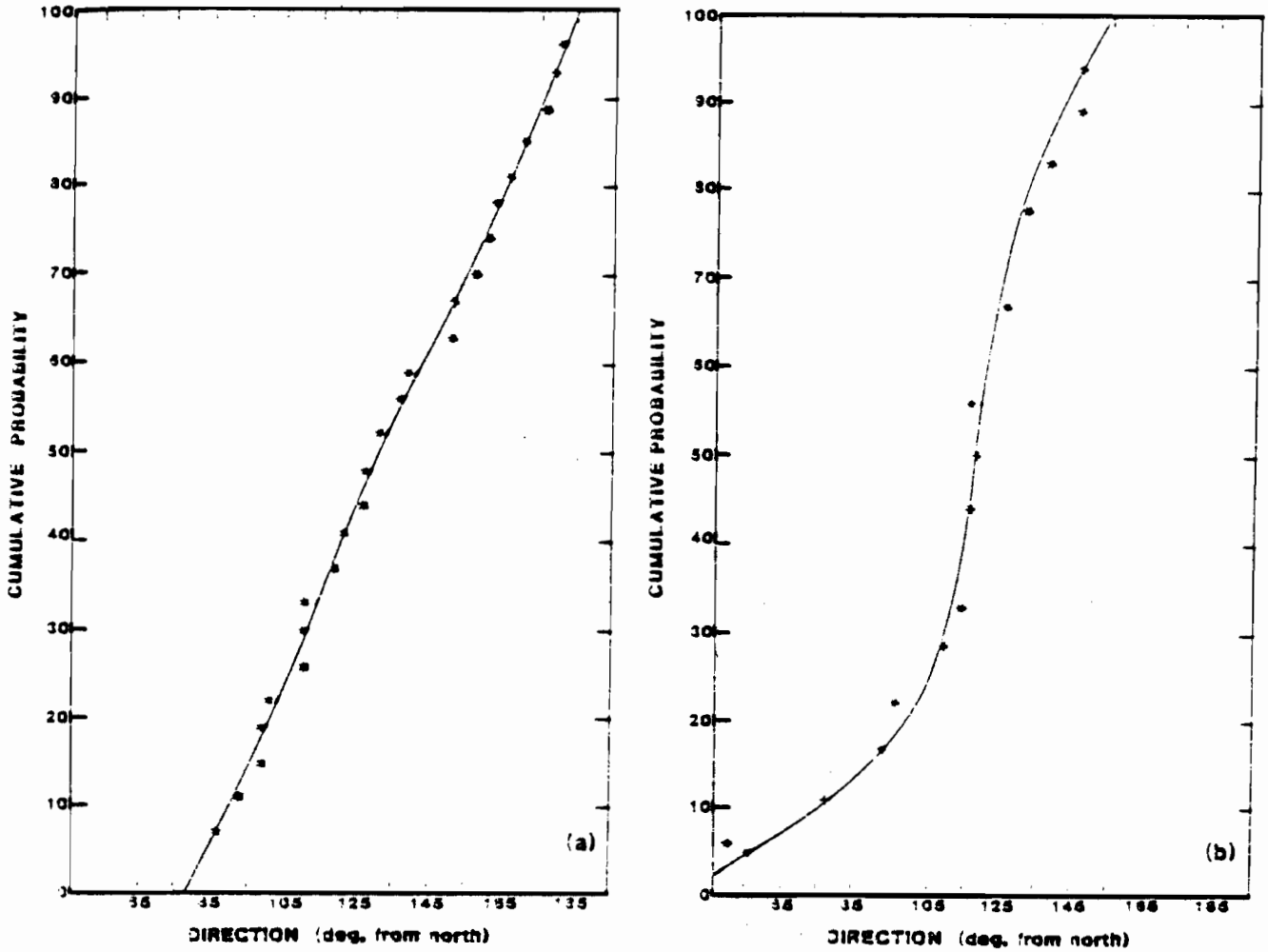

Figure 42.—Cumulative probability curve of direction of motion of tropical cyclones landfalling within (a) 100 nmi of milepost 250, near Corpus Christi, Texas, and (b) 100 nmi of milepost 1600, near Vero Beach, Florida.

Cumulative probability curves for direction of storm motion for landfalling tropical cyclones were constructed using the Weibul plotting position formula given in Section 7.2. Figure 42 shows examples of these curves for two coastal locations near Corpus Christi, Texas, and Vero Beach, Florida. Each of the cumulative probability curves was divided into class intervals, and the values at selected percentiles were analyzed for three sections along the coast: the Gulf coast (fig. 43), and the Atlantic coast south (fig. 44) and north (fig. 45) of Cape Hatteras.

9.2.1.2 Results and Discussion. The direction of landfalling storm motion is closely related to the coastal orientation curve because the definition of landfalling restricts the storm direction data selection, exiting and alongshore storm motions being excluded. Under the influence of the easterly circulation of the lower latitudes (the Azores-Bermuda high) the tracks of most storms in the tropics is westward. There is a tendency for these low latitude storms to drift slowly northward at the western end of the high pressure system. As the storms drift toward higher latitude, they come under the influence of westerly winds and recurve northeastward.

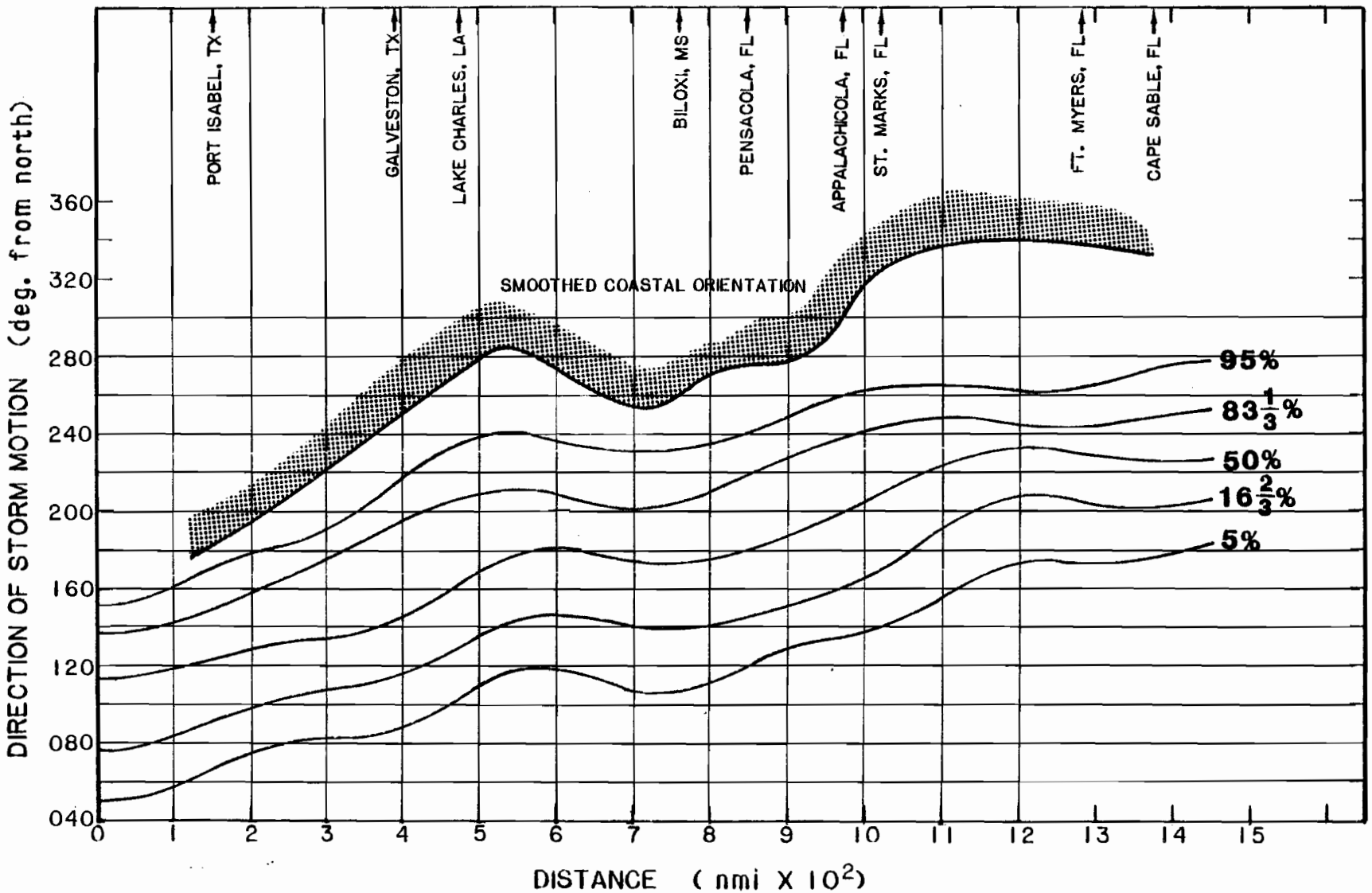

Figure 43.—Probability distribution for direction of storm motion for tropical cyclones landfalling on the Gulf coast (1900-84). Numbered lines denote the percentage of storms with θ equal to or less than the value indicated along the ordinate.

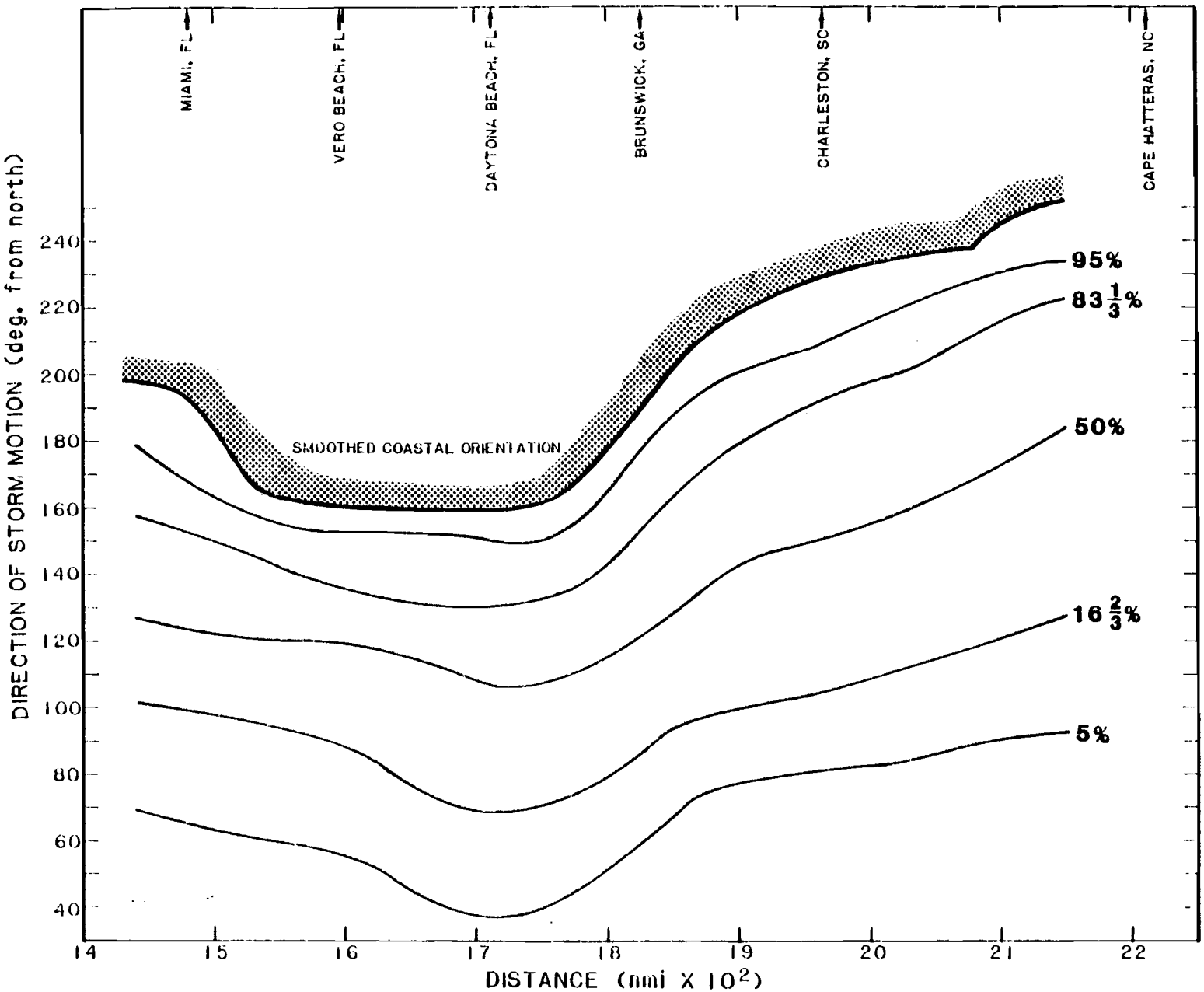

Figure 44.--Same as Figure 43, but for the Atlantic coast south of Cape Hatteras.

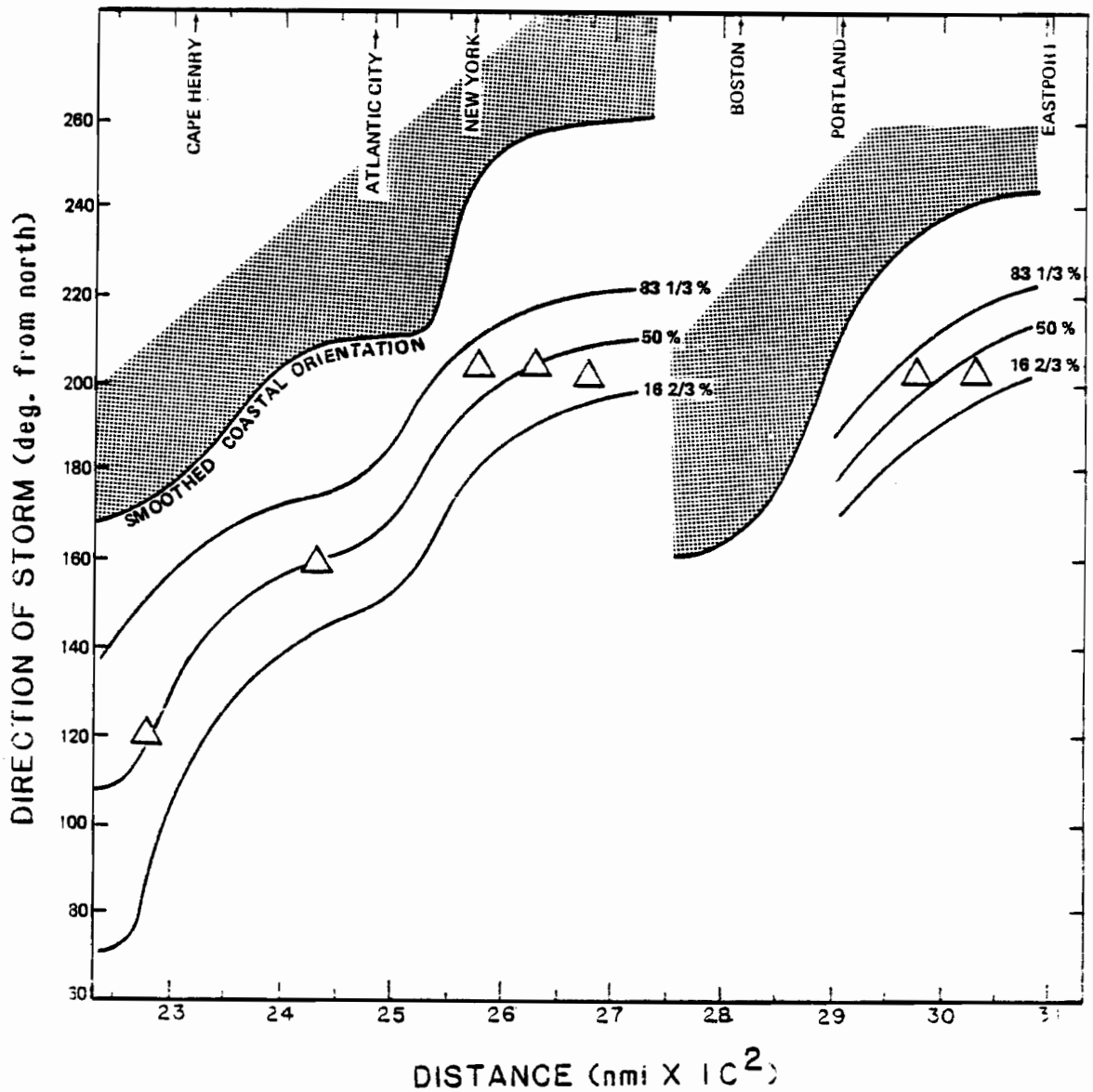

Figure 45.—Same as Figure 43, but for the Atlantic coast north of Cape Hatteras.

As indicated in preceding paragraphs, data sampling for the present analysis departed slightly from that used in TR 15. The analyzed results generally agree with the previous study. On the Gulf coast, 50 percent of the storms occurring between coastal reference points 900 and 1300 appeared to have greater southerly and easterly components than previously determined in TR 15. This difference may be attributed to the data samples of different time periods. Thirty-four storms occurring prior to 1900, with directions from 200 to 270° were not included in the present analysis.

9.2.1.2 (a) Gulf coast Figure 43 shows smoothed profiles at selected percentiles for direction of motion for landfalling tropical cyclones for the Gulf coast. As expected, the tropical cyclones striking the west coast of Florida come from the southwest direction and those striking the Texas coast are generally from the southeast. Along the mid-Gulf, coastal areas are vulnerable to storms approaching from both southeast and southwest.

9.2.1.2 (b) East coast, south of Cape Hatteras. Figure 44 confirms that for landfalling storms near Miami, Florida, the predominant direction of storm motion is from the east or southeast. In the vicinity of Daytona Beach, Florida, there is higher percentage of landfalling storms coming from the south and southeast. North of the Florida-Georgia state line, the percentage of north to northeastward moving storms increases gradually northward, which reflects the increasing number of recurving storms. This group of landfalling storms includes recurving tropical cyclones of Atlantic origin and storms that exited the Florida coast and may have reentered the coast south of Cape Hatteras. More than 50 percent of the landfalling tropical cyclones near Cape Hatteras are north-northeastward moving storms.

9.2.1.2 (c) East coast, north of Cape Hatteras. For the period since publication of TR 15 (1974-84), only two storms made landfall north of Cape Hatteras. The directions of motion for these two storms were consistent with those used in TR 15. Given the very small number of storms affecting this part of the coast, we believe that no changes to the earlier analysis were necessary for this stretch of the coast. Figure 45 has been taken from TR 15 for areas north of Cape Hatteras, North Carolina. The stretch of coast south of Cape Henry, Virginia, is vulnerable to landfalling tropical cyclones coming mainly from the easterly directions; the coastal orientation excludes the northeastward moving storms from the landfalling category. Tropical cyclones striking this part of the coast from the northeast have generally been weak. Figure 45 also reveals that tropical cyclones striking the coast east of New York consist mostly of northward to northeastward moving storms.

9.2.1.3 Areas of Discontinuous Direction Profile. The directions of landfalling storm profiles along the east coast are not continuous in the vicinity of Cape Hatteras, North Carolina and Cape Cod, Massachusetts, because of abrupt turning of the coast. The probability distribution of landfalling storm direction and its relation to P_o and T for Cape Hatteras area was discussed in Section 5.4. For the Cape Cod area, it is advisable to use the direction distributions from the south and west of the eastern extremity of the cape (lower milepost number), since the maximum wind region of a hurricane lies to the right of the hurricane track. The values indicated for Cape Sable (fig. 43) may be used as representative for hurricanes striking the mainland coast of Florida Bay.

9.2.2 Direction of Storm Motion for Bypassing Tropical Cyclones

Bypassing storms, by definition, do not strike the coast in the vicinity of interest. Variation of coastal orientation and the restriction imposed by the definition make specification of a generalized distribution of directions impossible. For practical computations, **we recommend assigning a direction parallel to a tangent to the coastal point of interest for bypassing storms,** with the general motion from east to west along the Gulf coast facing south, and for coasts such as Texas, Florida and along the Atlantic, the general direction should be from south to north.

10. ADJUSTMENT OF HURRICANE INTENSITY FOR FILLING OVERLAND

10.1 Introduction

The tropical cyclone is a thermally driven circulation in which the vertical flux of sensible and latent heat is the primary source of energy for both its formation and maintenance. One of the factors that diminishes hurricane intensity is the increased dissipation of kinetic energy by friction overland. In a steady-state hurricane, the frictional dissipation of kinetic energy near the core of a hurricane is approximately balanced by the energy supplied by sensible and latent heat. Overland, the heat sources are greatly reduced or may be lacking altogether. Hence, the energy balance between heat and frictional dissipation is upset after the hurricane moves overland. It has been suggested by Bergeron (1954) and Palmen (1956) that the removal of the sensible heat source (hence also the removal of the latent heat source) is the most important factor which contributes to the filling process overland. Miller (1963) confirmed the earlier work of Bergeron (1954) and others in stating that filling stems principally from the reduction of equivalent potential temperature (0_e) of the rising air around the hurricane core. Miller also noted that filling due to surface friction was of minor importance compared to the removal of the oceanic heat source.

Palmen and Newton (1969) state that "Owing to the removal of the oceanic heat source in the inner region, the baroclinity is reduced since the air ascending in the inner cloud wall now has somewhat lower θ_e. As a result, the outward radial wind component in upper levels is reduced. The previous balance between the mass inflow is thus temporarily disturbed and pressures rise."

In this chapter the term "filling" is used in the generally accepted sense. As discussed by Petterssen (1956), filling of a center of low pressure refers to an increase in the central pressure. Petterssen further distinguishes deepening and filling from intensification and weakening: while the former terms apply to the pressure, the latter apply to the pressure gradient. Changes in intensity or in pressure gradients are not dependent entirely on changes in central pressure. Nevertheless, it has been generally assumed that there is a high degree of correlation between the two factors (e.g., Hess 1945). Recent studies on inner core structure of mature hurricanes generally support this assumption. Most of the studies on Atlantic hurricanes based on reconnaissance flight data since the 1940's have focused on the inner core region (within 1° latitude radius). There is a scarcity of upper air data between 2-3° from the center. Frank and Gray (1980) used compositing techniques to determine an average radius and frequency of 30-kn winds around tropical cyclones. Merrill (1984) found no significant correlation of the radii of outer closed isobars with core intensity in a comparison of large and small tropical cyclones. Weatherford (1985) examined flight-level wind data obtained by reconnaissance aircraft flown into tropical cyclones in the northern Pacific during the period 1980-82. She showed that the outer strength (as measured by the magnitude of winds between 1°- and 3°-latitude radius of the storm center) is highly correlated with the extent of 30-kt surface winds, while the core intensity was a far more variable feature.

10.2 Index for Overland Filling

In defining climatological hurricane parameters for this study, we assumed a steady-state hurricane moving on a constant course during the time period required for storm surge computation. Strictly, these assumptions cannot be

carried through to determine a filling rate for hurricanes over land. However, transient phenomena of the hurricane core will not be considered. After the center of a hurricane crosses the coast, the hurricanes' central pressure rises faster than the change in peripheral pressure and the pressure deficit decreases. The decreasing intensity of the hurricane affects the level of storm surge, especially in bays and estuaries. It has been shown that the coastal surge and the surge producing forces in bays and estuaries vary proportionally with pressure deficit (e.g., Harris (1959), Ho and Myers (1975)). These surge-producing forces in bays and estuaries are, mainly, the propagation of open ocean surge into the bay and wind setup. The open coast storm surge increases with increasing kinetic energy of the wind which acts on the water surface, other factors being held constant. In a mature hurricane, the kinetic energy of the wind is approximately proportional to the pressure deficit. Hence, the coastal surge and the propagation of the open coast surge into a bay are approximately proportional to the pressure deficit in a hurricane. The second major factor in the bay and estuary response is wind setup. The magnitude of the wind setup effect is also proportional to the kinetic energy of wind for given conditions and, thus, is also approximately proportional to the concurrent pressure deficit.

Having considered the cause and effect of filling of hurricanes, it is logical to select pressure deficit as an index in defining the rate of filling overland. The advantages in selecting such an index is its direct and simple application to numerical surge models. Its application is, however, restricted because the averaging process used in the analyses tends to ignore the extremes. Recognizing that wind profiles in individual hurricanes do not always vary with the change in central pressure, the resultant rate of filling is best utilized in an idealized hurricane model. The user is cautioned against using an average filling rate for individual hurricane case studies for the purpose of replicating storm surge levels, especially in bays and estuaries.

10.3 Previous Observational Studies

Hubert (1955) observed that filling is most pronounced in the innermost region of the hurricane. Malkin (1959) stated that both filling and decrease in intensity proceed at a lesser rate when the ratio of water to land of the underlying surface increases along the track. Malkin analyzed the change in central pressure after landfall of 13 selected hurricanes and evaluated the average change in pressure gradient after landfall. Schwerdt et al. (1979) analyzed eight selected hurricanes which occurred during the period 1957-70 with central pressure less than 949 mb. They accepted the previous data and analyses made by Malkin and developed the filling rates in terms of reduction in wind speed for 3 different zones along the Gulf and Atlantic coasts of the United States. Jarvinen et al. (1985) suggested a quadratric filling rate of central pressure for hurricanes along the Texas coast and stated that the largest intensity changes occurred in the most intense storms within the first 6 hours after landfall.

10.4 Analysis of Data

In this chapter, the decrease in hurricane intensity after landfall was determined by using the ratios of pressure deficits at specified times after landfall (ΔP_t) and the pressure deficit at the time of landfall (ΔP_c). The

pressure deficit was obtained by subtracting the central pressure (P_o) from the peripheral pressure (P_n). These ratios give the percentage decrease in intensity and, thus, a rate of filling for hurricanes overland.

In order to determine the pressure deficit, an analysis of P_o and P_n must be made for the duration of the storm over land. Values of P_n were estimated from 3-hourly weather maps. For P_o, graphs were constructed showing sea-level pressure readings from stations with available continuous pressure records during the time period when a hurricane approached and passed by that station. These pressure readings and corresponding distances from the storm center were used in composite pressure-distance profiles analyzed at 3-hour intervals for a duration of 24 hours after landfall. These profiles were then extrapolated to the storm center, yielding estimated central pressures at various times.

Observations are taken at regular reporting stations as well as by many private individuals and corporations for their own uses. In some cases, this material is filed with the National Climatic Data Center (NCDC), NOAA's Cooperative Reporting Network. Additionally, after many severe storms, surveys are made to obtain supplementary data that are not routinely collected. With improvement of the observational network, analyses of observed data have proven to yield fairly good estimates of central pressure. These analyses, supplemented by analyzed synoptic maps, were relied on heavily in determining P_o of recent hurricanes.

Available data were plotted and a profile was fit to the data by eye. This allowed meteorological considerations to influence the resulting profiles. Figure 46 is an example of central pressure-time profiles for Hurricanes Frederick (1979) and Alicia (1983). Both hurricanes struck the Gulf coast; Frederick made landfall near the Alabama-Mississippi state line, while Alicia entered the coast just south of Galveston, Texas.

10.5 Filling Rates by Region

Table 19 shows a list of selected hurricanes which were analyzed individually to estimate the decrease in hurricane intensity after landfall. The data sample of 23 hurricane events was separated into three groups, based on the location where each hurricane crossed the coast. These regions are shown in Figure 47. Region A is the area along Gulf coast from Port Isabel, Texas, to Apalachicola, Florida, region B, the coast of Florida south of 29°N, and region C, the Atlantic coast from South Carolina to Rhode Island. Hurricane Camille, listed with other hurricanes in region A, was both intense and small in size, and had the steepest filling rate within the first 6 hours after landfall. Its central pressure rose from 909 mb to 965 mb in 6 hours, an average increase of more than 9 mb per hour. Camille stands out as a special case, presumably representative of the most intense storms. Since our hurricane sample indicates that there is a tendency for the more intense hurricanes to fill more rapidly, we have chosen to provide separate filling rates for extreme hurricanes.

For region A, filling rates were determined for each of the six Gulf hurricanes since 1971, following the procedures outlined in Section 10.4. Figures 48 a and b show the variation with time after landfall of filling rates of hurricanes listed in part A of Table 19. The filling rate is the ratio of pressure deficit at specified times (t) after landfall (ΔP_t) to the pressure deficit at the time of landfall (ΔP_c), or $\Delta P_t/\Delta P_c$. The filling rate for Hurricane Camille was adopted from analyses made in an earlier study (Schwerdt et al. 1979). Filling

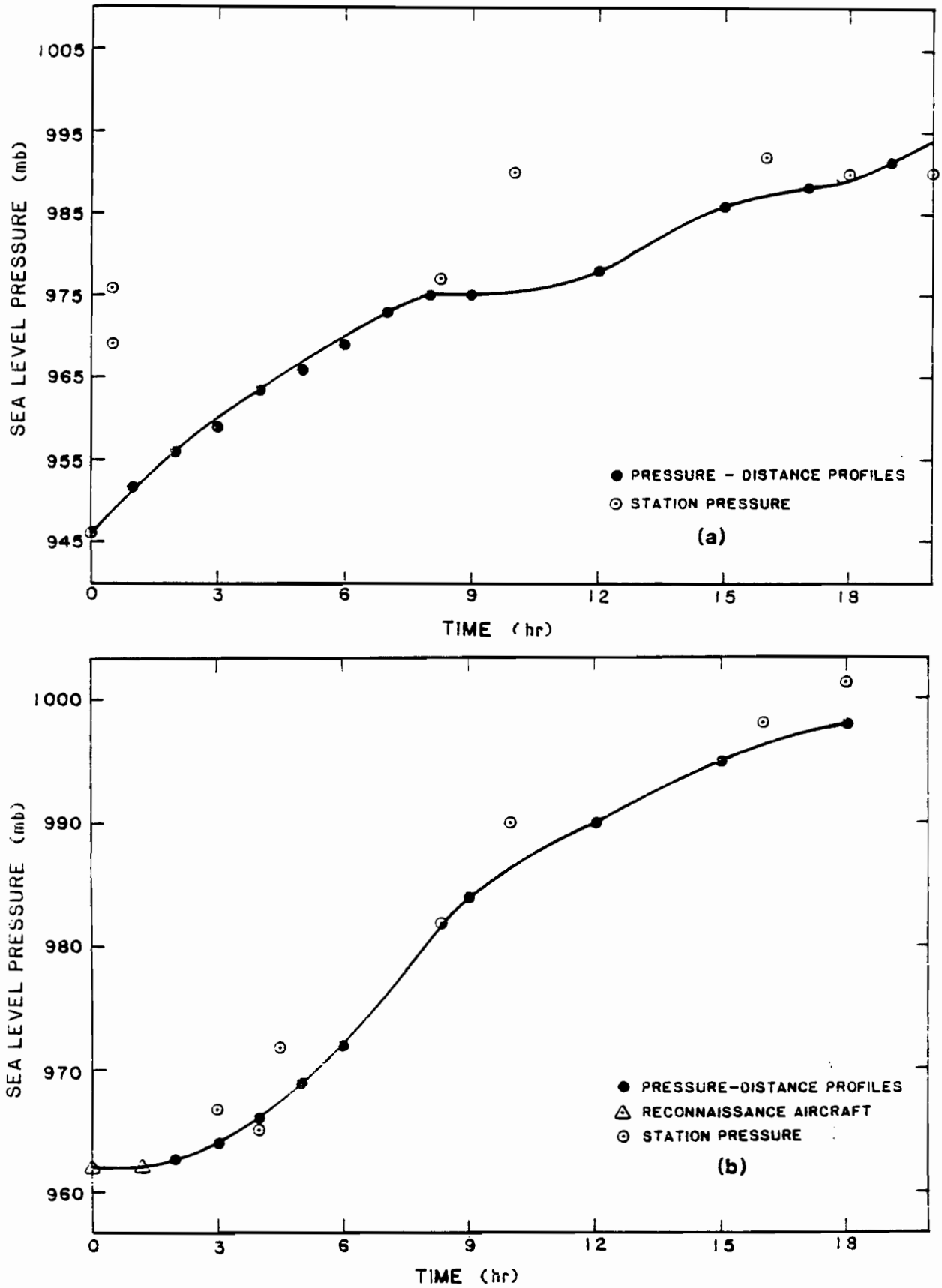

Figure 46.—Pressure profiles after landfall for (a) Hurricane Frederick, September, 1979 and (b) Hurricane Alicia, August, 1983.

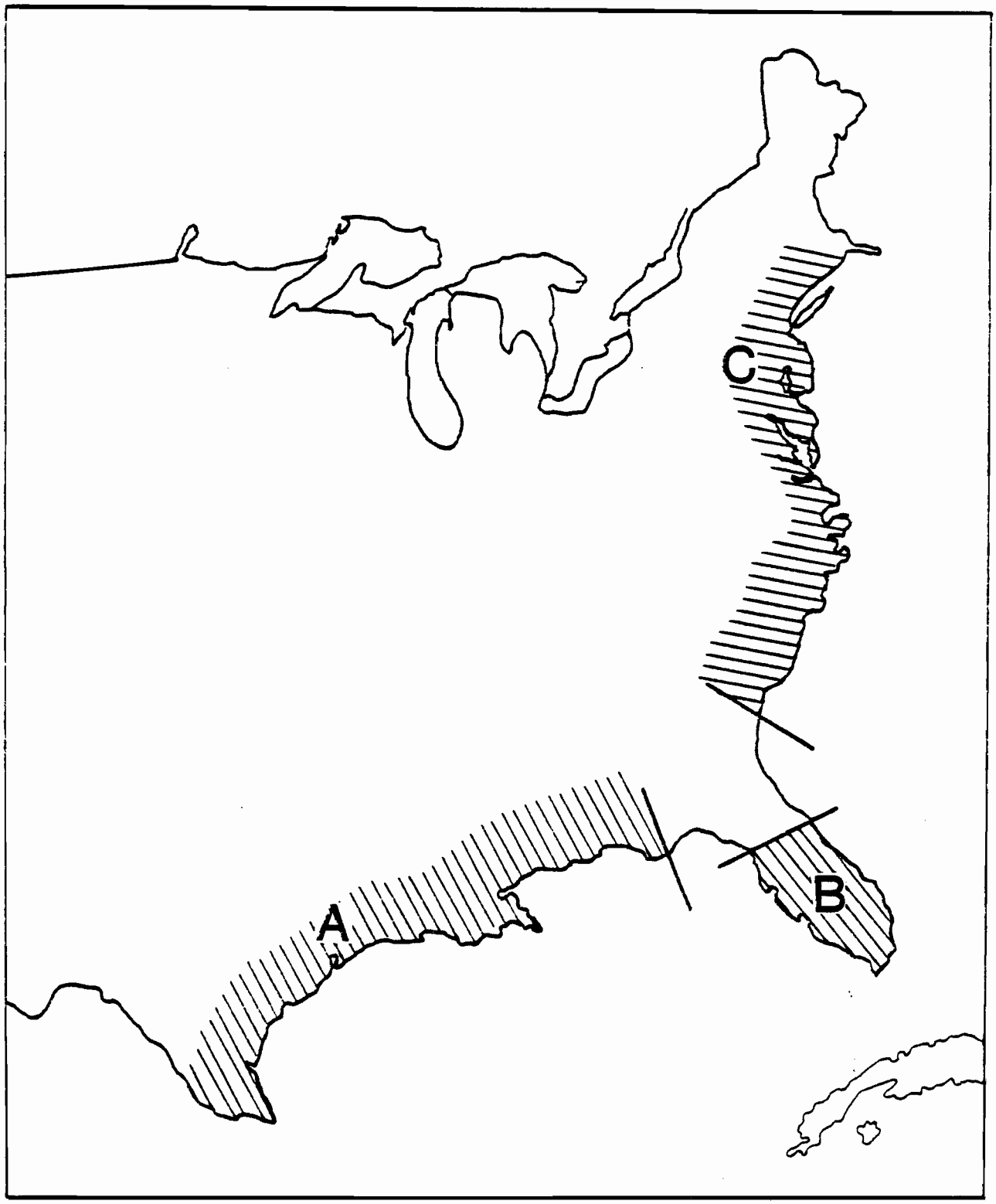

Figure 47.—Map showing geographical regions used to study filling rates.

Table 19.--Selected landfalling hurricanes (1928-1983) used to estimate overland filling rates.

No. of Storms	Hurricane	State of Landfall	Region
11	Audrey (1957)	Louisiana	A (Gulf coast from Apalachicola, FL westward)
	Carla (1961)	Texas	
	Betsy (1965)	Louisiana	
	Camille (1969)	Mississippi	
	Celia (1970)	Texas	
	#Edith (1971)	Louisiana	
	#Carmen (1974)	Louisiana	
	#Eloise (1975)	NW Florida	
	#Frederick (1979)	Mississippi-Alabama	
	#Allen (1980)	S. Texas	
	#Alicia (1983)	Texas	
4	Sept. 17, 1928	S. Florida	B (Florida south of 29°N)
	Sept. 15, 1945	S. Florida	
	Aug. 27, 1949	S. Florida	
	Donna (1960)	S. Florida	
8	Sept. 21, 1938	New York	C (Atlantic coast from South Carolina northward)
	Sept. 15, 1944	New York	
	Carol (1954)	New York	
	Hazel (1954)	North Carolina	
	Gracie (1959)	South Carolina	
	Donna (1960)	New York	
	#Belle (1976)	New York	
	#David (1979)	Georgia	

# Indicates storms since 1971

rates for other hurricanes prior to 1971 determined by Schwerdt et al. were checked for consistency by using observed minimum pressure data as previously discussed. Minor changes were made whenever warranted.

The filling rates at selected time intervals for the 11 hurricanes listed in Table 19 for region A were averaged to develop a filling rate for hurricanes of lesser intensity. Separate filling rates for more intense hurricanes were estimated by taking into consideration this average filling rate and the extreme filling rate associated with Camille. Intense hurricanes were arbitrarily defined as storms with ΔP_c greater than 85 mb, which have approximately the same intensity as category 5 hurricanes according to the Saffir/Simpson scale (Saffir 1977). Figure 49 shows the filling rate curves for hurricanes with ΔP_c less than or equal to 85 mb, ΔP_c equal to 100 mb, and ΔP_c equal to 110 mb. These curves have been used to develop the pressure deficits in part (a) of Table 20. Linear interpolation between values in Table 20 should be used instead of recourse to Figure 49 to assure a higher degree of accuracy and consistency.

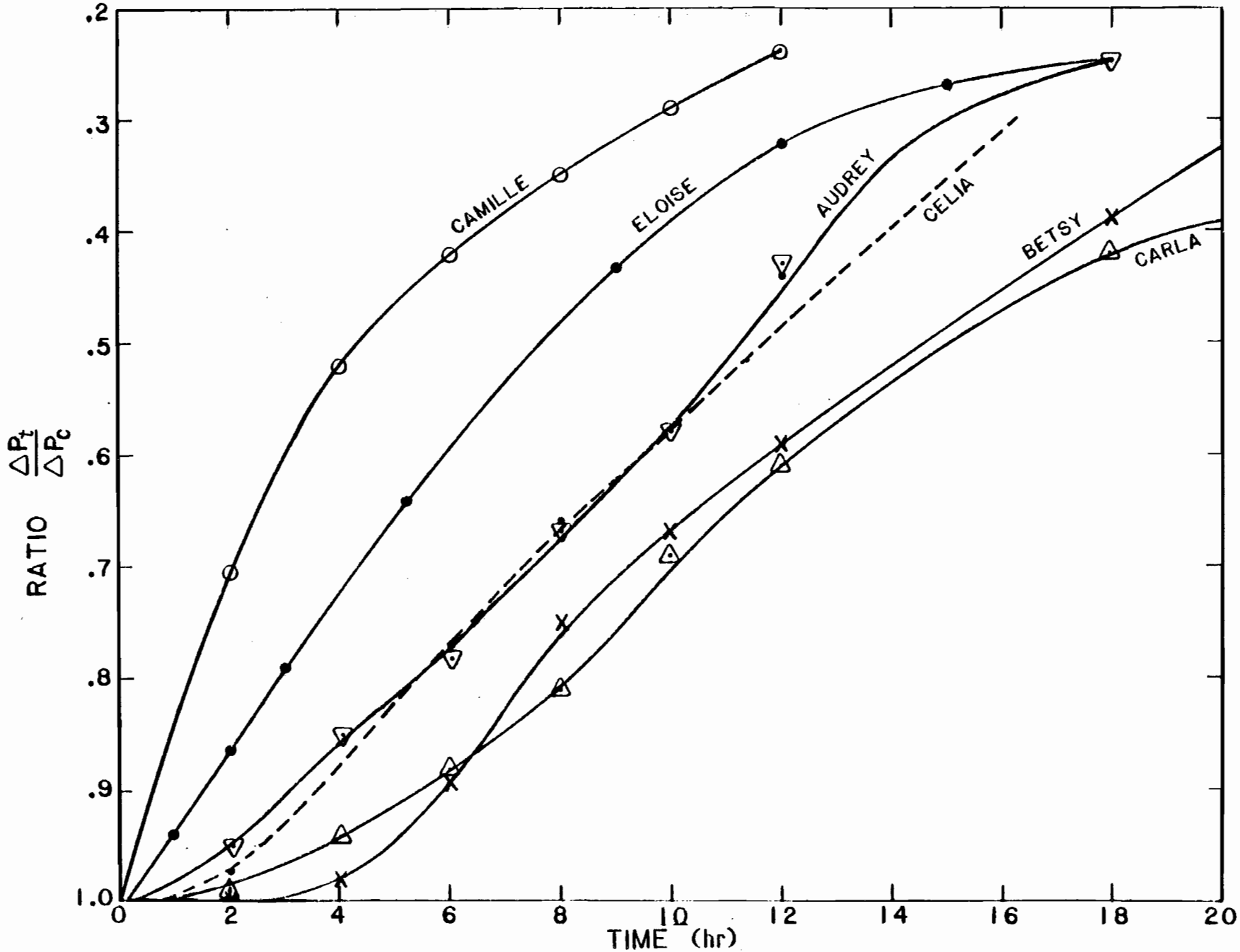

Figure 48a.--Variation with time after landfall of filling rate of hurricanes listed in region A of Table 19. Filling rate is expressed in terms of $\Delta P_t/\Delta P_c$.

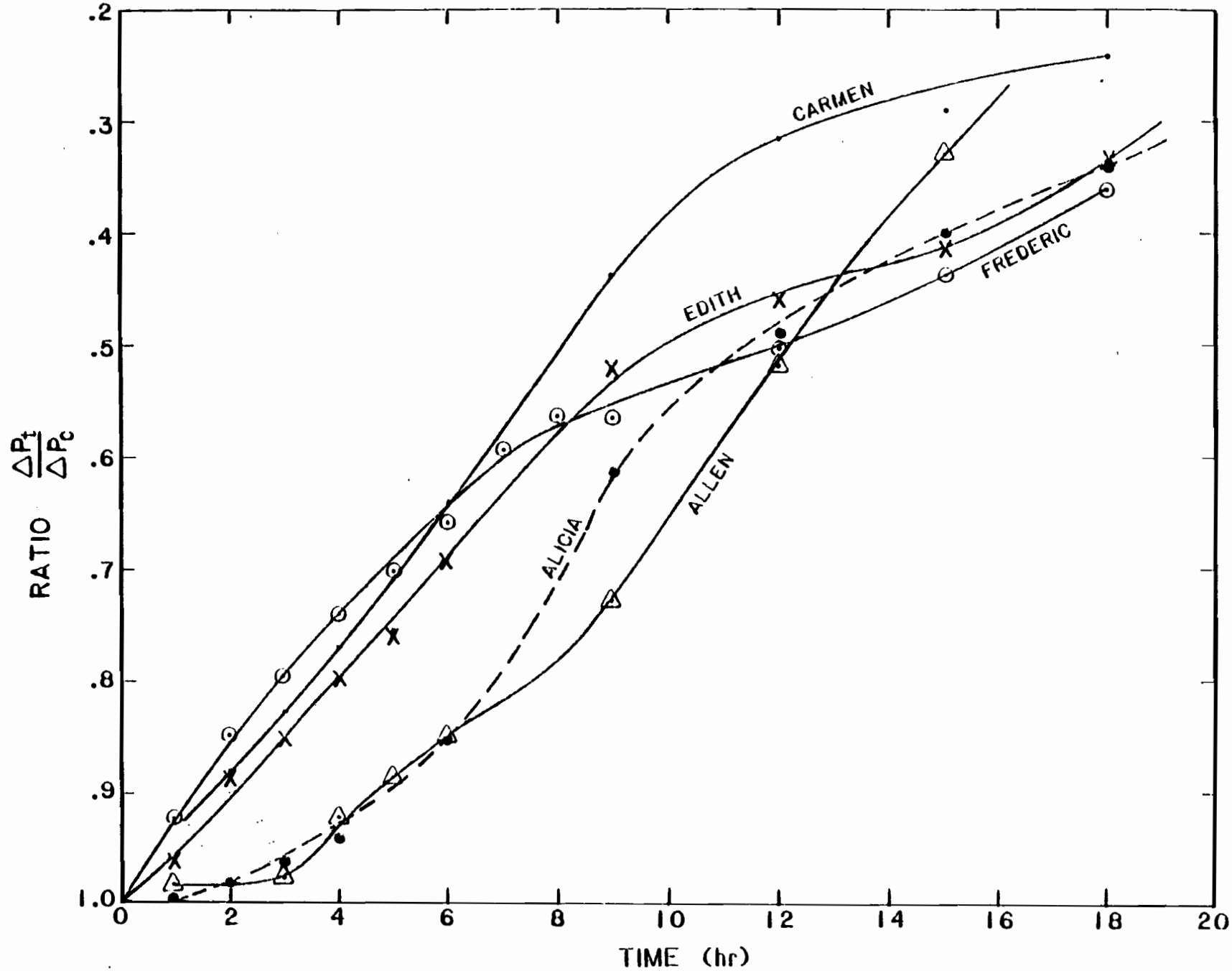

Figure 48b.--Same as Figure 48a.

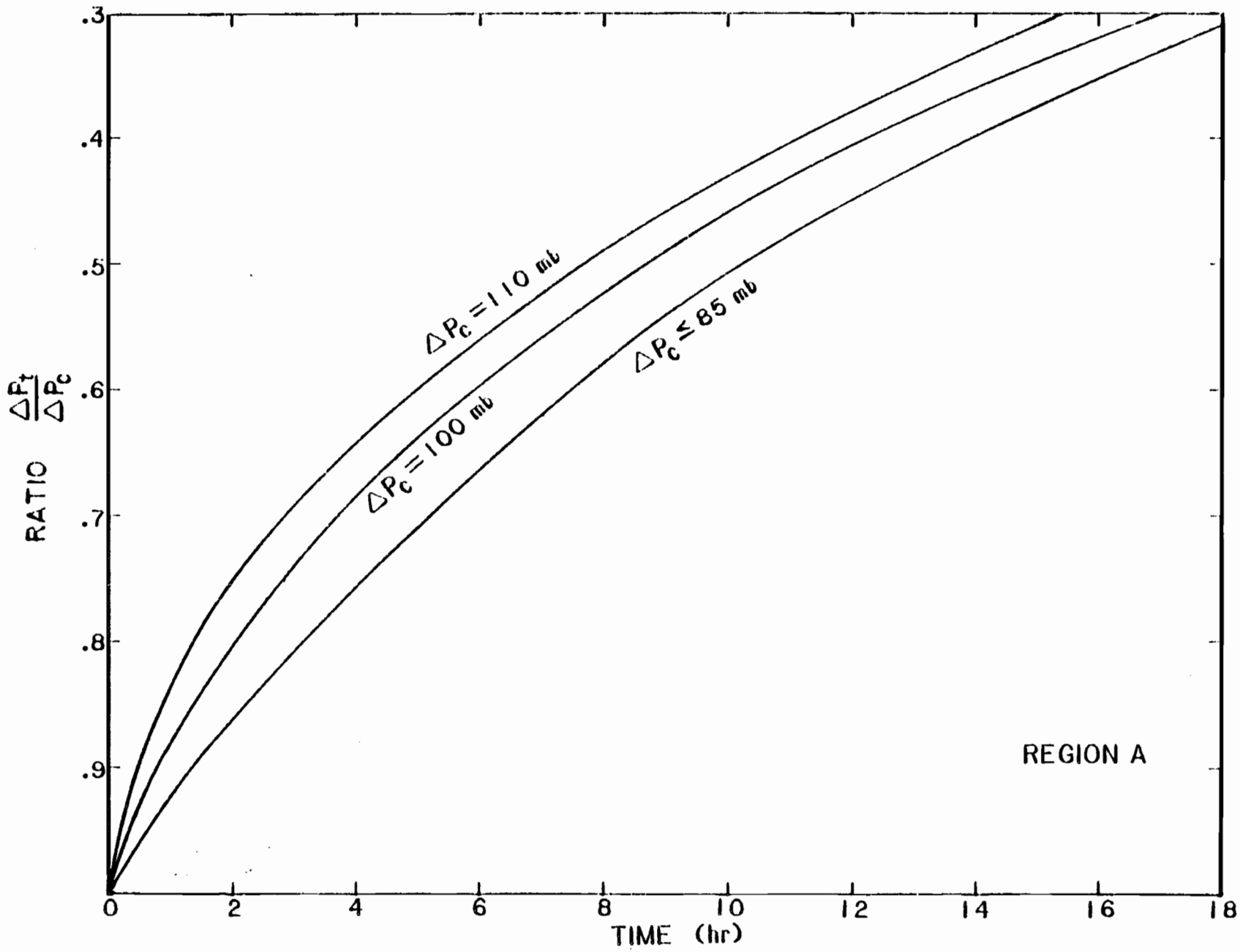

Figure 49.--Filling rates for hurricanes of various intensities for region A (Gulf coast, west of Apalachicola, Florida).

Table 20.--Changes in hurricane pressure deficits due to overland filling

Time After Landfall (hr)	Pressure Deficit (mb)								
(a) Gulf hurricanes, west of Apalachicola, Florida									
0	40	60	80	85	90	95	100	105	110
2	34	51	68	72	76	78	80	81	82
4	30	44	59	63	66	67	68	69	70
6	26	40	53	56	58	59	60	61	62
8	22	34	45	48	50	51	52	53	54
10	20	30	40	42	44	45	46	47	47
12	18	27	36	38	39	40	41	41	42
14	16	24	32	34	35	36	36	36	36
16	14	21	28	30	31	32	32	32	32
18	12	19	25	26	27	28	28	28	28
(b) Florida hurricanes, south of 29°N									
0	40	60	80	85	90	95	100	105	110
2	38	57	75	80	85	88	90	91	92
4	36	54	70	75	79	81	82	83	84
6	34	51	67	71	75	76	77	78	79
8	32	48	63	67	71	72	73	74	75
10	30	45	59	63	67	68	69	70	71
12	28	42	56	60	63	64	65	66	67
14	26	40	53	56	59	60	61	62	63
16	25	37	50	53	55	56	57	58	59
18	24	35	47	50	52	53	53	54	55
(c) Atlantic hurricanes, north of Georgia-South Carolina state line									
0	40	60	80	85	90	95	100	105	110
2	36	54	72	76	81	86	90	94	99
4	32	49	65	68	73	77	81	85	89
6	28	44	58	61	65	68	72	76	79
8	25	39	51	54	57	60	64	67	70
10	22	34	44	47	50	53	56	59	61
12	19	29	38	41	43	46	48	51	53
14	17	25	34	36	38	40	42	44	46
16	15	22	30	31	33	35	37	39	40
18	13	19	26	27	29	30	32	34	35

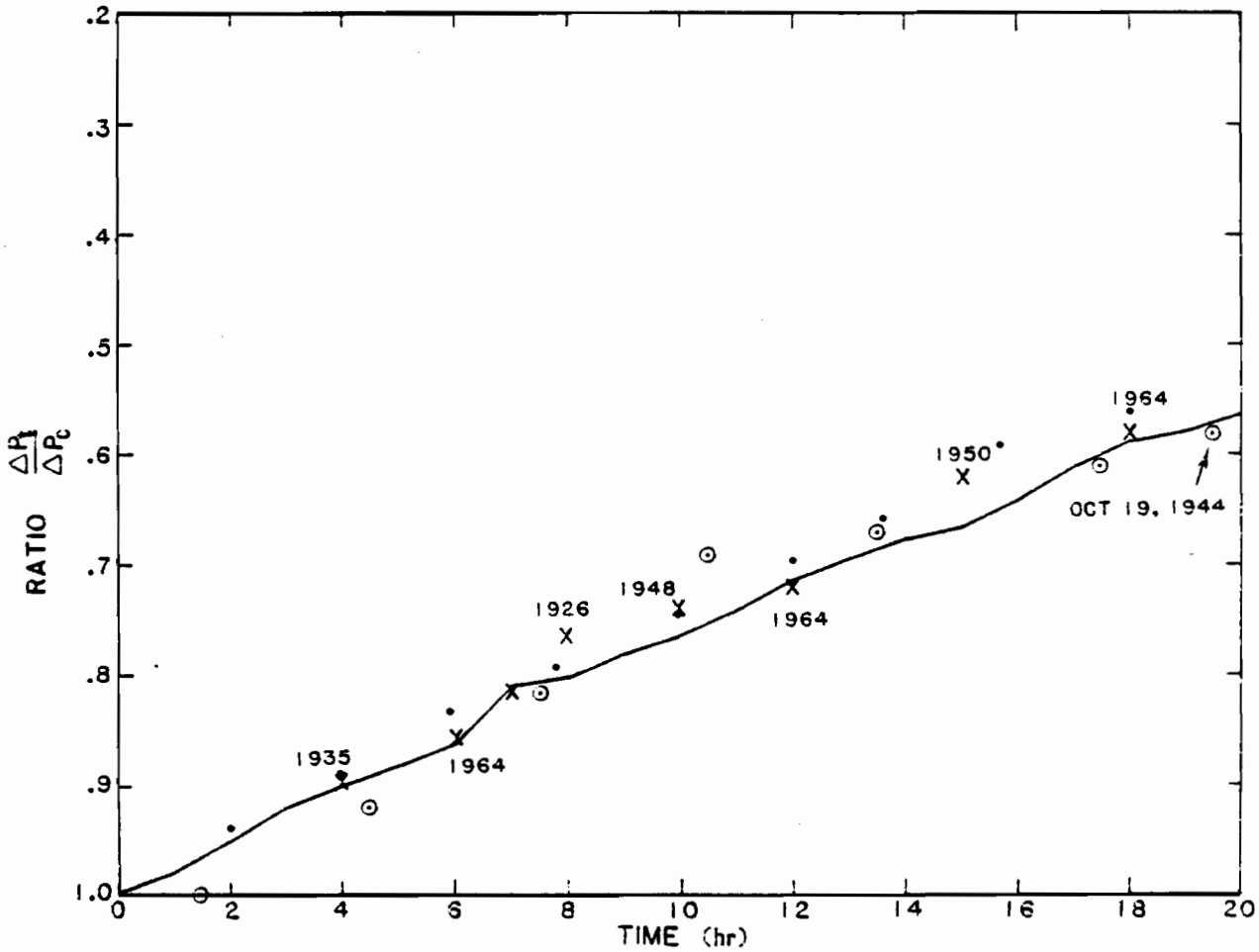

Figure 50.—Comparison of filling rates for various hurricanes crossing the Florida peninsula and the filling curve for region B from Schwerdt et al. (1979).

There were no additional storms that affected region B since 1971. The average filling rate curve determined by Schwerdt et al. (1979) was adopted after checking for consistency by comparing $\Delta P_t/\Delta P_c$ ratios for several hurricanes. No attempt was made to obtain separate filling rate curves for each of these hurricanes because data was scanty. Figure 50 shows a plot of these ratios at various times after landfall and the filling rate curve for region B from Schwerdt et al. It is again recommended that filling rates be obtained from the values in Table 20b by linear interpolation. Figure 51 shows filling rate curves for selected pressure deficit levels in region B.

Figure 52 shows the filling rate at various times after landfall for Hurricane Hazel (1954) and Gracie (1959). These two hurricanes entered the Atlantic coast, crossed the Carolinas, and recurved towards the north. Filling rates for a 12-hr period after landfall are shown in the figure because both hurricanes became extratropical soon after that period of time. The changes in intensity during their extratropical stage would not be representative of hurricanes. Only the rate of weakening for the first 12-hr period, as indicated by the solid line, was used in this analysis. Figure 52 also shows the rate of weakening for Hurricane David (1979) after entering the coast just south of Savannah, Georgia. The obvious difference between the curves reveals that David had a much slower

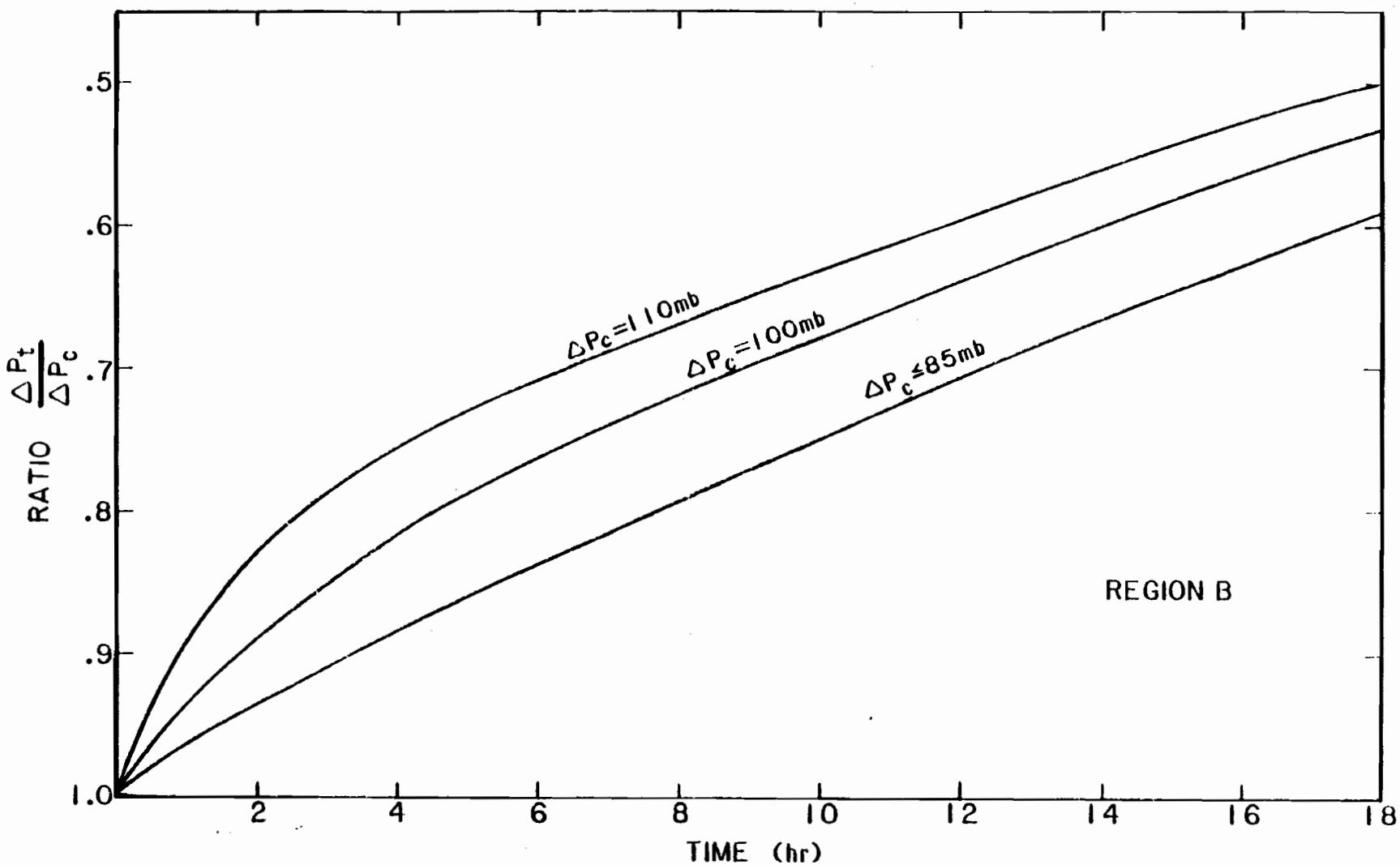

Figure 51.--Filling rates for hurricanes of various intensities for region B (southern Florida).

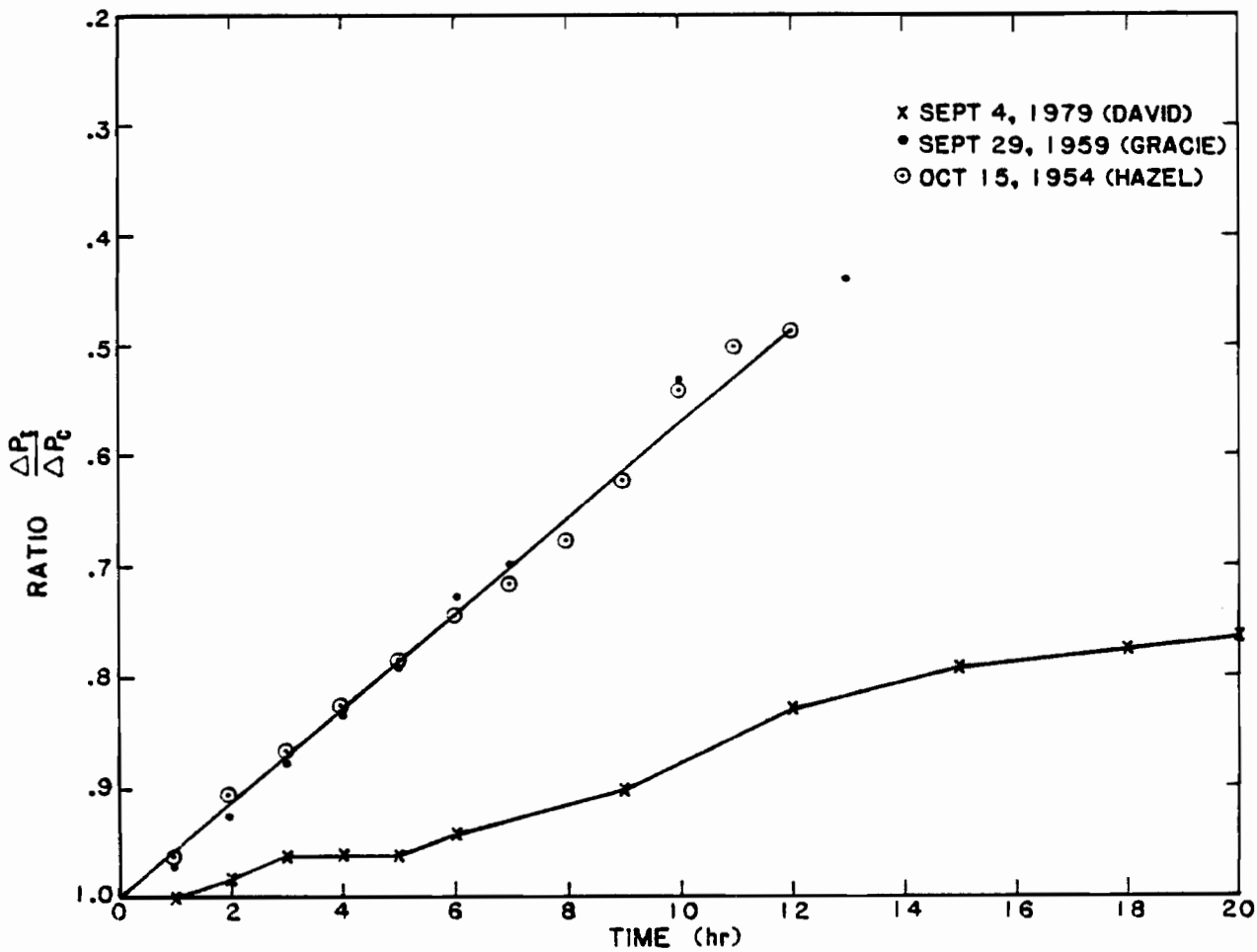

Figure 52.—Variation with time after landfall of filling rates for Hurricanes Hazel (1954), Gracie (1959), and David (1979).

filling rate than those of Hazel and Gracie. This can be partially explained by the fact that David traveled inland, parallel to the coast, with half of the cyclonic circulation of the storm remaining over water. The heat supply from the underlying sea acted to minimize the filling process. For this reason, David was not used in obtaining an average filling rate for Atlantic coast hurricanes.

Figure 53 shows a plot of filling rate versus time after landfall for hurricanes which crossed the shores of Long Island, New York and the New England states. Data obtained during the first 12-hr period after landfall were used in the analysis because these hurricanes were fast moving storms. In a 12-hr period after landfall, they would have either moved across the United States border into Canada or become extratropical. The average filling rates for these hurricanes agree fairly well with the filling curve for Hurricanes Hazel and Gracie (fig. 52). Combining both sets of data, we obtained the average filling curve as shown in Figure 54. Since region C has not experienced any extreme hurricanes, this curve was adopted to represent the filling rates of landfalling hurricanes of all intensities in this region. Again, linear interpolation from Table 20 should be used to determine pressure deficits.

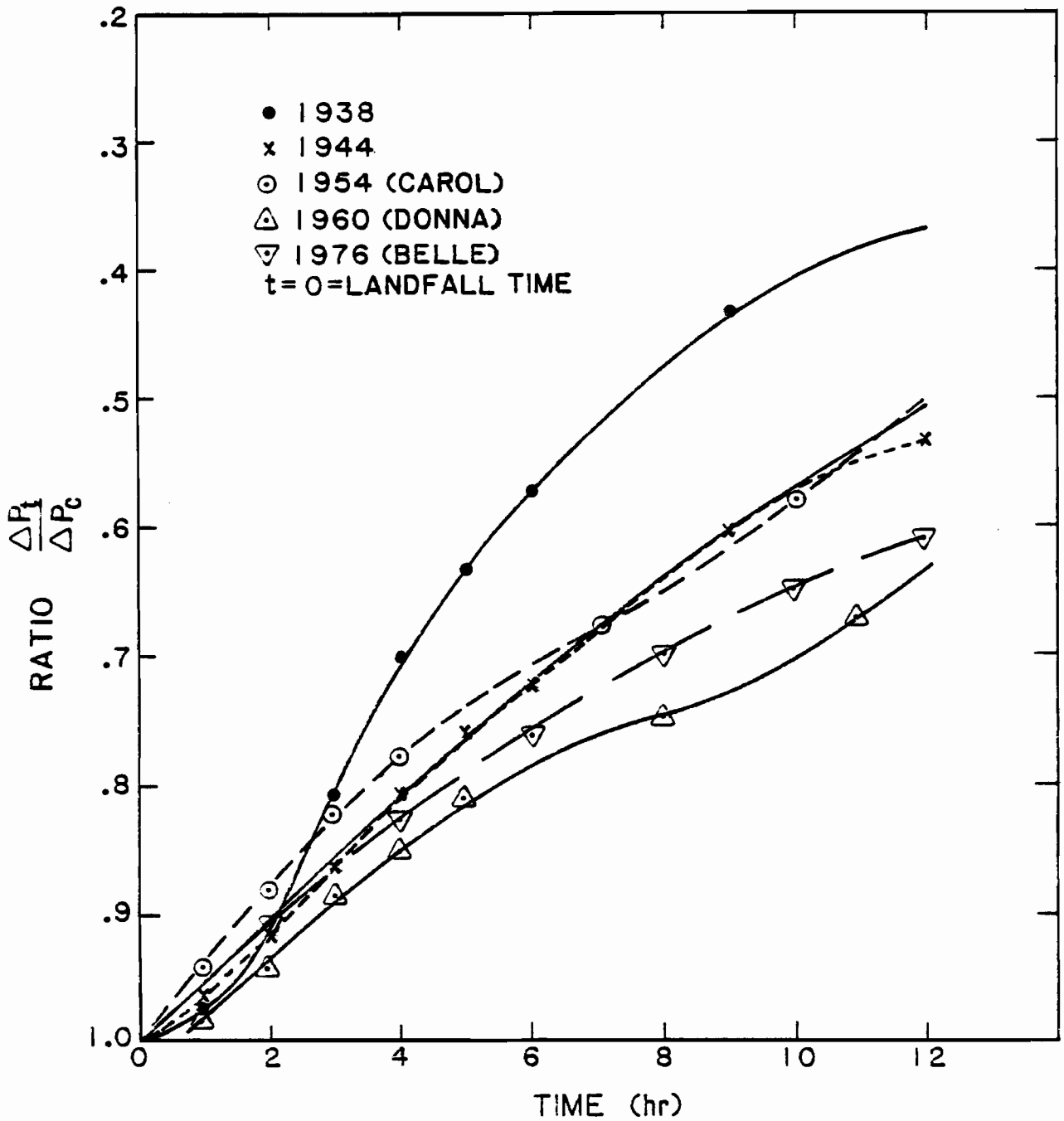

Figure 53.—Variation with time of filling rates for New England hurricanes.

10.6 Results

The lower filling rate curves for regions A and B in Figures 49 and 51 are applicable to hurricanes with pressure deficits less than or equal to 85 mb at the time of landfall. For hurricanes with pressure deficits greater than 85 mb, filling rates may be obtained from interpolation of pressure deficit values given in Tables 20a and 20b for regions A and B, respectively. There is no separate filling rate determined for hurricanes of the most intense category in region C.

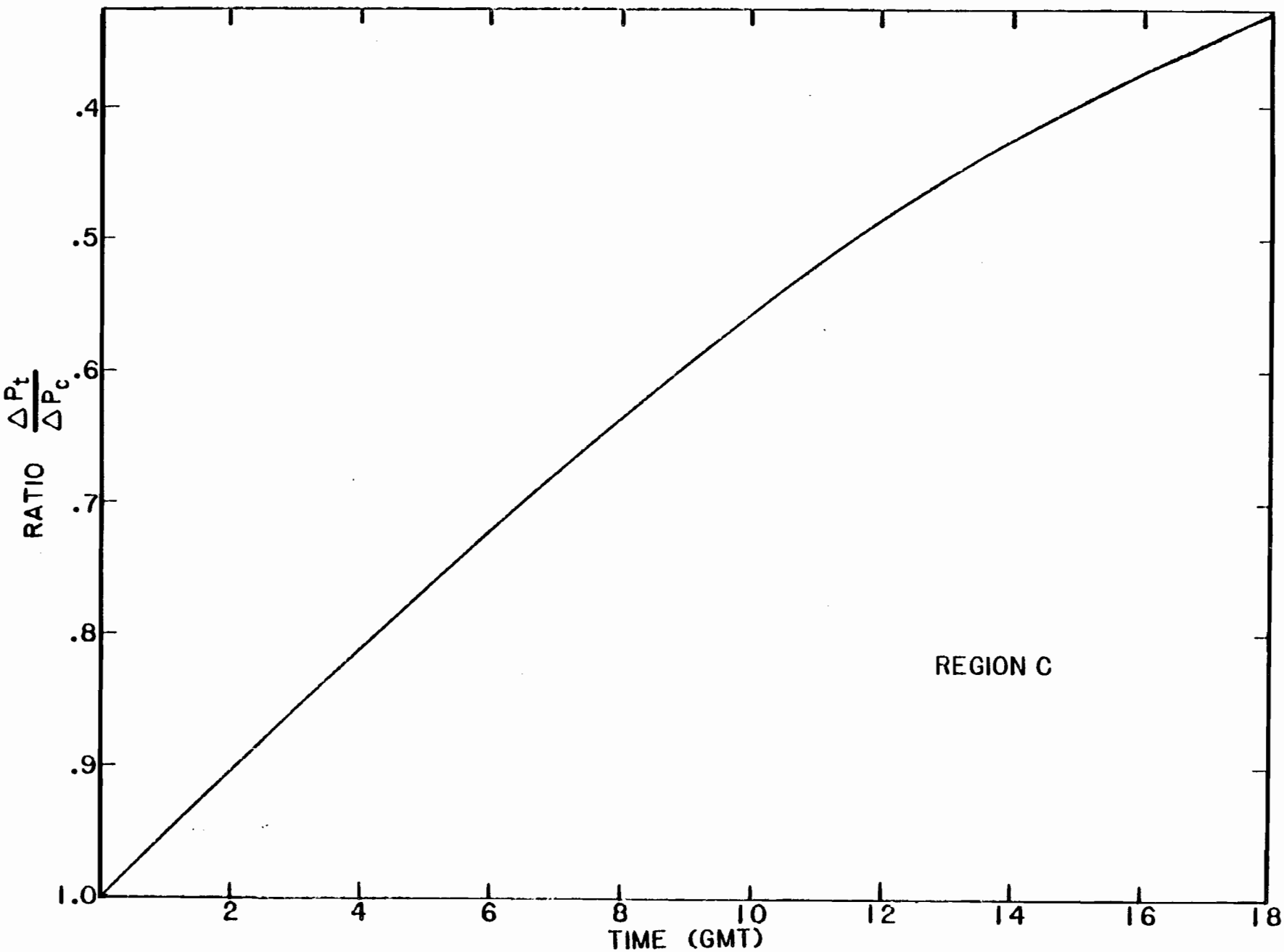

Figure 54.--Filling rate for hurricanes in region C (Atlantic coast north of Georgia).

The filling rate for region C, shown in Figure 54, was extended to depict filling up to 18 hr after landfall, for consistency. One should realize that the degree of accuracy decays with increasing time after landfall. The curve for region C is also applicable to areas north of Long Island, New York in order to include the entire coastline.

Assuming that the rate of filling is linear for the first 10-hr period after landfall, we can draw a straight line joining the point indicating the filling rate at 10 hr after landfall and the point of origin for each of the three regions. We obtained slopes of .051, .075, and .056 for regions A, B, and C, respectively. Linear interpolation of the slopes may be used as an aid to develop intermediate curves in estimating appropriate filling rates for areas lying between designated regions.

11. APPLICATION OF HURRICANE PARAMETERS

11.1 Introduction

An objective of this report has been to define climatological probability distributions of hurricane central pressure (P_o), radius of maximum winds (R), forward speed (T), and direction of motion (θ) along the Atlantic or Gulf coasts of the United States. In some applications of these data -- for example, in flood insurance studies -- it would be necessary to calculate frequency distributions of hurricane-induced surges on the coast by combining the analysis of hurricane climatology with the application of a numerical storm-surge model. Also needed in such application is the overall frequency with which hurricanes enter the coast in terms of strikes per mile per year, or some equivalent unit, within certain discrete distances. The landfall point of a hurricane is another parameter needed in a surge-frequency analysis. If storm track is parallel to the coast, then distance from the coast is needed instead of direction. This chapter outlines procedures to be followed in selecting hurricane parameters, their corresponding probabilities, and the representative storm tracks and frequencies for surge-frequency analyses as currently adopted in flood insurance studies.

11.2 Landfall Point

The cyclonic wind field of a hurricane usually increases from the edge of the storm to the highest value at the radius of maximum winds (R) then rapidly decreases to low values near the center. There is usually some asymmetry to the approximately circular pattern, with the highest winds on the right side as the storm moves forward. From the geometry of the hurricane wind field pattern, the maximum shoreward component is experienced at a given coastal site when the hurricane center landfalls approximately at distance R to the left. On a straight coast with uniform bathymetry, the highest surge along the coast will be experienced at this point of highest wind. Variable bathymetry can modify this location somewhat. Similarly, a bay experiences the strongest winds from a hurricane of given intensity and lateral extent when the storm track is about at distance R to the left of the center of the bay, as viewed from the sea.

In addition to the inverse barometer effect and the convergence of wind affecting surge levels near a storm's center, the major driving force for coastal surges is the stress of the wind on the water, roughly proportional to the square of the wind speed. Average wind profiles show that surface winds of a hurricane

at a distance five times the radius of maximum winds (5R) from the storm center are less than half of its maximum magnitude (Schwerdt et al. (1979), chapt. 13) and the magnitude of the corresponding peak surge heights are only about 25 percent of the peak. Except for the most intense storms, hurricane-induced surges of any significant level would not affect the coast if the hurricane made landfall at a distance exceeding 5R to the left of the point of interest or at a distance of more than 3R to the right. The distance 3R is chosen because coastal surge heights drop off much more rapidly to the left of the landfall point.

11.3 Peripheral Pressure

The linkage between the climatologically-defined hurricane central pressure (P_o) and the pressure deficit (ΔP) used in a storm-surge model is the peripheral pressure (P_n). P_n is used to compute the pressure deficit ($\Delta P = P_n - P_o$), which is a measure of the intensity of a hurricane. P_n is frequently considered the average pressure around the hurricane where the isobars change from cyclonic to anticyclonic curvature. This pressure occurs at a distance from the storm center near where storm inflow begins and, therefore, has physical meaning. In this study, P_n is used in conjunction with climatologically determined hurricanes. The use of a climatological mean value for P_n is considered adequate for this purpose.

Schwerdt et al. (1979) described several techniques for evaluating P_n and indicated that there is no significant variation of P_n with latitude. They compiled peripheral pressures for Gulf and Atlantic coast hurricanes with P_o less than 982 mb since 1900. **The average value of these given peripheral pressures is 1013 mb. We recommend that this climatological mean value be adopted as a representative peripheral pressure to compute pressure deficits in storm-surge frequency analysis.**

11.4 Probability Distributions of Hurricane Parameters and Frequency of Occurrence

This chapter describes the application of hurricane parameters needed to calculate storm surge levels on the coast. The assessment of probability distributions of these parameters assumes a steady-state hurricane moving on a constant course during the time period required for storm-surge computations. The averaging process along the Gulf and Atlantic coasts assures a smooth continuous variation of individual parameters along the coast. Exceptions to these basic assumptions and specific treatment of discontinuities have been discussed in preceding chapters. These include frequencies of landfalling tropical cyclones for the Florida Keys (sec. 6.2), refinements in alongshore hurricane track counts and probability distributions of landfalling storms for the North Carolina coast (sec. 5.4), frequencies of exiting storms (sec. 6.3), and filling of storms as they pass overland (chapt. 10). The procedure to estimate probability distributions of hurricane parameters for exiting storms will be discussed further in subsequent paragraphs.

The probability distribution of P_o is determined for landfalling tropical cyclones (sec. 7.3). There is no reason to believe that the pressure distribution of alongshore storms would be different from that of landfalling storms because both classes of storms experience an area with climatologically similar atmospheric and sea-surface conditions. Hence, this probability distribution of P_o can also be applied to alongshore storms. The probability distribution of R is

assumed to be the same for the landfalling, bypassing and exiting categories of storms. Probability distributions for direction and speed of storm motion for landfalling storms are given in Chapter 9. For alongshore storms, the direction is, by definition, assumed to be parallel to the coast and the probability distribution of forward speed is assumed to be the same as for landfalling hurricanes.

The frequency of tropical cyclone occurrence is defined as the number of tracks per year per nautical mile of a smoothed coast for each of the landfalling and exiting categories of storms (chapt. 6). Figure 27 depicts variation of frequencies of landfalling tropical cyclones along a smooth coastline. We have implicitly smoothed out the coast while smoothing out the accidental landfalling points of storms. A stretch of the coast that turns sharply in a direction almost parallel to that of the predominant storm motion is less exposed than adjacent coastal segments more normal to the track direction. For areas where the coast turns abruptly, such as the Mississippi Delta, Apalachee Bay, and the tip of Florida, special consideration must be given in using the generalized results in this report. An example of the treatment of a discontinuity in landfalling storm frequencies at Cape Hatteras, North Carolina, is discussed in Section 5.4. In areas where variations of frequencies along the coast are large, the effects of the steep gradient of hurricane frequencies along the coast on resultant coastal surge frequencies must be considered (see examples given in the following section).

For alongshore hurricanes, the bypassing distance is a significant parameter instead of the landfalling point discussed in Section 11.2. The frequency of an alongshore hurricane event is treated in the same way as the landfalling storms, except that the frequency is defined as the number of storms per year passing through a given distance interval along the line perpendicular to the coast. It is the counterpart of the frequency per year for landfalling storms multiplied by the length of coastal segment, determined by the spacing of storm tracks for computations. The application of this is further discussed in the following section. Figures 31 and 32 depict the variation along the Gulf and Atlantic coasts of tropical cyclone tracks bypassing the coast at sea. These figures give accumulated track count at selected intervals from the coast. With this information, plots of the cumulative count of tracks versus distance from the coast can be constructed for any coastal point. Figure 55 is an example of the accumulated track count plotted against distance from the coast for Vero Beach, Florida. The difference in accumulated track count between two points read off the graph gives the number of storms, per 100 years, crossing the given distance interval. It is advisable to use small distance intervals near the coast, using the selected R values for landfalling storms as a guide. This would ensure that the effect of maximum winds on coastal waters would maximize generated surge levels.

The frequency of tropical cyclones bypassing the coast overland is not treated as such in this report. First, these storms tend to weaken after traversing over land and the surge frequencies resulting from these storms are usually not significant (see for example fig. 29). Second, the contribution of this class of storms to surge frequencies varies greatly in different localities. Coastal surges of significant levels can be produced by such storms in areas near the Outer Banks of North Carolina and in the southern portion of the Florida peninsula. For the treatment of this class of storms in North Carolina, the reader is referred to the report by Ho and Tracey (1975). The North Carolina

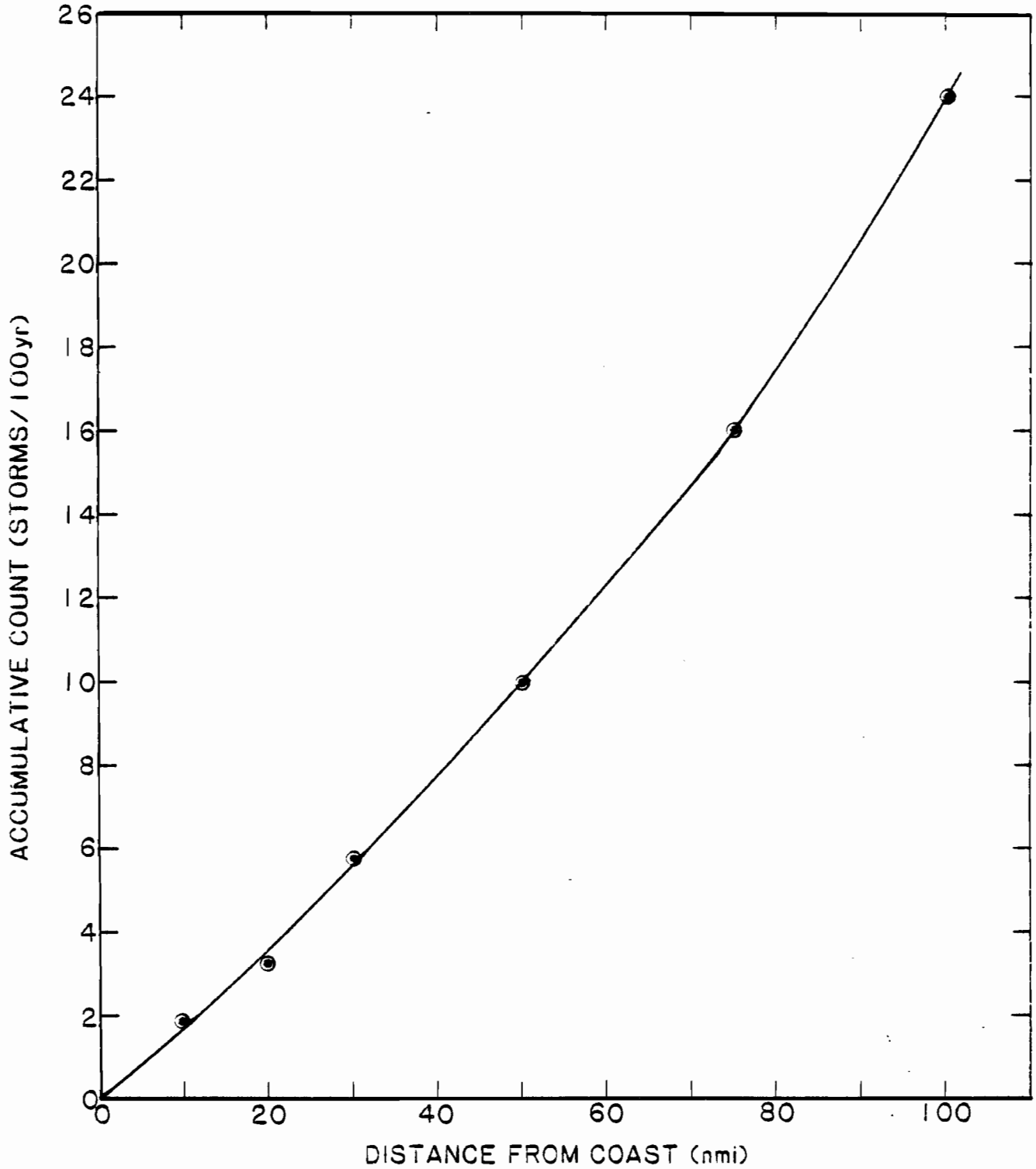

Figure 55.—Plot of cumulative count of alongshore storms versus distance from coast for Vero Beach, Florida (milepost 1600).

study may be used as a guide for the Florida peninsula area. A good example of these storms in Florida is the hurricane of October 1950 which entered the coast of south Miami and moved north-northwestward over the entire length of the peninsula. Its intensity weakened to that of a tropical storm after passing near Orlando, Florida. Another hurricane that entered the southern tip of Florida and weakened rapidly while moving northward is the hurricane of 1935. It was the most intense Atlantic hurricane ever recorded (P_o = 892 mb while crossing the Florida Keys). It weakened to minimal hurricane intensity (P_o = 960 mb) by the time it crossed the northern Florida coast, near 30°N. Hurricanes that move northward over the Florida Peninsula seem to fill faster than hurricanes that cross the peninsula in a east-west duration. It should be noted that the filling rate in Chapter 10 for Florida should not be applied to this class of northward moving hurricanes. The treatment of such tropical cyclones passing the coast inland needs further investigation.

11.5 Applications of Profiles of Probability Distributions for Hurricane Parameters

Hurricane parameters for storm-surge frequency computations can be obtained by constructing cumulative probability curves for each of the hurricane parameters from smoothed alongshore graphs. Table 21 itemizes the information needed by the user. Items 1-4 are information to be listed for identification. Item 5 lists the meteorological information needed for surge-frequency computations and where it can be found in this report. Numerical values to be filled in (5a through 5j) are hurricane parameter values for designated percentiles and frequencies read from the appropriate figures for the location (milepost) listed in Item 4. Using these values for the designated percentiles, the full range of individual parameters of climatologically possible hurricanes that can make landfall at the point of interest can be determined. The cumulative probability curve, thus obtained, is then divided into class intervals that can be used in frequency computations.

In storm-surge frequency analysis, landfall points should be selected by taking into consideration the lateral extent of the coast affected by an individual hurricane. Based on the geometry of the hurricane wind field, as discussed in Section 11.2, we recommend that the coastal area of influence for the purpose of surge computations be limited to a distance 5R to the left and 3R to the right of the point of interest. Hurricane tracks crossing landfalling points at 10-25 nmi intervals should be considered in estimating overall surge levels. The computed peak surge at the point of interest for a given storm passing along each of the selected hurricane tracks is assumed to be representative of a "surge event" that could occur within the distance interval (10-25 nmi) between two landfalling points. Hence, the selection of track spacing should be guided by (1) the alongshore gradient of the bathemetry, (2) the storm size and (3) the configuration of coastal areas. For example, tracks spaced at larger distance intervals may be specified for a straight coastline with uniform bathymetry while computation for storms crossing landfalling points at close intervals would be needed to produce representative surge levels on the shorelines of bays and estuaries. To obtain the frequency of this "surge event" multiply the frequency of landfalling storms (storms/nmi/yr, given in item 5h of table 21) by the selected distance interval between landfalling points.

Table 21--Summary sheet of information needed from this report for surge-frequency computations

1. Geographic location _____
2. Latitude _____
3. Longitude _____
4. Milepost [fig. 1] _____

5. Hurricane parameters

	Percentile						
	1	5	15	30	50	70	90
a. Central pressure (P_o) [fig. 35]							
b. Pressure deficit ($1013-P_o$)							

	Percentile					
	5	20	40	60	80	95
c. Forward speed (T) [fig. 41]						

	Percentile				
	5	16.67	50	83.33	95
d. Direction (θ) [fig. 44]					
e. Coastal orientation					
f. Angle of approach (d-e)					
g. Radius of maximum winds (R) [fig. 38]					

h. Frequency of landfalling storms [fig. 27] _____ storms/10 nmi/100 yr, or
_____ storms/nmi/yr

i. Frequency of exiting storms [fig. 28] _____ storms/10 nmi/100 yr, or
_____ storms/nmi/yr

j. Frequency of alongshore storms (accumulative counts) [fig. 32]

Distance from coast (nmi)	Frequency (storms/100 yr)	Frequency (storm/yr)	Frequency within distance interval
10			
20			
30			
50			
75			
100			

After completing the appropriate number of forms for the coastal area of interest, the information can be used to reconstruct cumulative probability curves for the parameters that describe the climatologically possible hurricanes for each of the selected locations. Intermediate cumulative probability curves, if required, may be estimated using linear interpolation. The reconstructed cumulative probability curves will provide values for any selected percentile within the full range of individual parameters. Intermediate curves will insure a smooth transition from one location to the next.

Table 22a is an example of a completed computation form for storm-surge frequency analysis at Vero Beach, Florida (milepost 1600). Tables 22b and 22c contain similar information for locations located 50 nmi to the north and south of Vero Beach, respectively. Figure 56 shows a plot of cumulative probability curves of P_o for the three locations. Curves for intermediate locations can be determined by linear interpolation. It should be noted that the lowest 1 percent of P_o for Vero Beach and the lowest 2 percent of P_o for the location 50 nmi to the south (fig. 56) fall into the intense hurricane category. As discussed in Section 4.5, these hurricanes should have an assigned R of 13 nmi. Similarly, cumulative probability curves can be plotted for the other parameters.

Figure 55 shows a plot of cumulative frequency of bypassing hurricane tracks versus distance from the coast for Vero Beach. The accumulated track counts for selected distances from the coast are taken from Item 5j of Table 22a. A smooth line was then drawn by eye joining the data points. From this curve, the frequency of bypassing storms within the first 10 nmi of the coast is 0.0170 storms/yr, the number of storms passing the distance interval of 10-30 nmi is (0.0575-0.0170) 0.0405 storms/yr and the track count for the distance interval of 30-75 nmi is (0.1600-0.0575) 0.1025 storms/yr. Similarly, frequencies within other distance intervals may be obtained (e.g., table 23).

The next step in determining hurricane probabilities requires that the hurricane parameters be divided into class intervals for the landfalling storms and that the mid-point value of each class interval be determined. The size and number of intervals cannot be specified **a priori**, but must involve judgment that considers factors that can vary from site to site; an example for P_o is given in Figure 57. It should be noted that Figure 57 shows only the fraction of all hurricanes with intensities below certain levels and makes no reference to frequency in terms of events per year. For storm-tide frequency computation, this continuous distribution could be divided into five class intervals, each represented by the pressure deficits at the mid-point of the class interval. This computational probability distribution is indicated by the dashed line on Figure 57. For computation purposes, the hurricanes are treated as if the most severe 1 percent all had pressure deficits of 95 mb, the next 6 percent had a deficit of 84 mb, the next 12 percent a deficit of 70 mb, the next 40 percent a deficit of 45 mb and the last 41 percent a deficit of 19 mb. These class intervals are representative values and their corresponding probabilities are listed in Table 23. It is of interest to note that these class intervals are not equally spaced. Closer intervals are used for parameters associated with intense hurricanes. Higher surge levels produced by the intense hurricanes contribute to the 100-yr or higher tide frequencies. Similarly, cumulative probability curves for other parameters can be divided into class intervals, and values for designated percentiles are listed in Table 23.

Table 22a—Summary sheet for Vero Beach, Florida

1. Geographic location: Vero Beach, Florida
2. Latitude: 27° 39' N
3. Longitude: 80° 27' W
4. Milepost [fig. 1]: 1600

5. Hurricane parameters

	Percentile						
	1	5	15	30	50	70	90
a. Central pressure (P_o) [fig. 35]	921	931	945	958	977	990	997
b. Pressure deficit ($1013-P_o$)	92	82	68	55	36	23	16

	Percentile					
	5	20	40	60	80	95
c. Forward speed (T) [fig. 41]	3.5	6.5	8.5	10.6	13.0	16.3

	Percentile				
	5	16.67	50	83.33	95
d. Direction (θ) [fig. 44]	055	087	118	135	153
e. Coastal orientation	020	020	020	020	020
f. Angle of approach (d-e)	035	067	098	115	133
g. Radius of maximum winds (R) [fig. 38]	5.5	11.0	18.0	28.0	37.0

h. Frequency of landfalling storms [fig. 27]: 0.76 storms/10 nmi/100 yr, or 0.00076 storms/nmi/yr

i. Frequency of exiting storms [fig. 28]: 1.20 storms/10 nmi/100 yr, or 0.0012 storms/nmi/yr

j. Frequency of alongshore storms (accumulative counts) [fig. 32]

Distance from coast (nmi)	Frequency (storms/100 yr)	Frequency (storm/yr)	Frequency within distance interval
10	1.70	0.0170	0.0170 (0 - 10 nmi)
20	3.30	0.0330	0.0160 (10- 20 nmi)
30	5.75	0.0575	0.0245 (20- 30 nmi)
50	10.00	0.1000	0.0425 (30- 50 nmi)
75	16.00	0.1600	0.0600 (50- 75 nmi)
100	24.00	0.2400	0.0800 (75-100 nmi)

Table 22b—Summary sheet for 50 nmi north of Vero Beach, Florida

1. Geographic location	Vero Beach + 50 nmi
2. Latitude	28° 30' N
3. Longitude	80° 42' W
4. Milepost [fig. 1]	1650

5. Hurricane parameters

	Percentile						
	1	5	15	30	50	70	90
a. Central pressure (P_o) [fig. 35]	925	935	949	963	981	991	997
b. Pressure deficit ($1013-P_o$)	88	78	64	50	32	22	16

	Percentile					
	5	20	40	60	80	95
c. Forward speed (T) [fig. 41]	3.8	6.8	8.8	11.0	13.2	16.5

	Percentile				
	5	16.67	50	83.33	95
d. Direction (θ) [fig. 44]	044	076	115	131	153
e. Coastal orientation	000	000	000	000	000
f. Angle of approach (d-e)	044	076	115	131	153
g. Radius of maximum winds (R) [fig. 38]	6.3	11.5	19.0	28.8	37.5

h. Frequency of landfalling storms [fig. 27] 0.74 storms/10 nmi/100 yr, or
0.00074 storms/nmi/yr

i. Frequency of exiting storms [fig. 28] 1.65 storms/10 nmi/100 yr, or
0.00165 storms/nmi/yr

j. Frequency of alongshore storms (accumulative counts) [fig. 32]

Distance from coast (nmi)	Frequency (storms/100 yr)	Frequency (storm/yr)	Frequency within distance interval
10	1.36	0.0136	0.0136 (0 - 10 nmi)
20	2.41	0.0241	0.0105 (10- 20 nmi)
30	4.32	0.0432	0.0191 (20- 30 nmi)
50	8.25	0.0825	0.0393 (30- 50 nmi)
75	14.10	0.1410	0.0585 (50- 75 nmi)
100	22.60	0.2260	0.0850 (75-100 nmi)

Table 22c—Summary sheet for 50 miles south of Vero Beach, Florida

1. Geographic location: Vero Beach - 50 nmi
2. Latitude: 26° 54' N
3. Longitude: 80° 11' W
4. Milepost [fig. 1]: 1550

5. Hurricane parameters

	Percentile						
	1	5	15	30	50	70	90
a. Central pressure (P_o) [fig. 35]	916	927	941	955	974	989	996
b. Pressure deficit ($1013-P_o$)	97	86	72	58	39	24	17

	Percentile					
	5	20	40	60	80	95
c. Forward speed (T) [fig. 41]	3.4	6.4	8.5	10.5	12.8	16.2

	Percentile				
	5	16.67	50	83.33	95
d. Direction (θ) [fig. 44]	059	093	120	142	155
e. Coastal orientation	020	020	020	020	020
f. Angle of approach (d-e)	039	073	100	122	135
g. Radius of maximum winds (R) [fig. 38]	5.0	10.0	17.5	28.0	37.0

h. Frequency of landfalling storms [fig. 27]: 0.97 storms/10 nmi/100 yr, or 0.00097 storms/nmi/yr

i. Frequency of exiting storms [fig. 28]: 0.90 storms/10 nmi/100 yr, or 0.00090 storms/nmi/yr

j. Frequency of alongshore storms (accumulative counts) [fig. 32]

Distance from coast (nmi)	Frequency (storms/100 yr)	Frequency (storm/yr)	Frequency within distance interval
10	2.34	0.0234	0.0234 (0 - 10 nmi)
20	4.02	0.0402	0.0168 (10- 20 nmi)
30	7.10	0.0710	0.0308 (20- 30 nmi)
50	12.50	0.1250	0.0540 (30- 50 nmi)
75	18.50	0.1850	0.0600 (50- 75 nmi)
100	25.80	0.2580	0.0730 (75-100 nmi)

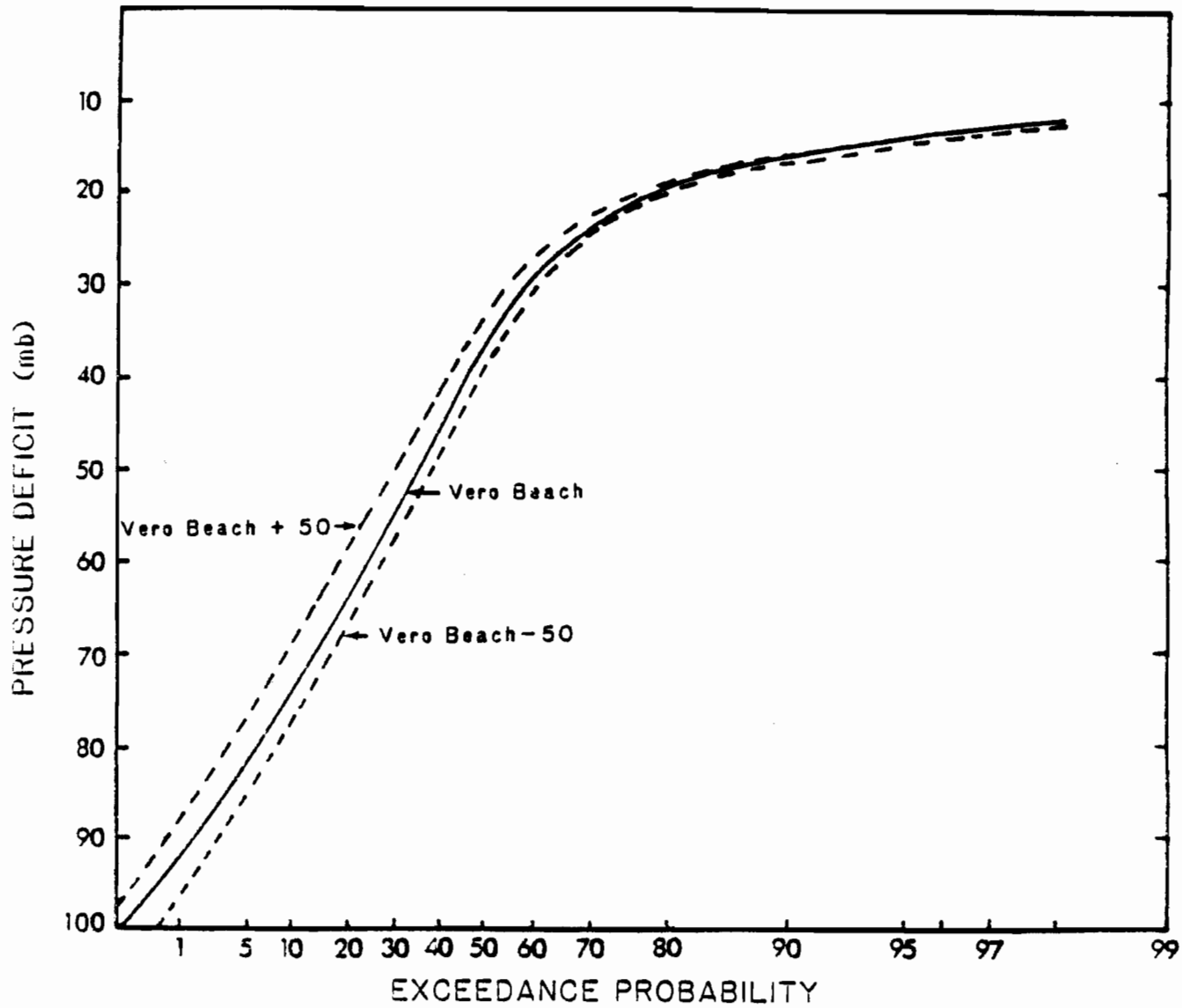

Figure 56.—Cumulative probability curves of P_o for designated locations.

The parameters adopted for Vero Beach, Florida, in Table 23 represent five pressure deficit categories, four R categories, three T categories and three θ categories. These factors are considered statistically independent except that the four R's are not the same for all pressure deficit categories, a small value being used with the class interval of most intense pressure deficits in line with the discussion in Section 4.5. Thus, in Table 23, the most intense hurricanes (1 percent of total count) are assumed to have an R of 13 nmi. The R's for weaker storms cover the full range of values. For these storms, the R class intervals need not be equally spaced. One needs to consider an appropriate class interval for the critical range of R near 30 nmi. This is because of the importance of the dynamic effect of winds near R on the surge calculation. For a hurricane with constant intensity crossing the continental shelf of average width, the induced peak surge reaches its maximum value for R at or slightly greater than 30 nmi. Similarly, there exists a critical motion relative to a coast that gives the highest possible surge under any given set of conditions. The critical speed generally is greater than 25 kn. Thus, the fastest moving storms, especially if they are large and moving directly toward the coast, pose the greatest hazard. Appropriate class intervals should also be designated for

Table 23.--Tropical cyclone parameters Vero Beach, Florida

P_o (mb)	ΔP (mb)	p_i	R (nmi)	p_r	T (kn)	p_t	θ_L (deg.)	p_θ
			Landfalling					
918	95	0.01	*		5.7	0.30	040	0.16
929	84	0.06	11.0	0.333	9.5	0.40	088	0.40
943	70	0.12	18.0	0.333	14.0	0.30	112	0.44
968	45	0.40	28.0	0.333				
994	19	0.41						

Landfalling storm frequency = 0.00076 storms/nmi/yr.

* R = 13 nmi is assigned a probability of 1.0 for P_o < 920 mb.

			Exiting					
950	63	0.07	13.8	0.5	8.8	0.5	067	1.0
961	52	0.12	23.5	0.5	18.0	0.5		
980	33	0.40						
999	14	0.41						

Exiting storm frequency = 0.0012 storms/nmi/yr.

L (nmi)	F (storms/yr)	R (nmi)	p_r	T (kn)	p_t	
		Alongshore				
5.0	0.017	13	.5	7.0	.5	P_o, ΔP, and P_i are the same as those for landfalling storms
15.0	0.016	25	.5	12.3	.5	
25.0	0.024					
40.0	0.042					
62.5	0.060					

P_o = Central pressure (mb)
ΔP = Pressure deficit (mb)
p_i = Proportion of total storms with indicated ΔP value
R = Distance from center of storm to principal belt of maximum winds (nmi)
p_r = Proportion of storms with indicated R value
T = Forward speed of storm (kt)
p_t = Proportion of storms with indicated T value
θ_L = Direction of entry or exit, measured clockwise from the coast (deg.)
p_θ = Proportion of storms with indicated θ_L value
L = Distance of storm track from coast (nmi)
F = Frequency of storm tracks crossing a line normal to coast (storm tracks/yr passing through the interval centered at L)

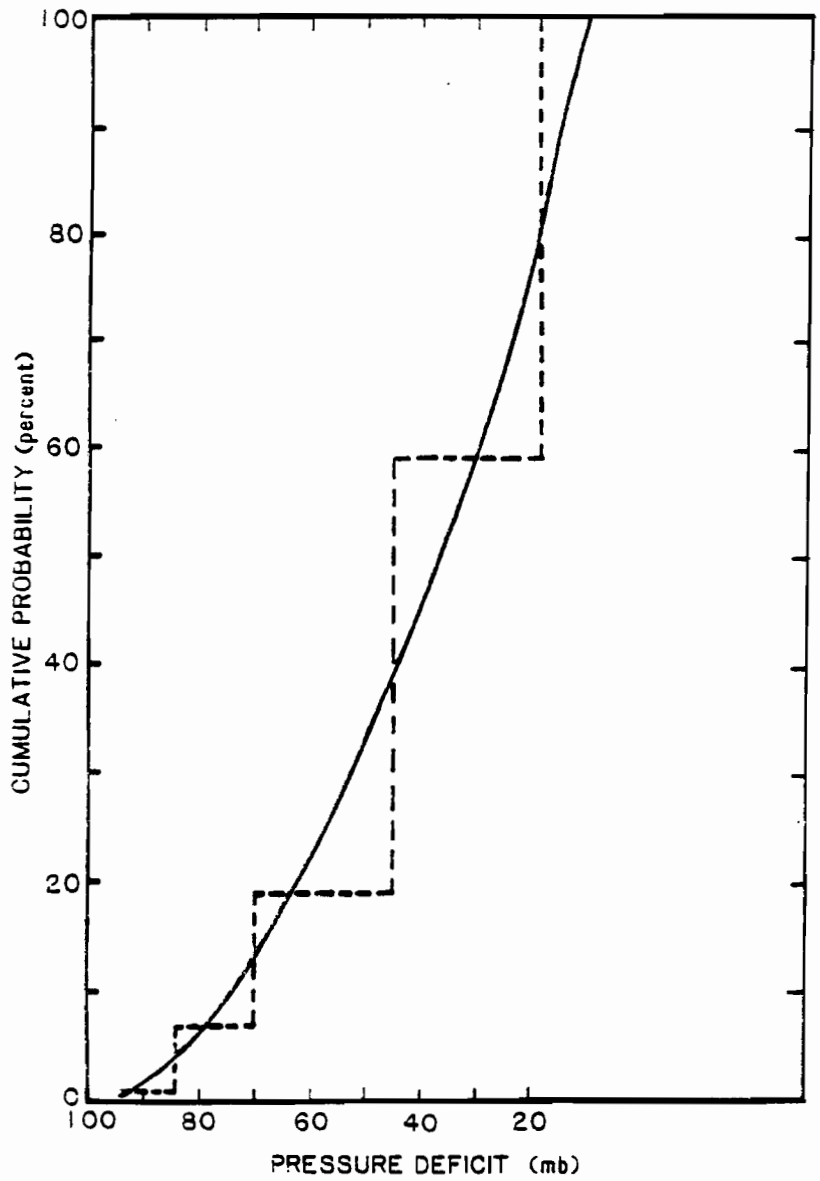

Figure 57.—Cumulative probability curve for pressure deficit at Vero Beach, Florida. Dashed lines shown selected class intervals.

the critical range of speed and direction. The direction of approach, 88°, was selected (table 23) to represent the most critical range of directions which would produce the highest coastal surge if other factors were the same.

In Table 23, the most intense landfalling hurricane class interval (1 percent of the total) is assumed to have an R of 13 nmi and one third of each class of less intense hurricanes are assumed to have R's of 11, 18, and 25 nmi. The P_o and R categories for landfalling storms given in Table 23 define 13 different hurricanes [$4(P)_o$ X 3(R) + (P_o = 918 and R = 13)]. The probability of each of these is obtained by multiplying the respective probabilities in the table. The sum of the probabilities of the 13 hurricanes, of course, equals 1. P_o and R are statistically independent of θ and T. Thus, the parameters for landfalling storms defines 117 different hurricanes (13 X 3(T) X 3(θ)). Each of the 117 discrete storms represent a portion of the probability domain, the probability of each

storm is obtained by multiplying the four parameter probabilities. For example, the probability of having a hypothetical hurricane with P_o = 929 mb, R = 18 nmi, T = 9.5 kn, and θ_L = 88°, is 0.0032 (0.06 X 0.333 X 0.4 X 0.4).

11.6 Exiting Tropical Cyclones

The intensity of exiting storms generally decreases because the overland trajectory reduces the energy supply (see chapt. 10). Central pressure data observed over the ocean in landfalling and alongshore storms may not be used to estimate the probability distribution of P_o for exiting storms. Because of insufficient data sample size, no attempt was made to construct cumulative probability curves of hurricane parameters for exiting storms based on observed data.

As previously indicated (sec. 6.3.2.3), exiting storms normally contribute little to the overall frequencies of storm surges, except for the Florida peninsula. Storms exiting the east coast of Florida frequently come from the southwest. Plots of cumulative probability curves of landfalling direction along the west coast of Florida show a median direction of about 227° (from north) along most of the coast. The median direction for storms crossing the Florida peninsula from the Atlantic to the Gulf varies from 110-130° (from north). The typical translation speed of these storms is about 10 kn (see figs. 40 and 41). Using the median landfalling direction on the opposite coast, and assuming that the storm direction remains constant as it crosses the peninsula, a representative overland storm track can be determined for exiting storms. The next step is to estimate the time it takes the storm to cross the peninsula, using the median landfalling speed, which is also assumed constant. This time can be used to determine filling-rate factors (sec. 10.5) that can be applied to the P_o distribution at the landfall point. The modified P_o distribution is then used to approximate the P_o distribution for exiting storms.

Except for P_o, we assume that there are no changes in other parameters as storms crossed the Florida peninsula. Cumulative probability curves developed for R, T, and θ at the point of landfall are applicable to storms exiting the opposite coast. For expediency and economic considerations it will usually be sufficient to assign two class intervals for each of the R and T distributions and four intervals for P_o (e.g., see table 23). The direction of storms exiting the east coast of Florida may be represented by 227° from north since the range of probable direction of exit is so small. Two class intervals for directions of storms exiting the west coast of Florida are recommended by assigning 50 percent probability each to the directions of 073° and 116° from north. Because of infrequent occurrence of storms exiting north of Tampa Bay on the west coast of Florida, it should not be necessary to attempt to define exiting storm parameters to the north of this point.

12. SUMMARY AND DISCUSSION

This report presents an analysis of the geographical distribution of major hurricane and tropical storm factors useful for flood insurance studies. Each of these factors influences the ability of the storms to produce storm tides. This report provides a climatology of hurricane factors needed for surge-frequency analyses and information useful for storm-surge modeling. Because our purpose was to develop climatological data in a probabilistic sense, judicious smoothing

Table 24.--Data used in this report for probability analyses

Climatological Characteristic	Data Source	Application	Figures
Storm frequency (landfalling, alongshore, exiting)	Tropical cyclone tracks of the North Atlantic Ocean, 1871-1984	Tropical cyclones	27, 28, 31, 32
Central pressure	Tables 1 to 3 (hurricanes with P_o<982 mb since 1900)	Tropical cyclones*	34, 35
Radius of maximum winds	Tables 1 to 3 (hurricanes with P_o<982 mb since 1900)	Hurricanes	37, 38
Direction and speed of forward motion	Tropical cyclone tracks of the North Atlantic Ocean, 1900-84, 'HURDAT' tape	Tropical cyclones	40, 41, 43 44, 45

*Cumulative probability curves for central pressure, based on hurricane data, were extended to include tropical storms.

was employed along the Atlantic and Gulf coasts and across the frequency spectra to eliminate the effect of sampling fluctuations. Results of our analyses are given in figures and tables with brief definitions and explanations. The figures depicting coastal profiles of probability distributions for selected percentiles give ranges of climatologically defined hurricane parameters. Users should determine for their particular application the critical class intervals within these ranges.

Table 24 summarizes the data sources and the classes of tropical cyclones represented. These are not the same for the all factors, for the reasons stated in the report.

12.1 Frequency of Tropical Cyclone Occurrences

The frequency of landfalling, exiting, and bypassing tropical cyclones were summarized in Figures 27, 28, 31 and 32, respectively. Of the three classes of storms, the most significant factor for storm-surge frequency computations is the frequency of landfalling storms. Coastal variation of landfalling storm frequencies is most rapid along the Atlantic coast of Florida and along the North Carolina and Virginia coasts (fig. 27). This steep gradient of hurricane frequency contributes to the potential for significant differences in the magnitude of resultant coastal surge frequencies in adjacent locations along these portions of the coast. Frequencies of alongshore storms are generally small (negligible) for most of the Gulf coast and, except for portions of the west coast of Florida, contribute little to the overall tide frequencies. High frequencies of exiting storms occurred on the Atlantic coast near Jacksonville, Florida and just north of Cape Hatteras. Exiting storms generally produce lower storm surges and they are usually weaker than landfalling or alongshore storms

for the same latitudes. Their contribution to the overall storm-surge frequencies is negligible in most cases. Because of coastal orientation, frequencies of landfalling storms are not continuous from Cape Sable, Florida, to the Florida Keys. Our treatment of the analysis in this area is discussed in Section 6.2.

12.2 Probability Distribution of Storm Parameters

Analysis of the data led to a set of graphs depicting the probability distribution of central pressure, radius of maximum winds, forward speed, and direction of storm motion. The central pressure distribution (figs. 34 and 35) is for tropical cyclones and is broken down for illustrative purposes into seven probability levels (percentiles) ranging from 1 to 90 percent. The probability levels were selected at intervals sufficiently close for the purpose of reconstructing smooth cumulative probability curves and should not be considered as a guide in selecting the number of class intervals appropriate for computational purposes.

Probability levels ranging from 5 to 95 percent were selected to depict the full range of other parameters (R, T, θ). The distribution for the radius of maximum winds (figs. 37 and 38) was derived from hurricane data only, and is illustrated for five selected probability levels. The resulting probability distribution may be considered applicable for both hurricanes and tropical storms. The forward speed distribution (figs. 40 and 41), based on tropical cyclones landfalling on the United States coasts, is illustrated for six selected probability levels. This distribution is also adopted for alongshore storms, as discussed in Section 11.4. The direction of storm motion distribution for landfalling tropical cyclones is illustrated for five probability levels in Figures 43 (Gulf) and 44 (Atlantic coast, south of Cape Hatteras). Because of the very limited number of storms affecting the Atlantic coast north of Cape Hatteras, only three probability levels are given for direction of storm motion for this portion of the coast (fig. 45).

12.3 Independence of Parameters

The parameters presented in this study can be considered statistically independent, except for central pressure (P_o) and radius of maximum winds (R). Limited historical data indicate that hurricanes with central pressure below 920 mb have small R's. Hurricanes with large R's are nearly always of moderate or weak intensity, but not all the weaker storms have large R's. Establishing the joint probability of two factors with a degree of reliability requires a much larger sample of data than that available in Tables 1 to 3. For this reason, we specify R values for only the most intense hurricanes (sec. 4.5).

Observations show that alongshore hurricanes generally move at a faster speed than landfalling hurricanes at the same latitude. The differences in forward speeds (T) were presumably related to the direction of storm motion, θ, (according to TR 15). There was no detectable interrelation between T and θ for landfalling hurricanes found in statistical tests of the present study. The small sample size does not allow us to establish any interrelation between T and θ for alongshore storms. With increased data in future years, it would be of interest to re-examine this relationship.

It is generally believed that hurricanes striking the Florida Keys from an easterly direction are more intense than hurricanes coming from the southwesterly direction. The data sample for that area is not sufficient for us to statistically establish an interrelation of P_o and θ for landfalling storms. A similar situation exists in the area north of Cape Hatteras, North Carolina. In the latter case, separate P_o probability distributions were evaluated for tropical cyclones coming from the northeasterly and southeasterly directions (see chapt. 5). Segregating the sample into subgroups would take care of the interdependence of P and θ for this particular area. This approach may be used to deal with similar problems in other regions.

ACKNOWLEDGMENTS

The authors are grateful for the help of numerous members of the Water Management Information Division, Office of Hydrology, National Weather Service, during the course of this study. In particular, we would like to thank Helen V. Rodgers for invaluable editorial assistance, and Roxanne Johnson who ably prepared many of the figures for this report. The guidance and critical review of the manuscript by E. Marshall Hansen, Chief of the Water Management Division, was especially helpful.

We would like to thank researchers at the National Hurricane Center, the Hurricane Research Division of NOAA's Atlantic Oceanographic and Meteorological Laboratories, and the National Weather Service's Techniques Development Laboratories for their extremely helpful discussions, both during the formative stages of our study, and as work progressed. We also want to thank Dr. Gerald F. Cotton of NOAA's Air Resources Laboratory, who advised us on some statistical procedures.

The authors especially want to express their appreciation to the staff of the Hurricane Research Division for providing us with data from their files. In particular, we wish to thank Mark D. Powell for sharing with us his data collections obtained in post-hurricane surveys, and Neil Dorst for preparing computer plots of hurricane wind data observed by reconnaissance aircraft.

Periodic meetings with the staff of the sponsoring agency, the Federal Emergency Management Agency, and their consultants, provided us with additional insight throughout the preparation of this report. Dr. Frank Tsai of the Federal Insurance Agency, Federal Emergency Management Agency, Dr. Chester P. Jelesianski of the Techniques Development Laboratory, and Charles Neumann of the National Hurricane Center, provided crucial reviews of drafts of this report. These reviews were most helpful in improving the quality of the final product.

REFERENCES

Alaka, M.A., 1968: Climatology of Atlantic Tropical Storms and Hurricanes, ESSA Technical Report WB-6, Environmental Sciences Services Administration, U.S. Department of Commerce, Washington, DC, 18pp.

Benson, M.A., 1962: Plotting Positions and Economics of Engineering Planning, Proceedings of American Society of Civil Engineers, 88 (HY6), part 1.

Bergeron, T., 1954: The Problem of Tropical Cyclones, Quarterly Journal of the Royal Meteorological Society, Vol. 80, No. 344, pp 131-164.

Bradbury, D.L., 1971: The Filling Over Land of Hurricane Camille, Satellite and Mesometeorology Research Project Paper No. 96, NOAA Grant E-198-68(B) MOD No. 2, Department of the Geophysical Sciences, The University of Chicago, Chicago, IL, 25 pp.

Case, R.A. and Gerrish, H.P., 1984: Atlantic Hurricane Season of 1983, Monthly Weather Review, Vol. 112, No. 5, pp. 1083-1092.

Chow, V.T. (ed.), 1964: Handbook of Applied Hydrology, McGraw-Hill, New York, NY.

Clark, G.B. and Staff, 1984: Annual Data and Verification Tabulation - Atlantic Tropical Cyclones, 1983, NOAA Technical Memorandum NWS NHC-21, National Hurricane Center, National Weather Service, National Oceanic and Atmospheric Administration, U.S. Department of Commerce, Miami, FL, 92 pp.

Cline, M., 1926: Tropical Cyclones, McMillan Company, New York, NY, 301 pp.

Colon, J.A., 1953: A Study of Hurricane Tracks for Forecasting Purposes, Monthly Weather Review, Vol. 81, No. 3, pp. 53-66.

Conover, W.J., 1971: Practical Non-parametric Statistics, John Wiley and Sons, New York, NY, 462 pp.

Craddock, J.M., 1969: Statistics in the Computer Age, American Elsevier Publishing Company, New York, NY, 214 pp.

Cry, G.W, 1965: Tropical Cyclones of the North Atlantic Ocean, Tracks and Frequencies of Hurricanes and Tropical Storms, 1871-1963, Technical Paper No. 55, Weather Bureau, U.S. Department of Commerce, Washington, DC, 148 pp.

DeAngelis, R.M., 1969: Enter Camille, Weatherwise, Vol. 22, pp. 173-179.

DeAngelis, R.M. and Nelson, E.R., 1969: Hurricane Camille August 5-22, Climatological Data National Summary, Vol. 20, No. 8, Environmental Science Services Administration, U.S. Department of Commerce, Washington, DC, pp. 451-474.

DeAngelis, D., 1979: Hurricane David - Preliminary Report, Weekly Weather and Crop Bulletin, National Oceanographic Data Center, Environmental Data and Information Service, National Oceanic and Atmospheric Administration, Washington, DC, pp. 16-17.

Dunn, G.E., Davis, W.R., and Moore, P.L., 1955: Hurricanes of 1955, Monthly Weather Review, Vol. 83, No. 12, pp. 315-326.

Frank, W.M. and Gray, W.M., 1980: Radius and Frequency of 15 m/s (30 kt) winds around tropical cyclones. Journal of Applied Meteorology, Vol. 19, pp 219-223.

Friedman, H.A., Brown, W.J., Jr., and Michie, J.D., 1982: Airborne Research Meteorological Data Collected by the National Hurricane Research Laboratory During the NOAA/RFC WP-3D ERA - Inventory and Availability, NOAA Data Report ERL AOML-2, National Hurricane Research Laboratory, National Oceanic and Atmospheric Administration, U.S. Department of Commerce, Miami, FL, 376 pp.

Friedman, H.A., Armholes, C.A., Dorst, N.M., Nelson, C.J., and Brown, W.J., Jr., 1984: Airborne Research Meteorological Data Collected by the National Hurricane Research Laboratory (HRD/AOML) During the 1982-1983 Hurricane Seasons - Inventory and Availability, NOAA Data Report ERL AOML-3, National Hurricane Research Laboratory, National Oceanic and Atmospheric Administration, U.S. Department of Commerce, Miami, FL, 158 pp.

Garcia, A.W. and Flor, T.H., 1984: Hurricane Alicia Storm Surge and Wave Data, Technical Report CERC-84-6, Coastal Engineering Research Center, Waterways Experiment Station, U.S. Army Corps of Engineers, Vicksburg, MS, 89 pp.

Graham, H.E. and Nunn, D.E., 1959: Meteorological Considerations Pertinent to Standard Project Hurricane, Atlantic and Gulf Coasts of the United States, National Hurricane Research Project Report No. 33, Weather Bureau, U.S. Department of Commerce, Washington, DC, 76 pp.

Graham, H.E. and Hudson, G.N., 1960: Surface Winds Near the Center of Hurricanes (and other cyclones), National Hurricane Research Project Report No. 39, Weather Bureau, U.S. Department of Commerce, Washington, DC, 200 pp.

Gumbel, E.J., 1958: Statistics of Extreme Events, Columbia University Press, New York, NY.

Hardy, A.V. and Carney, C.B., 1962: North Carolina Hurricanes, Weather Bureau, U.S. Department of Commerce, Raleigh, NC, 26pp.

Harris, D.L., 1959: An Interim Hurricane Storm Surge Forecasting Guide. National Hurricane Research Project Report No. 32, Weather Bureau, U.S. Department of Commerce, Washington, DC, 24 pp.

Hawkins, H.F., Christensen, F.E., Pearce, S.E., and Staff, 1962: Inventory, Use and Availability of National Hurricane Research Project Meteorological Data Gathered by Aircraft, National Hurricane Research Project Report No. 52, Environmental Research Laboratories, National Oceanic and Atmospheric Administration, U.S. Department of Commerce, Boulder, CO, 48 pp., plus data.

Hebert, P.J. and Poteat, K.O., 1975: A Satellite Classification Technique for Subtropical Cyclones, NOAA Technical Memorandum NWS SR-83, National Weather Service, National Oceanic and Atmospheric Administration, U.S. Department of Commerce, Fort Worth, TX, 25 pp.

Hebert, P.J., 1980: Atlantic Hurricane Season of 1979, Monthly Weather Review, Vol. 108, No. 7, pp. 973-990.

Hebert, P.J. and Staff, 1980: Annual Data and Verification Tabulation Atlantic Tropical Cyclones, 1979, NOAA Technical Memorandum NWS NHC 13, National Hurricane Center, National Weather Service, National Oceanic and Atmospheric Administration, U.S. Department of Commerce, Miami, FL, 77 pp.

Hess, S.L., 1945: A Statistical Study of the Deepening and Filling of Extratropical Cyclones. Journal of Meteorology, Vol. 2, No. 3, pp. 179-184.

Ho, F.P. and Myers, V.A., 1975: Joint Probability Method of Tide Frequency Analysis Applied to Apalachicola Bay and St. George Sound, Florida. NOAA Technical Report NWS 18, National Weather Service, National Oceanic and Atmospheric Administration, U.S. Department of Commerce, Silver Spring, MD, 43 pp.

Ho, F.P., Schwerdt, R.W., and Goodyear, H.V., 1975: Some Climatological Characteristics of Hurricanes and Tropical Storms, Gulf and East Coasts of the United States, NOAA Technical Report NWS 15, National Weather Service, National Oceanic and Atmospheric Administration, U.S. Department of Commerce, Silver Spring, MD, 87 pp.

Ho, F.P. and Tracey, R.J., 1975: Storm Tide Frequency Analysis for the Coast of North Carolina, North of Cape Lookout, NOAA Technical Memorandum NWS HYDRO-27, National Weather Service, National Oceanic and Atmospheric Administration, U.S. Department of Commerce, Silver Spring, MD, 46 pp.

Ho, F.P. and Miller, J.F., 1982: Pertinent Meteorological and Hurricane Tide Data for Hurricane Carla, NOAA Technical Report NWS 32, National Weather Service, National Oceanic and Atmospheric Administration, U.S. Department of Commerce, Silver Spring, MD, 111 pp.

Ho, F.P. and Miller, J.F., 1983: Pertinent Meteorological Data for Hurricane Allen of 1980, NOAA Technical Report NWS 35, National Weather Service, National Oceanic and Atmospheric Administration, U.S. Department of Commerce, Silver Spring, MD, 73 pp.

Howell, G., Lee, D.Y., and Wang, H., 1982: Storm Surge Measurements and Computations for Hurricane David, Coastal and Oceanographic Engineering Department, University of Florida, for Office of Nuclear Regulatory Research, U.S. Nuclear Regulatory Commission, Washington, DC, 67 pp.

Hubert, L.F., 1955: Frictional Filling of Hurricanes. Bulletin American Meteorological Society, Vol. 36, No. 9, pp. 440-445.

Jarvinen, B.R., Neumann, C.J., and Davis, M.A.S., 1984: A Tropical Cyclone Data Tape for the North Atlantic Basin, 1886-1983: Contents, Limitations, and Uses, NOAA Technical Memorandum NWS NHC 22, National Hurricane Center, National Weather Service, National Oceanic and Atmospheric Administration, U.S. Department of Commerce, Coral Gables, FL, 21 pp.

Jarvinen, B.R., Damiano, A.B., and Lockett, G.J., 1985: A Storm Surge Atlas for Corpus Christi, Texas. NOAA Technical Memorandum NWS NHC 27, National Hurricane Center, National Weather Service, National Oceanic and Atmospheric Administration, U.S. Department of Commerce, Coral Gables, FL, 438 pp.

Jordan, C.L., 1957: Estimating Central Pressure of Tropical Cyclones from Aircraft Data, National Hurricane Research Project Report No. 10, Weather Bureau, U.S. Department of Commerce, West Palm Beach, FL, 12 pp.

Jordan, H.M. and Stowell, D.J., 1955: Some Small-scale Features of the Track of Hurricane Ione, Monthly Weather Review, Vol 83, pp. 315-326.

Kuo, H.L., 1959: Dynamics of Convective Vortices and Eye Formation. In The Atmosphere and Sea in Motion, Rockefeller Institute Press, New York, NY, pp. 413-424.

Lambeth, B., 1983: Hurricane Alicia: Special Report, Radian Corporation, Austin, TX, 20 pp.

Lawrence, M.B., 1978: Atlantic Hurricane Season of 1977, Monthly Weather Review, Vol. 106, pp 534-540.

Lawrence, M.B. and Pelissier, J.M., 1981: Atlantic Hurricane Season of 1980, Monthly Weather Review, Vol. 109, pp. 1567-1582

Ludlam, W., 1963: Early American Hurricanes, 1492-1870, American Meteorological Society, Boston, MA, 198 pp.

Malkin, W., 1959: Filling and Intensity Changes in Hurricanes Over Land. National Hurricane Research Project Report No. 34, Weather Bureau, U.S. Department of Commerce, Washington, DC, 18 pp.

Marks, F.D., Jr., 1985: Evolution of the Structure of Precipitation in Hurricane Allen, Monthly Weather Review, Vol. 113, No. 6, pp. 909-930.

Marshall, R.D., 1984: Fastest-mile Windspeeds in Hurricane Alicia, NBS Technical Note 1197, National Bureau of Standards, U.S. Department of Commerce, Washington, DC, 61 pp.

Merceret, F.J., Davis, H.W., DeVivo, R., Lewis, W.M. Mallinger, W.D., and Zysko, A., 1980: In-Flight Calibration of the NOAA/RFC Meteorological Research Aircraft Instruments at the Air Force Eastern Test Range: 1977-1978, NOAA Technical Memorandum ERL-RFC-6, Environmental Research Laboratories, National Oceanic and Atmospheric Administration, U.S. Department of Commerce, Miami, FL, 64 pp.

Merrill, R.T., 1984: A Comparison of Large and Small Tropical Cyclones, Monthly Weather Review, Vol. 112, pp. 1408-1418.

Miller, B.I., 1958: The Three-Dimensional Wind Structure Around a Tropical Cyclone, National Hurricane Research Project Report No. 15, Weather Bureau, U.S. Department of Commerce, Miami, FL.

Miller, B.I., 1963: On the Filling of Tropical Cyclones Over Land, with Particular Reference to Hurricane Donna of 1960, National Hurricane Research Project Report No. 66, Weather Bureau, U.S. Department of Commerce, Washington, DC, 82pp.

Myers, V.A., 1954: Characteristics of United States Hurricanes Pertinent to Levee Design for Lake Okeechobee, Florida, Hydrometeorological Report No. 32, Weather Bureau, U.S. Department of Commerce, and Corps of Engineers, U.S. Department of the Army, Washington, DC, 106 pp.

Myers, V.A., 1975: Storm Tide Frequencies on the South Carolina Coast, NOAA Technical Report NWS-16, National Weather Service, National Oceanic and Atmospheric Administration, U.S. Department of Commerce, Silver Spring, MD, 79 pp.

National Academy of Science, 1983: Evaluation of the FEMA Model for Estimating Potential Coastal Flooding from Hurricanes and Its Application to Lee County, Florida, Committee on Coastal Flooding From Hurricanes, Advisory Board on the Built Environment, Commission on Engineering and Technical Systems, National Research Council, National Academy Press, Washington, DC, 154 pp.

National Hurricane Center, 1980: Hurricane Allen, Climatological Data, National Summary, National Climatic Center, Environmental Data and Information Services, National Oceanic and Atmospheric Administration, U.S. Department of Commerce, Asheville, NC.

National Hurricane Center, 1983: Hurricane Alicia, Climatological Data, National Summary 1983, National Climatic Data Center, National Environmental Satellite, Data and Information Service, National Oceanic and Atmospheric Administration, U.S. Department of Commerce, Asheville, NC.

NOAA Data Buoy Center, 1984: NDBC Observations During Hurricanes Alicia and Barry, 1983, National Weather Service, National Oceanic and Atmospheric Administration, U.S. Department of Commerce, NSTL, MS, 34 pp.

Neumann, C.J., Cry, G.W., Caso, E.L., and Jarvinen, B.R., 1981: Tropical Cyclones of the North Atlantic Ocean, 1871-1981, National Climatic Center, National Oceanic and Atmospheric Administration, U.S. Department of Commerce, Asheville, NC, 174 pp.

Palmen, E., 1956: Formation and Development of Tropical Cyclones, Proceedings of the Tropical Cyclone Symposium, Brisbane, Australia, pp. 212-231.

Palmen, E. and Newton, C., 1969: Atmospheric Circulation Systems, Their Structure and Physical Interpretation, Academic Press, New York, NY, and London, pp. 515-522.

Petterssen, S., 1956: Weather Analysis and Forecasting. McGraw-Hill Book Co., Inc., New York, NY, Vol. 1, 428 pp.

Powell, M.D., 1982: The Transition of the Hurricane Frederic's Boundary-Layer Wind Field from the Open Gulf of Mexico to Landfall, Monthly Weather Review, Vol.110, pp. 1912-1932.

Powell, M.D., Marks, F.D., Jr., and Black, P.G., 1984, The Asymmetric Structure of Alicia's Windfield at Landfall, Proceedings, Conference on Coastal Engineering, Galveston, TX, American Society of Civil Engineers.

Riehl, H., 1954: Tropical Meteorology, McGraw-Hill Book Company, New York, NY, 392 pp.

Roberts, N.C., Jr., 1969: The Story of Extreme Hurricane Camille, August 14 Through August 22, 1969. Privately published report, Copyright by Nash C. Roberts, Jr., New Orleans, LA, 135pp.

Saffir, H.S., 1977: Design and Construction Requirements for Hurricane Resistant Construction, American Society of Civil Engineers, New York, Preprint Number 2830, 20 pp.

SAS Institute, 1982: SAS User's Guide: Basics, SAS Institute, Inc., Cary, NC.

Schloemer, R.W., 1954: Analysis and Synthesis of Hurricane Wind Patterns Over Lake Okeechobee, Florida, Hydrometeorological Report No. 31, Weather Bureau, U.S. Department of Commerce, and Corps of Engineers, U.S. Department of the Army, Washington, DC, 49pp.

Schwerdt, R.W., Ho, F.P., Watkins, R.R., 1979: Meteorological Criteria for Standard Project Hurricane and Probable Maximum Hurricane Windfields, Gulf and East Coasts of the United States, NOAA Technical Report NWS 23, National Weather Service, National Oceanic and Atmospheric Administration, U.S. Department of Commerce, Silver Spring, MD, 317 pp.

Shapiro, L.J., 1977: Tropical Storm Formation from Easterly Waves: A Criterion for Development, Journal of the Atmospheric Sciences, Vol. 34, pp. 1007-1021.

Shea, D.J. and Gray, W.M., 1972: The Structure and Dynamics of the Hurricane's Inner Core Region, Atmospheric Science Paper No. 182, NOAA Grant N22-65-72(G), NSF Grant GA 19937, Department of Atmospheric Science, Colorado State University, Fort Collins, CO, 134 pp.

Sheets, R.C., 1977: On the Evolution of Hurricane Anita, Presented at the Eleventh Technical Conference on Hurricanes and Tropical Meteorology, Miami Beach, FL pp. 495-465.

Simpson, R.H., Sugg, A.L., and Staff, 1970: Atlantic Hurricane Season of 1969, Monthly Weather Review, Vol. 98, pp. 295-300.

Sugg, A.L., Pardue, L.G., and Carrodus, R.L., 1971: Memorable Hurricanes of the United States Since 1873, NOAA Technical Memorandum NWS SR-56, National Weather Service, National Oceanic and Atmospheric Administration, U.S. Department of Commerce, Fort Worth, TX, 52 pp.

Taylor, G. and Staff, 1981: Annual Data and Verification Tabulation, Atlantic Tropical Cyclones - 1980, NOAA Technical Memorandum NWS NHC 15, National Hurricane Center, National Weather Service, National Oceanic and Atmospheric Administration, U.S. Department of Commerce, Miami, FL, 78 pp.

U.S. Army Corps of Engineers, 1983: Hurricane Alicia, 15-18 August 1983, Army Engineer District, Galveston, TX, 44 pp.

Weather Bureau, 1968: Interim Report -- Meteorological Characteristics of the Probable Maximum Hurricane, Atlantic and Gulf Coasts of the United States, unpublished memorandum HUR 7-97, U.S. Department of Commerce, Silver Spring, MD, 45 pp.

Weatherford, C.L., 1985: Typhoon Structure Variability. Department of Atmospheric Science Paper No. 391, Colorado State University, Ft. Collins, CO, 77 pp.

Willoughby, H.E., 1979: Some Aspects of the Dynamics in Hurricane Anita of 1977, NOAA Technical Memorandum ERL-NHEML-5, Environmental Research Laboratories, National Oceanic and Atmospheric Administration, U.S. Department of Commerce, Miami, FL, 30pp.

Willoughby, H.E., Clos, J.A., and Shoreibah, M.G., 1982: Concentric Eye Walls, Secondary Wind Maxima, and the Evolution of the Hurricane Vortex, Journal of the Atmospheric Sciences, Vol. 39, pp. 395-411.

Willoughby, H.E., 1985: Confirmatory Observations of Concentric Eyes in Hurricanes, Extended Abstracts, 16th Conference on Hurricanes and Tropical Meteorology, American Meteorological Society, Boston, MA.

APPENDIX A

Detailed Analysis of Selected Storms

A.1 Introduction

Data for storms that have occurred since TR 15 and are included in Tables 1 to 3 were based on consideration of research work done by others and our own detailed analyses. This Appendix provides examples of the analyses leading to development of the parameters used in this study. The first storm discussed is Hurricane Alicia, which is representative of Gulf storms. We then discuss Hurricane David which affected the Atlantic coast. David was also used in Chapter 4 to examine the relation between P_o and R. Finally, we conclude with an examination of Hurricane Allen. Allen was used in Chapter 4, and is an example of an intense storm undergoing a number of strengthening and weakening cycles.

A.2 Hurricane Alicia, August 15-21, 1983

A.2.1 Introduction

Hurricane Alicia was the first hurricane since Carla (1961) to cause extensive damage in the Houston-Galveston, Texas area (estimated at 1.8 billion [1983] dollars). By hurricane standards, Alicia was only a medium sized hurricane that reached a minimal category 3 status (based upon the Saffir/Simpson scale) at landfall. Carla was a much larger and more intense hurricane than Alicia, but Alicia struck a highly urbanized coastal area. Alicia caused more damage than Carla - the estimated total damage of nearly 2 billion dollars is the largest dollar damage ever recorded for a hurricane striking Texas. If a hurricane the size and strength of Carla were to strike close to the Galveston Bay area today, the losses have been estimated to be two to three times more than those caused by Alicia (Case and Gerrish 1984).

While the analyses described in this Appendix can provide useful information on a single storm event for calibration of hurricane surge computation using a numerical model, the purpose of the analyses was to specify climatological hurricane parameters. These are central pressure, speed and direction of forward motion, and the radius of maximum winds.

A.2.2 Previous Reports

The National Hurricane Center provided a description of significant features of all Atlantic tropical storms that occurred during 1983, including Hurricane Alicia, in the Monthly Weather Review (Case and Gerrish 1984) and in the National Summary of Climatic Data (National Hurricane Center 1983). These publications also included a smoothed "best" track for Alicia. The NHC publication on annual data and verification tabulation for the 1983 Atlantic tropical cyclones (Clark and Staff 1984) also includes a list of Alicia's center-fix positions obtained by aerial reconnaissance penetrations, satellite images, and land-based radar. The hurricane's central pressure, maximum winds and other data observed by reconnaissance aircraft are also included in that report. Meteorological data collected at data buoy stations in the Gulf of Mexico can be found in the report "NDBC Observations During Hurricanes Alicia and Barry, 1983," published by the NOAA Data Buoy Center (1984).

Lambeth (1983) provided a summary of available information about Hurricane Alicia. It included maximum wind, minimum pressure, and times of occurrences of both, reported from regular reporting stations and other sources, including the Texas Air Control Board (6 stations), Houston Regional Monitoring Corporation (12 monitoring stations) in the Houston-Galveston area, and the Dow Chemical Plant in Freeport, Texas.

Marshall (1984) used surface windspeeds recorded during the passage of Alicia to estimate fastest-mile windspeeds at 10 m above ground and compared these speeds with recommended windspeed criteria for the design of buildings and other permanent structures. Powell et al. (1984) described the asymmetric character of the windfield in Hurricane Alicia and the changes in the winds during landfall. They found that the strongest surface and flight-level winds showed a close relationship to the precipitation structure of the storm as depicted by radar. Willoughby (1985) also described the evolution of Alicia's windfield as the hurricane made landfall.

The Galveston District of the U.S. Army Corps of Engineers (1983) evaluated storm damage caused by Alicia and published summaries of hydrologic, meteorologic and damage data. Garcia and Flor (1984) compiled coastal and inland tide gage data and high-water marks associated with Hurricane Alicia. They also included wave data and wave spectra in their report.

A.2.3 Sources of Data

The reports discussed in the previous section were used to the maximum extent possible in the present study. We also examined original records to ensure the accuracy and completeness of this study and to enable us to provide more detailed information on track position, speed, central pressure, etc. This permitted us to perform the most comprehensive and detailed analysis yet developed for meteorological factors associated with Alicia and important to storm-surge modeling.

The basic information was obtained from the regularly reporting network of weather stations operated by NWS, NOAA and the military services. These reports are maintained at the National Climatic Data Center in Asheville, North Carolina. Supplemental data, available in the NCDC archives, included ship observations, radar observations, radiosonde records, reconnaissance flight data and satellite observations.

In addition, meteorological data collected by research aircraft of NOAA's Office of Aircraft Operations (OAO) were processed by computer and stored on magnetic tapes at the Hurricane Research Division (HRD) of NOAA's Atlantic Oceanographic and Meteorological Laboratory (AOML) in Miami, Florida. This information was made available to us for this report. A detailed description of the collection of meteorological information by aircraft, including the instrumentation, its calibration, and reliabilities, has been included in Hawkins et al. (1962). A more recent discussion of the calibration and instrumentation of present-day NOAA research aircraft can be found in other publications (e.g., Merceret et al. 1980). Availability of airborne research meteorological data collected by HRD/AOML are included in Friedman et al. (1982, 1984).

A.2.4 General Meteorological Situation

The system which developed into Hurricane Alicia on August 17, 1983, initially formed in the northern portion of the central Gulf of Mexico. This system intensified into a tropical storm around mid-day of August 15 and drifted westward for the next 24 hours. Surface pressures were high over the Gulf of Mexico and remained high during the early stages of the storm's development. Several ships located near the storm reported pressures of 1015 to 1016 mb late on the 15th. During this time the storm remained quite small and generated winds stronger than usually observed in storms with similar minimum central pressures. Alicia turned toward the west-northwest on the afternoon of August 16 and attained hurricane intensity on the morning of the 17th. Hurricane Alicia moved northwestward at the a steady pace and crossed the Texas coast about 30 nmi southwest of Galveston at 0700 GMT on August 18. The minimum pressure at the time of landfall was 962 mb. Maximum sustained winds of 78 kn were reported by a Coast Guard Cutter near Galveston. Alicia maintained its hurricane intensity for the 6 hours after making landfall. Maximum winds of 77 kn were reported at 1050 and 1524 GMT at Pearland, Texas, and 70 kn at 1300 GMT at Baytown, Texas. After passing the southwestern suburbs of Houston, Texas, Alicia weakened rapidly and moved northwestward over Texas and then northward over western Oklahoma.

A.2.5 Detailed Meteorological Analysis

A primary focus of this study was to analyze in detail hurricane parameters used in storm-surge models in order to develop a statistical climatology. For this purpose, we analyzed raw observational data. The intent of these analyses was to develop specific values of the hurricane's central pressure, radius of maximum winds, direction and speed of forward motion, and location of its center at various time intervals. Particular attention was focused on the period just before and after the hurricane made landfall since this is the time interval most critical for storm-surge computation.

A.2.5.1 Storm Track. Generally, the analyses of meteorological data are weighted toward synoptic-scale motion. The hurricane track, thus obtained, is the best estimate of the large-scale motion and not necessarily the most precise location of the eye at discrete time intervals. Track differences of a few miles, insignificant in determining the large-scale motion, can be significant for replicating high water on the open coast and inside bays and estuaries in surge-model computations.

Figure A.1 shows the final track determined for Hurricane Alicia from 0000 CST (0600 GMT) on August 16 through 1200 CST (1800 GMT) August 18 together with locations of meteorological stations used in this report. Except for Baytown, the stations are either NWS offices or military installations reporting regularly to the NWS. The positions of the storm center are shown at 6-hour intervals. The central pressure (mb) and the radius of maximum winds (nmi) are plotted to the left of 12-hour positions. Direction of storm motion at landfall was determined from figures such as this.

Any final determination of the track and speed of forward motion of a hurricane, especially over data-sparse regions, has inherent uncertainties. The track that was finally chosen was based on subjective analysis of all available information. Figure A.2 is an example of the information used in our analysis.

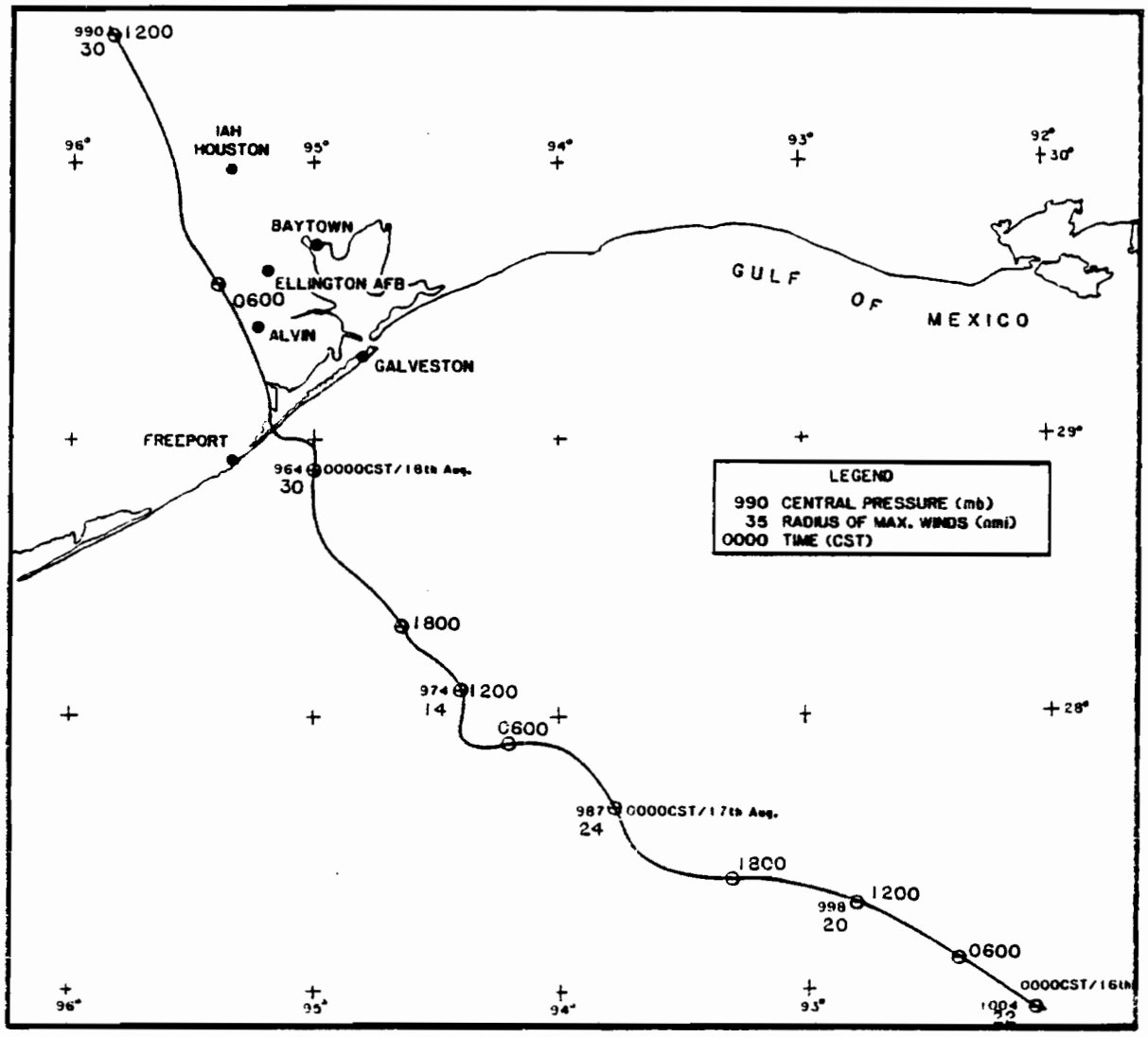

Figure A.1.—Hurricane track for Alicia, 0000 CST August 16 through 1200 CST August 18, 1983.

Hurricane eye positions based on radar observations reported from Galveston, Texas, and Lake Charles, Louisiana, are shown as solid dots. Aircraft reconnaissance penetration fixes are shown by triangles. Locations of the hurricane's center determined from satellite observations are given by diamonds. The data from radar fixes and aircraft penetrations were the primary sources used in determining the track and speed of the hurricane over the open ocean. However, information obtained from satellite observations and from ships and oil rigs operating in the area was considered in determining the final track and speed of motion.

A.2.5.2 Forward Speed. The translation speed of the hurricane is an important factor in determination of the surge along the open coast and in bays and estuaries. Hourly positions were the basic data used to determine the forward speed. Speeds between successive hours from positions along the best track were first determined and plotted on a time scale and smoothed. Then smooth curves drawn from these data were used to adjust the hourly locations. The new locations were examined with regard to the observed data and, if necessary, some further adjustments were made. This process was continued in an iterative fashion until the best combination between smooth forward speeds and observed eye

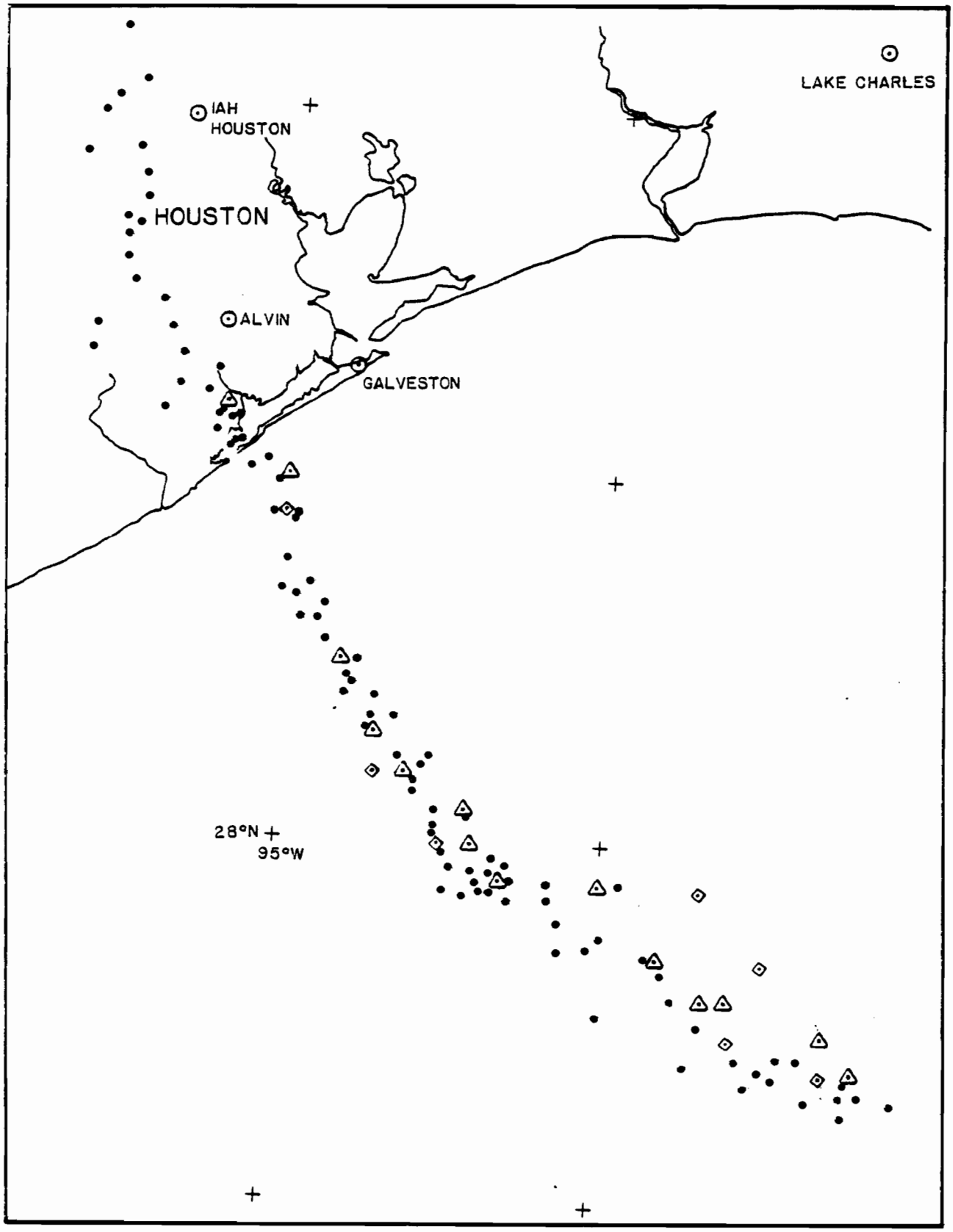

Figure A.2.—Hurricane eye position obtained from radar (●), aircraft reconnaissance penetration fixes (△), and satellite observations (◇).

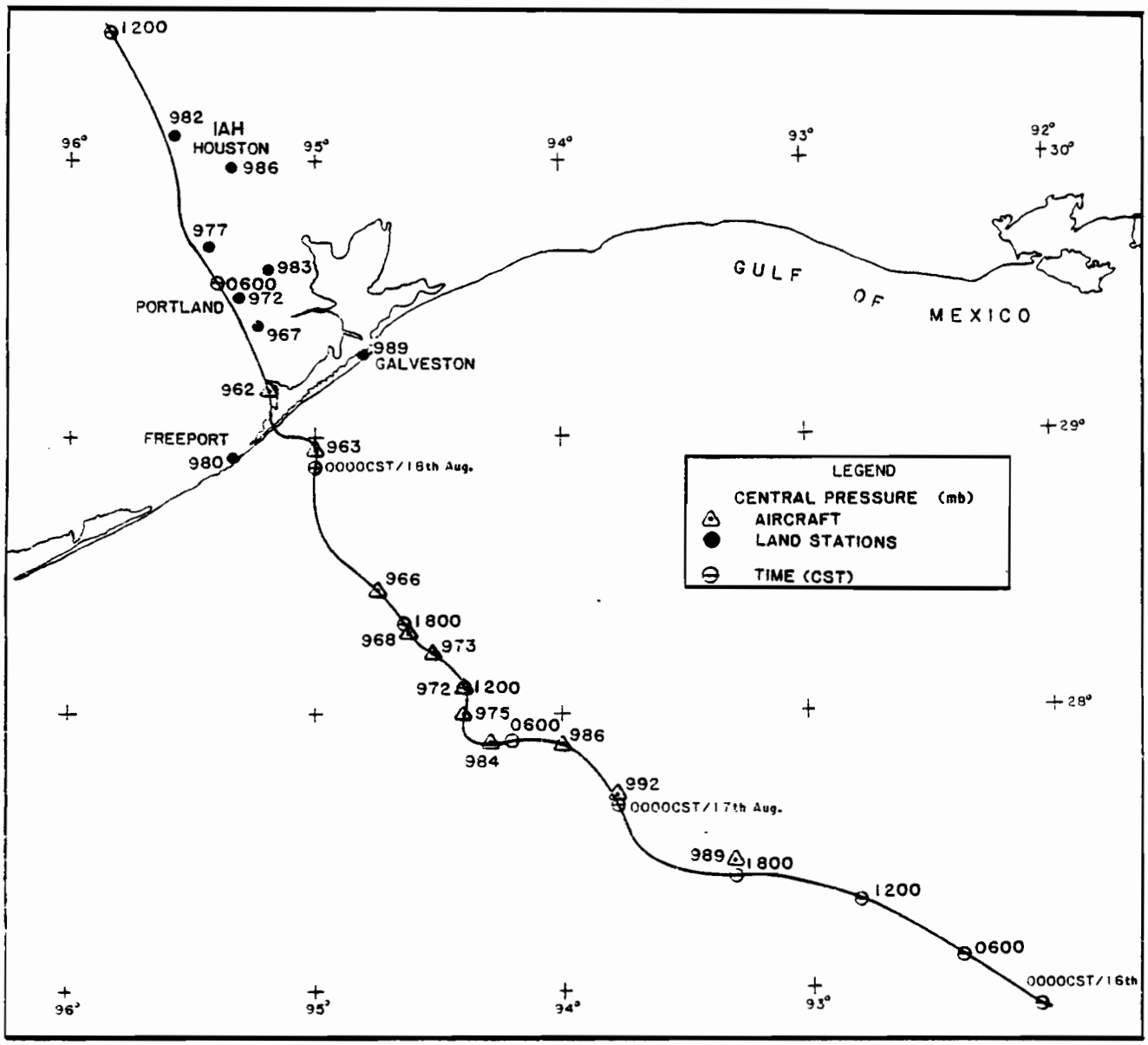

Figure A.3.—Minimum pressure recorded at land stations and by aircraft reconnaissance during Hurricane Alicia (1800 CST August 16 - 1200 CST August 18, 1983).

positions was obtained. This process helped to obtain the best possible estimate of forward speed and hourly locations.

A.2.5.3 Central Pressure. The most important meteorological input to storm-surge models is the intensity of the hurricane which can be parameterized in terms of its central pressure. Minimum pressures observed at stations and during reconnaissance aircraft penetrations are presented in Figure A.3. These observations were not all obtained at the same time. Since the track of the eye did not cross any land station location, none of the values reported at land stations are equal to the minimum central pressure in the storm.

Figure A.4 shows our analysis of pressure data from land stations and aircraft reconnaissance flights used to obtain a time history of Alicia's central pressure. A smooth curve was fit to the data by eye. Alicia deepened gradually

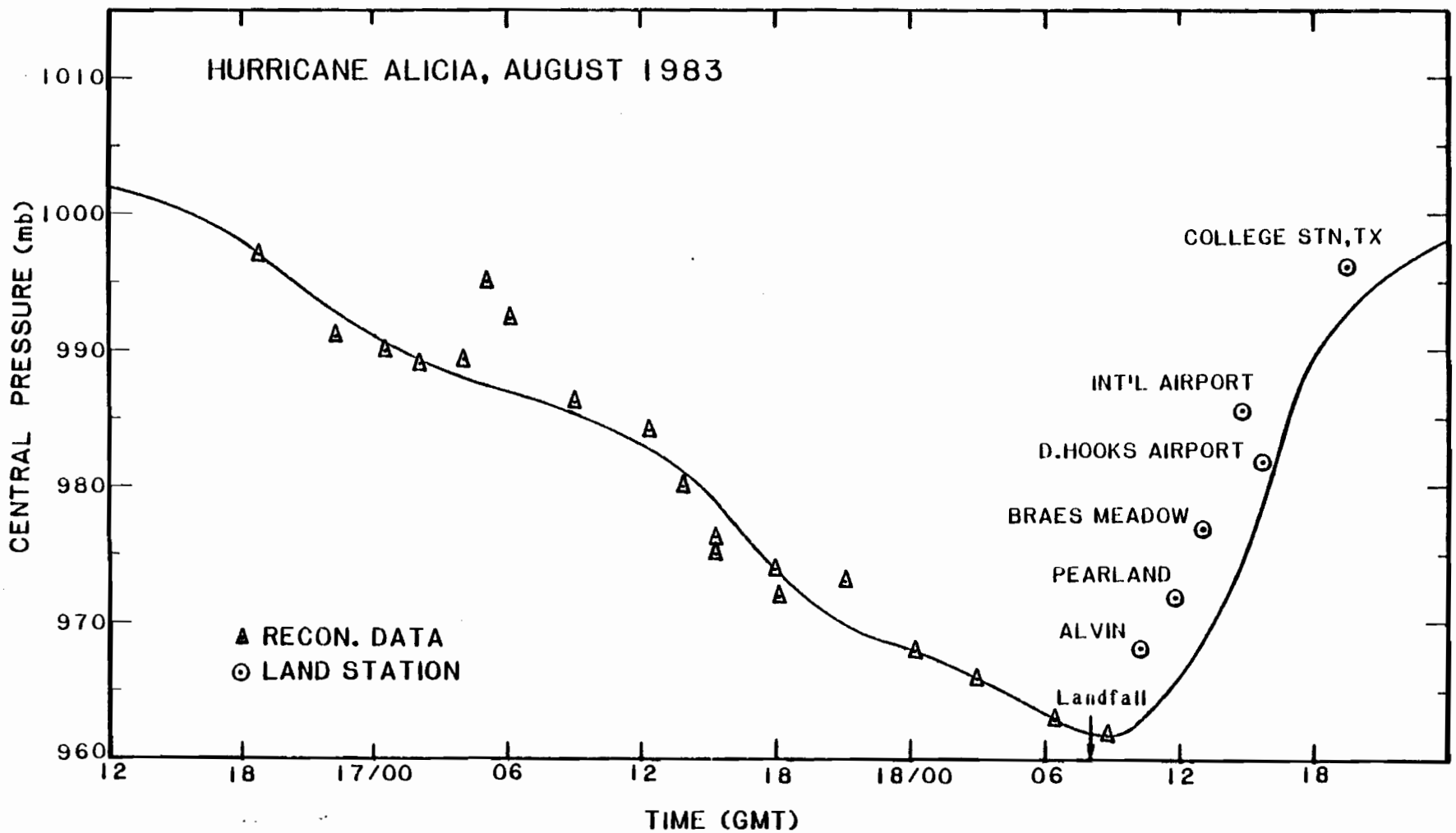

Figure A.4.—Variation of minimum central pressure estimates for Hurricane Alicia (August 16-18, 1983).

at an average rate of 1 mb per hour starting from 1200 GMT on August 16 until it reached a minimum value almost 2 hours after landfall. A reconnaissance aircraft recorded the minimum pressure of 962 mb at 0842 GMT on August 18 (fig. A.4). We consider this pressure to be the lowest that occurred in Hurricane Alicia. The short time intervals between central pressures obtained by aircraft, combined with other information (cited in sec. A.2.2), did not indicate any lower pressure at intermediate times.

As Alicia continued its north-northwesterly course overland, its intensity weakened only gradually over the next several hours. Alicia's central pressure reached its minimum and stayed nearly unchanged for another 2 to 3 hours after the hurricane center crossed the coast. Hurricane central pressure usually rises rapidly after the storm center moves over land. The central pressure of Camille (1969), which was a small and intense hurricane, rose at a rate of about 10 mb per hour for about 5 hours after its center crossed the Mississippi coast. For Alicia, the lowest sea-level pressure recorded at Alvin, Texas, was 967 mb and at Pearland, Texas, it was 972 mb. Alicia weakened rapidly soon after it passed the southwestern suburb of Houston, Texas. Its central pressure rose to 980 mb as its center passed near Spring, Texas, just 14 nmi west by north of Houston Intercontinental Airport (sea-level pressure at Spring reached 982 mb at 0952 CST or 1552 GMT - see fig. A.3).

A.2.5.4 Wind Analysis. In addition to the minimum pressure reported at stations during hurricane passage, surface winds were recorded at several weather stations operated by the NWS and the military services. The Hurricane Landfall Program executed by the HRD of the AOML, NOAA, recorded radar data and collected post-storm surface meteorological data from numerous NWS and private sources (Powell et al. 1984). This data collection was made available to us for this study. We analyzed the windfield for Alicia in two ways. We first examined the wind observations of land stations. Next, we did composite streamline analyses of the windfields at various intervals near the time of landfall. This wind analysis was used to aid in the determination of the radius of maximum winds. It also provided some guidance in determining the best track.

Figure A.5 shows the time variation of windspeed and sea-level pressure recorded at Houston Intercontinental Airport, Texas. The figure shows that the maximum wind of 51 kn occurred some 3 hours before the minimum pressure was reached at about 1450 GMT on August 18. The maximum wind was observed when the hurricane center was about 28 nmi (51.8 km) south of the station. Figure A.6 shows similar curves for pressure and windspeed recorded at the EXXON office in Baytown, Texas. A maximum wind of 70 kn was observed at 1300 GMT when the storm center was 31 nmi (57.4 km) to the west.

Since surface data were too limited and scattered to analyze the winds when the hurricane was located some distance off the coast, all reconnaissance aircraft observations within intervals of several hours were combined and plotted. This technique, called composite analysis, makes use of the hurricane center as the basis of the coordinate system. The position of each observation taken in aerial reconnaissance was measured in terms of azimuth angle and radial distance relative to the hurricane center at the time of observation. Each wind observation was then transposed to the relative location with respect to the hurricane center at map time. Figure A.7 shows a composite analysis based on the flight-level wind observations taken from 2040 GMT on the 17th through 0040 GMT on the 18th. The transposed observations are shown in this chart. The figure

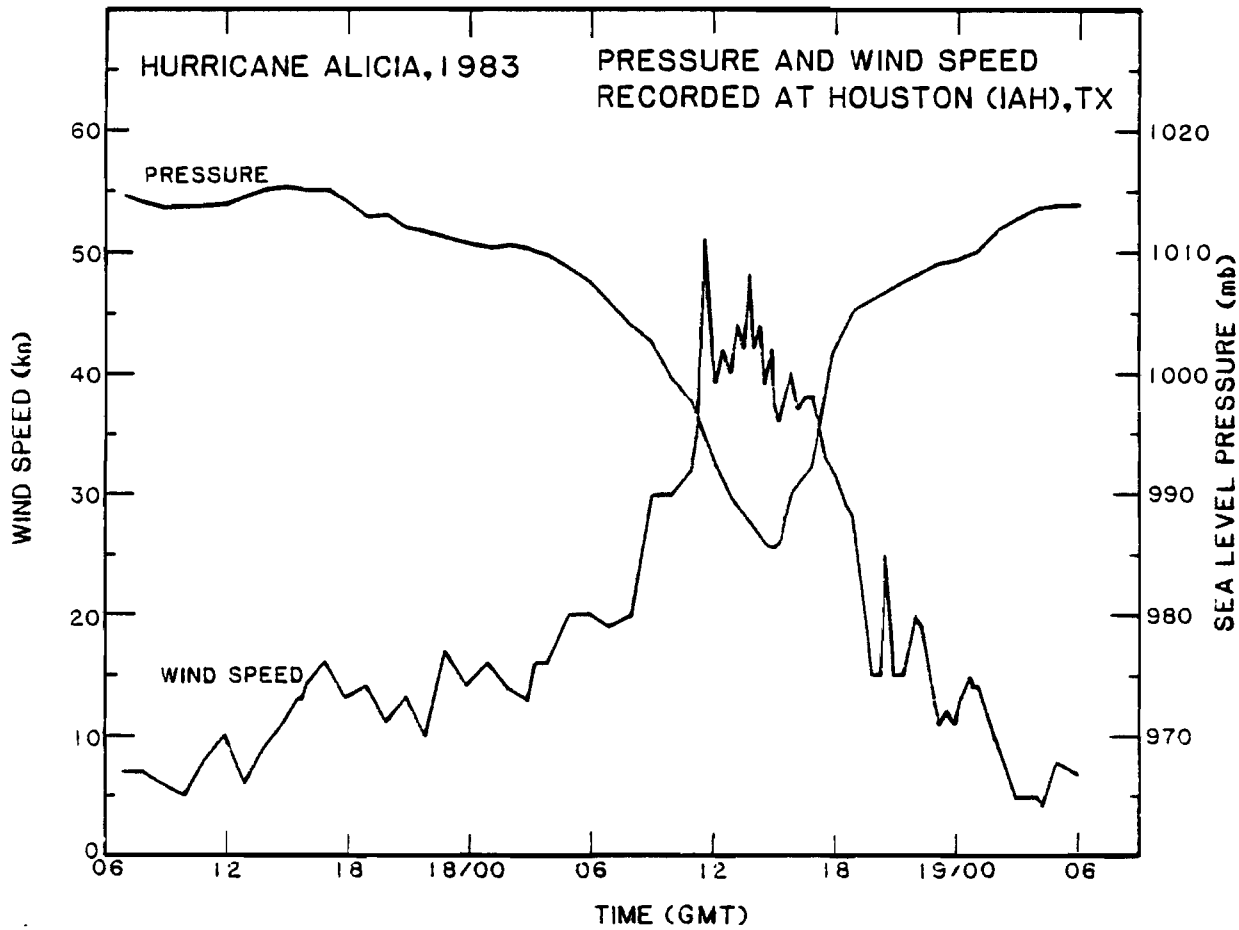

Figure A.5.—Hourly observations of sea-level pressure and surface wind speed recorded at Houston Intercontinental Airport, Texas, (0600 GMT August 17 - 0600 GMT August 19, 1983).

shows an isotach (isolines of constant windspeed) analysis of flight-level (1,500 m or 5,000 ft) winds. The isolines are labeled in kn. The analysis is assumed to apply to the center time (2240 GMT) of the composite period. Maximum winds of about 85 kn were observed in the front semi-circle at about 15 nmi (27.8 km) from the storm center.

Powell et al. (1984) constructed composite maps using mean surface and flight-level wind data, adjusted to the 10-m level. The observations were plotted at transposed locations, relative to the wind center of the storm, as determined from aircraft reconnaissance fixes, surface winds, sea-level pressures and radar data. Figure A.8 shows the streamline and isotach analysis of a composite map from Powell et al., near the time of landfall (0730 GMT). The analysis assumed that the storm structure and intensity had not changed during the period of composite, 0400-1100 GMT on August 18. At this time, Alicia exhibited a double eye structure. The maximum winds observed during this period in the storm (39 m/sec or 78 kn) were found in the outer radius by a Coast Guard cutter near Galveston, Texas. The extreme winds near the inner core (eyewall) were slightly less than those of the outer maximum which was about 30 nmi (55.6 km) from the storm center. Analysis of flight-level winds for the same period (diagram not shown) revealed maximum flight-level winds of 90-100 kn occurring at about 30 nmi

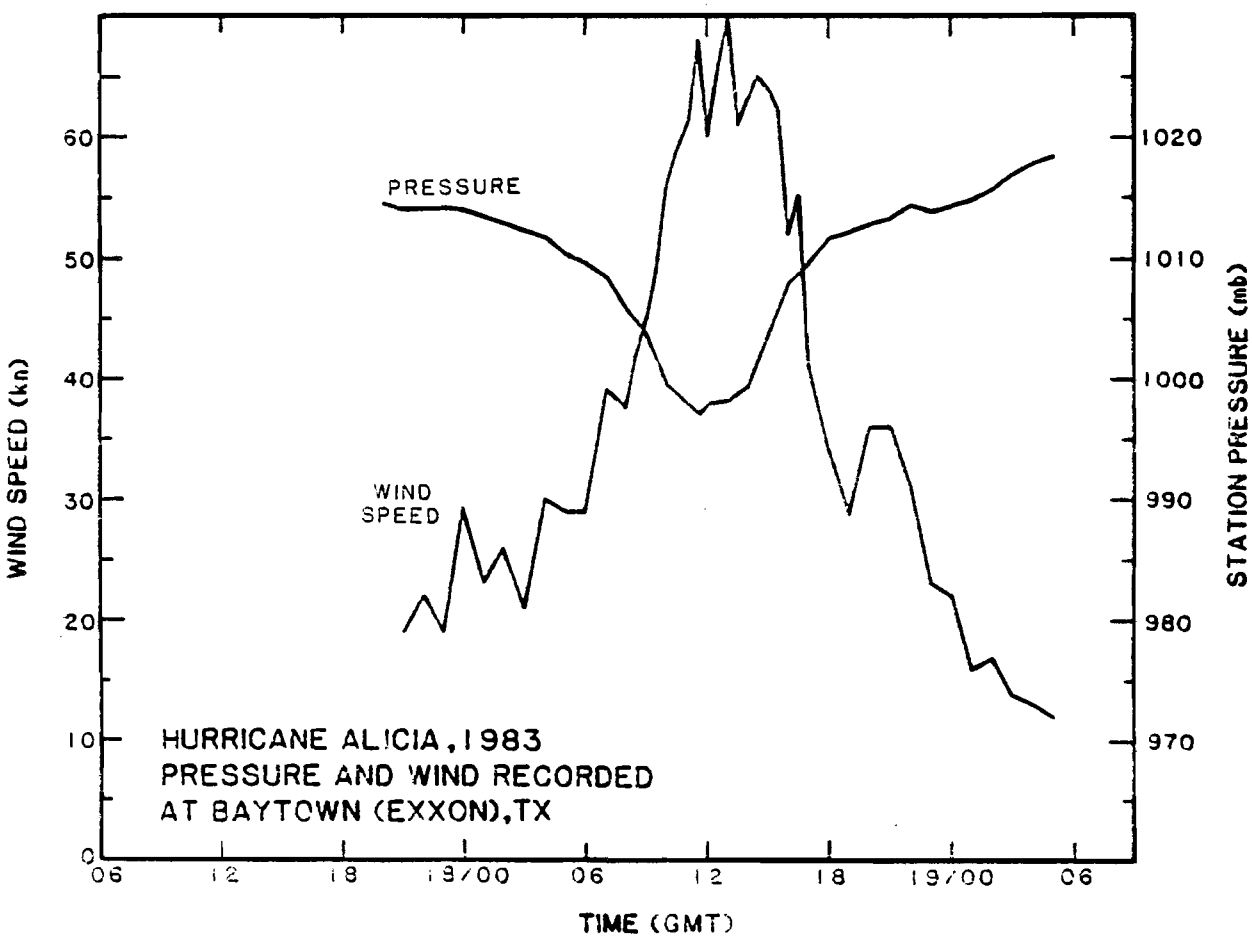

Figure A.6.--Same as Figure A.5 for Baytown, Texas.

(55.6 km) to the right of the storm center. This agrees very well with surface wind observations. A secondary wind maximum (80-85 kn), nearer the eye at flight-level, was located in the right rear quadrant of the storm.

A.2.5.5 Radius of Maximum Winds. A common measure of hurricane size is the distance between the storm center and the band of highest winds. The determination of the radius of the maximum winds was made on the basis of all available data for this storm. Three different types of observations were used. The first included maximum flight-level winds and estimated surface winds as reported by reconnaissance aircraft. The second was the radar-estimated eye wall diameter, as well as data on the size of the eye as reported by reconnaissance aircraft and by surface stations. Some visual reports were used when the reconnaissance aircraft were in the eye of the storm. The third measure, useful only after the hurricane was near shore, was the estimated radius deduced from wind records at land stations. In Alicia, we relied heavily on the first and the third measures to determine the R value.

Figure A.9 shows flight-level winds recorded at the 850-mb level between 1352-1433 GMT on August 17. The winds were recorded at 1-second intervals by reconnaissance aircraft of NOAA's Office of Aircraft Operations and were processed and plotted as a function of radial distance from the hurricane center. The winds obtained during a traverse of the eye along a path 349° to 169° revealed that maximum winds of about 45 m/sec (90 kn) occurred near 30 km

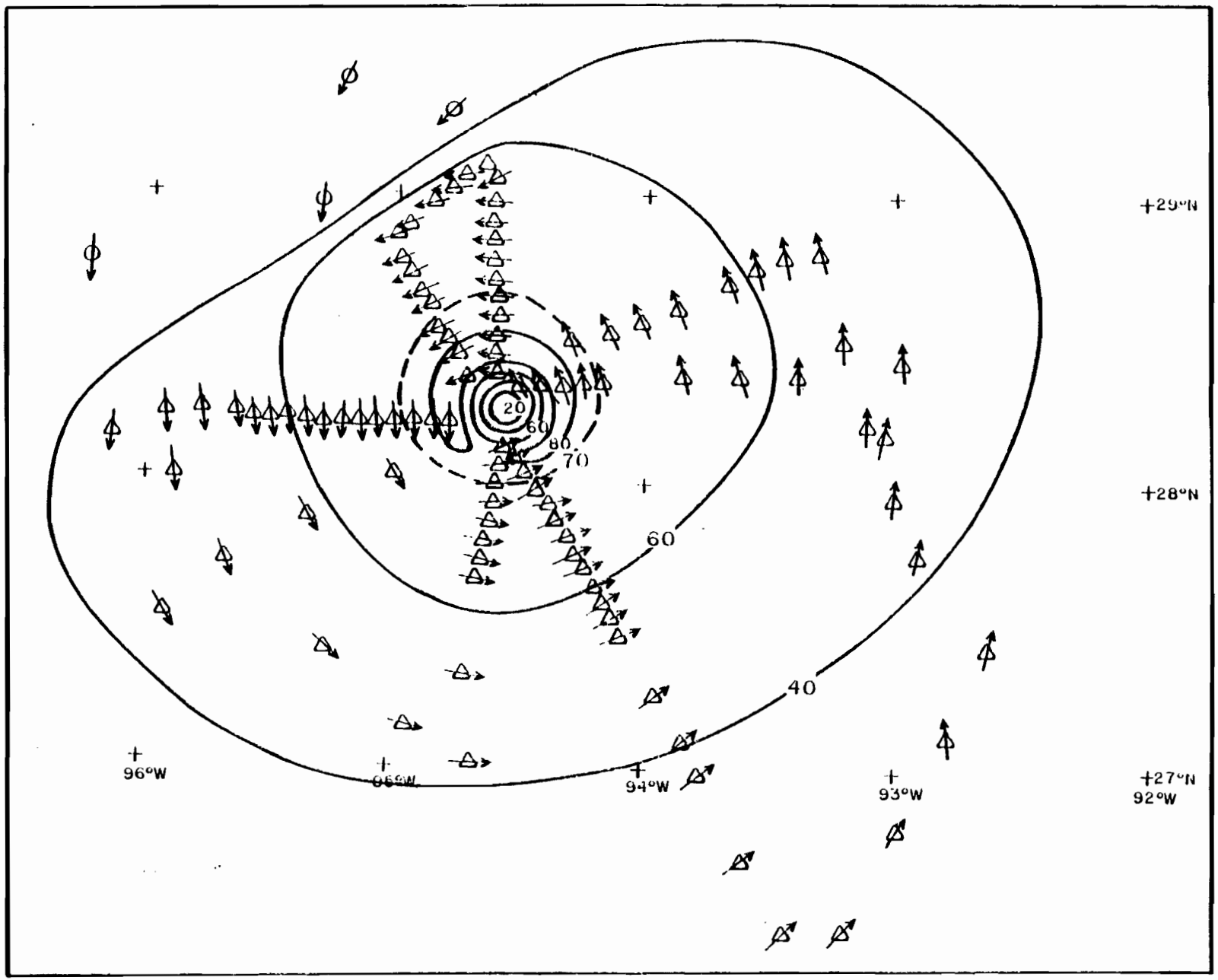

Figure A.7.—Composite isotach analysis for Hurricane Alicia, centered at 2240 GMT August 17, 1983.

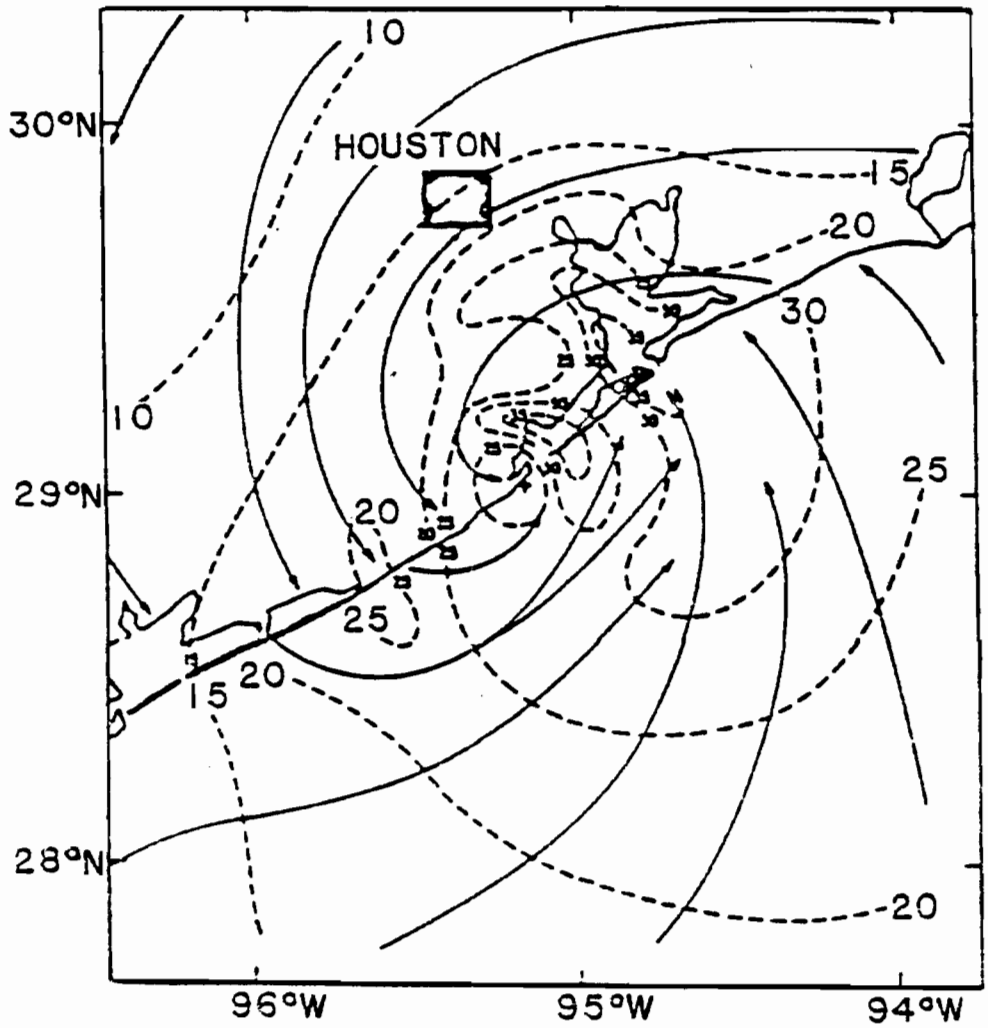

Figure A.8.—Streamline (solid lines) and 10-m isotach (dashed lines) analysis for Hurricane Alicia, 0730 GMT August 18, 1983 (from Powell et al. 1984).

(16 nmi) from the storm's center. Similar radial wind profiles constructed from winds recorded in each traverse of the hurricane eye were plotted by computer and made available to us by the HRD/AOML, NOAA. Examining a series of wind profiles, we obtained estimates of R at various times. Further analysis of composite charts of flight-level winds, previously discussed, provided additional insight into the time history of R in Alicia.

Figure A.10 shows the radial distance of wind maxima, thus obtained, at various times between 0600 GMT on August 17 and 0000 GMT on the 19th. Smooth lines drawn through these data points provided us with curves from which the radius of maximum winds was determined. Radial distances of maximum winds obtained from analysis of flight-level winds are shown by solid boxes; those deduced from surface winds recorded at land stations are given by triangles. The magnitude of extreme winds recorded at a given time was classified into two categories, a primary and a secondary wind maximum. The primary wind maximum is denoted by a solid line, while the secondary wind maximum is indicated by a dashed line. A shift of the primary wind maximum from a radial distance of about 15 nmi (27.8 km) to about 30 nmi (55.6 km) from the center seems to have occurred around 0600 GMT on August 18.

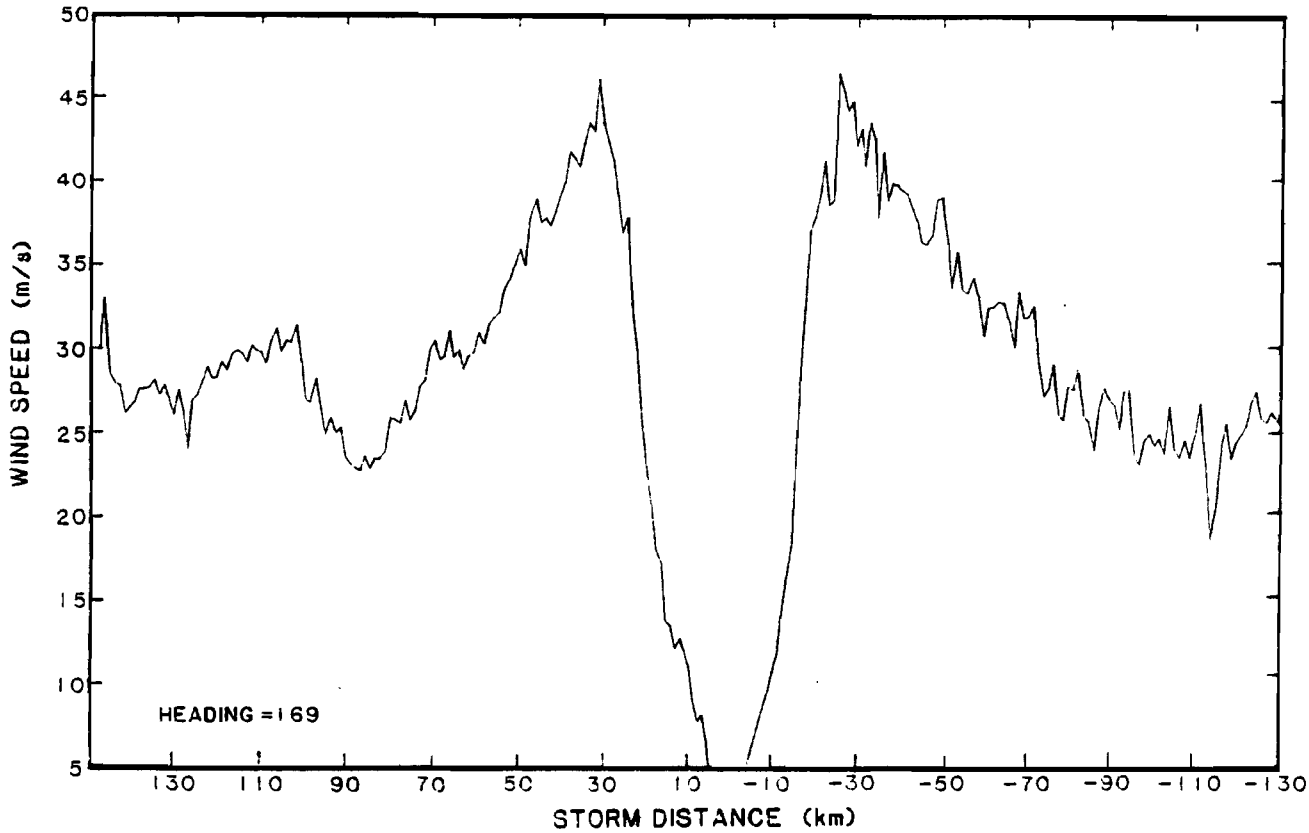

Figure A.9.--Flight-level (1500 m) winds recorded along radials through the center of Hurricane Alicia, 1352-1433 GMT August 17, 1983.

A.2.6 Discussion

The value of R is one of the important factors to be prescribed in a numerical computation of hurricane surges at the coast as well as in bays and estuaries. The R value, together with a precisely determined storm track specify the location of maximum winds along the coast. This, in turn, influences the water level produced by surface wind stress in a storm-surge model. It is important for surge modelers, as well as users of hurricane surge models, to have precise meteorological information in order to calibrate or verify a numerical surge model. The radius of maximum winds for Alicia shifted from 15 nmi (27.8 km) to 30 nmi (58.6 km) near the time of landfall. The transformation of storm size for Alicia took several hours to complete. The high winds near the inner core caused severe damages to downtown Houston, Texas. However, high-water levels in Galveston Bay (close to 11 ft above MSL at Baytown, Texas) were generated by the winds within the region of highest winds. After examining all available data, we concluded that R for Alicia shifted from 15 nmi (27.8 km) to 30 nmi (55.6 km) just before the hurricane made landfall and that the larger R should be applied to surge computations for the Galveston Bay area.

Hurricane data of recent years have shown large variabilities in hurricane parameters at various stages of a hurricane's life cycle. After a hurricane moves over land, its characteristics often change abruptly, due to larger surface friction and modifications to the heat and energy supply. Such changes in the characteristics of the hurricane would result in a departure from the standardized wind profile of the storm-surge model. Hurricane parameters, especially the index R, given in Tables 1 through 3 may not be the best values

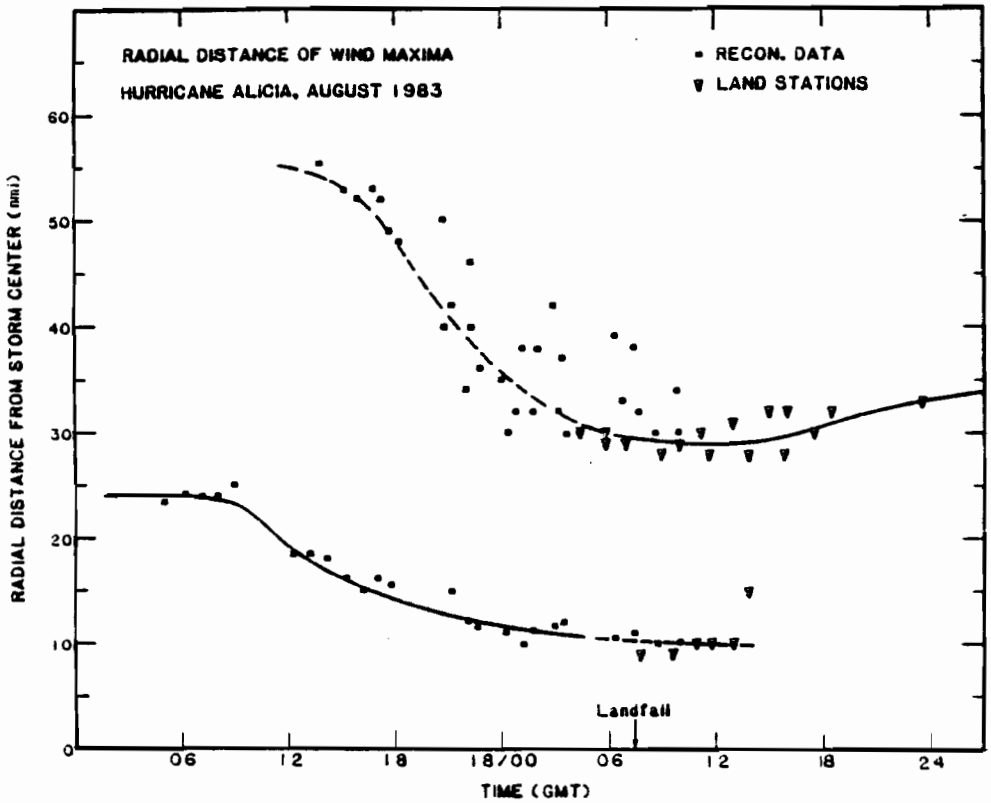

Figure A.10.—Radius of primary (solid line) and secondary (dashed line) wind maxima in Hurricane Alicia, August 17-18, 1983.

for replicating observed surges with a standardized wind profile. The variation in R near landfall might have to be examined on a case-by-case basis before a suitable value can be determined for the calibration of a numerical surge model. In the calibration process, the computed model winds, in addition to the computed high-water level, should be verified using observed data to ensure the adequacy of the wind model used in the numerical surge computation.

A.3 Hurricane David, September 2-5, 1979

A.3.1 Introduction

Hurricane David emerged from the central Caribbean on September 2 after devastating the Dominican Republic and rapidly weakening to tropical storm strength over the mountains of Hispanola. David was the strongest hurricane to hit Santo Domingo, Dominican Republic since 1930 (Hebert 1980). Once over water north of Cuba, David began to reintensify as it moved northwestward and approached Andros Island in the western Bahamas with winds of 61-69 kn (DeAngelis 1979). As the center crossed the island late in the afternoon on September 2, it appeared to be heading toward the Miami area (fig. A.11). A turn to the north-northwest, however, brought the slowly strengthening hurricane about 50 nmi (92.6 km) east of Miami on Labor Day, September 3. Winds of 50 kn were reported buffeting Miami Beach by 0800 GMT September 3. David continued moving north-northwestward and passed within 25 nmi (46.3) of West Palm Beach with a minimum central pressure of 973 mb at 1445 GMT September 3. Winds of 50 kn were experienced at West Palm Beach shortly before David's nearest approach. At 1730 GMT on September 3, the storm center made landfall just south of Stuart, FLorida, with a central pressure of 968 mb. Winds of 60 kn were recorded

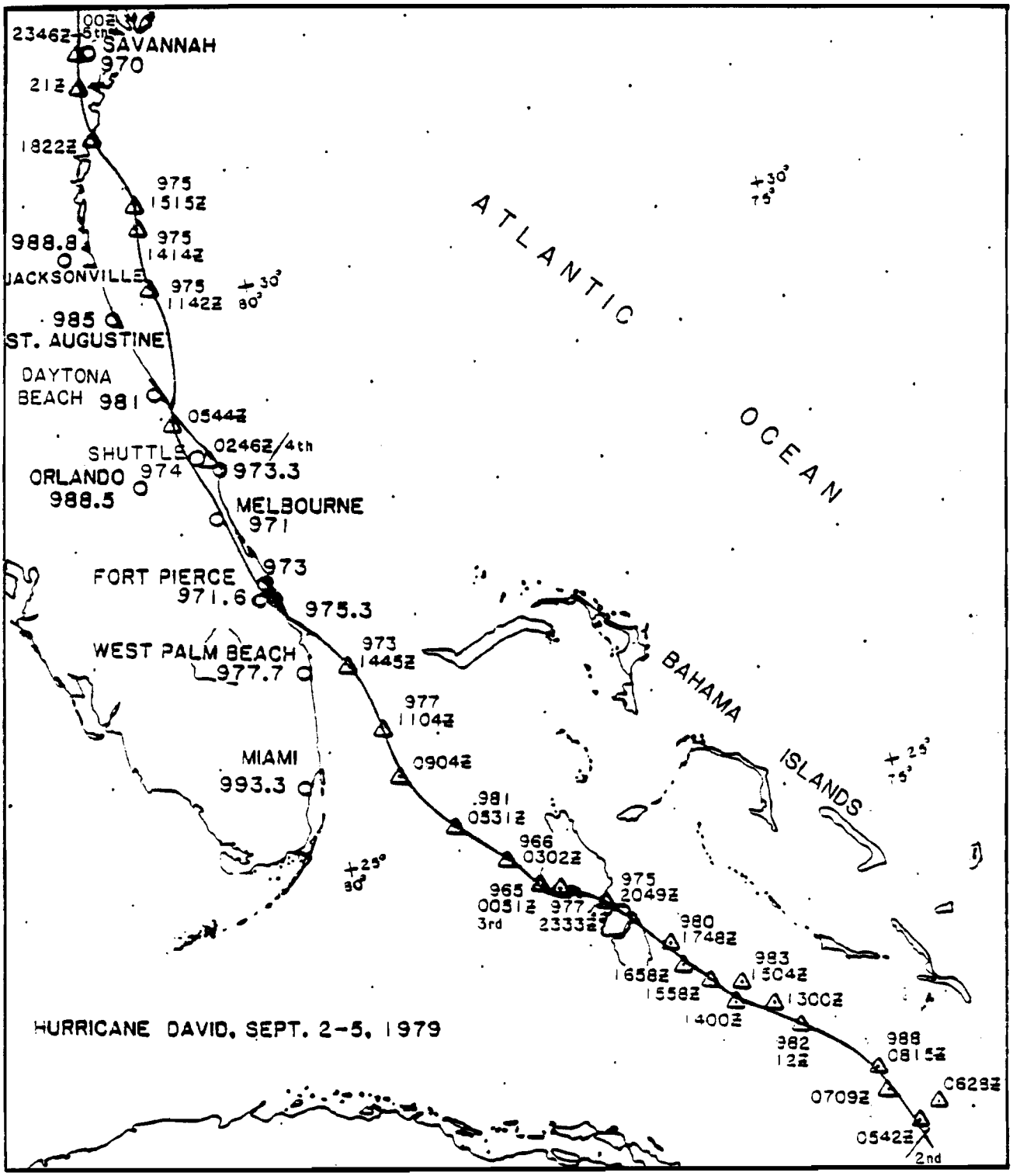

Figure A.11.—Track with central pressures (mb) for Hurricane David, September 2-5, 1979.

Table A.1.—Time, flight pattern, and flight level of NOAA/RFC missions into Hurricane David, September 1979

Mission*	Time period (GMT)	Pattern	Flight level(s) (ft)
790902F	02/0145-0925	east-west race track	5,000
790902I	02/1130-1853	star	variable
790902H	02/2002-03/0454	Recon.	variable
790903F	03/0504-1240	star (see fig. A.12)	5,000
790903I	03/2312-04/0641	along FL coast	variable
790904H	04/1723-05/0128	modified star (eye partly onshore)	variable

*The missions are designated by an identification code, YYMODAAC where:
YY = year
MO = month
DA = day of the month
AC = aircraft { F = NOAA/RFC C130B aircraft 41; H = NOAA/RFC WP-3D aircraft 42; I = NOAA/RFC WP-3D aircraft 43

at Stuart at 1600 GMT. David remained close to the Florida east coast for the next 11 hours as it moved north-northwestward over land. By 0600 GMT September 4, the storm center had moved back over open water north of Cape Canaveral. David was the first hurricane to strike the Cape Canaveral area since 1926 (Hebert 1980). Central pressures in David remained steady as it made its way north toward Georgia. Landfall occurred for a second time in the United States at 1822 GMT September 4 north of Brunswick, Georgia, with a minimum central pressure of 968 mb. David continued on a northerly track and passed just west of Savannah, Georgia, at 2346 GMT September 4.

A.3.2 Previous Studies

Hebert (1980) prepared a detailed description of Hurricane David and included meteorological data from land stations as far south as the Lesser Antilles, and as far north as Mt. Washington, New Hampshire. He compiled meteorological data from regularly reporting stations, as well as various unofficial sources which were used in the analysis of the variation of central pressure with time (shown in fig. A.15). The National Hurricane Center published an annual verification and data tabulation for Atlantic tropical cyclones of 1979 which included Hurricane David (Hebert and Staff 1980). The compiled data tabulations give David's center-fix positions obtained by aerial reconnaissance penetrations, satellite images, and land-based radar. Central pressures, maximum winds and other data observed by aerial reconnaissance were also included for Hurricane David.

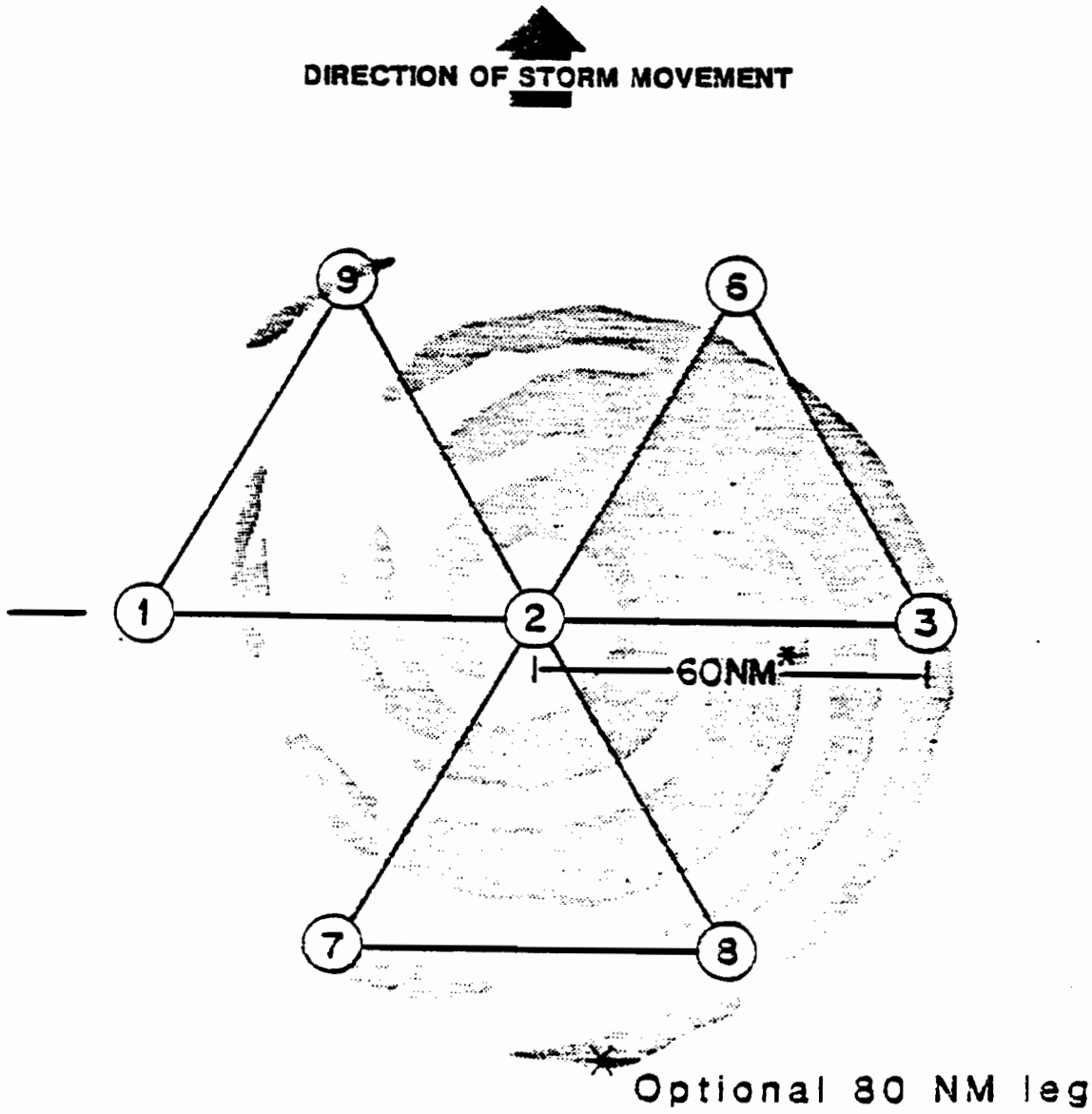

Figure A.12.—Reconnaissance flight pattern, designated as star pattern, used in Hurricanes David and Allen (refer to Friedman et al. 1982).

Howell et al. (1982) provided a report of tide data during the passage of Hurricane David at Miami Beach, Palm Beach, and Vero Beach, Florida. Storm surges at Palm Beach and Vero Beach were computed by Howell et al. using a numerical storm-surge model and compared with observed values.

A.3.3 Aircraft Data

NOAA research aircraft flew six missions into Hurricane David during the period September 2-5. Table A.1 summarizes the flight patterns, flight levels and the time periods for which meteorological and flight data were recorded. The flight patterns flown in these missions included a 'star' type (fig. A.12) and a 'Recon' type. The 'Recon' flight pattern was a deviation from typical flight patterns. In this case, the actual pattern completed was designed to optimize both the determination of the storm center location and collection of research data. A

detailed inventory of airborne research meteorological data is described by Friedman et al. (1982). This set of NOAA flight data was supplemented by Air Force reconnaissance flight data recorded on the morning of September 4.

A.3.4 Central Pressure

A.3.4.1 P_o From Aerial Reconnaissance. Minimum central pressures were recorded nearly continuously from September 2-4 by NOAA and Air Force reconnaissance aircraft when Hurricane David was moving over open water. Pressure values were obtained from Hebert et al. (1980). These pressure values were used in Figure A.15. When Hurricane David moved over land, reconnaissance aircraft did not penetrate the eye to obtain a pressure reading because of increased turbulence over land.

A.3.4.2 P_o From Land Station Observations. Once Hurricane David was over land, station reports of hourly weather observations and barograph traces were used to determine minimum pressures. If the center of the hurricane eye passed directly over a land station, then the minimum pressure could be readily determined. Hurricane David, however, did not pass directly over any land stations. Since several stations were very close to the track, their minimum pressures were used to estimate the storm's minimum pressure. Figure A.13a shows the time variation of minimum pressures recorded at Shuttle Airport, Florida every 3 hours. From this plot, the lowest pressure observed during the passage of David, 974 mb, occurred at about 0300 GMT September 4, when the storm's eye was located only about 5 nmi (9.3 km) to the west of the station. This estimate was plotted in Figure A.15. Another example of (hourly) station pressure data is shown in Figure A.13b for Savannah Municipal Airport, Georgia. A minimum pressure of 970 mb was experienced at 2300 GMT September 4 when David was about 7 nmi (13 km) to the west. This estimate was also used in the analysis shown in Figure A.15.

A.3.4.3 Pressure Fit at the Coast. Minimum pressures determined at the Florida and Georgia coasts were not based on any single source. Observed pressures were extrapolated inward to P_o using visually-fitted radial pressure profiles based on equation 1. Figure A.14a shows a subjectively fit pressure profile curve at the Florida coast, near the time of landfall, at 2100 GMT September 3. Pressure observations from several land stations were plotted against distance from storm center at 2100 GMT. Then a curve was drawn to fit the data. Figure A.14b is another example of the pressure profile curve except at 1800 GMT September 4, at the Georgia coast. In both cases, a minimum central pressure of 968 mb was estimated. In the case of the Georgia coast, a NOAA research aircraft measured a minimum 700 mb height of 2820 m at 1822 GMT September 4. Using a nomogram for estimating surface pressure in the eye of tropical cyclones (Jordan 1957), a central pressure of 968 mb was also estimated.

A.3.4.4 Time Variation of P_o. Hurricane David was most intense (central pressure of 924 mb) while still located in the Caribbean Sea, south of Puerto Rico. The analysis for this period was used in Chapter 4. As David emerged from the central Caribbean Sea, however, central pressures moderated considerably (see fig. A.11). Figure A.15 shows the time variation of central pressure in David for the period of September 3-5. Minimum pressures recorded by reconnaissance aircraft and land stations at various times were used to obtain a time history of David's central pressure. The line drawn is a curve fit to the data by eye.

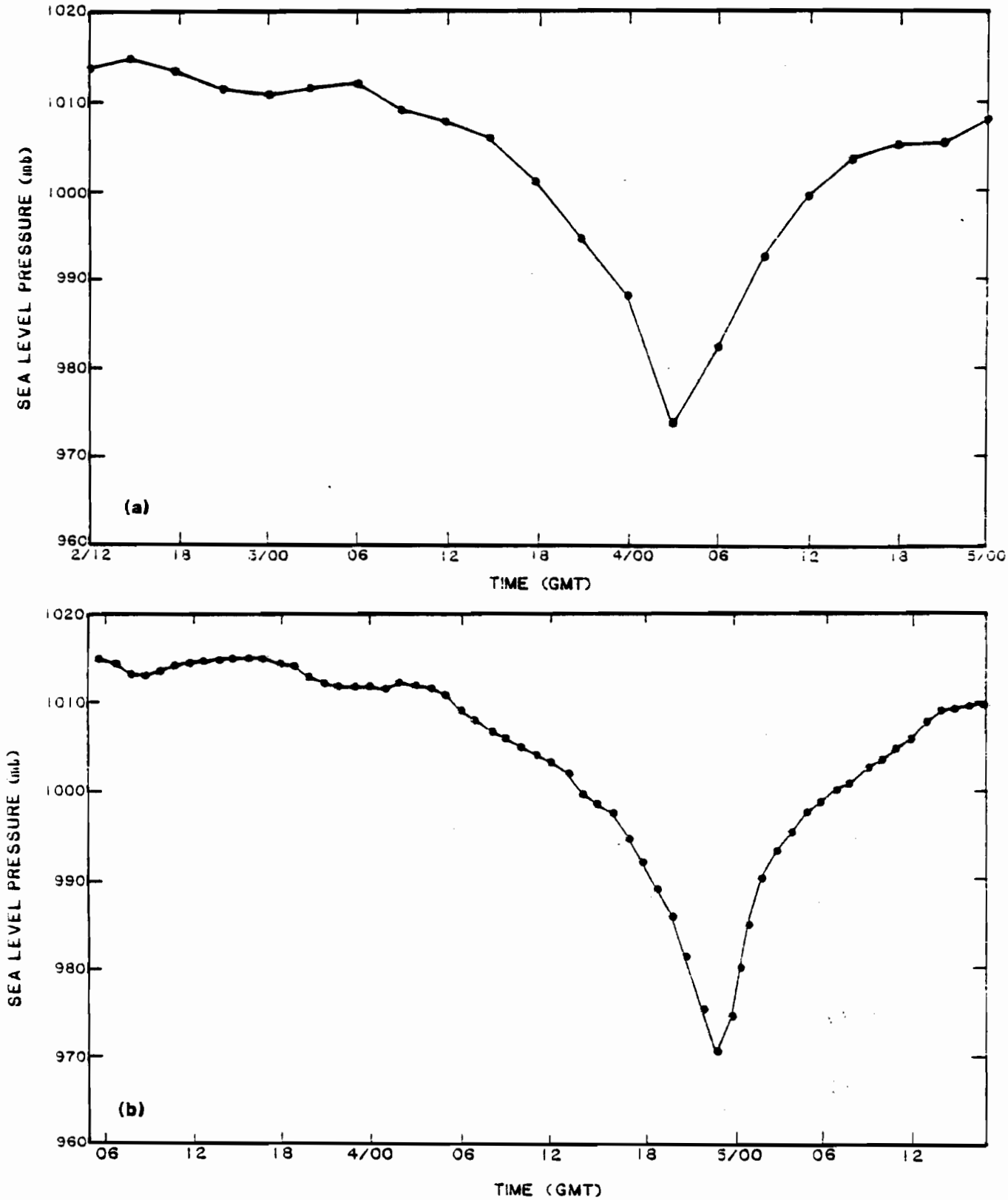

Figure A.13.—Sea-level pressure observed during passage of hurricane David (September 1979) at (a) Shuttle Airport, Florida, and (b) Savannah (Municipal Airport), Georgia.

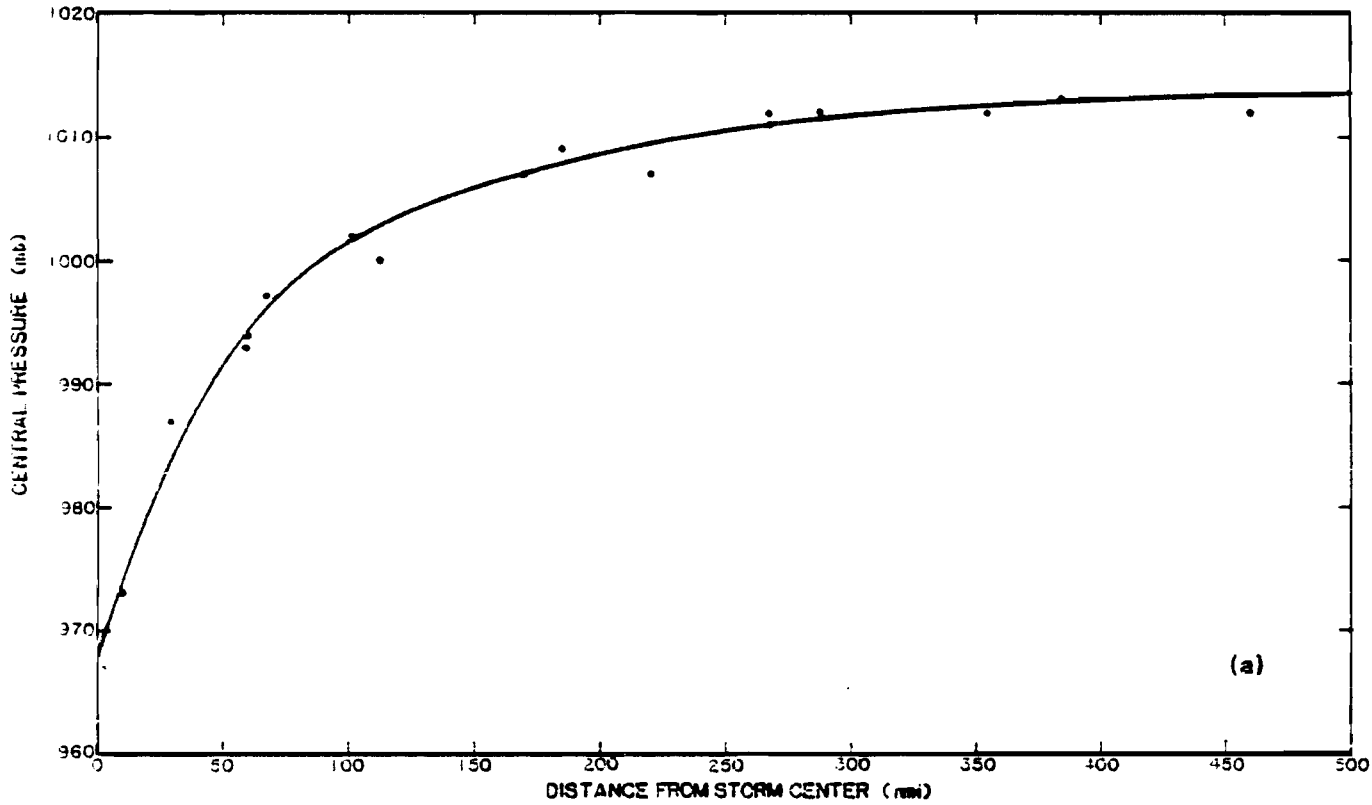

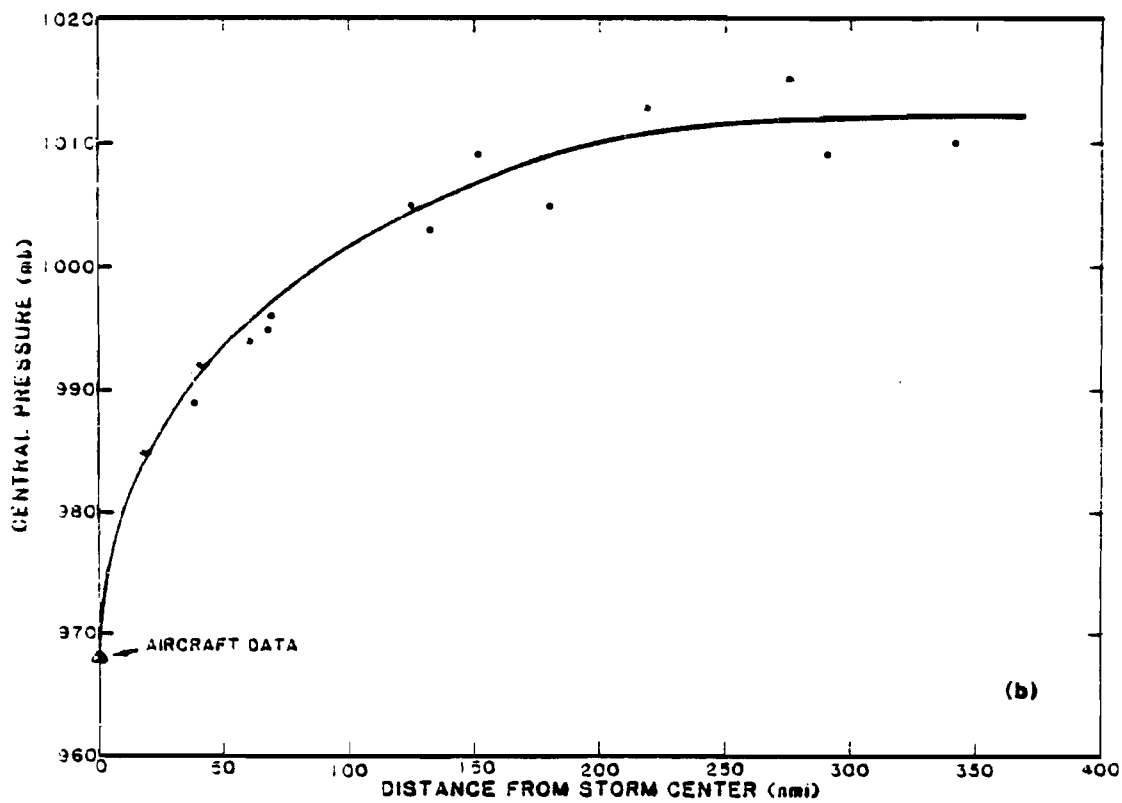

Figure A.14.—Pressure-profile curve during Hurricane David for (a) Florida coast at 2100 GMT, September 3, 1979, (b) Georgia coast at 1800 GMT, September 4, 1979.

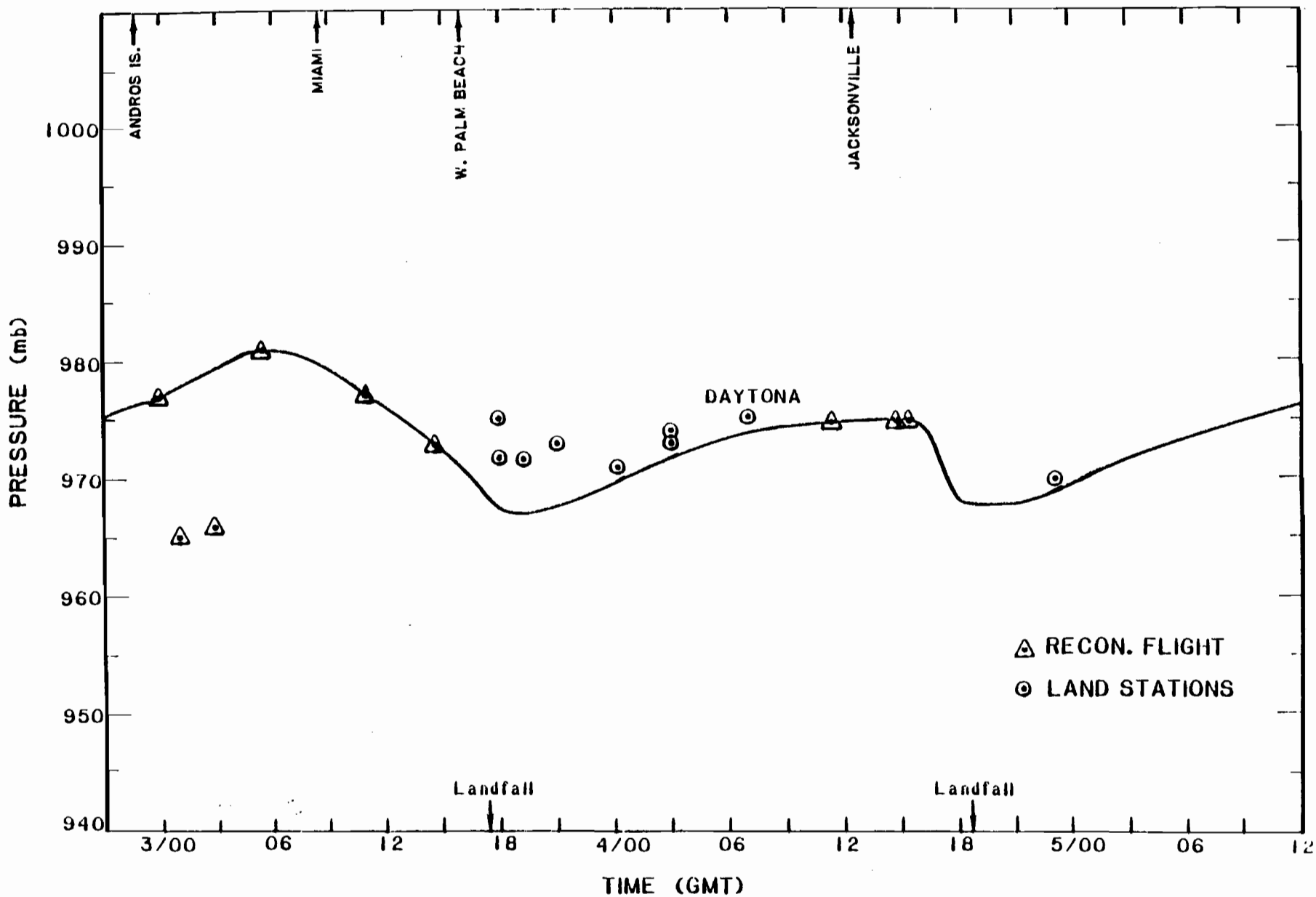

Figure A.15.--Central pressure (sea-level) for Hurricane David, September 3-5, 1979.

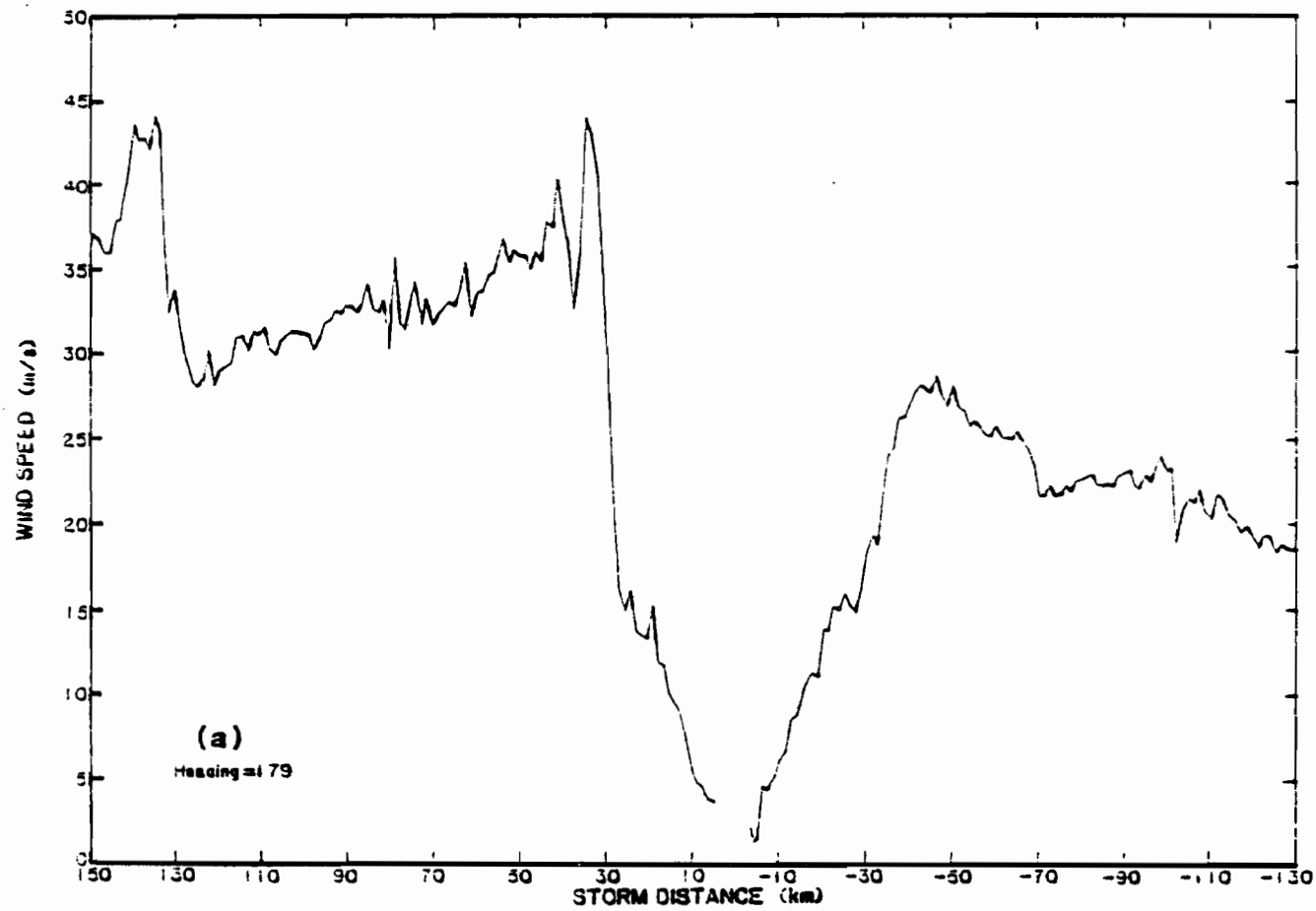
WIND SPEED (m/s)
STORM DISTANCE (km)
(a)
Heading = 179

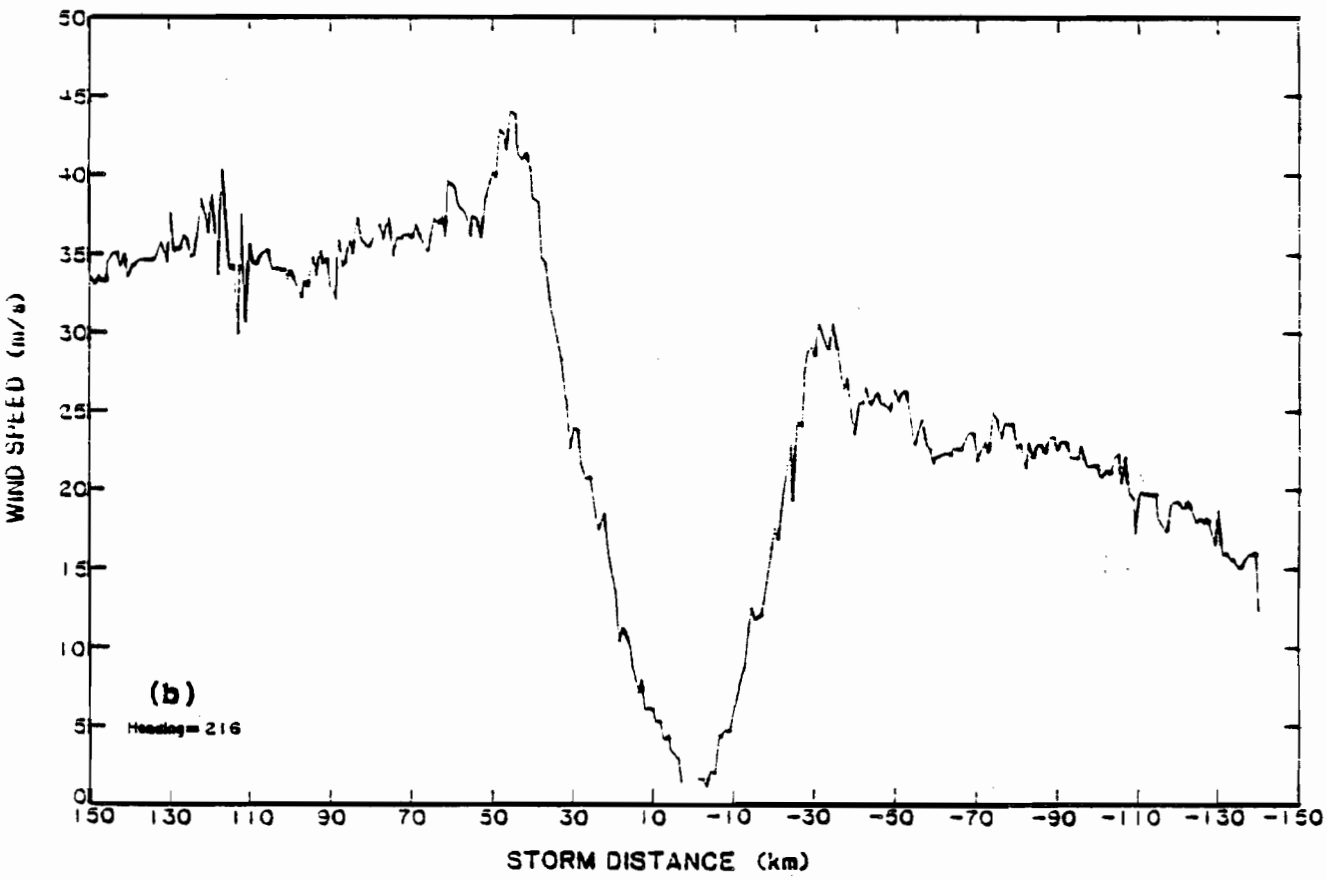
WIND SPEED (m/s)
STORM DISTANCE (km)
(b)
Heading = 216

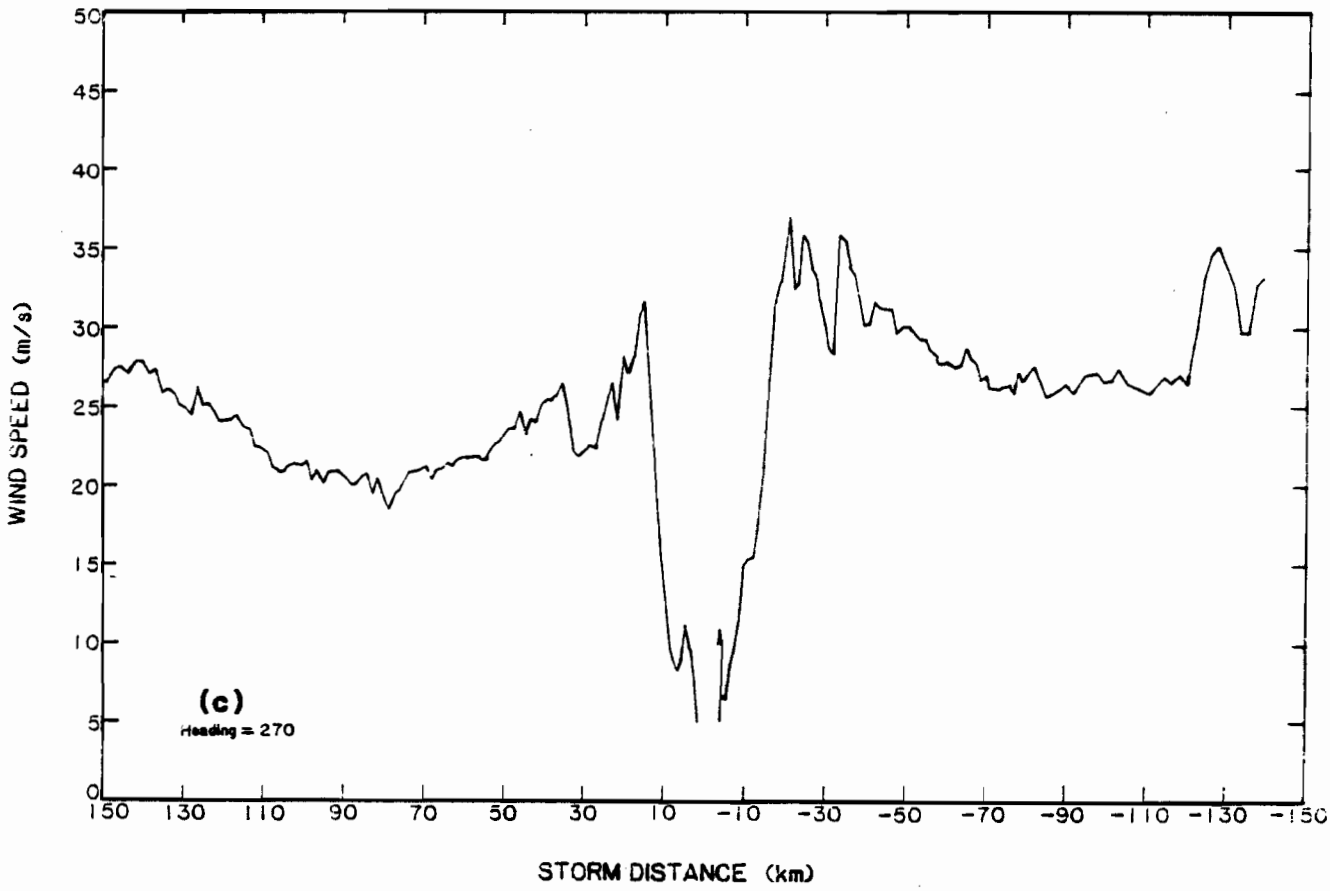

Figure A.16.—Flight-level winds recorded along radials through the center of Hurricane David, (a) 2308-2356 GMT, September 2, (b) 0644-0748 GMT, September 3, and (c) 1751-1841 GMT, September 4, 1979.

Reconnaissance aircraft reported a minimum pressure of 965 mb at 0051 GMT September 3 just as David crossed Andros Island, about 120 nmi (222 km) southeast of Miami, Florida. A central pressure of 966 mb was recorded by aerial reconnaissance at 0302 GMT. By 0531 GMT September 3, another mission reported a central pressure of 981 mb. The pressure difference in these 2.5 hours was 15 mb. This large pressure rise seems to be inconsistent with the other data as Figure A.15 shows and no explanation can be given. Hurricane David approached the southeast coast of Florida at a speed of about 10 kn, and a central pressure of 968 mb was determined at landfall at about 1730 GMT September 3. This value is the pressure recorded in Table 2. As David moved northwestward over land along the Florida coast (fig. A.11), central pressures increased very gradually until the storm exited the coast and moved over water again. A central pressure of 975 mb was consistently reported by Air Force reconnaissance aircraft from 1142-1515 GMT September 4. During this time, David was moving over water north of Cape Canaveral at about 12 kn. As the hurricane approached the Georgia coast, pressures dropped at about 2 mb/hr from 1515 GMT until a low pressure of 968 mb was determined at landfall (see sec. A.3.4.3), about 1822 GMT September 4. David moved inland at about 10 kn and weakened slowly. Savannah, Georgia experienced a minimum pressure of 970 mb when the center of David was only about 7 nmi (13 km) to the west and 40 nmi (74 km) inland.

A.3.5 Radius of Maximum Winds

A.3.5.1 R From Aerial Reconnaissance. Figure A.16a shows a wind profile constructed from flight-level wind data recorded between 2308-2356 GMT September 2. The winds were recorded during a north-south traverse through the eye and are plotted against radial distance from the storm center. The figure indicates that a wind maximum is located to the north of the center at a radial distance of about 35 km (18.9 nmi). This value was plotted in Figure A.18 at 2332 GMT September 2. Figure A.16b is another wind profile for Hurricane David constructed from flight-level winds recorded between 0644-0748 GMT September 3. At this time, the storm center was located over open water about 68 nmi (126 km) east-southeast of Miami, Florida (see fig. A.11). Flight-level winds were recorded during a northeast-southwest traverse through the eye. The wind profile indicates that maximum winds occurred at a radial distance of about 45 km (24 nmi) northeast of center. This value was plotted in Figure A.18 at 0716 GMT September 3. Figure A.16c shows another wind profile constructed from data recorded between 1750-1841 GMT September 4. At this time, the storm center was over water north of Cape Canaveral and approaching landfall on the Georgia coast. The winds were recorded during an east-west traverse through David's eye. Figure A.16c indicates a maximum wind at a radial distance of about 20 km (10.8 nmi) west of center. This value is plotted at about 1815 GMT September 4 in Figure A.18. Figures A.16a through A.16c suggest the existence of secondary maxima (indicated by solid dots in fig. A.18) which were relatively short-lived. Analysis of composite maps (diagrams not shown) revealed that these secondary maxima were scattered and quite disorganized. They were not considered relevant in the specification of the parameters that are the focus of this study.

A.3.5.2 R From Land Station Observations. Once the storm moved inland, land stations were the primary source of data. Data from these stations were obtained from the NCDC in Asheville, North Carolina, where all raw data from station observations are stored.

Figure A.17a shows a time variation of windspeed and wind direction for Shuttle Airport, Florida from 1200 GMT September 2, to 0000 GMT September 5. This plot consists of hourly wind observations as Hurricane David passed just west of the station (0300-0400 GMT September 4). Note the shift in wind direction as the storm center passed. Winds veered from the east to east-southeast then south indicating the path of the storm center was to the west of the station. A maximum wind of about 37-38 kn (19-20 m/s) was experienced at Shuttle Airport at 0530 GMT September 4 when the storm center was located approximately 20 nmi (37 km) away from Shuttle Airport (see hurricane track on Fig. A.11). Figure A.17a also shows the distance of the storm from Shuttle Airport (dashed line). Using this information, a radial distance of 20 nmi (37 km) was determined for the wind maxima and was plotted in Figure A.18 at 0530 GMT September 4. Figure A.17b shows another plot of hourly windspeed and direction against time for Savannah Municipal Airport, Georgia from 0600 GMT September 3 to 1700 GMT September 5. The wind direction at Savannah as David's center passed nearby shifted from the east to east-southeast then south and finally south-southwest. This indicates that the hurricane passed to the west of the station (fig. A.11). A maximum wind of about 37 kn (19 m/s) occurred at Savannah at 2230 GMT September 4. The track in figure A.11 indicates that the hurricane center was only about 10 nmi (18.5 km) away from Savannah at 2230 GMT September 4.

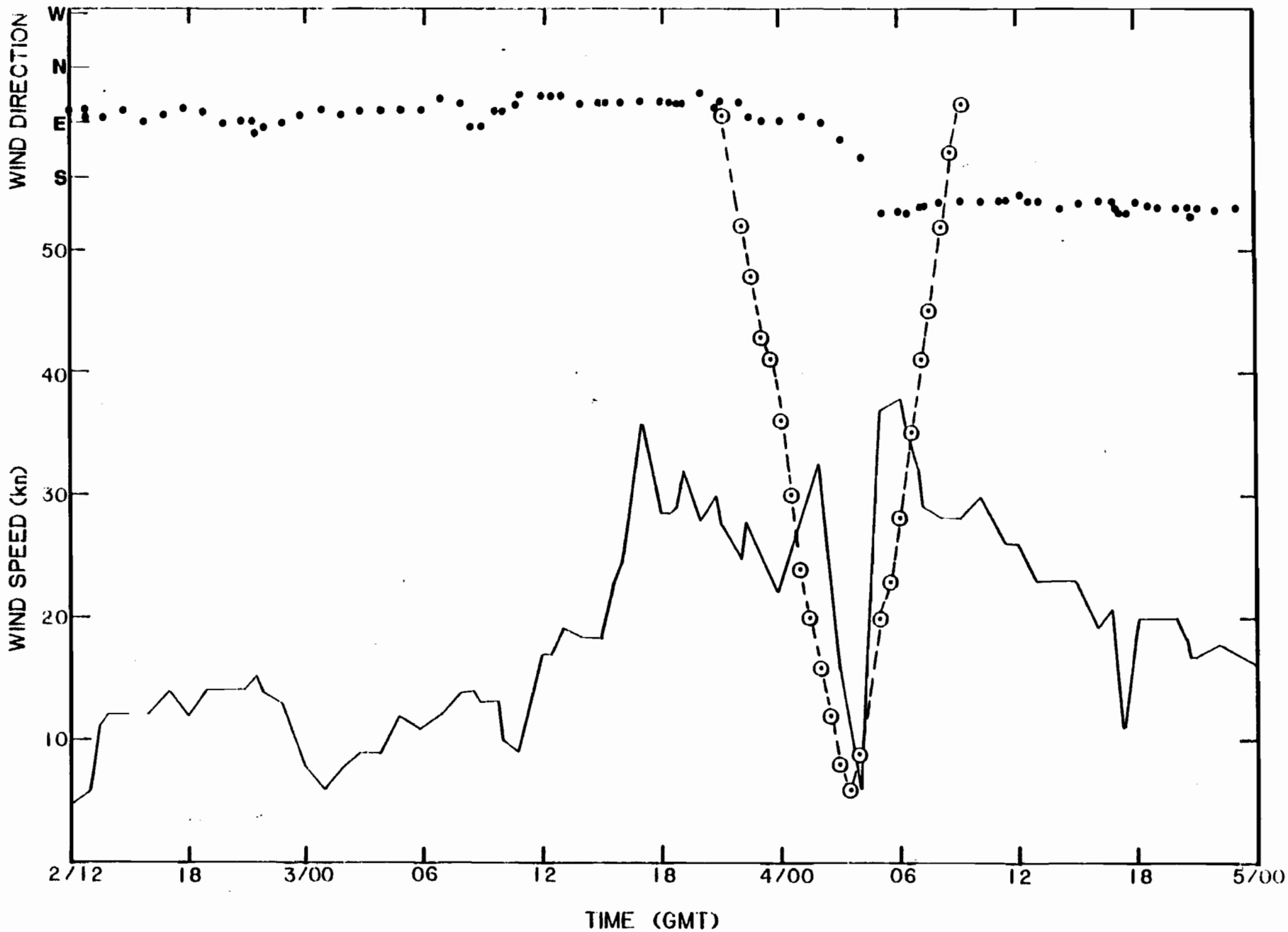

Figure A17a.--Wind speed (solid line) and direction (dots) at Shuttle Airport, Florida, during the passage of Hurricane David, Seoptember 2-4, 1979. Dashed line shows distance of storm from station.

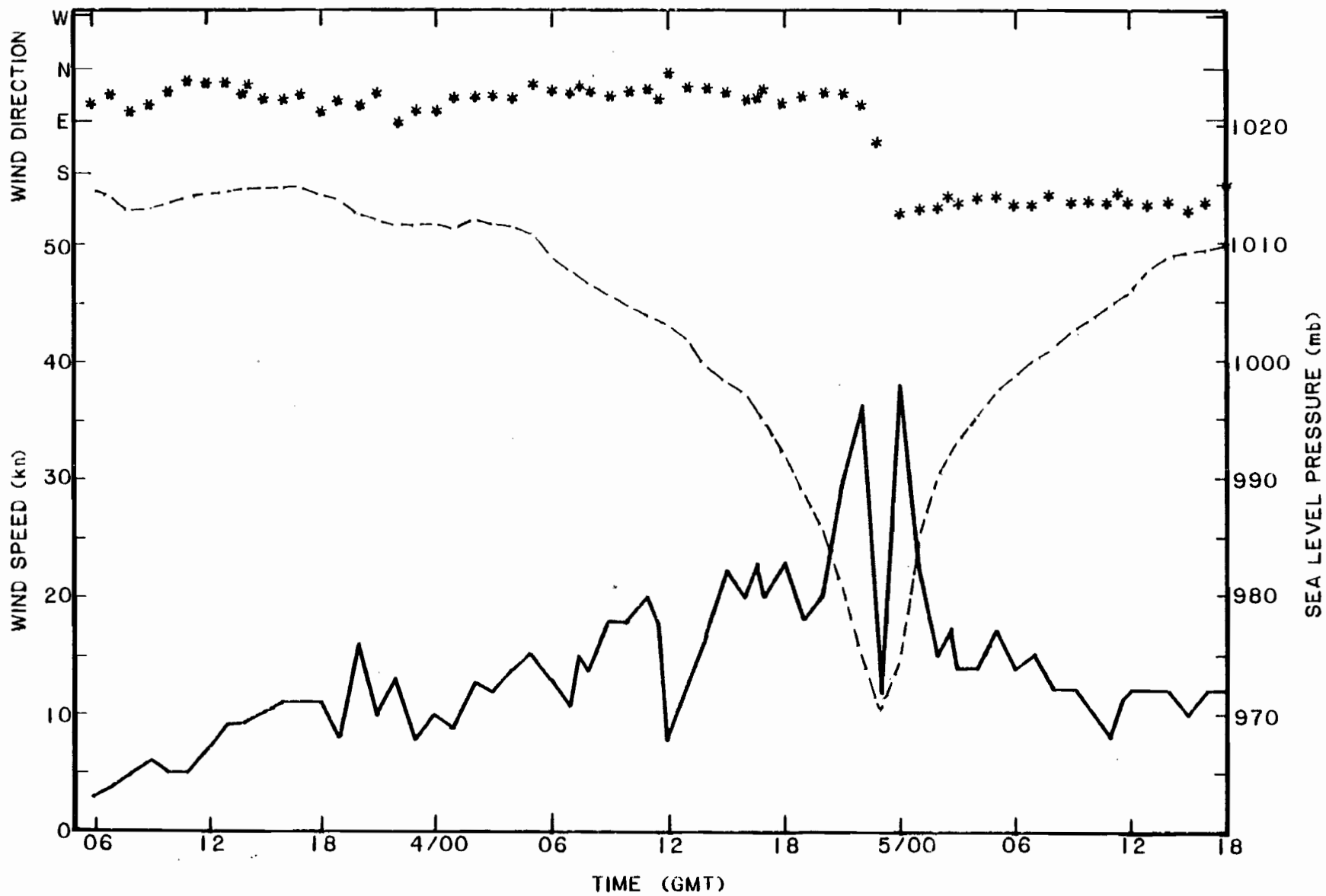

Figure A17b.--Wind speed (solid line) and direction (stars) at Savannah, (Municipal Airport), Georgia, during the passage of Hurricane David, September 3-5, 1979. Dashed line shows the time variation of central pressure.

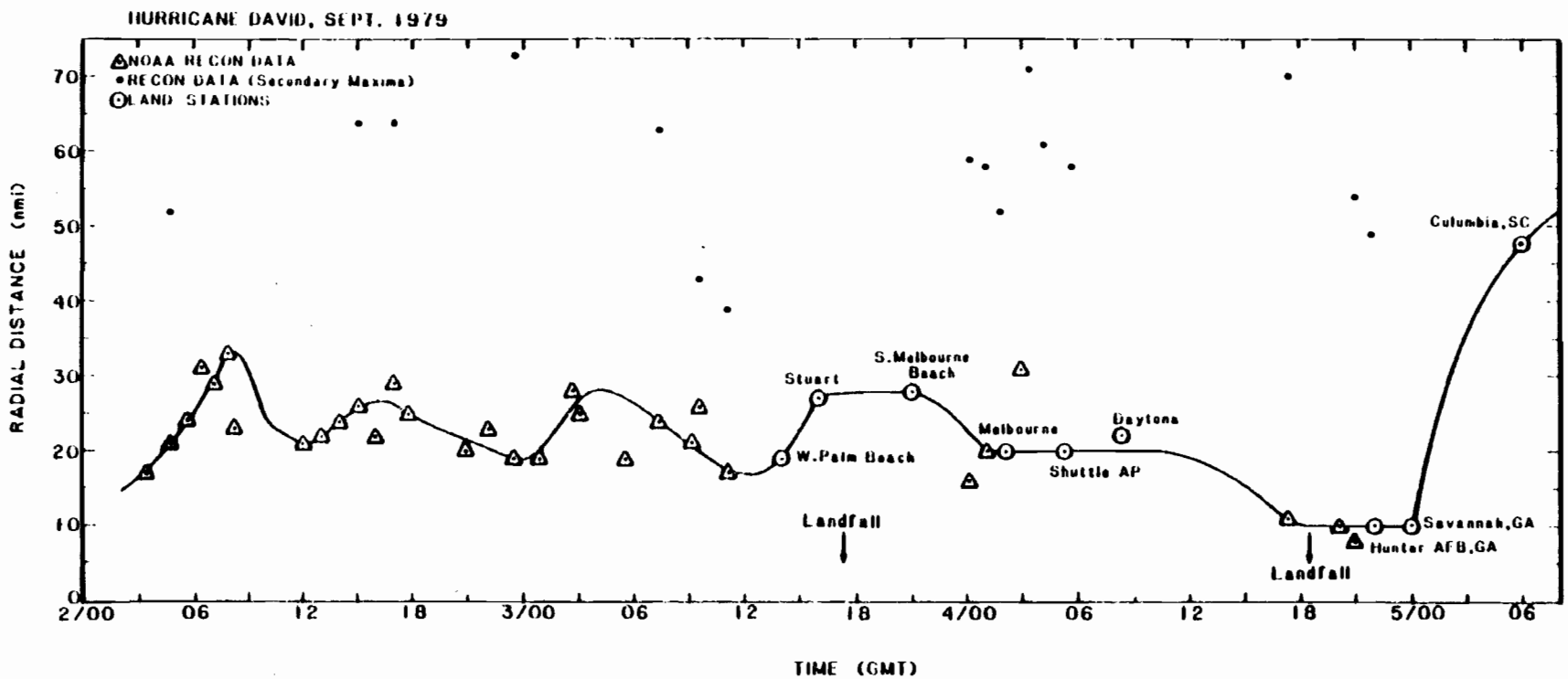

Figure A.18.--Radial distances (from eye center) of wind maxima in Hurricane David, September 2-5, 1979.

A.3.5.3 Time Variation of R. Figure A.18 shows the time variation of the radius of maximum winds in Hurricane David from 0300 GMT September 2 to about 0800 GMT September 5. Radial distances of maximum winds from the storm center measured by reconnaissance aircraft at various times, and those obtained from analyses of land-station wind records were used to obtain this time history. Reconnaissance aircraft reported the majority of maximum winds needed for R-value analyses, especially before 1200 GMT September 3. The line shown was drawn to the data by eye.

As Figure A.18 shows, the radius varied from about 17 to about 28 nmi (31.5-51.9 km) between 2100 GMT September 2 and 1200 GMT September 3. By 1400 GMT September 3, land stations were beginning to experience maximum winds. West Palm Beach, Florida experienced maximum winds when the hurricane center was about 18 nmi from the station. Stuart, Florida recorded maximum winds at about 1600 GMT September 3 or 1.5 hours before the storm center made landfall in Florida. The radius of maximum winds remained steady at 26 nmi (48.1 km) during landfall. By 2100 GMT September 3, the radius began decreasing again until about 0100 GMT September 4 when a reconnaissance aircraft reported maximum winds at a radius of 20 nmi (37 km). The radius remained steady once again at 20 nmi (37 km) as the storm moved out over water north of Cape Canaveral (see fig. A.11). Both Melbourne and Shuttle Airport, Florida, experienced maximum winds when David was located 20 nmi (37 km) from the station before exiting the coast. From about 1030 GMT September 4 until landfall in Georgia at 1822 GMT, the radius of maximum winds decreased to 10 nmi (18.5 km), as determined from maximum winds recorded by a reconnaissance aircraft at about 2000 GMT. This was the smallest radial distance reported within 150 nmi (278 km) of the east coast. Hunter AFB and Savannah, Georgia, both recorded maximum winds soon after the storm center made landfall when David was located 10 nmi (18.5 km) to the south. After passing Savannah, Georgia, the radius of maximum winds expanded rapidly. Columbia, South Carolina, experienced maximum winds when the storm was located at a distance of about 47 nmi (87 km) from the station at 0600 GMT September 5.

Because of the abrupt change in storm size after making landfall, using an R value of 10 nmi (18.5 km) in a numerical surge computation could not replicate surge heights along the coast produced by Hurricane David (Jarvinen 1985, private communication). As David moved parallel to the coast and passed some 40 nmi (74 km) inland of Charleston, South Carolina, its track and R influenced the position of the band of strongest winds along the coast. This factor, in turn, affected the coastal surges and the maximum wind setup effects in Charleston Harbor. In replicating high water levels experienced in Charleston, either varying R with time or using a large R value in a numerical surge computation would be required in order to obtain realistic results.

A.4 Hurricane Allen, August 2-10, 1980

A.4.1 Introduction

Hurricane Allen originated near the Cape Verde Islands, off the west coast of Africa, and developed into the second most severe Atlantic hurricane in modern records. It reached tropical storm strength in the early hours of August 2, 1980, and attained hurricane strength that evening (see fig. A.19). Its central pressure dropped to 951 mb by the evening of the 3rd as the eye passed just north of Barbados and south of St. Lucia. The hurricane continued westward into the Caribbean at about 20 kn and passed south of Puerto Rico during

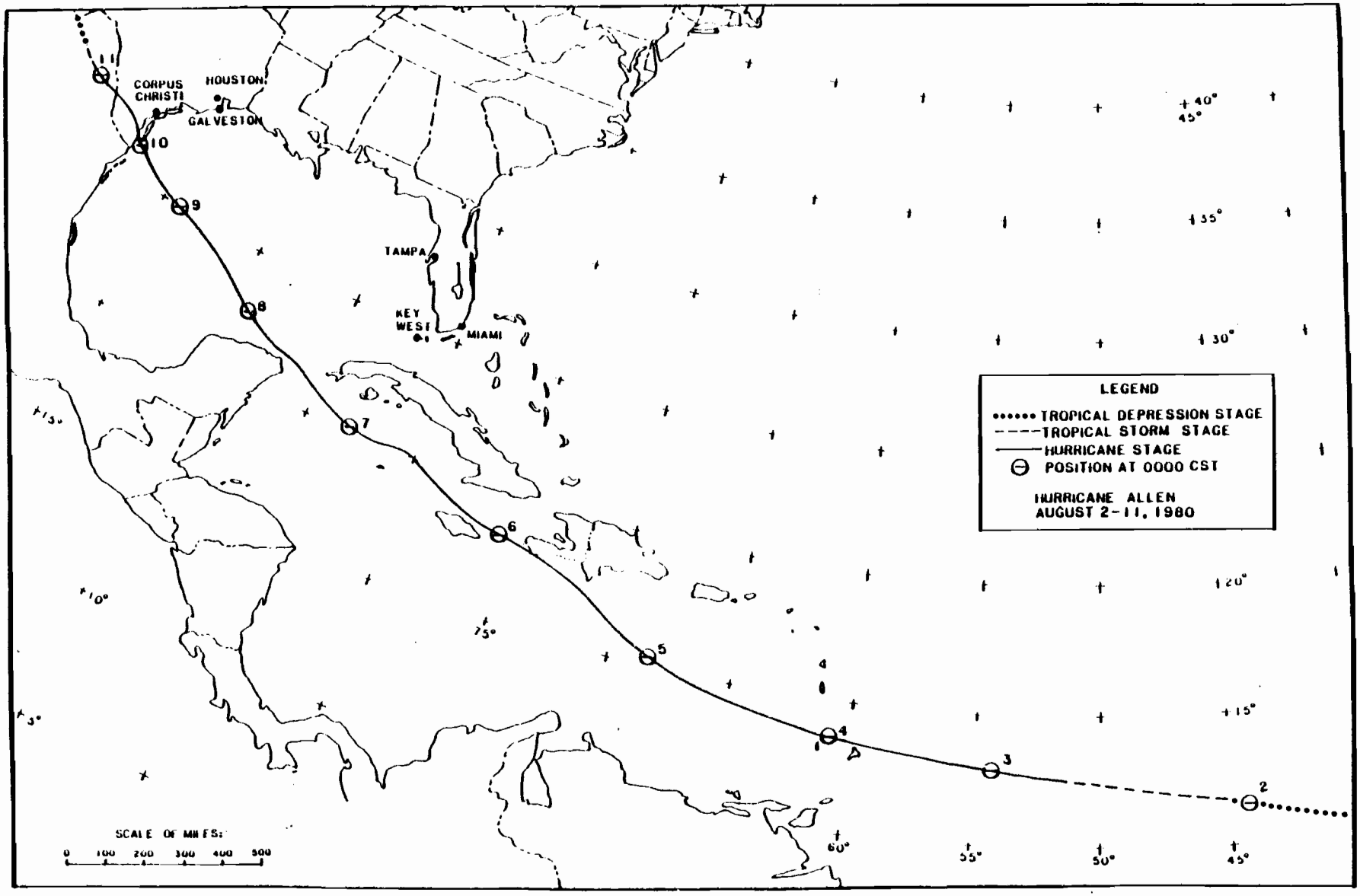

Figure A.19.--Track of Hurricane Allen, August 2-11, 1980.

the evening of the 4th. Its central pressure deepened and reached 911 mb, the lowest pressure ever recorded in the eastern Caribbean, on the early morning of the 5th.

The hurricane weakened as it passed the southwest tip of Haiti and moved between Jamaica and Cuba. This was the first of three strengthening-weakening cycles in Allen's life history that are unprecedented in hurricane records. Allen reintensified rapidly as the circulation moved over the northwestern Caribbean Sea. Arriving at Yucatan Channel on the 7th, its central pressure deepened to 899 mb, the lowest pressure ever observed in the western Caribbean and the second lowest ever recorded for an Atlantic storm. The hurricane weakened for the second time when it moved past the north coast of the Yucatan peninsula. Its central pressure rose rapidly, reaching 961 mb on the morning of the 8th. As the hurricane continued west-northwestward across the warm open water of the Gulf of Mexico, Allen deepened once again with a minimum pressure of 909 mb observed during the night of the 8th.

As the hurricane approached the Texas coast on the 9th, its intensity weakened and the forward speed decreased. Allen held to its west-northwesterly course until mid-day and then turned northwestward. After crossing the southern end of Padre Island just northeast of Brownsville, Texas, Allen continued in a northwesterly direction. By early morning of the 10th, Allen moved inland at a slightly faster speed and turned gradually towards the west-northwest. In addition to the damage from the hurricane winds and storm surge, Hurricane Allen also spawned at least a dozen tornadoes over Texas.

A.4.2 Previous Reports

The National Hurricane Center provided a description of significant features of all Atlantic tropical storms that occurred during 1980, including Hurricane Allen. This information was published in the Monthly Weather Review (Lawrence and Pellissier 1981) and in the National Summary of Climatic Data (National Hurricane Center 1980). Significant features mentioned in regard to Allen were the minimum central pressure of record, the rapid deepening, and the fluctuations in intensity during its life cycle. The appearance of a double eye configuration was noted in a Brownsville radar picture taken when Allen was 100 nmi (185 km) off the coast.

Willoughby et al. (1982) described secondary wind maxima associated with concentric eye walls and the evolution of the hurricane vortex in Allen and a few other hurricanes. They described the sequence of events as reported near Allen's inner core by reconnaissance aircraft on August 5 and 8, 1980. Based on data collected in Allen and other hurricanes, they concluded that an outer maximum is frequently observed to constrict about a pre-existing eye and replace it and the central pressure tends to decrease during the constriction. They suggest that the concentric eye phenomenon is most frequently observed in intense, highly symmetric systems.

The NHC publication on annual data and verification tabulation for the 1980 Atlantic tropical cyclones (Taylor and Staff 1981) also includes a list of Allen's center fix positions obtained by aerial reconnaissance penetrations, satellite images, and land-based radar. The hurricane's central pressure, maximum winds, and other data observed by reconnaissance aircraft are also included in that report.

Ho and Miller (1983) analyzed available meteorological data for Hurricane Allen during the period surrounding landfall to provide information for use in dynamic storm surge models. Detailed analyses were made of the storm track, forward speed, central pressure, and radius of maximum winds.

Marks (1985) studied the evolution of the structure of precipitation in Hurricane Allen. He used reflectivity data from airborne radar systems on board the three NOAA aircraft to specify the horizontal and vertical precipitation distributions within 111 km (60 nmi) of the hurricane center. He found that the most striking changes in structure during the 6-day period were the rapid contraction in eyewall radius and the development of a secondary ring of intense reflectivity 80-100 km (43-54 nmi) from the storm center. He further stated that these changes in eye radius appeared to be related to the vortex evolution, as discussed by Willoughby et al.

A.4.3 Reconnaissance Flight Data

NOAA/RFC research aircraft flew 12 missions into Allen during the 6 day period, from August 5-10. Table A.2 lists the flight patterns, flight levels and the time periods for which meteorological and flight data were recorded in each of the 12 missions. The table lists two 3-aircraft missions flown on August 5 and August 8 and single-aircraft missions on other days. Willoughby et al. (1982) compared the calculated and observed properties of Hurricane Allen on August 8 for all three different flight levels (500-, 600-, and 850-mb levels). He concluded that one can obtain reliable indications of the evolution of the symmetric vortex from any lower tropospheric flight level above the boundary layer.

A.4.4 Central Pressure Analysis

Figure A.21 shows our analysis of the pressure information from reconnaissance aircraft that was used to obtain a time history of Allen's central pressure. This figure clearly shows the three strengthening-weakening cycles. Allen reached a record low pressure (for specific areas) at each of its deepening stages. A minimum pressure of 899 mb observed at 1742 GMT on August 7 was the lowest observed in Hurricane Allen. The central pressure was only 7 mb higher than the record pressure of 892mb observed in the Labor Day, 1935 storm that struck the Florida Keys. The low pressure of 909 mb, observed at 0558 GMT on August 9, was considered to be the lowest that occurred in Hurricane Allen as it approached the coast. The short time interval between central pressures obtained by aircraft, combined with other information, did not indicate any lower pressure at intermediate times. As Allen continued its course west-northwestward, approaching the Texas coast, its intensity weakened. While the hurricane's central pressure rose steadily, the characteristics of its inner core appeared to have undergone dramatic changes, as discussed in the next section.

A.4.5 Wind Analysis

Flight-level winds on each traverse were plotted by computer and made available to us by the Hurricane Research Division of NOAA/AOML. The aircraft locations for observation of flight-level winds were translated to positions relative to the storm center. From these records, composite maps of winds at given intervals were constructed. Another source of information came from Air Force reconnaissance aircraft that flew into the hurricane.

Table A.2.--Time, flight pattern, and flight level of NOAA/RFC missions into Hurricane Allen, August 1980

Mission	Time period (GMT)	Pattern(s)	Flight level(s) (ft)
800805F	05/1028-1742	figs. A.20a, A.20b	10,000
800805H	05/1021-1933	fig. A.20a fig. A.20b	variable variable
800805I	05/1015-1932	fig. A.20a, A.20b	1,500, 5,000
800806H	06/1239-1910	fig. A.12	1,500, 10,000 (last half)
800806I	06/1825-07/0031	fig. A.20a (modified)	5,000
800807H	07/1601-08/0017	fig. A.20a (modified)	variable
800808F	08/1620-09/0059	cross	12,000
800808H	08/1631-09/0107	cross	18,000, 20,000
800808I	08/1617-09/0110	cross	5,000
800809I	09/1625-10/0210	cross	10,000
800809H	09/2324-10/0947	along coast	variable
800810F	10/1006-1630	25 nmi off coast	700- and 850-mb levels

*The missions are designated by an identification code, YYMODAAC where:
YY = year
MO = month
DA = day of the month
AC = aircraft { F = NOAA/RFC C130B aircraft 41; H = NOAA/RFC WP-3D aircraft 42; I = NOAA/RFC WP-3D aircraft 43 }

Figure A.22 is an example of flight-level windspeeds plotted against radial distances from the storm center. The wind data were recorded in a 312° to 132° traverse through the eye between 1535 and 1627 GMT on August 5. The maximum winds can be located at radial distances of 15 and 19 nmi (27.8 and 35.2 km). A secondary maximum appeared near radial distances of 50-60 nmi (82.6-111 km) at the rear quadrant of the storm. At this time, Allen's central pressure had risen to 937 mb, after having reached a minimum of 911 mb at 0000 GMT on the 5th (fig. A.25). Figure A.23 is another example of flight-level windspeed plotted against radial distances from the storm center. This plot shows wind data observed between 1844 and 1945 GMT on August 7. The maximum winds recorded during this north to south traverse through the storm center were located at radial distances of 5 and 10 nmi (9.3 and 18.5 km). The maximum winds decreased rather rapidly with increasing distance away from the center. Allen, at this time, was a small and extremely intense hurricane, having reached its minimum pressure of 899 mb less than 2 hours earlier (see fig. A.21). Figure A.24 is an

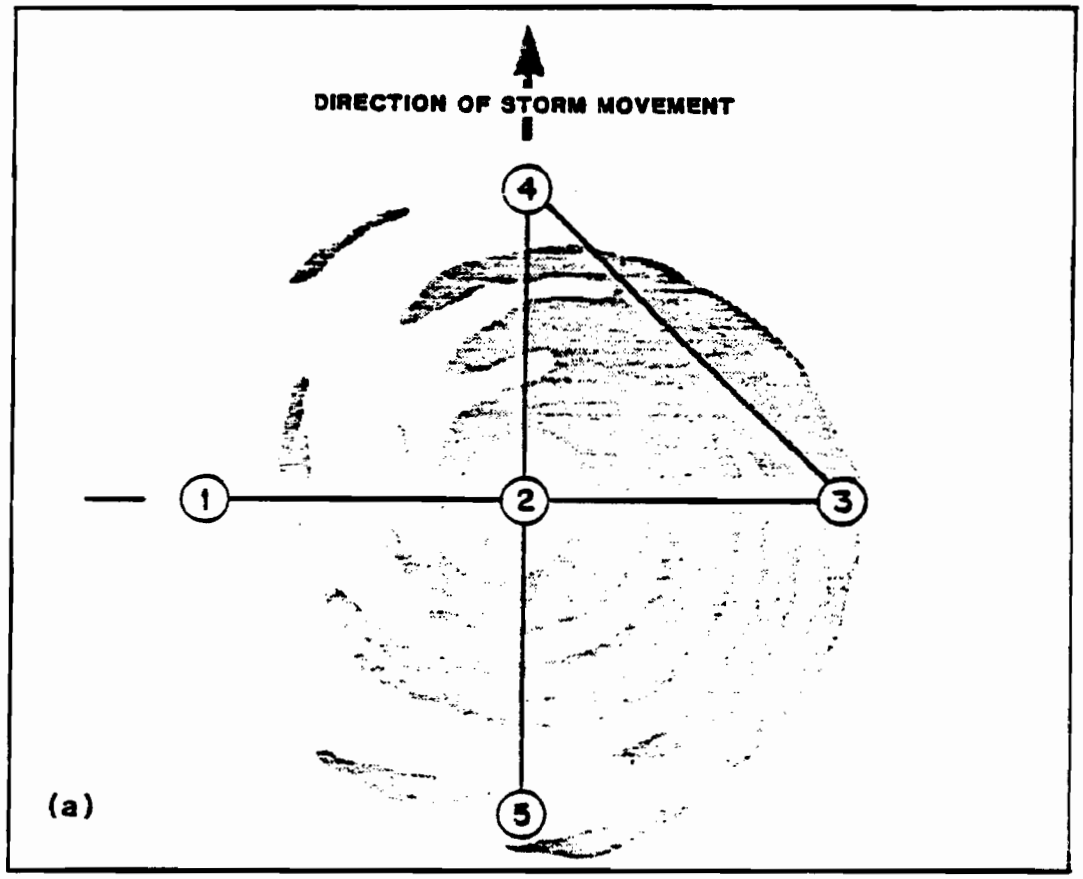

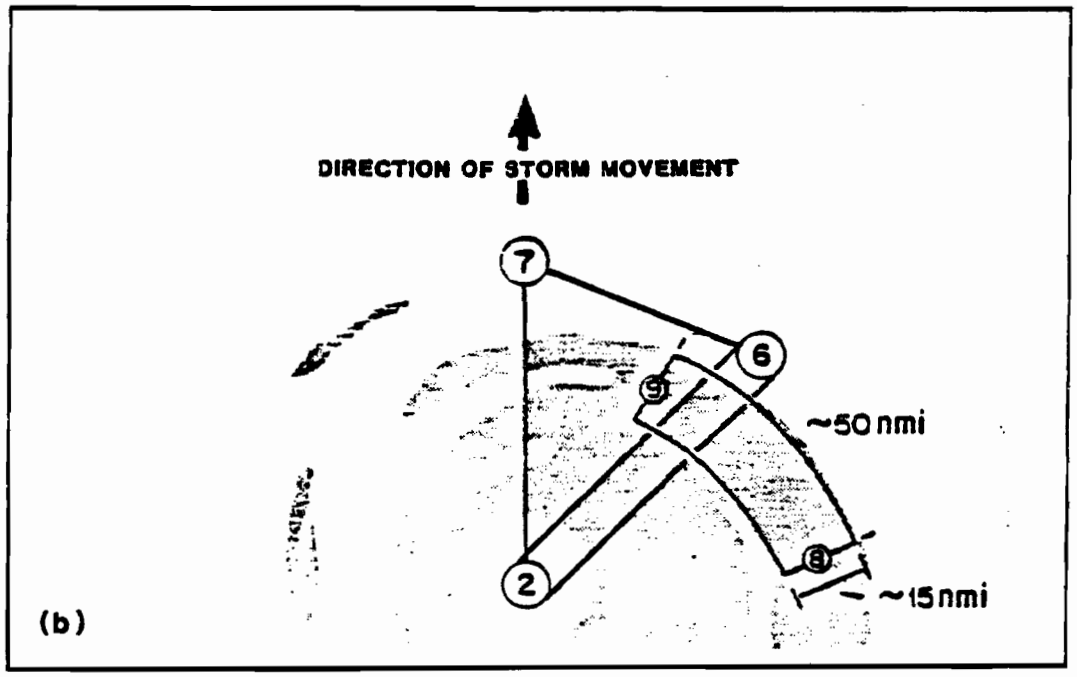

Figure A.20.--Reconnaissance flight patterns used in Hurricane Allen (refer to Friedman et al. 1982).

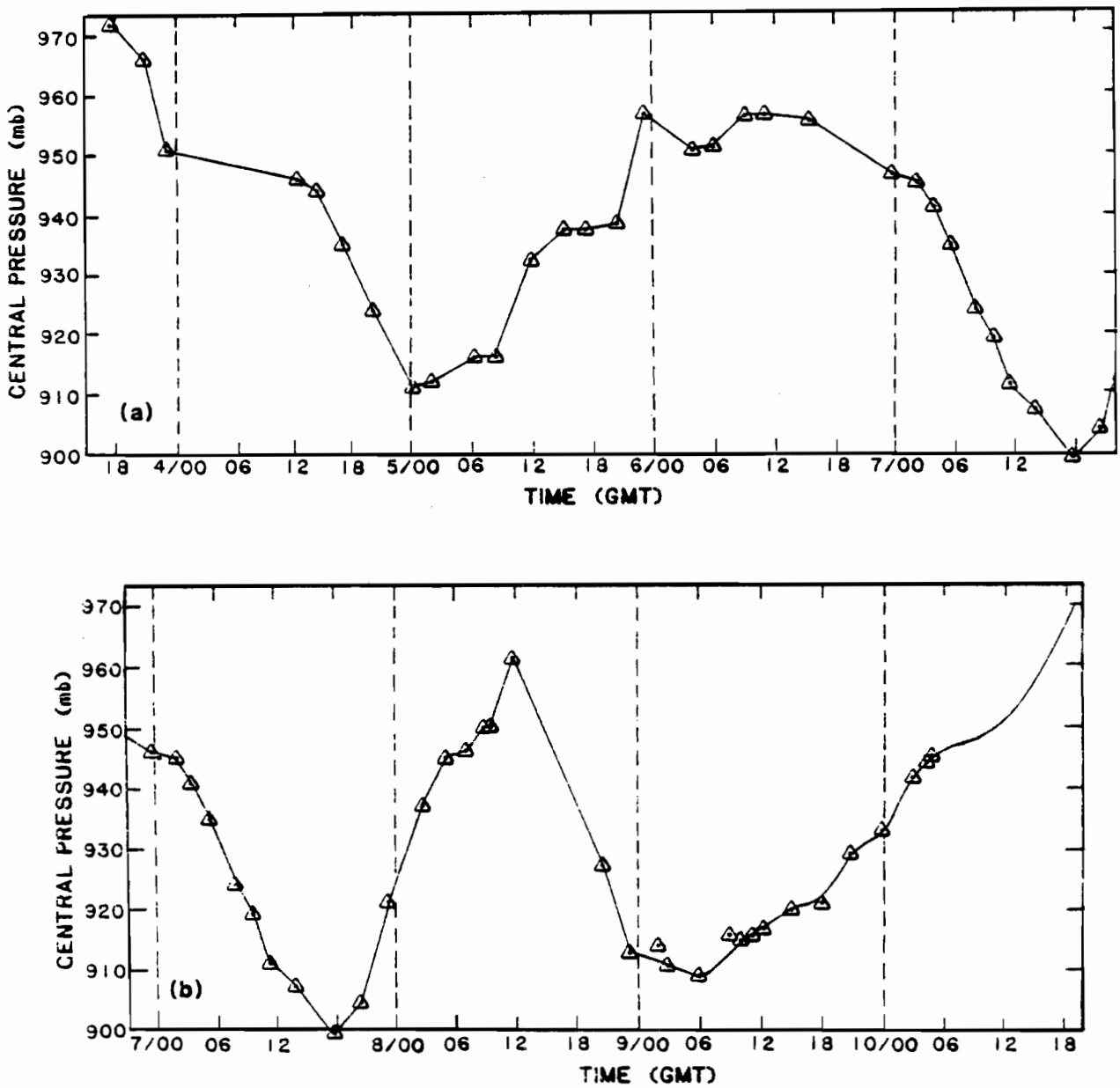

Figure A.21.—Central pressure (sea level) for Hurricane Allen, (a) August 3-7, and (b) August 7-10, 1980.

example of flight-level windspeed plotted at translated positions relative to the storm center. The wind data were observed between 0200 and 0400 GMT on August 9 during the third deepening cycle within Allen's life span. The wind distribution indicates that maximum winds occurred at radial distances of 11 nmi (20.4 km) and about 54 nmi (100 km) from the center. Similar distributions of flight-level winds can be identified in composite maps of other time periods (diagrams not shown) as Allen approached the Texas coast. The evolution of the wind distribution in Allen during this period, shifting from a small size hurricane to one with R of about 40 nmi (74 km), was described by Ho and Miller (1983).

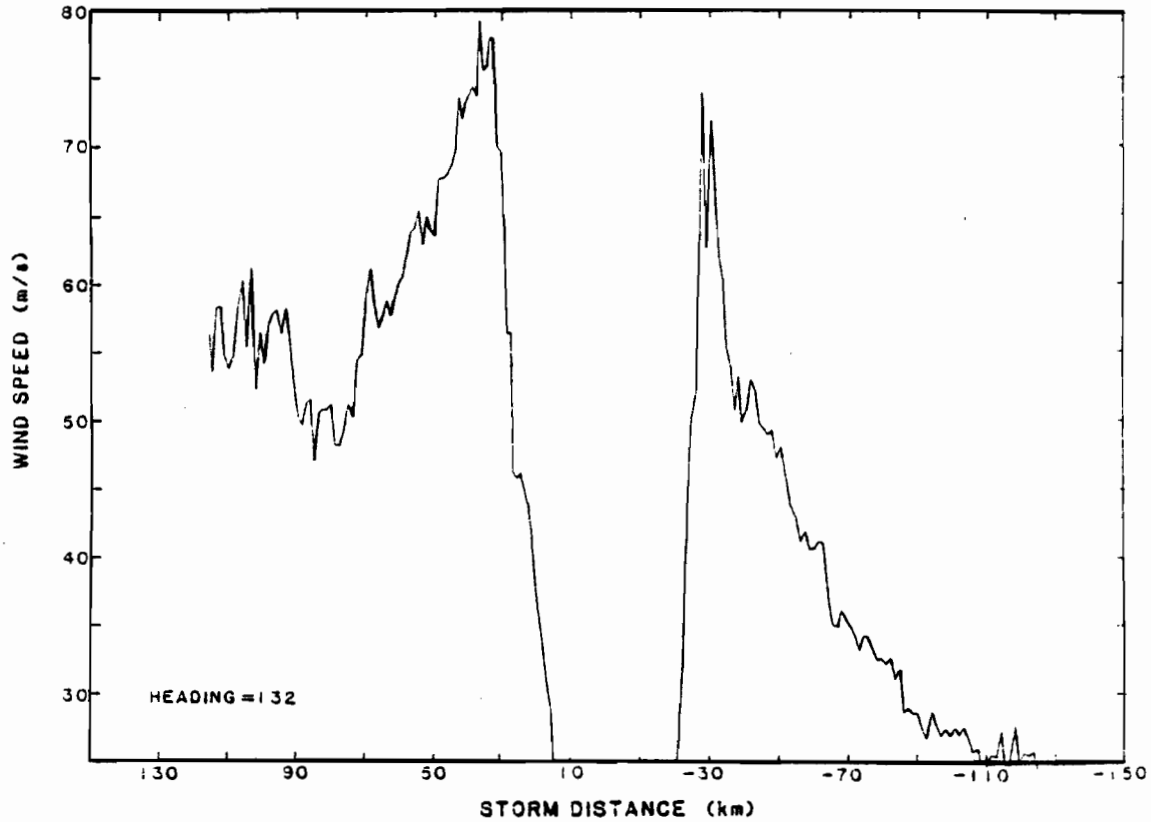

Figure A.22.—Flight-level winds recorded along radials through the center of Hurricane Allen, 1535-1627 GMT, August 5, 1980.

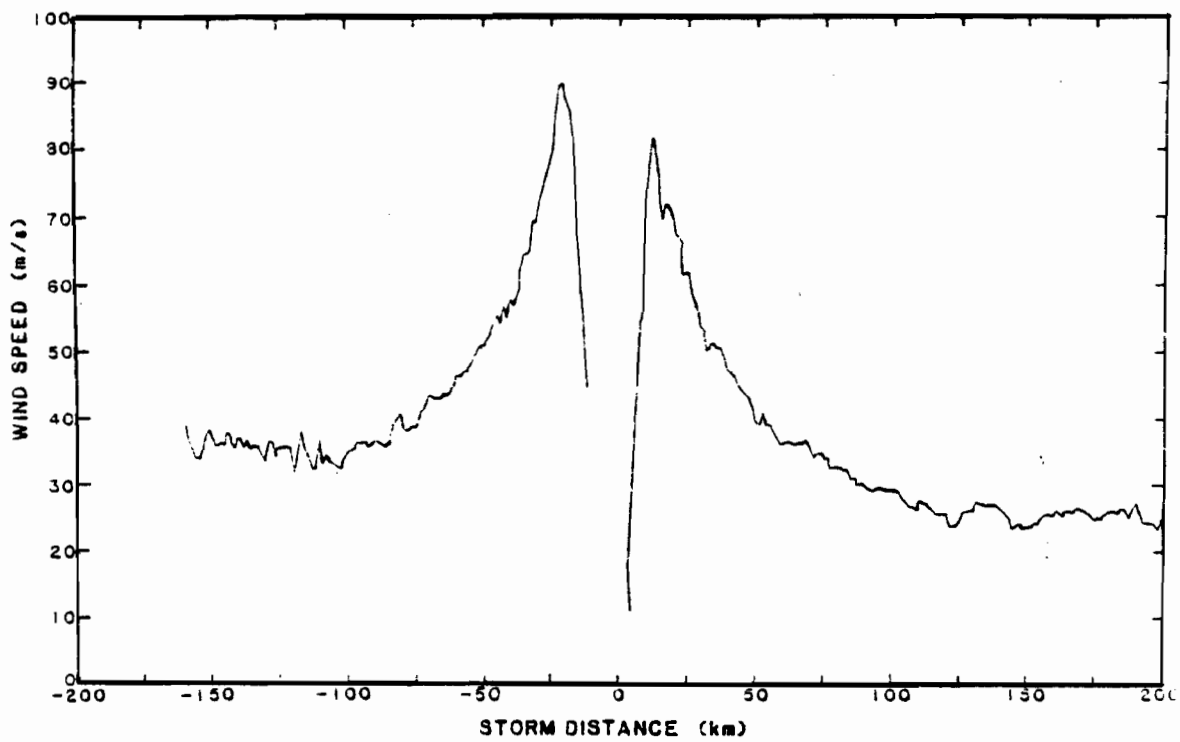

Figure A.23.—Flight-level winds recorded along radials through the center of Hurricane Allen, 1844-1945 GMT, August 7, 1980.

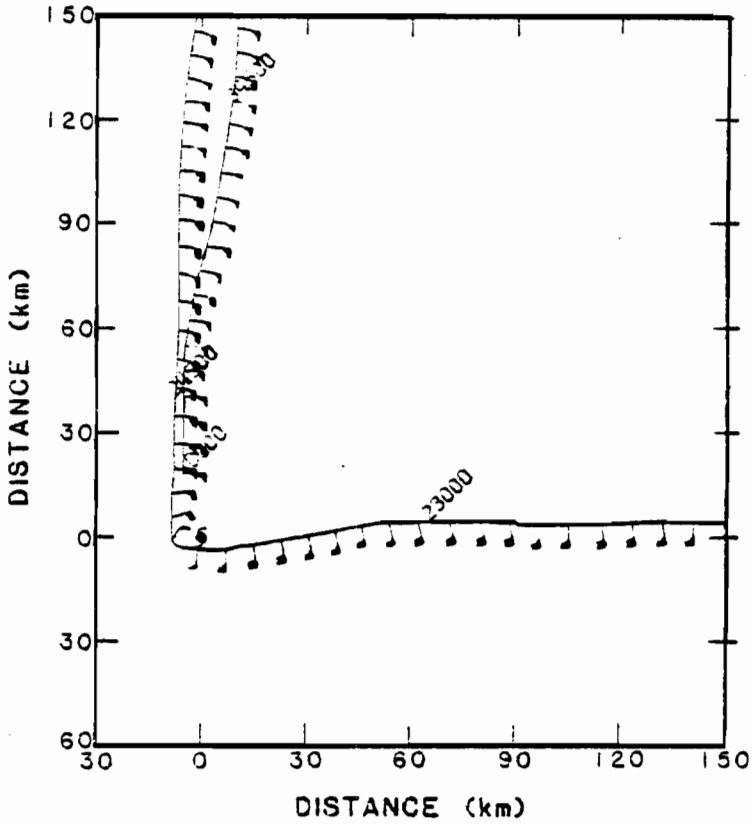

Figure A.24.—Composite map of flight-level winds (m/sec) recorded between 0200 and 0400 GMT, August 9, 1980.

A.4.6 Time Variation of Central Pressure and Radius of Maximum Winds

Figure A.25 shows the time history of central pressure for Allen (from fig. A.21) together with radial distances of observed maximum winds recorded at each traverse of the hurricane center. Analysis of these radial distances yielded the variation with time of the radius of maximum winds. Generally speaking, Allen was a small hurricane except for the period when it approached the Texas coast and moved over land. Prior to this period (9 hr before landfall) the time variation of maximum winds indicated that the radial distances of wind maxima increased to 20-25 nmi (37-46.3 km) during Allen's two weakening stages. However, radial distances of wind maxima stayed within 4 to 15 nmi (7.4-27.8 km) of the center when Allen's central pressure dropped below 930 mb in each of the three deepening stages. The fact that Allen's minimum pressure in each of the three deepening cycles occurred some distance from land, does not exclude the possibility that a hurricane could attain its maximum intensity (or minimum central pressure) at or near the time of landfall. Hurricane Camille (1969) is an example of a hurricane which maintained its intensity of about 905 mb for some 36 hours before it crossed the Mississippi coast.

A.4.7 Relation of P_o and R in Hurricane Allen

Figure A.26 is a plot of central pressure versus radial distance of maximum winds recorded by aircraft reconnaissance during the period August 3 through August 9. Data points used in the plot included those instances when both wind

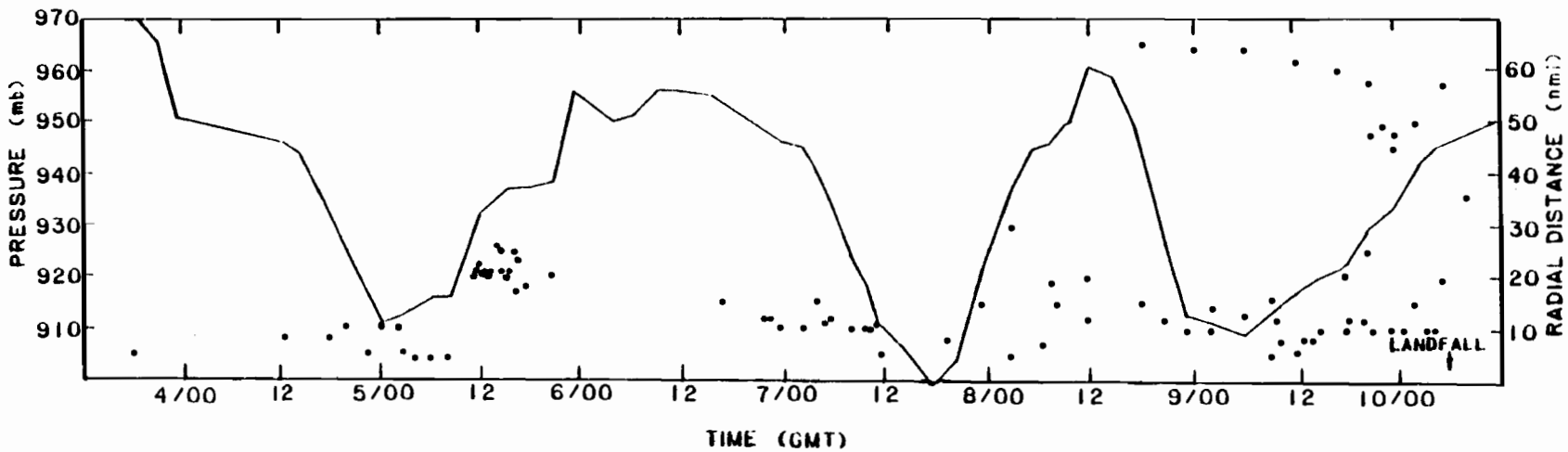

Figure A.25.--Central pressure (solid line) and radial distances (from eye center) of wind maxima (dots) in Hurricane Allen, August 3-10, 1980.

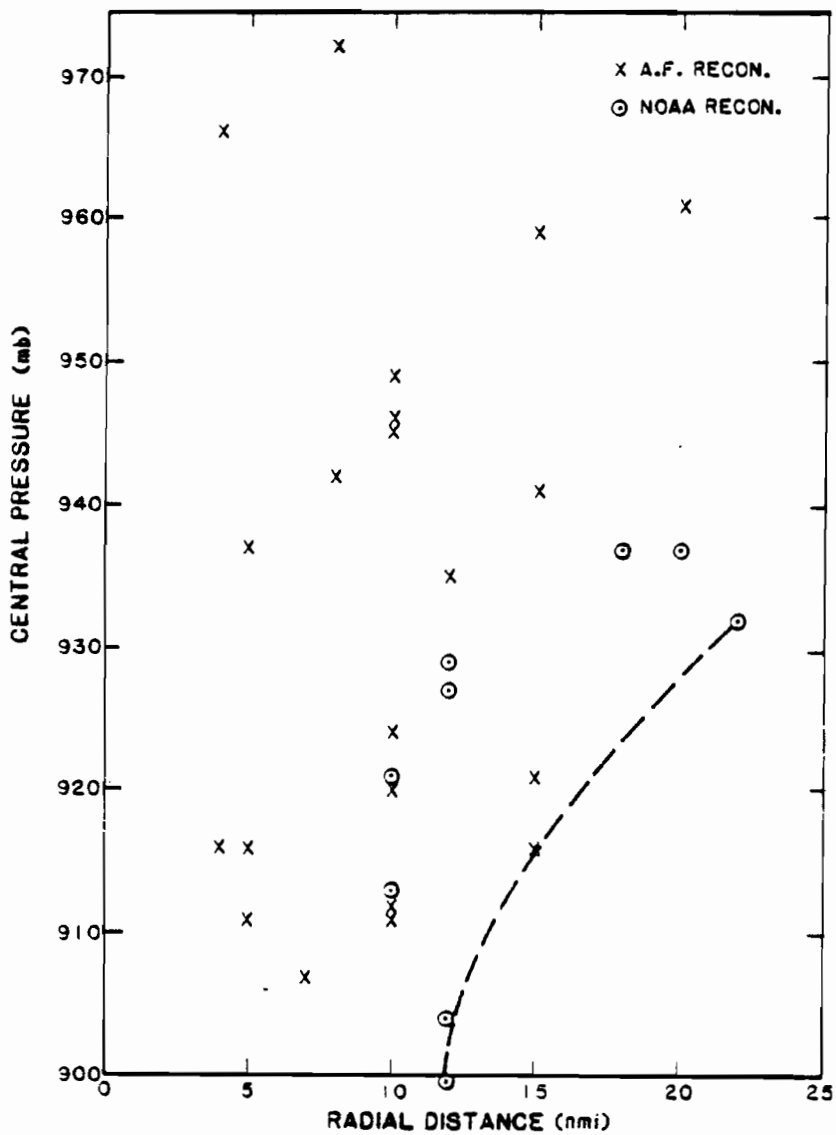

Figure A.26.—Concurrent observations of central pressure and radius of maximum winds for Hurricane Allen, August 3-9, 1980.

and pressure data were recorded in a traverse of the hurricane center. Some of the data points (with no concurrent observations of P_o and R) shown in previous diagrams were not included in this plot. During the period of observation (August 3-9), Allen traveled from the Caribbean through the Yucatan Channel into the Gulf of Mexico. It covered a distance of about 2,000 nmi (3704 km) from latitude 14°N through 27°N. Except for a few instances of large R observed in the weakening stages, Allen's maximum winds stayed within 15 nmi (27.8 km) of the center. Allen was essentially characterized by small R's before it reached the Texas coast. However, the R values in Allen, as well as in other intense Atlantic hurricanes, tend to be small and a non-linear relation may exist between P_o and R.

APPENDIX B

Statistical Methods for Tests of Homogeneity and Independence

B.1 Introduction

The statistical methods used in this report to test the homogeneity of hurricane parameters and interrelations between them are discussed in this appendix. The methods used to test for homogeneity include cluster analysis, discriminant analysis, principal component analysis, and the Mann-Whitney test; those for the test of independence include the Spearman test and contingency table analysis using the Chi-square test.

For these methods, this appendix describes assumptions, and where appropriate, the null hypotheses, the confidence levels, and decision rules. We also briefly discuss the rationale for choosing a method, its limitations, and the guidelines for interpreting the test results.

B.2 Methods for the Test of Homogeneity

Among the methods for the test of homogeneity, cluster analysis, discriminant analysis and principal component analysis each consider several parameters, whereas the Mann-Whitney test is based on only a single parameter.

B.2.1 Cluster Analysis

B.2.1.1 Description of the Method. In cluster analysis, objects are assigned to groups or clusters suggested by the data sample, not by any grouping defined **a priori.** In this study, a hurricane was considered an object for the purpose of statistical analysis. That is, all parameters associated with a given storm were used to characterize the hurricane. There are many clustering methods (e.g., SAS 1982); we chose the centroid method for this study.

The actual computation was performed using the CLUSTER procedure in the SAS* system. The procedure computes the Euclidean distances between objects and assigns those objects that are close to each other to the same cluster. In this study, the Euclidean distance was computed using coordinates represented by P_o, R, θ, T, m, ϕ and λ. In the centroid method, the distance between two clusters is defined as the Euclidean distance between their centroids (vector means).

The procedure provided a cluster hierarchy from level one to level N, where N is the number of objects in the data sample. In this study, N is the number of hurricanes; if any hurricane parameter was missing, that hurricane was omitted. In the cluster hierarchy, there is only one cluster at level one and there are N clusters at level N. The cluster at level one contains all the objects in the data sample, and every cluster at level N contains only one object. As shown in Figure B.1, every cluster at a given level is completely contained in a cluster at the preceding level. For example, a cluster at level four may contain

---

* Mention of a particular commercial product should not be considered an endorsement by the federal government.

MILEPOST RANGE	NUMBER OF CLUSTERS							
	2	3	4	5	6	7	8	9
11-243							7	8
296-500				1	1	1	1	1
560-671	1	1	1					5
716-904				4	4	4	4	4
966-1201					5	5	5	6
1292-1584		2	2	2	2	2	2	2
1752-1945	2		3	3	3	3	3	3
2043-2294		3				7	8	9
2582-2750			4	5	6	6	6	7

Figure B.1.--Levels two through nine of the hierarchical clusters of landfalling hurricanes, based on parameters P_o, R, θ, T, m, ϕ and λ. The circled numbers are the cluster identification numbers.

exactly the same objects of one cluster at level five (cluster 2 in fig. B.1), or it may contain exactly the same objects of two clusters at level five (cluster 1 at level 4, and clusters 1 and 4 at level 5 in fig. B.1). The user must determine the most appropriate number of clusters. When the number of clusters is chosen, the parent cluster of each object (hurricane) can be identified using the TREE procedure of the SAS system.

B.2.1.2 Rationale for Choice. Some clustering methods require that the sample data be normally distributed. The hurricane data sample has large natural variability, and the normality of our data could not be reliably tested. We chose to use the SAS CLUSTER procedure since it did not require that the data sample be normal.

B.2.1.3 Limitations of the Method. No satisfactory method has been developed to determine the appropriate number of clusters. This is dependent on the data sample and nature of the phenomena being considered.

B.2.1.4 Interpretation of the Results. Conclusions drawn from cluster analysis are dependent on the selection of the number of clusters and must be interpreted cautiously. Scatter diagrams of the original parameters were helpful for the determination of the optimum number of clusters. Other methods, both nonstatistical and statistical, were also considered to help interpret the results of cluster analysis. In this study, we relied heavily on meteorological judgment; in addition we used discriminant analysis and principal component analysis to help evaluate the results of the cluster analysis.

B.2.2 Discriminant Analysis

B.2.2.1 Description of the Method. Discriminant analysis uses one classification variable and several continuous quantitative variables to assign each object to a class corresponding to a value of the classification variable using the information contained in the continuous variables. In this study, hurricanes were the objects to be classified, the cluster identification number obtained from the cluster analysis was the classification variable, and hurricane parameters were the continuous variables.

There are several types of discriminant analysis, some are based on the assumption that each class can be considered normally distributed while others use non-parametric methods and do not require the assumption of normality. In this study, we used the "k-nearest-neighbor" discriminant analysis, where k was chosen to be seven, equal to the number of parameters (P_o, R, θ, T, m, ϕ and λ) used in the analysis.

Considering each hurricane as an object represented by a vector of seven components (P_o, R, θ, T, m, ϕ and λ), the method computes the distance between two objects based on the total-sample covariance matrix (Mahalanobis distance), and, for each object, it saves the distances of the seven nearest objects (because k = 7). Based on these distances, it computes the probability that an object would fall into the class with the selected nucleus object. If the probability exceeds a specified threshold, the associated object is classified into that class. The actual computation was performed using the NEIGHBOR procedure of the SAS system. More details of the method are given in the SAS User's Guide (SAS 1982).

B.2.2.2 Rationale for Choice. The k-nearest-neighbor approach was non-parametric and did not require the assumption of normality. It allowed us to evaluate the results of the cluster analysis and to determine a number of clusters that could be characterized as homogeneous for testing the independence of the various hurricane parameters.

B.2.2.3 Limitations of the Method. The variables, except for the classification variable, must be continuous so that the computation of distances can be performed. The classification variable can be either categorical or numerical, but there can only be one classification variable. It is recommended that the classification variable be limited to a finite number of values, so that the classes can be kept to a manageable number.

B.2.2.4 Interpretation of the Results. The discriminant analysis gives the classification of each object and probabilities of its membership in all the classes in which it could have been placed. By comparing the class that the object was placed in and the class assigned a **priori**, misclassified objects can be identified. The probability of membership in a particular class can be used to judge whether the classification of the object was appropriate. The threshold probability for the classification is user specified. In this study, the threshold probability was not assigned and objects were classified into the class which was associated with the largest membership probability.

B.2.3 Principal Component Analysis

B.2.3.1 Description of the Method. Given N numerical characteristics that describe a set of objects, the principal component analysis procedure computes N principal components; each principal component is a linear combination of the original characteristics (variables). The coefficients of this linear combination are the elements of an eigenvector of the correlation or covariance matrix of the original variables. The eigenvectors are normalized to have unit length (unit norm). The eigenvalues are the variances of the associated principal components. The first principal component has the largest eigenvalue and the N-th principal component has the smallest. The eigenvectors are orthonormal, i.e., they represent perpendicular directions in the space of original characteristic variables. In this study, the original characteristic variables were P_o, R, θ, T, m, ϕ and λ therefore, there were seven principal components.

The computation of the principal components of the hurricane parameters was performed using the PRINCOMP procedure of the SAS system. The procedure gives the percentage and cumulative percentage of all eigenvalues ordered from the largest to the smallest, i.e., from the first principal component to the seventh principal component. These percentages show the relative amount of variance accounted for by the principal components. The procedure also gives eigenvectors whose elements are interpreted as the loadings on the original variables; the loadings explain the relative importance of the hurricane parameters in each principal component.

B.2.3.2 Rationale for Choice. After investigating the results of cluster analysis and discriminant analysis, we decided to examine the importance of various parameters in the grouping of hurricanes. The loadings provided with the principal component analysis allowed us to evaluate the weight of individual parameters. By plotting one principal component versus another and using the cluster identification number of each hurricane for the plotting symbol, we could examine the clustering patterns of the hurricanes. Using such a plot, we could deduce which parameter(s) had most control on the clustering.

B.2.3.3 Limitations of the Method. Principal component analysis required that all seven parameters P_o, R, θ, T, m, ϕ and λ be available for each hurricane. Storms with missing values had to be excluded from the analysis.

B.2.3.4 Interpretation of the Results. As explained above, the results of the principal component analysis can be used to explain the relative importance of the original variables for the grouping of hurricanes. By investigating the percentage of variance accounted for by each principal component, we were able to

select the more important principal components. Then, by examining the eigenvectors associated with these principal components, we found the original variables that were most important in defining these principal components. Although the results of the principal component analysis can be used to explain some linear relations between the hurricane parameters, interpretation of these relations was not always clear. Sometimes scatter diagrams of the original variables were used for additional guidance in understanding the results.

B.2.4 Mann-Whitney Test

B.2.4.1 Description of the Method. The Mann-Whitney test is a rank test (non-parametric). In this study, we divided the hurricanes into several a **priori** groupings based on location along the coast. For each test, we selected two groups of hurricanes: one group had N hurricanes and the other had M hurricanes. Assuming that each group was a random sample drawn from its respective population and two groups were mutually independent, we performed the Mann-Whitney test on each of the hurricane parameters P_o, R and T.

The test was performed in the following manner: We first combined the group of N hurricanes (group 1) with the group of M hurricanes (group 2). To test whether parameter P_o, for example, has the same distribution function in groups 1 and 2, we first arranged the P_o in the mixed sample from the smallest to the largest value and assigned rank values from 1 to N+M to these P_o values. For tied values of P_o, an averaged rank value was assigned to each of them as shown in the following example (note rank 6.5 for P_o = 961.7).

Example*:

P_o	Rank	Group Origin
943.0	1	2
947.2	2	2
955.3	3	2
956.7	4	1
959.0	5	2
961.7	6.5	2
961.7	6.5	1
966.5	8	1
975.0	9	1
979.0	10	2
981.0	11	1

Then, the sums of ranks (S) were computed separately for groups 1 and 2. In the example, S_1 = 38.5 and S_2 = 27.5. The corresponding test statistics of the Mann-Whitney test were computed using the formulae:

* This example is for illustration only, not to be confused with any actual grouping in this study.

$$W_1 = S_1 - \frac{1}{2} N (N + 1), \qquad W_2 = S_2 - \frac{1}{2} M (M + 1)$$

respectively for groups 1 and 2. In the example, N = 5 and M = 6, thus $W_1 = 23.5$ and $W_2 = 6.5$.

For given sample sizes N and M, percentiles of the Mann-Whitney test statistic can be computed (see Conover, 1971, table 8). We used a two-tailed test at 5-percent significance level and the null hypothesis that P_o had the same distribution function in both groups of hurricanes. For N = 5 and M = 6 in the example, the 0.025-th percentile was 4 and the 0.975-th percentile was 26. Comparing the test statistics W_1 and W_2 with these percentiles, we found that W_1 and W_2 were within the range between 4 and 26 (respectively, 0.025-th and 0.975-th percentiles), and we accepted the null hypothesis for the above example.

The test was repeated for R and T for every selected pair of groups of hurricanes in this study. For more details of the Mann-Whitney test, see Conover (1971).

B.2.4.2 Rationale for Choice. The limited sample size and large natural variability of our hurricane data sample prevented us from reliably estimating the distribution functions of hurricane parameters for formal hypothesis testing. Since the Mann-Whitney test is a non-parametric test, it does not require a **priori** assumptions about the distribution function of the data sample and is suitable for our hurricane data.

B.2.4.3 Limitations of the Method. The basic assumption for the Mann-Whitney test is that both groups are drawn as random samples. For the reasons discussed in Section 3.2.1.2, we did not consider it appropriate to use direction of landfalling hurricanes as a random variable, and this parameter was excluded from the Mann-Whitney test. Another assumption of the Mann-Whitney test is that two samples must be mutually independent. There was no evidence that our hurricane data samples for the selected coastal segments violated this assumption.

B.2.4.4 Interpretation of the Results. The Mann-Whitney test examines the similarity of two distributions of rankings, but not the distributions of the actual values of the hurricane parameters. For this reason, the results must be interpreted with caution, and any conclusions drawn from the test results must recognize that the distributions of rankings may not fully correspond to the distributions of the actual values.

B.3 Methods for the Test of Independence

To test independence among hurricane parameters, we used two methods: the Spearman test and contingency tables with the Chi-square test. The Spearman test is a rank test while the contingency tables with the Chi-square test is for categorical data.

B.3.1 Spearman Test

B.3.1.1 Description of the Method. As an example, consider the Spearman test for P_o and R for a group of hurricanes. P_o was ranked from the smallest to the largest value and rank numbers were assigned to each value; for tied values of P_o, an average rank value was assigned to each of them as was done in the Mann-Whitney test (see sec. B.2.4.1). For the same group of hurricanes, R's were also ranked and assigned a rank number. Then the Spearman correlation was computed using the following formula:

$$\rho = 1 - \frac{6W}{N\,(N^2-1)} \quad ,$$

$$\text{where} \quad W = \sum_{i=1}^{N} [r(P_{o_i}) - r(R_i)]^2 \quad .$$

The parameter N is the sample size of the group of hurricanes, and r is the rank value of parameters P_o or R. Spearman's correlation can be used as a test statistic. Given the sample size, N, and the probability of a percentile, this percentile can be computed.

There are three ways to test the Spearman correlation. The null hypothesis for all three tests is that P_o and R are mutually independent, that is, the correlation coefficient is not significantly different from zero. The alternate hypothesis for the first test is that P_o and R are positively correlated, for the second, that P_o and R are negatively correlated, and for the third, that P_o and R are correlated (either positively or negatively). In this study, when the probability associated with a specific estimate of ρ was greater than 95th percentile, we rejected the null hypothesis of the first test, when ρ was less than 5th percentile, we rejected the null hypothesis of the second test, and when ρ was either less than 2.5 percent or greater than 97.5 percent, we rejected the null hypothesis of the third test. The significance level for all the tests was 5 percent. For more details, see Conover (1971).

B.3.1.2 Rationale for Choice. We chose Spearman test for the hurricane parameters because it offered the possibility of detecting the nature of interrelations, if they existed.

B.3.1.3 Limitations of the Method. As with many non-parametric tests, weak relations between two parameters may not be detected.

B.3.1.4 Interpretation of the Results. The Spearman test detects the correlation of ranks of random variables instead of the actual values of the variables. The interpretation of these correlations should be limited to the correlations of ranks only; independence between ranks of random variables may imply independence of the random variables.

B.3.2 Contingency Table with Chi-square Test

B.3.2.1 Description of the Method. The contingency table with a Chi-square test was used at the 0.05 level and is described in detail in Section 4.2 of this report. Additional details may be found in Conover (1971).

B.3.2.2 Rationale for Choice. There was no requirement that the sample meet conditions other than it be a random sample of sufficient size. This made it suitable for use with our data sample.

B.3.2.3 Limitations of the Method. The contingency table with the Chi-square test was designed for categorical data samples, thus, we had to choose specific values to partition the parameters into categories to establish the cell frequencies in the contingency table. There cannot be more than 20 percent of cells which have expected frequency less than 5 in each of them. This limitation is to ensure that the Chi-square approximation is valid for the test.

B.3.2.4 Interpretation of the Results. The results of this test were sensitive to the values selected to partition the data into categories. A small change of the dividing value sometimes caused the result to change from not significant to significant, or vice versa. Therefore, we had to be careful in interpreting the results using this approach.

APPENDIX C

Plotting Position Formula

C.1 Introduction

A plotting position formula was used to determine the location along the abscissa of ranked data in the cumulative frequency curves for the hurricane parameters. A plotting position formula was selected for this purpose from eight existing formulae based upon five evaluation criteria.

Existing plotting position formulae are listed in Table C.1. The symbols used in the formulae are explained in the note underneath the table. In each line, the name of the formula is given in the left column, and the year in which the formula was introduced is given in the right column. This table does not include all existing formulae. The Beard (1943) formula is not included because it only applies to $m = 1$, and the Samsioe formula (see Reinius 1949, p. 51) is not included because its computation involves solving a N-th power equation and it is not easy to use. For convenience of computation, only easy-to-use formulae were considered.

C.2 Criteria for Evaluation

The plotting position formula listed in Table C.1 were evaluated according to the criteria listed below.

1. The plotting position must be such that all the observed data can be plotted on probability paper.

Table C.1.--List of plotting position formulae

Name	Formula*	Year
California	$P_m = \frac{m}{N}$	1923
Hazen	$P_m = \frac{2m-1}{2N}$	1930
Weibull	$P_m = \frac{m}{N+1}$	1939
Chegodayev	$P_m = \frac{m-0.3}{N+0.4}$	1955
Blom	$P_m = \frac{m-3/8}{N+1/4}$	1958
Tukey	$P_m = \frac{3m-1}{3N+1}$	1962
Gringorten	$P_m = \frac{m-0.44}{N+0.12}$	1963
Reinius	$P_m = \frac{m-0.37}{N+0.26}$	1982

* P_m = probability;
N = total number of items;
m = rank of an item
$m \leq N$.

2. The plotting position should lie between the observed frequencies (m-1)/N and m/N. (For the explanation of m and N, see the footnote of Table C.1.)

3. The return period of a value equal to, or larger than, the largest observed value should converge towards N.

4. The observed values should be equally spaced on the frequency scale.

5. The plotting position should have an intuitive meaning, be analytically simple, and be easy to use.

Table C.2.--List of plotting position formulae in the descending order of their p_m's. (See table C.1 for the meanings of symbols.)

m = 1	m = N
California	California
Weibull	Hazen
Chegodayev	Gringorten
Tukey	Blom
Reinius	Reinius
Blom	Tukey
Gringorten	Chegodayev
Hazen	Weibull

C.3 Evaluation of Plotting Position Formulae

All formulae in Table C.1 meet criteria 4 and 5. All except the California formula meet criteria 1 and 2. Only the California and Weibull formulae meet criterion 3. The most important problem with the California formula is that it gives p_m = 100 percent for m = N, and this p_m can not be plotted on a probability paper. The most important advantage of Weibull formula is that the return period for m = 1 converges towards N as $N \longrightarrow \infty$. Among formulae listed in Table C.1, only the Weibull formula meets all the criteria listed above. Thus, the Weibull formula was the choice used in this study.

C.4 Comparison of Formulae

To reveal more about the characteristics of the various formulae, we compared them for the special cases: m = 1, m = N, and $N \longrightarrow \infty$. For m = 1 and N, the names of formulae are listed in Table C.2 in the descending order of their values of p_m. The order of names for m = N is exactly the reverse of that for m = 1, except for California formula. For $N \longrightarrow \infty$, the values of p_m computed using all the formulae in Table C.1 approach m/N.

Since the sample size of hurricane climatological data is usually small, we choose N = 10 for an example to compare values of p_m of the formulae in Table C.1. These values are plotted in Figure C.1. The Weibull formula gave the largest p_m for m = 1 and the smallest p_m for m = N. Except for the California formula, the largest difference in p_m between different formulae was less than 5 percent. For m = 1, the p_m of the Weibull formula is approximately two times that of the Hazen formula. For m = N, the p_m of the Weibull formula is close to that of the Hazen formula: approximately 91 percent compared to 95 percent.

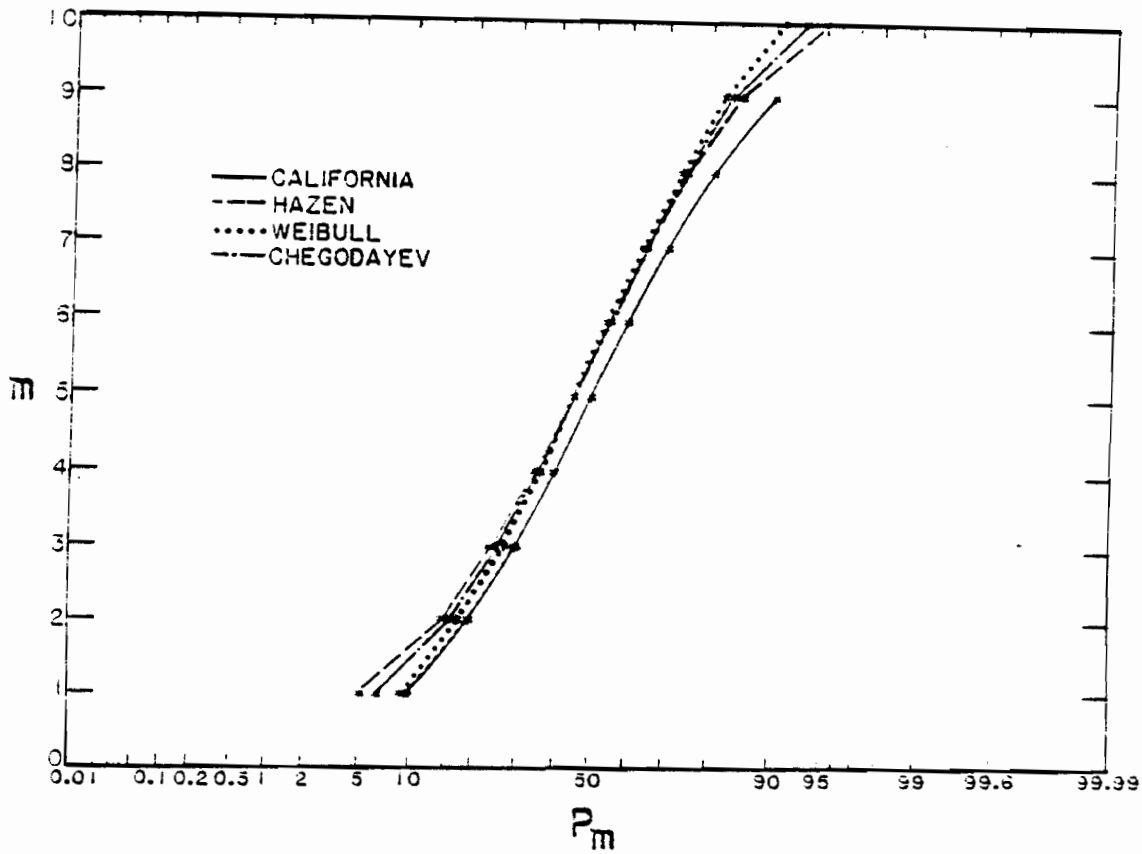

Figure C.1.—Comparison of plotting position formulae for N = 10. (See table C.1 for the meanings of symbols.)

1013 mb = 29.92 in

1